



Doctoral Thesis

QCD corrections for WH and $\gamma^*\gamma^*$ production

Author(s):

Cancino, Julián V.

Publication Date:

2014

Permanent Link:

<https://doi.org/10.3929/ethz-a-010246982> →

Rights / License:

[In Copyright - Non-Commercial Use Permitted](#) →

This page was generated automatically upon download from the [ETH Zurich Research Collection](#). For more information please consult the [Terms of use](#).

Diss. ETH No. 22037

QCD corrections for WH and $\gamma^*\gamma^*$ production

A thesis submitted to attain the degree of

DOCTOR OF SCIENCES of ETH ZÜRICH

(Dr. sc. ETH Zürich)

presented by

Julián Vincent Cancino

MSc ETH Physics, ETH Zürich

born on 08.11.1985

citizen of Versoix GE and Chile

accepted on the recommendation of

Prof. Dr. C. Anastasiou, examiner
Prof. Dr. G. Dissertori, co-examiner

2014

Abstract

The Standard Model of particle physics describes the interaction of elementary particles using a local gauge symmetry. This symmetry prevents us from writing mass terms for fundamental particles and we must rely on a mechanism to spontaneously break this symmetry to give mass to elementary particles. The Higgs mechanism introduces a scalar field which takes up a finite vacuum expectation value. After the spontaneous symmetry breaking, a spin-0 particle – the Higgs boson – remains in the spectrum and has specific interactions with the other elementary particles of the Standard Model.

After many years of searching for the Higgs boson, the ATLAS and CMS collaborations at CERN announced the discovery of a new boson in July 2012. Their analyses were based on diphoton and four-lepton events. These two clean decay channels of the Higgs boson are signatures of the loop-induced decay to a photon pair and the direct decay to a pair of Z bosons, respectively. So far, the measurements of the properties of this new boson coincide with the expectations for the Standard-Model Higgs boson.

To assess its identity, we need to measure its coupling to other fundamental particles of the Standard Model. At a collider such as the LHC the access to the couplings is challenging because of the hadronic environment. Therefore, we need reliable theoretical predictions for signal and background processes. To achieve this goal, we need to compute higher-order corrections in quantum chromodynamics (QCD) for the processes of interest. In this thesis, we will present the work done on two different processes.

After reviewing the theoretical framework, we present the phenomenological analysis we have performed for the process in which a Higgs boson is produced along with a W boson, and decays into a bottom-antibottom pair. We study the effect of next-to-leading order QCD corrections to both initial- and final-state in the context of the “boosted regime”, which provides a way to measure the coupling of the Higgs boson to bottom quarks at a hadron collider.

Then we turn to the production of two off-shell photons with different virtualities, which represents a first step towards the diboson production process. We present the computation of the QCD corrections up to next-to-next-to-leading order of the differential cross section for a gauge-invariant subset of the full correction, namely by computing diagrams that are proportional to the number of light quark flavors. There we focus on the treatment of virtual and real amplitudes before showing differential distributions of interest.

Zusammenfassung

Das Standardmodell der Teilchenphysik beschreibt die Wechselwirkung der Elementarteilchen aufgrund einer lokalen Eichsymmetrie. Diese Symmetrie verbietet es fundamentale Teilchen mit ein Massenterm auszustatten. Um das in der Natur vorgefundene Spektrum beschreiben zu können, ist es folglich notwendig einen Mechanismus einzuführen, welcher erlaubt diese Symmetrie spontan zu brechen. Der Higgs-Mechanismus erlaubt dies durch Einführung eines skalaren Feldes, welche einen endlichen Vakuumerwartungswert annimmt. Nach der spontanen Symmetriebrechung bleibt ein Spin 0 Teilchen – das Higgs-Boson – im Spektrum übrig, welches spezifische Wechselwirkungen mit den anderen Elementarteilchen des Standardmodells aufweist.

Nach einer vieljährigen Suche nach dem Higgs-Boson haben die ATLAS und CMS Kollaborationen am CERN im Juni 2012 die Entdeckung eines neuen Bosons verkündet. Ihre Analysen basierten auf Streu-Ereignissen mit zwei Photonen und vier Leptonen. Diese zwei klar messbaren Zerfallskanäle für das Higgs-Boson sind die Signaturen des schleifen-induzierten Zerfalls zu einem Photon-Paar, sowie respektive des direkten Zerfalls in ein Z-Boson-Paar. Bis anhin stimmen die gemessenen Eigenschaften des neuen Bosons mit den Vorhersagen des Standardmodells für das Higgs-Boson überein.

Um die Identität des neuen Bosons festzustellen, müssen wir seine Kopplungen mit anderen fundamentale Teilchen des Standardmodells messen. An einem Speicherring wie dem LHC ist der Zugang zu diesen Kopplungen wegen der hadronischen Umgebung eine Herausforderung. Wir brauchen deswegen zuverlässige theoretische Vorhersagen, sowohl für Signal- als auch für Hintergrundprozesse. Zu diesem Zweck müssen wir Störungsrechnungen zu höheren Ordnungen in Quantenchromodynamik (QCD) für die Prozesse von Interesse durchführen. In dieser Doktorarbeit werden wir die unternommene Arbeit an zwei verschiedene Prozesse präsentieren.

Nachdem wir den theoretischen Rahmen erörtert haben, werden wir die phänomenologische Analyse präsentieren, welche wir für den Prozess, bei dem ein Higgs-Boson zusammen mit einem W-Boson produziert wird und danach in ein Bottom-Antibottom Quark Paar zerfällt, durchgeführt haben. Wir werden die Konsequenzen der QCD Korrekturen in nächst-zu-führender Ordnung sowohl zu Anfangs- und Endzustand im Kontext des sogenannten “boosted Regime” studieren, welches eine Möglichkeit darstellt, die Kopplung des Higgs-Bosons zum Bottom-Quark an einem Hadron-Speicherring zu messen.

Danach werden wir die Produktion von Photonen mit nichtverschwindenden und unterschiedlichen Virtualitäten besprechen, welche ein erster Schritt in die Richtung des Diboson-Prozess darstellt. Wir präsentieren die Rechnung der QCD Korrekturen bis zur nächst-zu-nächst-zu-führenden Ordnung für eine eichinvariante Teilmenge der vollen Korrekturen, nämlich jene proportional zur Anzahl der leichten Quark-Flavors. Wir werden uns auf die Behandlung der virtuellen und reellen Amplituden fokussieren bevor wir einige Distributionen zeigen.

Résumé

Le Modèle Standard de la physique des particules décrit l'interaction des particules élémentaires au moyen d'une symétrie de jauge locale. Cette symétrie nous interdit d'introduire des termes de masse pour les particules fondamentales et il nous faut utiliser un mécanisme pour briser cette symétrie spontanément et donner une masse aux particules élémentaires. Le mécanisme de Higgs introduit un champ scalaire qui acquiert une valeur moyenne finie dans le vide. Après la brisure spontanée de symétrie, une particule de spin 0 – le boson de Higgs – reste dans le spectre et possède des interactions spécifiques avec les autres particules élémentaires du Modèle Standard.

Après de nombreuses années de recherche du boson de Higgs, les collaborations ATLAS et CMS du CERN ont annoncé en juillet 2012 la découverte d'un nouveau boson. Leur analyse était basée alors sur les événements à deux photons et à quatre leptons. Ces deux modes de désintégration propres du boson de Higgs sont les signatures respectives de la désintégration en deux photons induite par une boucle et de la désintégration directe en une paire de bosons Z . Jusqu'ici les mesures des propriétés de ce nouveau boson coïncident avec celles qu'on attend du boson de Higgs du Modèle Standard.

Afin de confirmer son identité, il convient de mesurer ses constantes de couplage aux autres particules fondamentales du Modèle Standard. L'extraction de ces constantes de couplage avec un collisionneur comme le LHC est rendue difficile en raison de l'environnement hadronique. Il nous faut donc des prédictions théoriques fiables pour les processus signaux et de fond. À cette fin, nous devons calculer les corrections d'ordres supérieurs en chromodynamique quantique (QCD) pour les processus d'intérêt. Cette thèse est dédiée à l'étude de deux processus différents.

Après avoir passé en revue le cadre théorique, nous présenterons l'analyse phénoménologique que nous avons faite pour le processus dans lequel un boson de Higgs est produit en association avec un boson W , et se désintègre en une paire de quark-antiquark bottom. Nous étudierons l'effet des corrections QCD au premier ordre à l'état initial comme à l'état final dans le contexte du "régime boosté", qui offre la possibilité de mesurer la constante de couplage du boson de Higgs aux quarks bottom sur un collisionneur de hadrons.

Ensuite nous traiterons la production d'une paire de photons à virtualités non nulles et distinctes, ce qui représente un pas dans la direction du processus diboson. Nous présenterons le calcul des corrections QCD au deuxième ordre pour un sous-ensemble invariant de jauge de la correction totale, à savoir celles proportionnelles au nombre de saveurs de quarks légers. Nous nous concentrerons sur le traitement des amplitudes virtuelles et réelles avant de présenter des distributions pertinentes.

Acknowledgements

There are many people I would like to thank for their direct or indirect contributions to this thesis, in particular:

Babis Anastasiou; for his central role in the last years: at first as an inspiring teacher of quantum mechanics and quantum field theory and then as a supervisor during my master thesis and my doctorate. He has shown support, care, and understanding no matter the circumstances and I am very grateful for that.

Romain Müller; much more than a study colleague and a roommate, a real friend with whom I could always have a chat or a break. I also need to mention his central support when it came to C++ implementation or introducing me to Python. We have a very different way of working, which has sometimes not been easy, but in the end it worked. I wish him a lot of success for his future challenges.

My parents Sarah and Roberto and my brother Hadrian; for their constant understanding for everything I have ever undertaken, and specifically their patience when I was talking passionately about what was going well, or cheering me up when motivation was down. It goes without saying that this extends far beyond the scope of the years of my doctoral studies, and I hope I will manage to be there for you as well.

I had the opportunity to work very intensely with Andrea Banfi at the beginning of my doctorate. He has been a very knowledgeable source for all my questions about perturbative QCD. I also had the privilege to collaborate with Federico Chavez and Claude Duhr concerning 2-loop virtual amplitudes and I was able to learn a great deal on the techniques of this topic from them. Regarding the reduction to master integrals Bernhard Mistlberger deserves a special thank for corroborating and performing reductions of the 2-loop 2-scale integrals. Finally, I was happy to work with Achilleas Lazopoulos, not only on research, but also for what became the most interesting (and challenging) teaching assistance I was to experience.

I would like to extend a special thank you to Stefanie Piebinga, who helped improve my spelling in this thesis and was always there when I needed someone with whom to talk, and to Federico, who was my thesis-writing buddy during the last couple of months after we shared a short theater career, travelled and organized an open-air cinema together.

Fortunately, I also had the occasion to share many activities outside of research with people I got to know during my years at ETH. These include but are not limited to my

officemates over the years: Franz, Stephan, Federico, Mathias, Bernhard, and Gizem; the people I had the occasion to work with in the AVETH, AMP, VSETH and VMP boards, the University Assembly and other commissions (with a special mention to Florian and Lars); the ski-enthusiasts of the group: Bernhard, and more recently Caterina and Simone; the D&D team: Claude, Falko, Stefanie, Dirk, Volker, Doug, and Tina; the many friends at the institute; and of course the scuba-diving aficionados of ASVZ.

Although it might look like I am slowly forgetting them, I would like to acknowledge the support I got from my friends from Geneva Akira, Alexandra, Alexander, Alexandru, Jeremy, Sonia, Violeta, and Tamara.

Declaration

The research presented in this thesis has been carried out in collaboration with C. Anastasiou, A. Banfi, F. Chavez, C. Duhr, A. Lazopoulos, B. Mistlberger, and R. Mueller.

Aspects of parts II and III have been part of the following publications:

- A. Banfi and J. Cancino, *Implications of QCD radiative corrections on high- p_T Higgs searches*, Phys.Lett. **B718** (2012) 499-506, [arXiv:1207.0674]. [1]
- C. Anastasiou, J. Cancino, F. Chavez, C. Duhr, A. Lazopoulos, B. Mistlberger, and R. Mueller, *NNLO QCD corrections to $pp \rightarrow \gamma^* \gamma^*$ in the large N_F limit*, submitted to JHEP, [arXiv:1408.4546]. [2]

Abbreviations

CKM	Cabibbo-Kobayashi-Maskawa
DIS	Deep-inelastic scattering
DGLAP	Dokhshitzer-Gribov-Lipatov-Altarelli-Parisi
DREG	Dimensional regularization
EW	Electroweak
HPL	Harmonic polylogarithm
IBP	Integration-by-parts identity
LHC	Large Hadron Collider
LI	Lorentz-invariance identity
LO	Leading order
MPL	Multiple polylogarithm
$\overline{\text{MS}}$	Modified minimal subtraction
N(N)LO	Next-to-(next-to-)leading order
OS	On-shell
PDF	Parton distribution function
QCD	Quantum chromodynamics
RGE	Renormalization-group equation
SM	Standard Model

Contents

Introduction	1
I Theory and methods	5
1 Particle physics in a nutshell	7
1.1 The Standard Model	7
1.2 Quantum chromodynamics	8
1.3 Electroweak theory	13
2 Calculation tools in perturbation theory	21
2.1 Decay rates and scattering cross sections	21
2.2 Phase space	22
2.3 Matrix elements	23
2.4 Hadronic cross sections	30
2.5 Jets	33
2.6 Loop integrals I: Reduction to master integrals	35
2.7 Loop integrals II: Computation of master integrals	41
II QCD corrections for WH production	49
3 Introduction	51
4 Higgs decay to bottom quarks	53
4.1 Leading order	53
4.2 Next-to-leading order	54
5 Higgsstrahlung at NLO	63
5.1 Setup	63
5.2 Higgs searches with the fat-jet method	65
5.3 Higgs searches at the LHC with $\sqrt{s} = 8$ TeV	70
6 Conclusion	77

III	QCD corrections for $\gamma^*\gamma^*$ production	79
7	Introduction	81
8	Virtual corrections	83
8.1	Generation	83
8.2	Mapping to topologies	84
8.3	Reduction with AIR	86
8.4	Double-virtual N_f amplitude	88
9	Real corrections	97
9.1	Single real amplitude	97
9.2	Double-real N_f amplitude	101
10	Numerical results	107
10.1	Equal virtualities	108
10.2	Unequal virtualities	111
11	Conclusion	115
	Outlook	117
	Appendices	121
A	Notations and useful formulae	121
B	Coefficients of the master integrals for the N_f-piece of the 2-loop amplitude of $q\bar{q} \rightarrow \gamma^*\gamma^*$	123
	Bibliography	158
	Curriculum vitæ	173

Introduction

The Standard Model of particle physics describes the electromagnetic, weak and strong interactions between matter particles (fermions) through the exchange of messenger particles (bosons). It is formulated as a gauge theory with gauge group $SU(3)_c \times SU(2)_L \times U(1)_Y$ with color, weak isospin and hypercharge as respective associated charges. It has been progressively formulated in the second half of the 20th century and is up to now one of the most precisely tested theories; its last missing piece having recently been discovered.

The strong part of the interaction is mediated by gluons which are colored and can thus interact among themselves. This part of the gauge group is not spontaneously broken and gluons are massless. Due to confinement, no colored particle is observed directly and partons (quarks and gluons) always hadronize in mesons and baryons yielding a typical jet structure in the detector. The strong interaction is not directly observable in our everyday life but it is responsible for the existence of nucleons (protons and neutrons) and nuclei (through residual nuclear interactions).

The electroweak part is spontaneously broken to $U(1)_{em}$ which corresponds to the usual electromagnetic interaction mediated by the massless photon and described by quantum electrodynamics (QED). The broken degrees are observed as massive W and Z bosons observed for the first time by the UA1 and UA2 experiments at the SPS collider (CERN). The massive W bosons manifest themselves in particular through the phenomenon of radioactive decay.

Spontaneous symmetry breaking is achieved by a scalar (spin-0) field acquiring a non-zero vacuum expectation value – measured to be approximately 246 GeV – which generates mass terms in the Lagrangian density. This is the essence of the Brout-Englert-Higgs-Guralnik-Hagen-Kibble mechanism [3–8]. By introducing a Yukawa coupling of the fermions to this scalar field, the vacuum expectation value also gives masses to quarks and leptons. The excitations of this scalar field from its vacuum expectation value should also be observable as a particle: the Higgs boson. In 2012, after many years of research, the ATLAS and CMS collaborations announced that they had observed a new particle at a mass around 125 GeV whose properties are consistent with those of the Higgs boson of the Standard Model [9, 10]. Previously the experiments around the Tevatron at Fermilab and around LEP and the Large Hadron Collider (LHC) at CERN had managed to exclude various mass ranges.

The assessment of the Standard-Model-likeness of the Higgs boson observed at the LHC will rely on careful measurements of its properties, in particular of its coupling to the

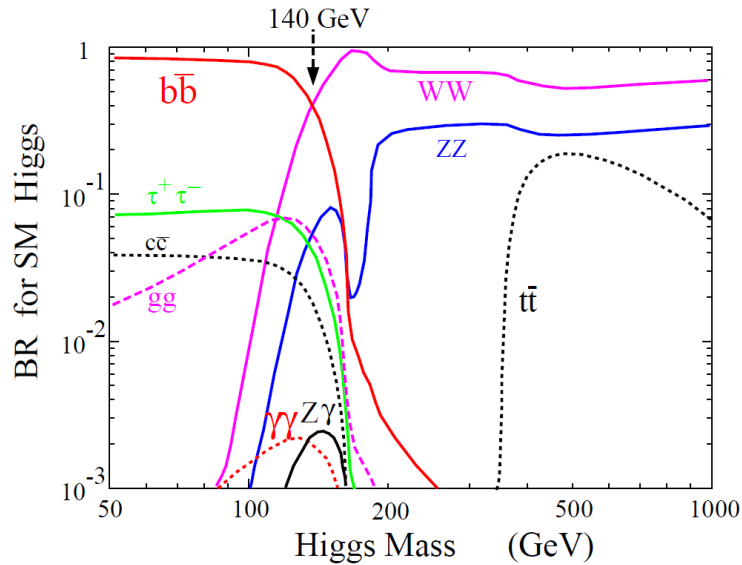


Figure 1: Branching ratios of the decay channels for the Standard-Model Higgs [11].

other elementary Standard Model particles. The branching ratios of the decay channels for the Standard-Model Higgs are shown in figure 1. One sees that the branching ratio for a decay into bottom quarks is very large in the case of a 125 GeV Higgs boson, but also that many other decay channels are in principle accessible, allowing to measure the couplings of the Higgs to these other particles. For example, we show in figure 2 the limits from the CMS analysis of different channels in the (κ_V, κ_f) -plane assuming that all couplings to vector bosons are scaled by κ_V and all couplings to fermions are scaled by κ_f .

In the meantime, some decay channels like $H \rightarrow \gamma\gamma$ or $H \rightarrow ZZ^* \rightarrow 4l$ have reached sufficient statistics to allow a discovery claim from them alone [13, 14]. As a showcase example we show the four-lepton mass distribution measured by ATLAS in figure 3 where a clear mass peak over the background is visible around 125 GeV. The study of the channels where the Higgs boson decays to a pair of vector bosons, like $H \rightarrow WW^*, ZZ^*, Z\gamma^*$, have smaller branching ratios, but are in principle easier as one can require the presence of leptons in the final state, which permits to reject unwanted backgrounds efficiently; furthermore the production cross sections partly compensate the lower branching ratios. They require however the careful assessment of the underlying “non-Higgs” initiated diboson production. The observation of the $H \rightarrow b\bar{b}$ channel is however much more challenging, as bottom quarks are produced abundantly at the LHC and overwhelm by many orders of magnitude the tiny signal from Higgs-related physics. Using the so-called Higgsstrahlung process, where the Higgs boson is produced in association with a vector boson, specific observables and kinematical regions can however offer a window into this channel.

Significant progress assessing the properties of the new boson at a hadron collider depends crucially on the capability to make precise predictions for the processes involved in the signal (where the Higgs boson is involved) and the background (where the Higgs

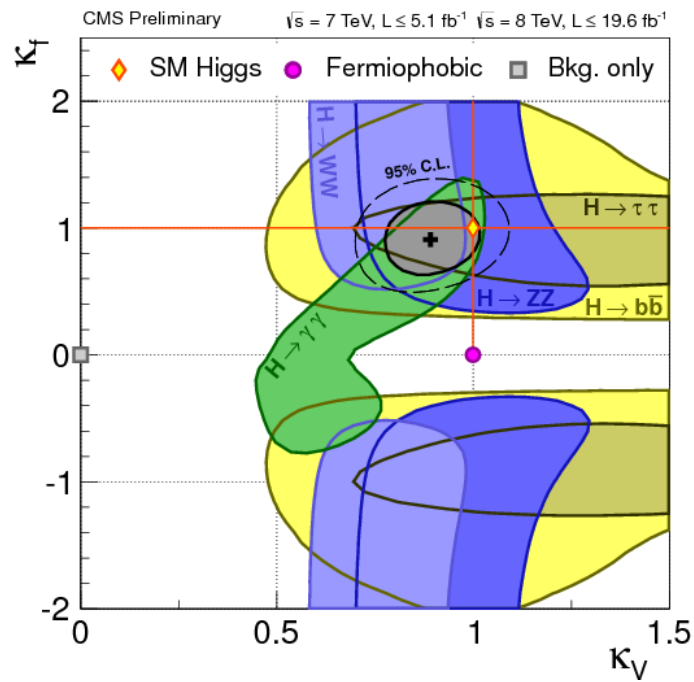


Figure 2: Limits on common vector/fermion strength modifiers for the Higgs couplings [12].

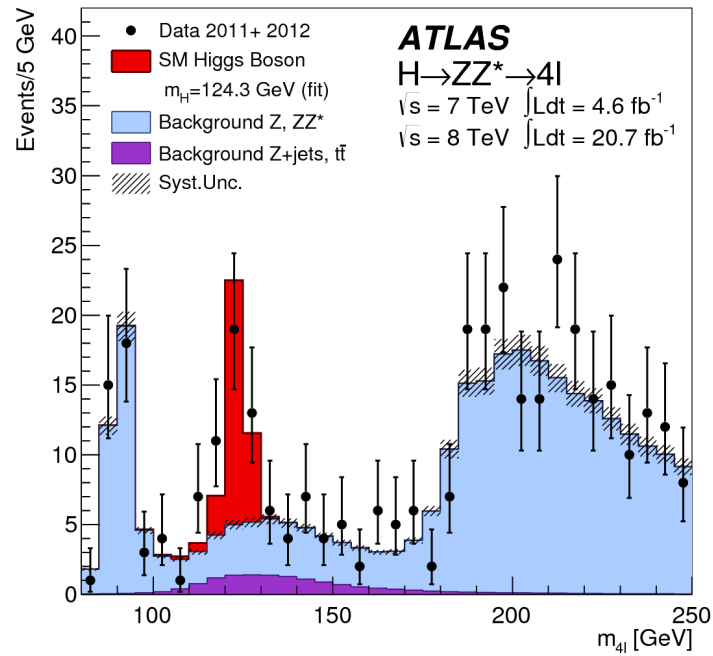


Figure 3: Distribution of the four-lepton invariant mass [13].

boson is absent). As was shown on multiple occasions in the last decades when higher-order corrections from the strong interactions were computed, their size is not negligible and taking them into account significantly improves the theoretical uncertainty. The first step when moving one order higher in the perturbative expansion of a process is to compute the inclusive cross section, i.e. in which we do not choose specific kinematics for the final state. This allows us to make estimates on the number of events to be expected in an experimental setup. In a second time, one usually wishes to perform the same computation differentially, i.e. in which we are able to select at specific kinematics of the final state. It provides a powerful way to select events that have the properties one is looking for, for example by requiring certain cut criteria to be met. The computation of differential cross sections is a highly non-trivial task as we need to consistently handle the divergences arising in the perturbative expansion and ensure their cancellation order-by-order to yield a finite result.

Of course, the completion of the spectrum of the Standard Model is only one of the many endeavors of high-energy physicists. It might be that experiments announce the observation of a discrepancy between the measurement and the prediction from the Standard Model tomorrow, but this is only possible if the theoretical predictions reach a high-enough level of precision.

We will not touch upon the wealth of models beyond the Standard Model that are on the market. In order to perform predictions that are experimentally testable one needs to compute the Standard Model “background” to these processes, which is yet another motivation to perform precise higher-order computations in particle physics.

This thesis is structured as follows: In part I we set up the framework of the Standard Model (chapter 1) and present the methods of perturbation theory used in this thesis (chapter 2). Part II presents the phenomenological discussion of the decay $H \rightarrow b\bar{b}$ for the Higgsstrahlung process when next-to-leading order perturbative corrections from quantum chromodynamics to decay (chapter 4) as well as production (chapter 5) are considered at a fully differential level. The third and last part focuses on the computation of the differential next-to-next-to-leading perturbative quantum chromodynamics corrections for the production of a pair of off-shell photons with different virtualities. We first tackle the double-virtual part (chapter 8) in the general case before specializing to the part proportional to the number of light quark flavors and handling the double-real contribution (chapter 9) and we present numerical distributions of interest obtained from their implementation (chapter 10). Parts II and III have their own introduction and conclusion chapters and we will present the outlook at the end of the thesis.

Part I
Theory and methods

Chapter 1

Particle physics in a nutshell

In this chapter we shall review the relevant features of the Standard Model of particle physics focusing on the elements that are of importance for the results presented in this thesis. It is not meant to be self-contained, but rather is based on multiple sources, which provide a more detailed treatment of the matter [15–21].

1.1 The Standard Model

As collision energies of nuclear physics grew and a zoo of particles started to appear, physicists started to look for organizing patterns in the new particles in the spirit of Mendeleev’s periodic organization of the elements with increasing atomic mass according to their recurrent chemical properties. Soon, it became clear that protons and neutrons are not the elementary building blocks of nature and modern particle physics was born.

Starting as an attempt to bring order in the chaos of the particle zoo, the quest for a description of the fundamental constituents of matter and their interactions at the sub-atomic scale during the second half of the 20th century – culminating with the discovery of the Higgs boson in 2012 – has yielded a coherent description known as the Standard Model of particle physics (SM): matter fields (fermions) interact through vector fields (bosons) that are the expression of a local gauge-symmetry.¹

In this model, matter particles – excitations of fermion fields – are subdivided into quarks and leptons, depending on whether or not they couple to the strong interaction that we shall describe in the next section. They come in three families of increasing mass with each family containing a quark doublet and a lepton doublet, see figure 1.1. All ordinary matter is made out of particles of the first family: as we learned in high school, the proton is made up of two up and one down quarks,² and the neutron is composed of two down and one up quarks. The electrically charged particles from the second and third

¹Note that gravity is not treated in the framework of the SM. There is in fact so far no consistent quantum field theory of gravity.

²As we will see below, this is only part of the composition of the proton. The other components will be relevant when we want to describe proton-(anti)protons collisions (see sections 1.2 and 2.4).

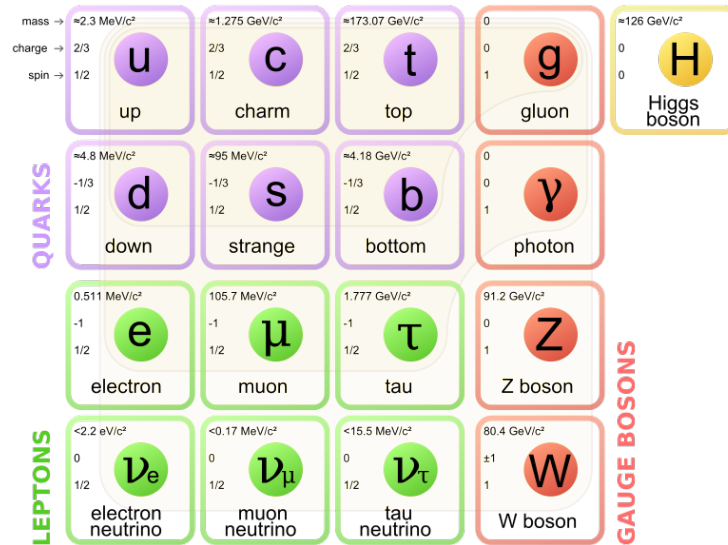


Figure 1.1: Fields of the SM with their respective masses and charges [22].

families decay through the weak interaction to particles of the first family.

While the SM is highly successful to describe most of the phenomenology of high-energy physics, we should remember that it cannot accommodate all of the observed phenomena and that it falls short of yielding a (satisfactory) explanation for some features of nature. Neutrino oscillations, which were confirmed in 2001 [23] and solve the solar neutrino problem, are not possible in the SM *strico sensu*, where neutrinos are exactly massless. The SM also does not explain why there are precisely three families or why the typical scale of gravity lies many orders of magnitude away from the electroweak scale (the hierarchy problem). And we are not even touching on the issue of dark matter and dark energy: according to the interpretation within the standard model of cosmology of the measurement of the homogeneity of the cosmic microwave background, ordinary matter makes up for less than 5% [24, 25] of the total amount of energy in the universe!

To tackle these issues one needs to go beyond the SM with typical examples being supersymmetry and warped extra-dimensions. These models predict the existence of states that can be looked for in collider experiments or that have an indirect effect on measured quantities. It is therefore essential to make precise predictions within the standard model, to be able to make out discrepancies, should there be any. As the saying goes: *“Today’s discovery is tomorrow’s background.”*

We will now present the two complementary components of the SM: quantum chromodynamics and the electroweak theory.

1.2 Quantum chromodynamics

The strong interaction affects only particles with a color charge: quarks and gluons. Quarks were initially proposed independently by Gell-Mann [26] and Zweig [27, 28] as an elegant

way to classify the hadronic states. They were then included in the parton model of the proton which was formulated by Feynman [29] based on the observation of Bjorken scaling [30]. Measurements of the momentum carried by partons in deep-inelastic scattering experiments (lepton-hadron collisions) showed that a substantial amount of momentum was not accounted for and had to be carried by an extra particle that was not interacting through the weak interaction. Gluons – discovered at the end of the 1970’s at DESY – went in to complete the parton model and are none other than the gauge field associated with the color symmetry.

The interaction is described by a Yang-Mills theory [31] for the non-abelian symmetry group $SU(N_c)$, where N_c denotes the number of colors. The coupling is denoted g_s . Quarks come in N_f flavors which are all equivalent for what concerns the strong interaction.³ They are described by spinor fields q_i , where $i = 1, \dots, N_c$ denotes the color index in the fundamental representation. Gluons are described by vector fields A_μ^a , where $a = 1, \dots, N_c^2 - 1$ denotes the color index in the adjoint representation.⁴ We define the field strength tensor and the covariant derivative⁵

$$F_{\mu\nu}^a \equiv \partial_\mu A_\nu^a - \partial_\nu A_\mu^a - g_s f^{abc} A_\mu^b A_\nu^c, \quad D_\mu \equiv \partial_\mu + ig_s T^a A_\mu^a, \quad (1.1)$$

where the f^{abc} ’s are the (totally antisymmetric) structure constants.

The $N_c^2 - 1$ generators of the fundamental representation of $SU(N_c)$ form the basis of a Lie algebra and can be represented by $N_c \times N_c$ matrices⁶ that satisfy the commutation relations

$$[T^a, T^b] = if^{abc} T^c. \quad (1.2)$$

The structure constants are common to all representations of $SU(N_c)$ and in particular define the adjoint representation through the $(N_c^2 - 1) \times (N_c^2 - 1)$ matrices defined entry-wise through

$$(t^a)_{bc} = if^{abc}. \quad (1.3)$$

When computing colored amplitudes one will at some point need to compute the trace of these color matrices. We shall use the most widely used normalization as well as the Casimir invariants for the fundamental and adjoint representations of $SU(N_c)$:

$$\text{Tr}(T^a T^b) = T_F \delta^{ab}, \quad T_F \equiv \frac{1}{2}, \quad (1.4a)$$

$$T^a T^a = C_F, \quad C_F \equiv \frac{N_c^2 - 1}{2N_c} \quad (1.4b)$$

$$t^a t^a = C_A, \quad C_A \equiv N_c. \quad (1.4c)$$

³It is common to designate the N_f flavors as massless, when dealing with QCD and to add the top as an extra flavor, or to consider its effect only within loops. Note that the evolution of PDF to relatively low energy where the mass of the bottom quark has to be taken into account, care needs to be taken as to what “ N_f ” represents.

⁴See reference [32] for a detailed discussion of group theory in the context of particle physics.

⁵As usual, repeated Lorentz and color indices are summed upon.

⁶For $N_c = 3$, the 8 generators are proportional to the Gell-Mann matrices.

We will discuss practical tools for the computation of the color-part of a diagram in section 1.2.2.

Note that in an abelian theory (such as QED, which is the gauge theory of $U(1)$) the field strength tensor does not involve the term which is quadratic in the fields. This implies that the gauge field is not self-interacting, whereas it is in a Yang-Mills theory as we will see below. Another way to see it is that the gluon fields themselves carry a color charge.

We would like to stress that we have allowed ourselves a small abuse of notation in the definition of the covariant derivative: the derivatives are hiding an $N_c \times N_c$ identity matrix, as do the definitions of the Casimir invariants.

With these notations, we can write down the classical Lagrangian density of the theory:

$$\mathcal{L}_{\text{cl.}} = -\frac{1}{4}F_{\mu\nu}^a F^{a,\mu\nu} + \sum_q \bar{q}_i (i\not{D} - m_q) q_i. \quad (1.5a)$$

Unfortunately, the theory is not quantizable in this form. We need to add a gauge-fixing term and Fadeev-Popov ghosts χ^a described by the Lagrangian densities

$$\mathcal{L}_{\text{gauge-fixing}} = -\frac{1}{2\xi} (\partial^\mu A_\mu^a) (\partial^\nu A_\nu^a) \quad (1.5b)$$

$$\mathcal{L}_{\text{ghost}} = \partial^\mu \chi^{a*} (\partial_\mu \delta^{ab} + g_s f^{abc} A_\mu^c) \chi^b. \quad (1.5c)$$

In these terms, ξ is the gauge parameter for the gauge fixing (we chose a covariant gauge fixing) and specific values correspond to the choice of a gauge; this ensures that gluons have only two polarizations, as they are massless spin-1 particles. The ghosts are complex scalar fields that obey fermion statistics. They interact with gluons, but only appear as internal particles (in loop diagrams) and are needed to maintain the gauge invariance.

The complete Lagrangian density $\mathcal{L}_{QCD} = \mathcal{L}_{\text{cl.}} + \mathcal{L}_{\text{gauge-fixing}} + \mathcal{L}_{\text{ghost}}$ can now be quantized allowing us to extract the Feynman rules for QCD that we shall list in the following next section.

To close this section, we would like to comment about confinement and asymptotic freedom, two characteristic features of QCD. Confinement forbids free colored particles. Qualitatively, it can be understood through the fact that the strong interaction grows with distance. Trying to take apart a quark-antiquark pair will result in more and more energy to be stored in the strong field, which at some point will be sufficient to create a quark-antiquark pair from the vacuum and creating again two bound states. When computing low-energy processes, the non-perturbative effects get more and more important, making a perturbative treatment in QCD useless. Fortunately for us, as we will see in section 2.3.1, QCD also exhibits asymptotic freedom – as first pointed out by Gross, Wilczek and Politzer in 1973 [33, 34] – which means that in the high-energy limit the strong coupling becomes vanishingly small. In terms of perturbation theory this means that the higher the energy we work at, the more convergent the perturbative QCD series become.

1.2.1 Feynman rules of quantum chromodynamics

In this section, we list the Feynman rules of QCD in a covariant gauge.

Propagators

$$i \begin{array}{c} \leftarrow p \\ \longrightarrow \end{array} j = \frac{i(\not{p} + m)\delta^{ij}}{p^2 - m^2 + i0} \quad (1.6a)$$

$$\mu, a \begin{array}{c} \leftarrow p \\ \text{oooooo} \end{array} \nu, b = \frac{i\delta^{ab}}{p^2 + i0} \left(-g^{\mu\nu} + (1 - \xi)\frac{p^\mu p^\nu}{p^2} \right) \quad (1.6b)$$

$$a \begin{array}{c} \leftarrow p \\ \text{.....} \end{array} b = \frac{i\delta^{ab}}{p^2 + i0} \quad (1.6c)$$

The $+i0$ specifies which of the poles need to be taken. In the following chapters it will be dropped when there is no doubt possible.

The polarization sum of the gluon is the expression in parenthesis.

The choice $\xi = 1$ is known as Feynman-'t Hooft gauge.

Vertices All momenta are ingoing.

$$\begin{array}{c} \mu, a \\ \text{oooo} \\ \swarrow \quad \searrow \\ i \quad \quad j \end{array} = -ig_s T_{ij}^a \gamma^\mu \quad (1.7a)$$

$$\begin{array}{c} \mu, a \\ \text{oooo} \\ \swarrow \quad \searrow \\ b \quad \quad c \end{array} \begin{array}{c} \leftarrow p \\ \text{.....} \end{array} = -g_s f^{abc} p^\mu \quad (1.7b)$$

$$\begin{array}{c} \mu, a \\ \text{oooo} \\ \swarrow \quad \searrow \\ \nu, b \quad \quad \rho, c \end{array} \begin{array}{c} p_1 \\ \text{oooo} \\ p_2 \quad \quad p_3 \end{array} = -g_s f^{abc} \begin{bmatrix} +g^{\mu\nu}(p_1^\rho - p_2^\rho) \\ +g^{\nu\rho}(p_2^\mu - p_3^\mu) \\ +g^{\rho\mu}(p_3^\nu - p_1^\nu) \end{bmatrix} \quad (1.7c)$$

$$\begin{array}{c} \mu, a \\ \text{oooo} \\ \swarrow \quad \searrow \\ \nu, b \quad \quad \rho, c \end{array} \begin{array}{c} p_1 \\ \text{oooo} \\ p_2 \quad \quad p_3 \\ \text{oooo} \\ p_4 \end{array} = ig_s^2 \begin{bmatrix} +f^{abe} f^{cde}(g^{\mu\rho} g^{\nu\sigma} - g^{\mu\sigma} g^{\nu\rho}) \\ +f^{ace} f^{dbe}(g^{\mu\sigma} g^{\nu\rho} - g^{\mu\nu} g^{\rho\sigma}) \\ +f^{ade} f^{bce}(g^{\mu\nu} g^{\rho\sigma} - g^{\mu\rho} g^{\nu\sigma}) \end{bmatrix} \quad (1.7d)$$

1.2.2 Computation of color factors

We present here a diagrammatic method that can be used to simplify or compute the color-factor of a given amplitude in QCD (we will keep the number of colors general to N_c). In this we follow the presentation made in reference [35]. All computations of cross sections involve squaring a given (sum of) matrix element(s). This will close in particular the color indices so that we need to compute a trace of a product of color matrices, which encodes the information about the color flows. This problem decouples from the rest of the computation as color and Lorentz indices do not talk to each other. The amplitude is then written as a color factor times a “color-free” amplitude. Note however, that this method cannot be applied directly when 4-gluon vertices are present, but one needs to use a trick [35]. This is however not needed for the computations we perform here.

We use the same diagrammatic representation as the one that we interpret with the Feynman rules and use the following rules:

1. All colorless objects as well as the cut of the amplitude are irrelevant and can be dropped.

2. Fundamental (quark) \rightarrow ———, Adjoint (gluon, ghost) \rightarrow ~~~~~

3. Simplify vertices:

$$\begin{array}{c} \text{triangle with wavy top} \\ \hline \end{array} = -\frac{1}{2N_c} \begin{array}{c} \text{triangle with wavy top} \\ \hline \end{array}, \quad \begin{array}{c} \text{triangle with wavy top} \\ \hline \end{array} = \frac{N_c}{2} \begin{array}{c} \text{triangle with wavy top} \\ \hline \end{array}, \quad \begin{array}{c} \text{triangle with wavy top} \\ \hline \end{array} = \frac{C_A}{2} \begin{array}{c} \text{triangle with wavy top} \\ \hline \end{array}.$$

4. Simplify propagators:

$$\begin{array}{c} \text{cloud} \\ \hline \end{array} = C_F \text{———}, \quad \begin{array}{c} \text{circle} \\ \hline \end{array} = \frac{1}{2} \text{~~~~~}, \quad \begin{array}{c} \text{star} \\ \hline \end{array} = C_A \text{~~~~~}.$$

5. Use:

$$\begin{array}{c} \text{circle} \\ \hline \end{array} = 0, \quad \begin{array}{c} \text{circle} \\ \hline \end{array} = N_c, \quad \begin{array}{c} \text{star} \\ \hline \end{array} = N_c^2 - 1.$$

6. Repeat 3 – 5 until it is no longer possible.

The proof of these steps is straightforward when looking at the color part of the Feynman rules of section 1.2.1.

In the next series of equations we work out a simple example following the steps cited above:

$$\left| \begin{array}{c} \text{triangle with wavy top} \\ \hline \end{array} \right|^2 \stackrel{1}{=} \left| \begin{array}{c} \text{triangle with wavy top} \\ \hline \end{array} \right|^2 \stackrel{2}{=} \begin{array}{c} \text{circle with wavy line} \\ \hline \end{array} \stackrel{4}{=} C_F \begin{array}{c} \text{circle} \\ \hline \end{array} \stackrel{5}{=} N_c C_F. \quad (1.8)$$

1.3 Electroweak theory

The formulation of quantum electrodynamics (QED) initiated by Dirac [36] and culminating in the formulation of a gauge theory of the electromagnetic interaction by Tomonaga [37, 38], Schwinger [39], and Feynman [40–42] has had formidable successes in the description of the related phenomenology: theoretical predictions including perturbative corrections agree with experimental measurements to a level of thirteen significant digits!

On the other hand, the β -decay of nuclei, the decay of the muon, as well as the decay of strange hadrons (i.e. hadrons containing strange quarks) were described through Fermi theory [43, 44]. A posteriori, the 4-fermion interactions of this model can be seen as the low energy limit of the electroweak (EW) interaction, where the W-boson exchange is not “resolved”.

The EW theory is a Yang-Mills theory based on the gauge group $SU(2) \times U(1)$. Glashow formulated the theory in 1961 [45]; while Salam [46] and Weinberg [47] independently applied the idea of spontaneous symmetry breaking to it. Fermions have now two types of charges: weak isospin, that couples to the gauge boson $W_\mu^i, i = 1, 2, 3$ with coupling g and hypercharge that couples to the gauge boson B_μ with coupling g' . Note that due to the V-A structure of the weak interaction, only left-handed fermions couple to the $W^{i\mu}$'s, while right-handed fermions only interact through B^μ . The covariant derivative is

$$D_\mu \equiv \partial_\mu - ig \frac{1}{2} \tau_i W_\mu^i - ig' \frac{Y}{2} B_\mu, \quad (1.9)$$

where τ_i denotes the Pauli matrices and Y is the hypercharge. We would like to stress that we have allowed ourselves a small abuse of notation in the definition of the covariant derivative: the derivatives and B_μ are hiding a 2×2 identity matrix.

The couplings g , g' and e (from QED) are actually in relation to each other:

$$e = g \sin \theta_W = g' \cos \theta_W, \quad (1.10)$$

where θ_W is called the weak mixing angle. Any two of the parameters is sufficient to parametrize the interaction, but the usual choice is e or g and the weak mixing angle θ_W . This relation shows that the weak interaction is not really weak, but has a coupling of the same order as the electromagnetic interaction. What makes it “weak” is the mass of the associated gauge bosons.

If it were to stick to this form, this model would have serious flaws to be phenomenologically meaningful:

1. Due to the requirement of gauge invariance, we cannot write mass terms for the gauge bosons.
2. Since left-handed fermions transform as a doublet under $SU(2)$ whilst right-handed fermions transform as two singlets it is also forbidden to write a mass term for them.

These problems are solved by the implementation of a mechanism that spontaneously breaks the symmetry that we shall present in the next section.

To conclude this section we would like to make a last remark which is of importance when implementing event generators for electroweak processes (as we will do in chapter 5). Mass eigenstates and weak eigenstates are not exactly aligned and are related through the Cabibbo-Kobayashi-Maskawa (CKM) matrix. It borrows its name from Cabibbo, who formulated the idea for two families [48], as well as Kobayashi and Maskawa, who extended the idea to three families [49]. An interesting fact is that with three families, there is room for CP violation in the SM, which is not the case if only two families exist. The violation of CP has been shown to happen experimentally. For our purposes however, the two-family formulation is sufficient as the top quark is not present in the proton. One only needs to remember that the process $u\bar{d} \rightarrow W^+$ and $c\bar{s} \rightarrow W^+$ should come with a weighting factor 0.975 while the process $u\bar{s} \rightarrow W^+$ and $c\bar{d} \rightarrow W^+$ with a weighting factor 0.222.

1.3.1 The Higgs mechanism

We will now present the mechanism that is used in the SM to break the $SU(2) \times U(1)$ symmetry, the celebrated *Higgs mechanism*. The mechanism is also known under the longer name Brout-Englert-Higgs-Guralnik-Hagen-Kibble mechanism, as all these authors independently came to similar conclusions around the same time [3–8].

The field content (quarks, leptons and the four gauge bosons) are supplemented with four real scalar fields in the form of an isospin doublet with hypercharge $Y = +1$,

$$\varphi \equiv \begin{pmatrix} \varphi^+ \\ \varphi^0 \end{pmatrix} = \frac{1}{\sqrt{2}} \begin{pmatrix} \varphi_1 + i\varphi_2 \\ \varphi_3 + i\varphi_4 \end{pmatrix}, \quad (1.11)$$

with Lagrangian density

$$\mathcal{L}_{\text{Higgs}} = (iD^\mu\varphi)^\dagger(iD_\mu\varphi) - V(\varphi), \quad (1.12)$$

where $V(\varphi)$ is the Higgs potential,

$$V(\varphi) = \mu^2\varphi^\dagger\varphi + \lambda(\varphi^\dagger\varphi)^2. \quad (1.13)$$

When $\mu^2 > 0$, the potential has a minimum in the origin and the symmetry is not broken. However, if for some reason $\mu^2 < 0$ (while $\lambda > 0$), the potential develops a minimum at

$$\varphi^\dagger\varphi = -\frac{\mu^2}{\lambda}, \quad (1.14)$$

and the field takes up a finite vacuum expectation value. Any choice of φ satisfying equation (1.14) will break $SU(2) \times U(1)$, but since we want to keep the photon massless the vacuum expectation value should have no electric charge, so we choose:

$$\varphi_0 = \frac{1}{\sqrt{2}} \begin{pmatrix} 0 \\ v \end{pmatrix}. \quad (1.15)$$

Inserting φ_0 in the covariant derivative of equation (1.12) and defining the fields

$$W_\mu^\pm \equiv \frac{W_\mu^1 \mp W_\mu^2}{\sqrt{2}} \quad Z_\mu \equiv \frac{gW_\mu^3 - g'B_\mu}{\sqrt{g^2 + g'^2}} \quad A_\mu \equiv \frac{gW_\mu^3 + g'B_\mu}{\sqrt{g^2 + g'^2}}, \quad (1.16a)$$

we can read out the masses of the fields:

$$m_W = \frac{1}{2}vg, \quad m_Z = \frac{1}{2}v\sqrt{g^2 + g'^2}, \quad m_A = 0. \quad (1.17)$$

We see that the photon remains massless while the other gauge bosons get a mass. It is also possible to obtain the relation

$$\frac{m_W}{m_Z} = \cos \theta_W. \quad (1.18)$$

As a last step, we reexpand the Higgs field around its vacuum expectation value via

$$\varphi(x) = \frac{1}{\sqrt{2}} \begin{pmatrix} 0 \\ v + H(x) \end{pmatrix}. \quad (1.19)$$

This describes a scalar boson H with self interactions and a mass

$$m_H = v\sqrt{2\lambda}. \quad (1.20)$$

Formally speaking, the breaking⁷ of $SU(2) \times U(1) \rightarrow U(1)$ generates four (massless) Nambu-Goldstone bosons [50, 51]. Three of these are absorbed in a redefinition of the three massive vector fields – as their third polarization – while the last one remains free as the photon stays massless, and remains in the spectrum as the Higgs boson. This observation was made by Higgs which lent his name to the postulated new particle and so began the long quest for the Higgs boson. In July 2012 the ATLAS and CMS collaborations at CERN announced the discovery of a new boson whose properties match those of the SM Higgs boson. Following this discovery, Englert and Higgs were jointly awarded the physics Nobel prize in 2013.

To end this section, we present how the Higgs field can be recycled to give a mass to the fermions, thus solving the second problem cited above. In the following we denote the component of a left-handed doublet with the highest (lowest) third component of the weak isospin U (D). This can be repeated for each family of quarks and leptons. The Higgs field is a isospin doublet and thus

$$\mathcal{L}_{\text{Yukawa}}^D = y_D \left[\overline{\begin{pmatrix} U_L \\ D_L \end{pmatrix}} \varphi D_R + \bar{D}_R \bar{\varphi} \begin{pmatrix} U_L \\ D_L \end{pmatrix} \right] \quad (1.21)$$

is an $SU(2)$ singlet and can be added to the Lagrangian density. When substituting 1.19 will give a mass term and interactions only for the component with the lowest isospin.

⁷Note that the $U(1)$ before the spontaneous symmetry breaking is associated to the hypercharge, whereas the $U(1)$ remaining afterwards is associated to the electric charge.

In general, we would be forced to include another Higgs field to give mass to the other fermions. In the case of $SU(2)$ however this can be achieved with the charge conjugate of the Higgs field:

$$\varphi^c \equiv i\tau_2\varphi^\dagger \quad (1.22)$$

using the term

$$\mathcal{L}_{\text{Yukawa}}^U = y_U \left[\overline{\begin{pmatrix} U_L \\ D_L \end{pmatrix}} \varphi^c U_R + \bar{U}_R \overline{\varphi^c} \begin{pmatrix} U_L \\ D_L \end{pmatrix} \right] \quad (1.23)$$

For a fermion f , we get the relation⁸

$$m_f = \frac{y_f v}{\sqrt{2}}. \quad (1.24)$$

The expansion (1.19) allows us to extract the coupling strengths of the Higgs boson to the vector bosons (equation (1.12)) and fermions (equations (1.21) and (1.23)). We will list them along with the other Feynman rules for the EW theory.

While the vacuum expectation value of the Higgs field allows us thus to give mass terms to the quarks and leptons, besides the W and Z bosons, the Higgs boson fulfills another important role within the SM. Should we compute the scattering amplitude of $W^+W^- \rightarrow W^+W^-$ in the absence of a Higgs boson, which would then consist of s - and t -channel exchange of a photon or a Z boson as well as the 4-W boson vertex, we would find that it grows indefinitely as we take the limit $s \rightarrow \infty$, thus destroying perturbative unitarity. Adding the diagrams where a Higgs boson is exchanged, with the specific couplings dictated by the EW theory, solves this problem and restores perturbative unitarity.

1.3.2 Feynman rules of the electroweak interaction

We will only state the Feynman rules that we will make use of in our computations. For a complete list of the Feynman rules, see for instance reference [16].

Propagators

$$\begin{array}{c} \leftarrow p \\ \text{---} \\ f \end{array} = \frac{i(\not{p} + m_f)}{p^2 - m_f^2 + i0} \quad (1.25a)$$

$$\begin{array}{c} \leftarrow p \\ \text{~~~~} \\ \gamma \end{array} \mu \nu = \frac{i}{p^2 + i0} \left(-g^{\mu\nu} + (1 - \xi) \frac{p^\mu p^\nu}{p^2} \right) \quad (1.25b)$$

$$\begin{array}{c} \leftarrow p \\ \text{~~~~} \\ Z \end{array} \mu \nu = \frac{i}{p^2 - m_Z^2 + i0} \left(-g^{\mu\nu} + (1 - \xi) \frac{p^\mu p^\nu}{p^2 - \xi m_Z^2} \right) \quad (1.25c)$$

$$\begin{array}{c} \leftarrow p \\ \text{~~~~} \\ W \end{array} \mu \nu = \frac{i}{p^2 - m_W^2 + i0} \left(-g^{\mu\nu} + (1 - \xi) \frac{p^\mu p^\nu}{p^2 - \xi m_W^2} \right) \quad (1.25d)$$

⁸Note that the normalization of the Yukawa coupling can be chosen differently!

$$\text{---} \xleftarrow{p} \text{---} = \frac{i}{p^2 - m_H^2 + i0} \quad (1.25e)$$

The $+i0$ specifies which of the poles need to be taken. In the following chapters it will be dropped when there is no doubt possible.

The polarization sum of each of the vector boson types are the parenthesis of the respective propagator.

The choice $\xi = 1$ is known as Feynman-'t Hooft gauge.

Vertices

$$\begin{array}{c} \mu \\ \gamma \\ \text{---} \\ \text{---} \end{array} = -ieq_f \gamma^\mu \quad (1.26a)$$

$$\begin{array}{c} \mu \\ Z \\ \text{---} \\ \text{---} \end{array} = -\frac{ig}{\cos \theta_W} \gamma^\mu \frac{1}{2} (c_V^f - c_A^f \gamma_5) \quad (1.26b)$$

$$\begin{array}{c} \mu \\ W \\ \text{---} \\ \text{---} \end{array} = -\frac{ig}{\sqrt{2}} \gamma^\mu \frac{1}{2} (1 - \gamma_5) V_{ff'} \quad (1.26c)$$

$$\begin{array}{c} \text{---} \\ \text{---} \\ \text{---} \end{array} = -i \frac{m_f}{v} \quad (1.26d)$$

$$\begin{array}{c} \text{---} \\ Z \\ \text{---} \end{array} = \frac{igm_Z}{\cos \theta_W} g^{\mu\nu} \quad (1.26e)$$

$$\begin{array}{c} \text{---} \\ W \\ \text{---} \end{array} = igm_W g^{\mu\nu}. \quad (1.26f)$$

In the last couple of equations, we have flavor-dependent constants. For the photon and the Z boson vertices, they are listed in table 1.1. For the W boson vertex, f and f' must have a charge difference of 1. Furthermore, if they are leptons $V_{ff'} \equiv 1$, while if they are quarks, $V_{ff'}$ is the corresponding CKM matrix element.

f	q_f	c_V^f	c_A^f
ν_e, ν_μ, ν_τ	0	$+\frac{1}{2}$	$+\frac{1}{2}$
e, μ, τ	-1	$-\frac{1}{2}$	$-\frac{1}{2} + 2 \sin^2 \theta_W$
u, c, t	$+\frac{2}{3}$	$+\frac{1}{2}$	$+\frac{1}{2} - \frac{4}{3} \sin^2 \theta_W$
d, s, b	$-\frac{1}{3}$	$-\frac{1}{2}$	$-\frac{1}{2} + \frac{2}{3} \sin^2 \theta_W$

Table 1.1: Constants involved in the Feynman rules of the EW theory. Antiparticles have the opposite values.

1.3.3 Treatment of γ_5

When dealing with the EW interaction, we will be confronted with the issue of using γ_5 in a way which is consistent with dimensional regularization (DREG). We will present shortly what options are available.

In four dimensions, we are used to γ_5 having two main properties:

1. Anticommutativity: $\{\gamma_5, \gamma^\mu\} \equiv \gamma_5 \gamma^\mu + \gamma^\mu \gamma_5 = 0$ for $\mu = 0, 1, 2, 3$.
2. Trace property: $\text{Tr}(\gamma^\mu \gamma^\nu \gamma^\rho \gamma^\sigma \gamma_5) = 4i \varepsilon^{\mu\nu\rho\sigma}$, where $\varepsilon^{\mu\nu\rho\sigma}$ is the totally antisymmetric Levi-Civita tensor with $\varepsilon^{0123} = +1$.

When going to $d \neq 4$ dimensions, using the cyclicity of the trace and property 1, we get the equation

$$(d-4)\text{Tr}(\gamma^\mu \gamma^\nu \gamma^\rho \gamma^\sigma \gamma_5) = 0, \quad (1.27)$$

which implies that the trace must vanish identically, contradicting property 2.

There are two options to solve it and they are equivalent in their results that we shall now present briefly together with their advantages and caveats.

't Hooft-Veltman prescription The most straightforward approach consists in giving up completely the anticommutativity and keep instead the trace property. It was first suggested by 't Hooft and Veltman [52], and equivalent to defining projectors to split the space-time in 4 and $(d-4)$ parts [53].

First, we need to make sure that the Feynman rules are written in a form that is slightly more symmetrical by replacing the axial-vector coupling

$$\gamma^\mu \gamma_5 \mapsto \frac{1}{2} (\gamma^\mu \gamma_5 - \gamma_5 \gamma^\mu). \quad (1.28)$$

Then, we replace each occurrence of γ_5 through

$$\gamma_5 \mapsto \frac{i}{4!} \varepsilon^{\mu\nu\rho\sigma} \gamma_\mu \gamma_\nu \gamma_\rho \gamma_\sigma, \quad (1.29)$$

where the indices associated with the Levi-Civita tensor are then restricted to 4 dimensions.

This procedure is quite straightforward and easy to implement, but it involves the computation of a lot of traces, and is not really practicable for processes that are not particularly simple.

Larin prescription Another approach proposed by Larin [54] makes the computation more efficient and allows to anticommute γ_5 .

First, one anticommutes γ_5 and uses $\gamma_5^2 = 1$ until it occurs only once per trace.

Then, one uses the replacement

$$\gamma^\mu \gamma_5 \mapsto \frac{i}{3!} \varepsilon^{\mu\nu\rho\sigma} \gamma_\nu \gamma_\rho \gamma_\sigma, \quad (1.30)$$

for the axial-vector coupling.

This leads to much less traces to be evaluated than with the 't Hooft-Veltman prescription. The price to pay is that one needs to take into account a finite renormalization constant Z_5 that depends on the exact vertex under consideration: pseudoscalar (that we are not concerned with), axial-vector non-singlet (as in the case of W bosons which is flavor-changing), or axial-vector singlet (as in the case of the Z boson, which is not flavor-changing).

Chapter 2

Calculation tools in perturbation theory

In this chapter we summarize the main theoretical tools that will be used in this thesis and give some examples when relevant.

2.1 Decay rates and scattering cross sections

The computation of decay rates and scattering cross sections in perturbation theory requires the consideration of both the kinematics of the process under study as well as its dynamics. The former is embodied in the phase-space $d\Phi$ of the process which parametrizes the allowed configurations of the final state which be elaborated upon in section 2.2 and the flux factor from the initial state. The latter consists of the squared sum of the matrix elements of all the subprocesses \mathcal{M}_i participating to the process at the perturbative order under consideration that we will detail upon in section 2.3.

For a $A \rightarrow 1 + \dots + n$ differential decay rate, we have

$$d\Gamma_{A \rightarrow 1 + \dots + n} = \frac{1}{2m_A} d\Phi_n(A \rightarrow 1 + \dots + n) \overline{|\mathcal{M}_{A \rightarrow 1 + \dots + n}|^2}, \quad (2.1)$$

where A denotes the initial state which consists of just the decaying particle with mass m_A while $1 + \dots + n$ denotes the whole n -particle final state. The (semi-)inclusive decay rate $\Gamma_{A \rightarrow 1 + \dots + n}$ is obtained by integrating the differential decay rate over (part of) the phase space. The total decay rate of a particle is simply the sum of the inclusive partial rates:

$$\Gamma_A = \sum_F \Gamma_{A \rightarrow F}, \quad (2.2)$$

where the sum runs over all allowed final states (with any number of particles). A final state is allowed if it has the same overall quantum numbers as A and it is kinematically allowed. For example, the decay rate of the top quark contains the decay channel $t \rightarrow W^+ b$

whereas the decay rate of the W^+ boson does not contain the channel $W^+ \rightarrow t\bar{b}$ because $m_t > m_W + m_b$.

We will mostly consider $A + B \rightarrow 1 + \dots + n$ differential scattering cross sections which take the form

$$d\sigma_{A+B \rightarrow 1+\dots+n} = \frac{1}{F} d\Phi_n(A + B \rightarrow 1 + \dots + n) \overline{|\mathcal{M}_{A+B \rightarrow 1+\dots+n}|^2}, \quad (2.3)$$

where $F \equiv 4\sqrt{(p_A \cdot p_B)^2 - m_A^2 m_B^2}$ is the collinear flux factor. Again the (semi-)inclusive cross section $\sigma_{A+B \rightarrow 1+\dots+n}$ is obtained by integrating the differential cross section over (part of) the phase space.

In both cases $\overline{|\mathcal{M}|^2}$ means that we have summed over the final-state spins/helicities and colors and averaged over the initial-state spins/helicities and colors.

2.2 Phase space

The phase space constrains the final-state particles of a process to be on-shell with positive energy, i.e. to fulfill $p_i^2 = m_i^2$, and ensures the conservation of the overall momentum [55]:

$$d\Phi_n(I \rightarrow 1 + \dots + n) = \left[\prod_{i=1}^n \frac{d^d p_i}{(2\pi)^d} (2\pi) \delta^{(+)}(p_i^2 - m_i^2) \right] (2\pi)^d \delta^{(d)} \left(p_I - \sum_{i=1}^n p_i \right), \quad (2.4)$$

where I denotes the total initial state and the ‘(+)’ superscript means that we only use the positive-energy solution of $p_i^2 = m_i^2$.

Note that we chose to directly work in $d = 4 - 2\varepsilon$ dimensions instead of 4 as we will use dimensional regularization (see the next section).

2.2.1 Phase-space decomposition

Multi-particle phase-space integrals become increasingly difficult to parametrize as the number of particle grows. Fortunately it is possible to organize the computation of the phase space in such a way that a phase space is broken down as a product of phase spaces with lower multiplicity [55].

This can be achieved in many different ways and they do not need to reflect the actual kinematics of the internal particles. The most illuminating example is the decomposition of the general n -particle phase space through

$$d\Phi_n(I \rightarrow 1 + \dots + n) = \int_{Q_-^2}^{Q_+^2} \frac{dQ^2}{2\pi} d\Phi_{n-1}(I \rightarrow 1 + \dots + (n-2) + Q) \times \\ \times d\Phi_2(Q \rightarrow (n-1) + n), \quad (2.5)$$

where the integration limits Q_{\pm}^2 are obtained through the kinematics of the remaining process, which can be thought of (up to the factor of 2π) as a concatenation of the production of $n - 2$ particles along with a particle of mass $\sqrt{Q^2}$ which subsequently ‘decays’ to two particles.

Using this decomposition recursively together with the phase space volume for the decay of a particle of mass M into 2 massive particles of mass m_1 and m_2 ,

$$\Phi_2(M; m_1, m_2) = \frac{2^{10-4d}(\sqrt{\pi})^{3-d}}{\Gamma((d-1)/2)} \left(\sqrt{\beta_1^4 + \beta_2^4 + 8\beta_1^2 + 8\beta_2^2 - 2\beta_1^2\beta_2^2} \right)^{d-3} M^{d-4}, \quad (2.6)$$

where we defined $\beta_i \equiv \sqrt{1 - 4m_i^2/M^2}$, it is *in principle* possible to compute the volume of any n -particle phase space. This provides a way to check the implementation of a parametrization of the phase space. In particular, the volume of the phase space for the decay of a particle of mass M into n massless particles is [56]

$$\Phi_n(M; \underbrace{0, \dots, 0}_n) = \frac{2^{1+d-dn}(\sqrt{\pi})^{2+d-dn}\Gamma(d/2-1)^n}{\Gamma((d/2-1)(n-1))\Gamma((d/2-1)n)} M^{-d+(d-2)n}.$$

2.3 Matrix elements

In this section, we shall take a closer look at the specific tools and techniques related to matrix elements.

Matrix elements are expressed as Feynman diagrams [57], which stand for their mathematical expressions and are interpreted using the specific Feynman rules¹ of the process (see sections 1.2.1 and 1.3.2). Computations using Feynman diagrams are representing a perturbative expansion in a small parameter. In the case of QED, the parameter is

$$\alpha \equiv \frac{e^2}{4\pi} \sim 10^{-2},$$

while in QCD the parameter is

$$\alpha_s \equiv \frac{g_s^2}{4\pi} \sim 10^{-1}.$$

Naively speaking, we expect perturbative corrections in QED to be much milder than in QCD because each order added comes with a factor of $\alpha \ll \alpha_s$ (at typical energies).

The computation starts with the leading-order (LO) diagram that is the basic process under consideration. Then when one further power of the coupling constant is present, we speak of a next-to-leading order (NLO) correction; and in general if k powers are present we speak of a N^k LO correction. When going one order higher in perturbation theory, two kind of diagrams will appear: diagrams involving one more loop (virtual), and diagrams involving one more external parton (real). For example, if studying the production of a Z

¹See e.g. reference [58] on the derivation of the Feynman rules for a given Lagrangian density.

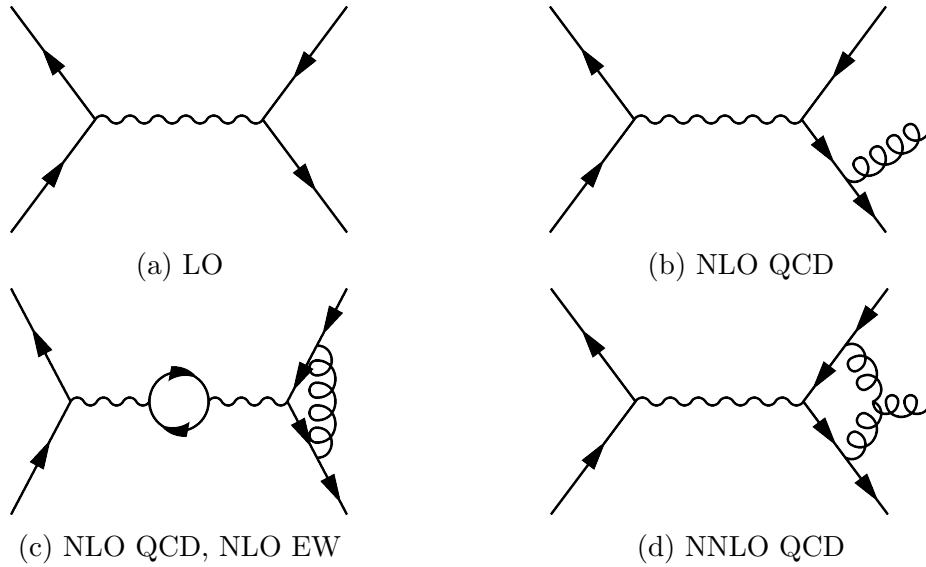


Figure 2.1: Examples of diagrams appearing at various perturbative orders in QCD and EW theory for the process $e^+e^- \rightarrow Z \rightarrow b\bar{b}$.

boson at an e^+e^- -collider and its subsequent decay to a bottom-antibottom pair the diagram shown in figure 2.1a is the LO diagram. When computing the NLO QCD correction to this process, we encounter the real diagram shown in figure 2.1b. Mixed NLO QCD and NLO EW corrections will contain diagrams like the double-virtual one of figure 2.1c. Finally figure 2.1d showcases a typical real-virtual NNLO QCD diagram.

The number of diagrams that one has to evaluate grows very fast as we move to higher orders (see e.g. chapter 8) and one typically has to rely on an automated procedure to generate them. For the computations we have performed we have used the program **QGraf** [59] which simply requires the external particles, propagators and vertices as input and gives the diagram together with the momentum flows. It is then possible to turn these into mathematical expressions and perform the usual algebraic manipulations like taking traces of strings of γ -matrices using e.g. **FORM** [60,61].

Unfortunately, starting already at NLO, the expressions are divergent. In the next sections we shall illustrate how this arises and how these divergences are taken care of.

2.3.1 Ultraviolet divergences and renormalization

The first kind of divergences that we encounter are characteristic of loop integrals and are called ultraviolet (UV) because they appear when the momentum in the loop becomes large. Let us see it appear for a simple loop integral – the (massless) bubble shown in figure 2.2. Performing a Wick rotation of the momenta to make them Euclidean

$$k_E^0 = ik^0 \Rightarrow d^4k = id^4k_E, k^2 = -k_E^2, \quad (2.7)$$

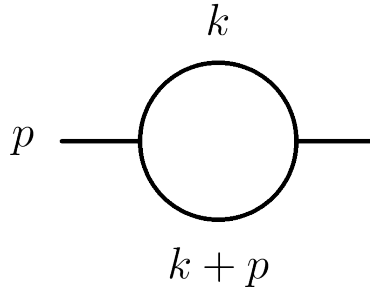


Figure 2.2: Massless scalar bubble.

and looking at the integrand in the limit $|k_E| \rightarrow \infty$, which means we can ignore the external momentum p , we get

$$\int \frac{d^4k}{(4\pi)^4} \frac{1}{k^2(k+p)^2} \sim \int_0^\infty \frac{d|k_E|}{|k_E|} \quad (2.8)$$

which diverges. In order to quantify the divergence we need to introduce a regulator. The most straightforward option is to introduce a cut-off Λ for the magnitude of the loop momentum, i.e. integrate up to Λ . In the example above,

$$\int_0^\Lambda \frac{d|k_E|}{|k_E|} = \ln \Lambda, \quad (2.9)$$

and we call the divergence logarithmic.

The main issue of the cutoff-regularization is that it violated the Lorentz invariance of the integral and care has to be taken when interpreting the result. Fortunately, there are other regularization schemes available that do not violate Lorentz invariance. One of them is the Pauli-Villars regularization, where massive auxilliary fields are introduced to cancel the divergence [62].

The modern method of predilection that we shall use in this thesis was introduced by 't Hooft and Veltman and is called dimensional regularization (DREG) [52]. In DREG, the dimension of space-time is taken to be $d = 4 - 2\varepsilon$, which means that the contraction of the metric tensor is now

$$g^\mu{}_\mu = d. \quad (2.10)$$

Using this, one is able to compute the modified traces of γ -matrices. The divergences are now appearing as poles in ε . We shall stick to conventional DREG, where the trace of the identity matrix is 4, the number of spin states of fermions is 2, massless gauge bosons have $d - 2$ helicities, and massive ones have $d - 1$. Phase-spaces (section 2.2) and external

momenta are also taken in d dimensions. For the example cited above²

$$\int \frac{d^d k}{(4\pi)^d} \frac{1}{k^2(k+p)^2} = \Gamma(\varepsilon) f(p^2, \varepsilon), \quad (2.11)$$

where $f(p^2, \varepsilon)$ is finite at $\varepsilon = 0$. The Laurent series of the Γ -function shows a pole in ε .

The modification of the dimension will affect the (mass) dimension of the fields as we want to keep the action $S = \int d^d x \mathcal{L}$ dimensionless. It is then easy to see from the kinetic terms that fermions and vector bosons will have dimension $(d-1)/2$ and $(d-2)/2$ respectively. In order to keep the gauge coupling dimensionless we need to introduce a scale via the substitution

$$g \rightarrow g\mu^\varepsilon. \quad (2.12)$$

This scale will be relevant when we perform renormalization [63].

We have now regularized our matrix elements dimensionally and we can proceed with the renormalization program. For a thorough treatment of the renormalization, the reader is invited to consult references [21, 53].

The 1-loop bubble presented above will come multiplied by a coupling $g^2\mu^{2\varepsilon}$ as an (infinite) contribution to that of the normal propagator.³ All we need to do is to find a consistent way to remove this infinity. This is achieved by adding a counterterm to the Lagrangian density of the theory under consideration, which exhibits the same pole structure as the dressed propagator with opposite sign when interpreted with the Feynman rules, such that the addition of both of them will have no poles left. This needs to be achieved for all the propagators and vertices of the theory that exhibit divergences.

The Lagrangian density \mathcal{L} – such as the QCD Lagrangian density (1.5) – can then be expressed via the bare fields,

$$q^b = \sqrt{Z_q} q, \quad A_\mu^b = \sqrt{Z_A} A_\mu, \quad \chi^b = \sqrt{Z_\chi} \chi, \quad (2.13)$$

and the bare parameters,

$$m_q^b = Z_{m_q} m_q, \quad \xi^b = Z_A \xi, \quad g_s^b = Z_g g_s \mu^\varepsilon. \quad (2.14)$$

In fact, each vertex, such as the gluon-ghost-ghost or the 4-gluon vertex could be renormalized independently, this would spoil the gauge invariance and in turn destroy the Slavnov-Taylor identities [64, 65], the equivalent of the Ward identities for non-abelian theories.

The pole structure of the renormalization constants Z_i is dictated by the poles we need to remove. The choice of the finite part is not crucially important (as long as it is done

²The steps of the calculation involve Feynman parameters which we will present in section 2.7.2 and properties listed in the appendix A. This integral actually also contains an infrared divergence, but as we will see in the next section, DREG can handle both.

³Both of them are combined to give by summing the geometric series of 1-particle irreducible diagrams and give the dressed propagator at 1-loop [17, 21, 53].

in such a way that the Slavnov-Taylor identities are preserved). Putting no finite part in the renormalization constant (i.e. keeping it to 1) is known as the minimal subtraction (MS) scheme [63]. The most common scheme for massless theories nowadays is the modified minimal subtraction ($\overline{\text{MS}}$) scheme, where along with the pole a universal finite part coming from the loop measure is also included. It consists in making the replacement [66]

$$\mu^2 \rightarrow \frac{e^{\gamma_E}}{4\pi} \mu_R^2. \quad (2.15)$$

When dealing with massive quarks (as we will do in chapter 4), another commonly used renormalization scheme is the on-shell (OS) scheme, which ensures that the pole of the propagator remains at the physical mass $p^2 = m^2$ and has a unit residue.

We will perform the renormalization in detail for the case of the Higgs decay to massive bottom quarks in chapter 4.2.3. For the other processes presented in this thesis, we will not present the renormalization explicitly.

A legitimate question is whether moving to more loops, the same procedure can be applied. This will of course be dependent on the theory we use. For renormalizable theories like the SM [67, 68], we can use the same renormalization constants and just compute them to some higher order in the coupling. A non-renormalizable theory would require the addition of genuinely new counterterms at every order, spoiling the predictive power of the theory.

When dealing with a quantum field theory such as the SM, we are bound to make a perturbative expansion up to some order in the coupling constant. At tree-level, we recover the classic theory with no quantum effects. From 1-loop on, the quantum effects become important. In a heuristic way, the virtual particles in the loop modify the classical behavior to make it quantum. The truncation of the perturbative series has the effect that the higher-order terms, that would be present if we were able to compute the non-perturbative solution, are missing. The renormalization scale μ_R allows us in a way to quantify the “error” that we make by truncating the series: in the later chapter, we will present plots where we vary the renormalization scale around a central value. If the variation is large, the perturbative series is still missing some significant pieces. Going one order higher will in general make the dependence on μ_R milder (the envelope will shrink), showing that the perturbative series is converging.

As the bare coupling does not depend on the renormalization scale, one can write a *renormalization group equation* (RGE) for the strong coupling, which will describe how it depends on μ_R :

$$\frac{da_s}{d \ln \mu_R^2} = a_s \beta(a_s), \quad a_s \equiv \frac{\alpha_s(\mu)}{\pi} \quad (2.16)$$

where we have now taken the limit $d \rightarrow 4$ as the β -function is finite. One usually needs the first coefficient of its expansion in a_s ,

$$\beta(a_s) = -4\pi \sum_{k=0}^{\infty} \beta_k a_s^{k+1}. \quad (2.17)$$

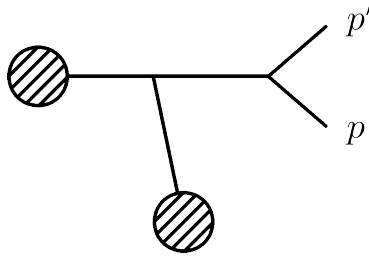


Figure 2.3: Typical presentation of an IR divergence.

As our tree-level diagrams in parts II and III shall not involve the strong coupling constant, even at NNLO we shall only need the first coefficient

$$\beta_0 = \frac{11N_c - 2N_f}{12}. \quad (2.18)$$

Before we close this discussion of renormalization we would like to make a last remark. Retaining only the first term in the expansion of the β -function, we can have the LO running of the coupling between the scales Q_0^2 and Q^2

$$\alpha_s(Q^2) = \frac{\alpha_s(Q_0^2)}{1 + \beta_0 \alpha_s(Q_0^2) \ln \frac{Q^2}{Q_0^2}}. \quad (2.19)$$

In QCD, since $N_f < 17$ and thus $\beta_0 > 0$, the coupling decreases with increasing energy: the theory exhibits asymptotic freedom as first pointed out by Gross, Wilczek and Politzer [33, 34]. This conclusion is not altered by retaining higher-order terms as well. Performing the same kind of analysis on the coupling of QED would show that α increases with energy.

2.3.2 Infrared divergences and subtraction

After renormalization has been performed UV divergences of loop amplitudes (arising when the loop momentum becomes very large) have been taken care of. When the loop momentum becomes very small, or in the case of real emission when a particle becomes unresolvable another type of divergence can occur, which are logically called infrared (IR). We used the word unresolvable for reasons that will become clear shortly.

Let us illustrate the typical IR divergence with the real emission diagram shown in figure 2.3. A particle (unprimed) of mass m emits a massless particle (primed). The blobs denote the rest of the diagram that we are not considering right now. Choosing some reference frame, say the lab frame, this diagram will have a propagator of the form⁴

$$(p + p')^2 - m^2 = 2p \cdot p' = 2EE' (1 - \beta \cos \theta), \quad (2.20)$$

⁴We are deliberately taking a scalar theory as it exposes the feature we want to illustrate. The generalization to a realistic theory like QCD does not alter the feature.

where $\beta \equiv |\vec{p}'|/E$, and θ denotes the opening angle between the momenta p and p' in this reference frame. The IR divergences appear whenever this propagator vanishes, which is the motivation to write it in this factorized form. Since $E^2 = \vec{p}^2 + m^2$, when $m > 0$, we have $E > 0$ and $\beta < 1$ and thus the only way for this propagator to vanish is if $E' = 0$, i.e. the emitted particle is actually “not there” any more. We say that it becomes soft and speak of *soft divergence*. If $m = 0$, $\beta = 1$ and the propagator vanishes if either particles become soft ($E = 0$ or $E' = 0$), or if they become collinear, i.e $\theta = 0$. This type of divergences is called *collinear divergence*. We will come across these divergences at various places in parts II and III.

Once again, we need to introduce a regulator for these divergences. For loop diagrams in the same spirit as in the UV case, we can introduce an infrared cutoff λ , or give massless particles a small mass m' . The usual choice nowadays is however again to regularize using the dimension of space-time $d = 4 - 2\varepsilon$ as for the UV case, and IR divergences appear once again as poles in ε .

Strictly speaking, we should introduce two different regulators $\varepsilon_{UV} > 0$ and $\varepsilon_{IR} < 0$. All poles in ε_{UV} are treated by renormalization, whilst the ε_{IR} poles cancel between the real and virtual contributions. In the following we will however not make a distinction between both regulators. Loop integrals will thus have both UV and IR divergences extracted (section 2.7.2), and only the IR part will remain after renormalization.

We now turn to the treatment of the IR divergences. We will focus on the case of real amplitudes but it can also be applied in the case of virtual amplitudes, see section 8.4.1. Over the years different approaches have been developed for the NLO case: the most common being Catani-Seymour dipole subtraction [69], antenna subtraction [70, 71], and Frixione-Kunszt-Signer subtraction [72]. The antenna approach has been extended to NNLO [73] and can handle radiation off initial state particles too [74].

The approach we will use relies on parametrizing the phase space on the unit hypercube and extract the singularities of factorized parameters with the help of the expansion in +-distributions (see e.g. reference [75]) defined via

$$\frac{1}{x^{1+n\varepsilon}} = -\frac{\delta(x)}{n\varepsilon} + \sum_{k=0}^{\infty} \frac{(-n\varepsilon)^k}{k!} \left[\frac{\ln^k x}{x} \right]_+ \quad (2.21)$$

where the +-distribution is defined via

$$\int_0^1 dx \left[\frac{f(x)}{x} \right]_+ g(x) \equiv \int_0^1 dx \frac{f(x)}{x} (g(x) - g(0)). \quad (2.22)$$

The critical point of this is choosing a parametrization which factorizes *all* the singularities. An integral such as

$$I \equiv \int_0^1 dx dy \frac{x^\varepsilon y^\varepsilon}{(x+y)^2} \quad (2.23)$$

has an overlapping one at $y = x = 0$ (i.e. the integrand is singular only when both variables vanish) so equation (2.21) cannot be used straightforwardly. One way to overcome this difficulty is called sector decomposition [76–78]. We decompose the integration domain into sectors: $I = I_1 + I_2$, such that for I_1 $x > y$ and for I_2 $y > x$ and perform a reparametrization in each integral:

$$I_1 = \int_0^1 dx \int_0^x dy \frac{x^\varepsilon y^\varepsilon}{(x+y)^2} \stackrel{y=zx}{=} \int_0^1 dx \int_0^1 dz \frac{x^{2\varepsilon} z^\varepsilon}{x(1+z)^2} \quad (= I_2). \quad (2.24)$$

The singularities being factorized, it is then possible to use equation (2.21), yielding the result

$$I = \frac{1}{2\varepsilon} - \ln 2 + \mathcal{O}(\varepsilon). \quad (2.25)$$

The main drawback of this method is that when the decomposition has to be performed with many variables, the number of integrals to evaluate explodes.

More recently, another method was developed, called non-linear mappings [79, 80]. It consists in making a non-linear mapping to factorize the singularities avoiding the splitting of the phase space into sectors. Taking the example above, we make the following substitutions:

$$\begin{aligned} I &= \int_0^1 dy \int_0^\infty dz \frac{y^\varepsilon}{(z + (1+z)y)^2} \left(\frac{z}{1+z} \right)^\varepsilon && : x = \frac{z}{1+z} \\ &= \int_0^1 dy \int_0^\infty dw \frac{y^{2\varepsilon}}{y(1+w+wy)^2} \left(\frac{v}{1+vy} \right)^\varepsilon && : z = wy \\ &= \int_0^1 dy \int_0^1 dv \frac{y^{2\varepsilon}}{y(1+yv)^2} \left(\frac{v}{1-v+yv} \right)^\varepsilon && : w = \frac{v}{1-v}, \end{aligned} \quad (2.26)$$

which has now a factorized singularity at $y = 0$ and of course yields the same result as before, but avoiding creating more integrals. Unfortunately finding the “right” transformation is not easy (in this case there is no advantage from using non-linear mappings instead of sector decomposition) and the method requires a significant amount of intuition. The original publication [79] provides many examples worked out in detail.

Although we have presented the method of non-linear mappings in the context of infrared divergences, it can as well be applied in the case of loop integrals, when the integral is represented using Feynman parameters (section 2.7.2) as we will see explicitly in chapter 8.

2.4 Hadronic cross sections

As we will compute cross sections for proton-proton collisions at the LHC, we review here the main elements specific to the presence of hadrons in the initial state.

2.4.1 Factorization and extraction of collinear counterterms

As the proton is not a point-like object but made of quarks, antiquarks, and gluons, we need a way to describe the distribution of momentum among these. This is achieved through parton density functions (PDFs) $f_i(x, \mu_F)$ which quantify the probability of finding a parton i (which can be a quark, an antiquark or a gluon) with a momentum fraction x in the proton. The PDF depends on μ_F , the *factorization scale*, which is introduced to separate the hard process (at small distances) from the soft-collinear process (at long distance): the emission of an extra parton with small transverse momentum $p_T < \mu_F$ is described by the hadron structure and thus the PDF, while if $p_T > \mu_F$ the parton is taken as part of the hard interaction and thus the partonic cross section.

Starting with the non-subtracted partonic cross section $d\hat{\sigma}(s_{12}, \mu_R)$, we introduce the scale μ_F to bring the soft/collinear divergence into the bare PDFs $f_i^b(x)$ in a given factorization scheme. As in the case of renormalization (section 2.3.1), the $\overline{\text{MS}}$ factorization scheme, which we shall stick to, includes only the poles in ε in the bare PDF. On the other hand, the DIS factorization scheme takes also the finite part. The behavior of the cross section in the collinear and soft limits is universal and we only need to compute the splitting kernels describing them once. The splitting process described by the Altarelli-Parisi splitting kernels $P_{ij}(z)$ is the splitting of j in a parton i which takes a momentum fraction z of the momentum of j and a another parton (which is not denoted as it is unambiguous) carrying the remaining fraction $1 - z$. The $\overline{\text{MS}}$ -factorized PDFs can be written

$$f_i(x, \mu_F) = [\Gamma_{ij} \otimes f_j^b](x, \mu_F), \quad (2.27)$$

where the sum over j is implicit and we have used the definition of the convolution of two functions (A.6). The function Γ_{ij} is called collinear counter term and can be expanded in a perturbative series in $a_s \equiv \frac{\alpha_s(\mu_R)}{\pi}$, up to order n ,

$$\Gamma_{ij}(z, \mu_F) = \sum_{k=0}^n a_s^k \left(\frac{\mu_R^2}{\mu_F^2} \right)^{k\varepsilon} \Gamma_{ij}^{(k)}(z) + \mathcal{O}(a_s^{n+1}) \quad (2.28)$$

The first three orders read (see e.g. reference [81]),

$$\Gamma_{ij}^{(0)}(z) = \delta_{ij} \delta(1 - z) \quad (2.29a)$$

$$\Gamma_{ij}^{(1)}(z) = -\frac{1}{\varepsilon} P_{ij}^{(0)}(z) \quad (2.29b)$$

$$\Gamma_{ij}^{(2)}(z) = -\frac{1}{2\varepsilon} P_{ij}^{(1)}(z) + \frac{1}{2\varepsilon^2} \left([P_{ik}^{(0)} \otimes P_{kj}^{(0)}](z) + \beta_0 P_{ij}^{(0)}(z) \right), \quad (2.29c)$$

where β_0 is the first coefficient of the expansion of the QCD β -function (see section 2.3.1 and appendix A) we have used the coefficients of the perturbative expansion of the splitting kernels defined through

$$P_{ij}(z) = \sum_{k=0}^{\infty} a_s^{k+1} P_{ij}^{(k)}(z). \quad (2.30)$$

It is common to take the renormalization scale and the factorization scale to be identical. Keeping them separate allows to derive the evolution of the PDF (see next section) and make estimates for the uncertainty coming from the variation of μ_F .

Note that it is customary to invert equation (2.27) to get the PDF counterterms that cancel with the remaining IR divergences of the cross section (see e.g. [82]),

$$f_i^b(x) = [\Delta_{ij} \otimes f_j](x). \quad (2.31)$$

This is achieved by solving order-by-order in a_s

$$[\Delta_{ij} \otimes \Gamma_{jk}](z) = \delta_{ik} \delta(1-z). \quad (2.32)$$

Expanding Δ_{ij} in a_s (for $\mu_R = \mu_F$)

$$\Delta_{ij}(z) = \sum_{k=0}^n a_s^k \Delta_{ij}^{(k)}(z) + \mathcal{O}(a_s^{n+1}) \quad (2.33)$$

the first three orders read

$$\Delta_{ij}^{(0)}(z) = \delta_{ij} \delta(1-z), \quad (2.34a)$$

$$\Delta_{ij}^{(1)}(z) = \frac{P_{ij}^{(0)}(z)}{2\epsilon}, \quad (2.34b)$$

$$\Delta_{ij}^{(2)}(z) = \frac{1}{2\epsilon} P_{ij}^{(1)}(z) + \frac{1}{2\epsilon^2} \left([P_{ik}^{(0)} \otimes P_{kj}^{(0)}](z) - \beta_0 P_{ij}^{(0)}(z) \right). \quad (2.34c)$$

The validity of the factorization of short- and long-distance effects has been proven for deep-inelastic scattering (DIS) and the Drell-Yan process⁵ [83]. It turns out to be working at a very good level of accuracy for other SM processes.

The hadronic cross section for a process after factorization takes the form

$$d\sigma_{h_1 h_2 \rightarrow X}(s, \mu_R, \mu_F) = \sum_{i,j} \int_0^1 dx_1 dx_2 f_{i/h_1}(x_1, \mu_F) f_{j/h_2}(x_2, \mu_F) d\sigma_{ij \rightarrow X}(s_{12}, \mu_R, \mu_F), \quad (2.35)$$

where the sum indices i, j run over the flavors of the partons in each hadron. The hard partonic cross section $d\sigma_{ij \rightarrow X}$ is evaluated at the center-of-mass energy $s_{12} = x_1 x_2 s$, where $s = (p_{h_1} + p_{h_2})^2$ is the center of mass energy of the two protons. We can compute the partonic process in its center of mass frame, but it is important to remember to boost the momenta back in the lab frame, which moves with momentum $x_1 p_{h_1} + x_2 p_{h_2}$. At the LHC, both hadrons are protons, while at the Tevatron one of them used to be an anti-proton.

⁵Hadron-hadron collision producing a lepton-antilepton pair through Z boson or an off-shell photon γ^* exchange

2.4.2 Evolution and measurement of PDFs

We will now derive the differential equation describing the change of the PDFs depending on the factorization scale in the same spirit as we presented the RGE for the strong coupling constant. As bare PDFs do not depend on μ_F ,

$$\frac{\partial f_i^b(x)}{\partial \ln \mu_F^2} = 0, \quad (2.36)$$

inverting equation (2.27) order by order, we can write the Dokshitzer-Gribov-Lipatov-Altarelli-Parisi (DGLAP) evolution equations, which were derived independently by these authors from either side of the iron curtain [84–86]:

$$\frac{\partial f_i(x, \mu_F)}{\partial \ln \mu_F^2} = [P_{ij} \otimes f_j](x, \mu_F). \quad (2.37)$$

The DGLAP evolution equations thus allow us to know how a change in scale affects the PDFs using the splitting functions that can be computed perturbatively. Heuristically, one can imagine that depending at what “resolution” one looks at the proton, the distribution of momenta between the partons will vary and the proton will look different, and the DGLAP evolution equations tells us how. The solution of this system of integro-differential equations can be achieved order-by-order using Mellin transforms, see e.g. reference [20].

It is possible to extract the PDFs at a high enough scale by comparing cross sections computed at this scale with the data as then we are in the perturbative regime, where the proton can be seen as a bunch of partons that do not interact with each other. DIS experiments on a fixed target or at a lepton-proton collider such as HERA at DESY were the primary sources of data for PDF determination by measuring the scattering for various values of the momentum transfer Q_0 . In order to pin down the gluon PDF, one needs to consider as well processes with a jet in the final state and it is also possible to use hadron-hadron data from e.g. the Tevatron and the LHC. Making a parametrization ansatz that is fitted to a data set taken at a certain value Q_0 one gets the PDFs at this scale $\{f_i(x, Q_0)\}$ that we can then evolve using the DGLAP evolution equations (2.37) to the scale of interest to obtain $\{f_i(x, Q)\}$.

The various collaborations fitting PDFs (MSTW, CTEQ, NNPDF,...) use different parametrizations and different datasets and will thus yield different sets of PDFs. For searches, like the search for the Higgs boson, it is essential to make predictions using different sets in order to obtain a reliable error [87]. Fortunately, the library LHAPDF [88] provides a unified framework for the implementation of event generators involving hadron collisions that can then be run with different sets at different scales.

2.5 Jets

In this section, we shall discuss the treatment of colored particles (partons) in the final state. This applies both to e^+e^- and hadronic initial states, although in the hadronic case

we have the additional possibility of radiation off the initial state partons, and the handling of this issue will thus be more critical. We will come back to this in the context of our analysis of the QCD corrections to the Higgsstrahlung process in chapter 5.

The presence of colored partons⁶ in the final state has two main consequences, which makes crucially important the definition of an object that can be related to the partonic process.

The first is due to the confinement of QCD. A typical final state will involve quarks, leptons, gauge and Higgs bosons, see e.g. figure 2.1, just after the process at some high scale. Going down to lower scales (larger distances) the partons will develop “strings” of color field between them. At some point the energy stored in the field is large enough to produce quark-antiquark pairs out of the vacuum. The confinement of QCD can then get fulfilled as the color charges of the individual partons are cancelled out in the formation of hadrons (mesons made out of a quark and an antiquark, and baryons, that consist of three (anti)quarks). Thus, even a simple partonic process like $e^+e^- \rightarrow q\bar{q}$ will produce a multitude of tracks in a detector, because both quarks will produce a fair share of pions, protons and neutrons. This process is called hadronization and is highly non-perturbative in nature and there are different models for hadronization on the market.

The second is schematically speaking the reverse process of factorization, that we have presented earlier in this section. Owing to their color charge, through which the coupling is enhanced by the associated color factors, partons tend to radiate off other partons, specifically at low relative transverse momentum, which is actually nothing else than the expression of soft/collinear IR divergences we have discussed in section 2.3.2 and lie at the center of parton shower event generators. As the calculations presented in this thesis are done at fixed-order, the main topic of concern is how to deal with the divergences. Fortunately for us Kinoshita, Lee and Nauenberg showed that for observables that are inclusive enough, the SM yields finite results [89,90]. We must thus be able to combine the radiation off the parton at small angle with the corresponding virtual contributions, and the IR divergences will cancel out.

The object which allows both experimentalists and theorists to deal with these features is called a *jet*. The layman definition of a jet would be a collimated spray of particles in a given direction. In practice, many definitions of a jet are available. They all rely on an algorithm which decides how particles will be grouped together to eventually become a jet. Some of these algorithms have only one step, while other recombine particles successively until some criterion is met, but each of them are referred to as a *jet algorithm*.

The first definition of a jet was made by Sterman and Weinberg in 1977 [91]: they defined a jet using two parameters describing the energy fraction deposited in a cone of a given opening angle. In chapter 5, we will make use of the Cambridge/Aachen jet algorithm [92,93], which needs one parameter R , which works as follows:

⁶In fact, leptons and photons exhibit the same behaviour, the only difference being the coupling strength and the absence of enhancing color factor. The effects are however milder, and the implementation of isolation cuts will take out the divergences.

1. Compute the distance

$$\Delta R_{ij} \equiv \sqrt{(y_i - y_j)^2 + (\phi_i - \phi_j)^2}, \quad (2.38)$$

where y_i and ϕ_i denote respectively the rapidity and the azimuthal angle of i , for each pair of partons (i, j) in the final state.

2. Find the pair (k, l) with the minimum ΔR_{kl} of the set $\{\Delta R_{ij}\}$.
3. If $\Delta R_{kl} \leq R$:
 - Then: replace partons k and l by a combination of both (adding their 4-momenta) into one parton and go to step 1.
 - Else: the algorithm terminates.

A jet algorithm needs to be IR safe to be useful for our purposes, i.e. the configuration of jets is not changed by the addition of a soft or collinear parton to the final state. Observables based on jets obtained from an IR-safe jet algorithm will fulfill the inclusivity condition and thus yield finite results.

Reference [94] gives a nice and transparent review of the most used jet algorithms. The library `FastJet` [95] contains many jet algorithms in a unified format which makes them particularly easy to implement. We have used it in the study presented in chapter 5.

2.6 Loop integrals I: Reduction to master integrals

In section 2.3.2, we discussed the extraction and treatment of divergences from diagrams that involve extra external partons. Once we have a suited parametrization for the dimensionally regularized phase space (section 2.2) one generally generates these numerically and implements the cuts that one wants. We will now turn to the other class of diagrams, namely those involving particle loops.

In this section we will focus our attention on the general treatment of loop integrals appearing in an amplitude and what methods and tools allow to reduce these to a significantly smaller subset of integrals called master integrals. We shall illustrate the techniques by taking the approaches presented in references [17, 35, 83] The computational tools to evaluate the master integrals will then be presented in the next section.

We deal at this level with loop amplitudes, i.e. squared sum of all the loop diagrams that are of the perturbative order under consideration. At N^N LO, this will consist of the interference of the N_l -loop diagrams with the tree-level diagrams, the interference of the $(N_l - 1)$ -loop diagrams with the 1-loop diagrams, and so on. We will restrict ourselves to the interference of the N_l -loop diagrams with the tree-level diagrams as the other involves a product of expressions with less loops and are thus intrinsically simpler. Using the

Feynman rules (sections 1.2.1 and 1.3.2) , we obtain a sum of terms of the form

$$\int \left(\prod_{i=1}^{N_l} d^d k_i \right) \frac{N^{\mu\nu\dots}(\{k_i, p_j\}, \dots)}{f(\{p_j\}) \prod_k P_k(\{k_i, p_j\}, m_k)} \quad (2.39)$$

where we denote the external momenta with p_j while the loop momenta are written k_i . The denominator is split between a function f that involves only the external momenta, and that does not play a role in the reduction, and a product of propagators that involves loop momenta and the masses of the particles propagating:

$$P_k(\{k_i, p_j\}, m_k) = \left(\sum_i a_{ki} k_i + \sum_j b_{kj} p_j \right)^2 - m_k^2, \quad a_{ki}, b_{kj} \in \{0, \pm 1\}. \quad (2.40)$$

On the other hand the numerator will in general be a tensor in all the momenta and contains also the coupling constants, the color factors, the space-time dimension etc. We will now show how to express them from scalar integrals.

2.6.1 Tensor integrals and Passarino-Veltman reduction

Depending on the process that one is computing it can be useful or necessary to keep indices open, i.e. to have a rank- n tensor in the loop momenta in the numerator. Straightforward examples are the electron self energy in QED,

$$I_e = \gamma^\nu \gamma_\mu \gamma_\nu I_e^\mu, \quad I_e^\mu = e^2 \int \frac{d^d k}{(2\pi)^d} \frac{k^\mu}{k^2 (k+p)^2}, \quad (2.41)$$

where we have a rank 1 tensor, and the self energy of the photon again in QED,

$$I_\gamma^{\mu\nu} = e^2 \int \frac{d^d k}{(2\pi)^d} \frac{\text{Tr} [\gamma^\mu \not{k} \gamma^\nu (\not{p} + \not{k})]}{k^2 (k+p)^2}, \quad (2.42)$$

which will be of rank 2. We made use of the shorthand notation $\not{k} = \gamma_\mu k^\mu$.

The Passarino-Veltman reduction [96] consists in making an ansatz for the result with the available Lorentz structures, i.e. 4-vectors and the metric tensor $g^{\mu\nu}$. In both the cases we just mentioned, there is only one vector available to construct the tensor structure: p^μ . Hence we can make the ansatz:

$$I_e^\mu = A_e p^\mu, \quad (2.43)$$

$$I_\gamma^{\mu\nu} = A_\gamma g^{\mu\nu} + B_\gamma p^\mu p^\nu. \quad (2.44)$$

We stress here that the coefficient functions are scalar functions, i.e. they can only depend on invariant quantities, of which there is only one available here. The next step consists in contracting on both sides with the same Lorentz structures to obtain scalar equations. In the case of the electron we have one equation:

$$p_\mu I_e^\mu = A_e p^2, \quad (2.45)$$

while for the photon we have a system of two equations:

$$g_{\mu\nu}I_\gamma^{\mu\nu} = A_\gamma d + B_\gamma p^2 \quad (2.46a)$$

$$p_\mu p_\nu I_\gamma^{\mu\nu} = A_\gamma p^2 + B_\gamma (p^2)^2. \quad (2.46b)$$

In both cases, we can invert the system to express the coefficients expressed from the contracted integral. The latter will not have any tensor anymore and can be expressed from p^2 and the denominators k^2 and $(k+p)^2$. The only scalar product is expressed from the other invariants via

$$k \cdot p = \frac{1}{2} [(k+p)^2 - k^2 - p^2]. \quad (2.47)$$

There only remains to evaluate the scalar integrals found.

We can thus reduce in principle any tensor integral into scalar integrals using the Passarino-Veltman reduction. This becomes however increasingly difficult when many vectors are available, as we need to build all the possible Lorentz structures.

We can apply the same method to integrals over the phase space of particles, instead of over a loop momentum. We will make use of this in chapter 8.

2.6.2 Scalar integrals and topologies

By applying the steps described above we are left with a large number of scalar integrals in the loop momenta. We will now use a set of propagators $\{D_i\}_{i=1}^{N_p}$ to represent each scalar integral through a monomial in these propagators. This is achieved by expressing the scalar products in the numerator through some linear combination of the propagators, as we have done during the step of Passarino-Veltman reduction. Beyond 1-loop, the set $\{D_i\}_{i=1}^{N_p}$ will involve N_p propagators that do not appear in the denominator, but are necessary to express all scalar products. A given set of propagators $\{D_i\}_{i=1}^{N_p}$ defines a *topology class* \mathcal{T} .

It is of course in principle possible to choose the set of propagators to accommodate all scalar integrals we want to reduce into one topology class. This is however seldom a good strategy as this will result into many possible “names” for the same integral. We prefer on the other hand to have as few different propagators as possible and define multiple topology classes. The 2-loop integrals that we will encounter in chapter 8 are a generic example: there we define a planar topology class \mathcal{P} and a crossed topology class \mathcal{X} , which share all but one propagator, which has the effect that only one of the scalar products is decomposed in a different way.

In practice, the diagrams are generated automatically and interpreted through the Feynman rules to mathematical expressions. The generator will assign the loop momenta of the diagrams, but we can remap them using transformations that do not alter the measure of the loop momenta, i.e. for which the determinant of the Jacobian of the transformation is 1. For example, $(k, l) \mapsto (k + p_1, l + p_1)$ or $(k, l) \mapsto (k + l, l + p_1)$ are allowed transformations whereas $(k, l) \mapsto (k, l + 2k)$ is not.

Each diagram from the topology class \mathcal{T} can then be expressed as a sum

$$\sum_i f_i(\{p_j\}) T(n_{1,i}, \dots, n_{N_p,i}, q_1, \dots, q_{N-1}) \quad (2.48)$$

where N is the number of external momenta p_i , and we have defined

$$T(n_1, \dots, n_{N_p}, q_1, \dots, q_{N-1}) \equiv \int \left(\prod_{i=1}^{N_l} d^d k_i \right) \prod_{i=1}^{N_p} D_i^{-n_i}(q_1, \dots, q_{N-1}). \quad (2.49)$$

Note that q_1, \dots, q_{N-1} may be any $N - 1$ independent of the N external momenta p_i . We will make use of this fact to further organize the reduction.

2.6.3 Identities between integrals

In the previous section, we have brought scalar integrals in the form

$$T(n_1, \dots, n_{N_p}, q_1, \dots, q_{N-1})$$

Due to their invariance under translations and boosts, integrals with different values of the indices are related by identities. *Integration-by-parts identities* (IBPs) [97, 98] are due to the invariance of the integral under infinitesimal shifts of the loop momentum. They are named this way because they take the form

$$\int d^d k \frac{\partial f(k)}{\partial k_\mu} = 0. \quad (2.50)$$

In our notation we can write the $N_p \times N_l$ identities:

$$\frac{\partial}{\partial k_j^\mu} [\eta_i^\mu T(n_1, \dots, n_{N_p}, q_1, \dots, q_{N-1})] = 0, \quad (2.51)$$

for $i = 1, \dots, N_p$, $j = 1, \dots, N_l$ and where $\eta_{i,\nu} \eta_i^\nu = D_i$. Following the usual product rule the derivative will act on η_i^μ (provided that the latter contains the momentum k_j^μ) as well as on each of the propagators D_i containing k_j^μ . The scalar products are then expressed through the propagators and the equations (2.51) become a set of algebraic relations between integrals of the same topology with shifted indices.

In the same spirit we can state $\frac{1}{2}(N - 1)(N - 2)$ *Lorentz-invariance identities* (LI) [99] which come from the invariance of loop integrals under infinitesimal boosts of the loop momentum:

$$(q_j^\mu q_k^\nu - q_j^\nu q_k^\mu) \sum_i \left(q_{i,\nu} \frac{\partial}{\partial q_i^\mu} - q_{i,\mu} \frac{\partial}{\partial q_i^\nu} \right) T(n_1, \dots, n_{N_p}, q_1, \dots, q_{N-1}) = 0, \quad (2.52)$$

for $j, k = 1, \dots, N - 1$, $j < k$. Proceeding in the same fashion as for the IBPs, the equations (2.52) become a set of algebraic relations between integrals of the same topology with shifted indices.

2.6.4 Off-shell classes and zero topologies

At this stage it is in principle possible to move directly to the reduction of all scalar integrals of the topology \mathcal{T} . For absolutely general choices of the momenta q_1, \dots, q_{N-1} , i.e. assuming they are all massive $q_i^2 \neq 0$ and different, the reduction will turn out to be computationally impossible.

Before proceeding to the reduction of each topology, we thus need to identify the (distinct) off-shell classes relevant to our process by deciding which momenta are massless. This step is evidently going to depend on the process under study, and we shall elaborate more on this in the computation of $q\bar{q} \rightarrow \gamma^*\gamma^*$ in chapter 8. Each integral will then fall into one of these off-shell classes, and this allows us to

1. Simplify the IBPs and LIs, by setting the corresponding invariants to zero,
2. Identify the *zero topologies*, which are set of integrals that vanish because they are scaleless.

Let us illustrate with an example: When treating the 2-scale 1-loop box ($N = 4, N_l = 1, N_p = 4$) we can write the general scalar integral of the topology \mathcal{B}

$$B(n_1, \dots, n_4, q_1, q_2, q_3) \equiv \int d^d k \frac{1}{D_1^{n_1} D_2^{n_2} D_3^{n_3} D_4^{n_4}}, \quad D_i \equiv (k + q_1 + \dots + q_{i-1})^2. \quad (2.53)$$

This topology can be divided in two off-shell classes that we shall denote suggestively by

$$\begin{aligned} q_1^2 = 0, q_2^2 = 0, q_3^2 \neq 0 &\Rightarrow B(\dots, q_1, q_2, q_3) \in \mathcal{B}_{ortho} \\ q_1^2 = 0, q_2^2 \neq 0, q_3^2 = 0 &\Rightarrow B(\dots, q_1, q_2, q_3) \in \mathcal{B}_{para} \end{aligned}$$

because the massive legs are next respectively opposite to each other. A topology from the off-shell class \mathcal{B}_{ortho} missing the propagators 3 and 4, i.e for which $n_3, n_4 \leq 0$, is a zero topology. As $n_3 = n_4 = 0$, the only external momentum involved is q_1 , which is light-like ($p_1^2 = 0$) and the integral vanishes.

It suffices to check that the integral vanishes when the indices are set to zero. The generalization of the statement to negative values is achieved through the use of Feynman parametrization (section 2.7.2): We spell out the case for our example when $n_3 = 0$ and $n_4 = -1$, focusing on the relevant part,

$$\int d^d k \frac{(k + q_1 + q_2)^2}{[k^2]^{n_1} [(k + q_1)^2]^{n_2}} \propto \int d^d k \frac{k \cdot q_2}{[k^2]^{n_1} [(k + q_1)^2]^{n_2}} \equiv I,$$

where we expanded the Minkowski square and kept only the term that does not give back the zero topology with $n_3 = n_4 = 0$. The Feynman parametrization combining the two propagators reads,

$$I = \frac{\Gamma(n_1 + n_2)}{\Gamma(n_1)\Gamma(n_2)} \int_0^1 dx (1-x)^{n_1-1} x^{n_2-1} \int d^d k \frac{k \cdot q_2}{[k^2 + 2xk \cdot q_1]^{n_1+n_2}}. \quad (2.54)$$

We shift the momentum by defining $k \mapsto k - xq_1$ and hence

$$I = \frac{\Gamma(n_1 + n_2)}{\Gamma(n_1)\Gamma(n_2)} \int_0^1 dx (1-x)^{n_1-1} x^{n_2-1} \int d^d k \frac{k \cdot q_2 - xq_1 \cdot q_2}{[k^2]^{n_1+n_2}}. \quad (2.55)$$

The term linear in k vanishes because it is antisymmetric. The remaining integral is completely scaleless and hence $I = 0$. The essential feature is that the shift does not generate a mass term in the denominator. The above can be generalized to include the other numerator or any polynomial in the loop momentum straightforwardly.

When the loop momenta are not decoupled, one applies the same strategy in two steps: one first combines the propagator associated to one loop momentum treating the other loop momenta as if it were external, integrate it, and then combine the result (which this time will involve a mass term containing the other loop momenta) using Feynman parameters with the remaining propagators. This will again produce no mass term and the integral vanishes.

Using the Heaviside function

$$\Theta(x) \equiv \begin{cases} 1, & x > 0 \\ 0, & x \leq 0 \end{cases},$$

and defining the shorthand,

$$\Theta(n_1, \dots, n_k) \equiv \sum_{i=1}^k \Theta(n_i),$$

we can list the zero topologies in a compact way: For our example of the off-shell class \mathcal{B}_{ortho} , the zero topologies can be found to be

$$Z[\mathcal{B}_{ortho}] = \{\Theta(n_1, \dots, n_4) < 2, \Theta(n_1, n_4) < 1, \Theta(n_3, n_4) < 1\}, \quad (2.56)$$

where a given integral vanishes as soon as one of the constraints is fulfilled. For the first one we end up with a tadpole, where we can shift away any momentum; the other two can only depend on a massless vector.

2.6.5 Reduction with AIR

We have now treated all the ingredients which enter in the reduction of scalar integrals to a subset of master integrals as it can be performed with the program **AIR** [78] which is based on an algorithm by Laporta [100] and implemented in **Maple** [101]. The algorithm diagonalises and solves a large system of algebraic equations produced by applying integration identities (IBPs and LIs) on selected ‘seed’ integrals.

Seeds Before starting with the reduction, **AIR** generates the list of seed integrals from which the identities with numerical integer values of the indices will be generated and on which Laporta’s algorithm will be applied. The set of seeds should contain all the scalar integrals appearing in the process for this off-shell class.

Iterative identification of the master integrals While it is in principle possible to run AIR with the most general set of indices for each off-shell class, this is computationally extremely demanding due to the extremely large number of identities generated. Instead, we construct the basis of master integrals by successively allowing more propagators in the integrals that we reduce. After each iteration, we identify which integrals AIR uses to express all the generated seed integrals from. The identified potential master integrals from the iteration with up to n propagators are declared as master integrals for the iteration with up to $n + 1$ propagator. This allows AIR to recognize directly these master integrals which it will not try to reduce further. All the combinations of declared master integrals are saved in a cache and do not interfere with the rest of the reduction, which ensures that the reduction deals with expressions as simple as possible, as only new master integrals will appear explicitly.

Starting at two loops, it is not possible to express all integrals out of a set of master integrals containing only simple propagators. The ordering criterion used by AIR makes it favor integrals containing numerators (i.e. with negative indices) on the right-hand side which we then choose as master integrals. It is however possible to choose a different base by translating them into integrals containing dotted propagators (i.e. with a 2 as entry).

The details of the treatment will be illustrated in the reduction of the integrals involved in the process $q\bar{q} \rightarrow \gamma^*\gamma^*$ in chapter 8. Relevant information for the practical use of AIR can be found in the original publication [78].

We have compared the speed of the reduction when including or not the LIs and found out that they do not lead to a speeding up of the reduction process. In intermediary steps, however, they avoid taking up spurious “master” integrals that are actually reducible.

2.7 Loop integrals II: Computation of master integrals

Once the set of master integrals of a given topology has been identified, we are left with the task of evaluating them. Besides the direct integration with the use of Feynman parameters that we will describe below, we can use the method of differential equations that we will shortly present with an example computation now.

2.7.1 Differential equations

The usual way to evaluate such integrals is to write down and solve a system of differential equations where the differentiation is done in the scales involved in the problem. We shall now shortly illustrate following the presentation of reference [99] how this is performed by computing the 2-scale 2-loop triangle integral that we will encounter in chapter 8. Other pedagogical examples can be found in references [102, 103].

The integral under consideration is shown in figure 2.4. As the integral is a scalar it can only be a function of the external momenta squared. In the case under consideration,

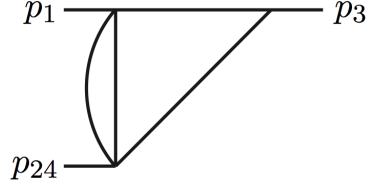


Figure 2.4: 2-scale 2-loop triangle.

only p_3 and p_{24} are non-light-like and independent (we have $p_1 + p_3 + p_{24} = 0$), and the result will depend only on the independent variables s_3 and s_{24} .

In order to set up a differential equation, we need to know how derivatives act on the integral. To achieve this, we note that the partial derivatives are given by

$$\frac{\partial}{\partial p_3^\mu} = \frac{\partial s_3}{\partial p_3^\mu} \frac{\partial}{\partial s_3} + \frac{\partial s_{24}}{\partial p_3^\mu} \frac{\partial}{\partial s_{24}} \quad (2.57a)$$

$$\frac{\partial}{\partial p_{24}^\mu} = \frac{\partial s_3}{\partial p_{24}^\mu} \frac{\partial}{\partial s_3} + \frac{\partial s_{24}}{\partial p_{24}^\mu} \frac{\partial}{\partial s_{24}}. \quad (2.57b)$$

Computing the partial derivatives and inverting the system (2.57b), we get

$$(s_{24} - s_3)^2 \frac{\partial}{\partial s_3} = -2s_{24} \left(p_3^\mu \frac{\partial}{\partial p_3^\mu} \right) + (s_3 + s_{24}) \left(p_{24}^\mu \frac{\partial}{\partial p_{24}^\mu} \right) \quad (2.58a)$$

$$(s_{24} - s_3)^2 \frac{\partial}{\partial s_{24}} = (s_3 + s_{24}) \left(p_3^\mu \frac{\partial}{\partial p_3^\mu} \right) - 2s_3 \left(p_{24}^\mu \frac{\partial}{\partial p_{24}^\mu} \right). \quad (2.58b)$$

The differential operators on the right hand side will act on the master integral by raising the propagator containing the corresponding momentum. We then make use of the relevant identities (section 2.6.3) to come back to the master integrals and simpler integrals, i.e. with fewer propagators – which we already computed, assuming we work our way up in complexity. This yields a system of inhomogeneous coupled partial differential equations:

$$s_3 \frac{\partial}{\partial s_3} \text{triangle} = \frac{d-4}{2} \frac{2s_3 - s_{24}}{s_3 - s_{24}} \text{triangle} - \frac{3d-8}{2} \frac{1}{s_3 - s_{24}} \text{circle} \quad (2.59a)$$

$$s_{24} \frac{\partial}{\partial s_{24}} \text{triangle} = -\frac{d-4}{2} \frac{s_{24}}{s_3 - s_{24}} \text{triangle} + \frac{3d-8}{2} \frac{1}{s_3 - s_{24}} \text{circle} \quad (2.59b)$$

This system is then solved using the standard methods for solving systems of differential equations. In particular, we need to specify the boundary conditions for $s_3 = 0$ and $s_{12} = 0$, which are instances of the simpler 2-loop 1-scale triangle that we will compute in the next section.

In the example that we just computed, the result reads [99]

$$\text{triangle} = A_4 \frac{(-s_3)^{-\varepsilon}}{(s_{24} - s_3)^\varepsilon} + A_3 \frac{2\varepsilon}{1 - 2\varepsilon} \frac{(-s_{24})^{1-2\varepsilon}}{-s_3} {}_2F_1 \left(1 - \varepsilon, 1; 2 - 2\varepsilon; \frac{s_{24}}{s_3} \right), \quad (2.60)$$

where we substituted $\varepsilon = \frac{4-d}{2}$. The computation of the constant A_4 will be sketched in the next section to illustrate the use of Feynman parameters. The constant A_3 can be obtained by computing the 2-loop sunset diagram. We refer the reader to [99] for the value.

In practical applications, the results are usually expanded in the dimension parameter ε . The expansion of the hypergeometric function ${}_2F_1$ yields harmonic polylogarithms (HPLs) [104]. This expansion can be performed using the `Mathematica` [105] package `HypExp` [106,107]. HPLs on the other hand are implemented in the package `HPL` [108,109], and their numerical evaluation can be achieved e.g. with the library `CHAPLIN` [110].

2.7.2 Feynman parameters

For simple loop integrals, it is sometimes more straightforward to compute them by introducing *Feynman parameters*. They permit to combine multiple denominators in a single one at the expense of introducing an integration. The basic identity reads:

$$\frac{1}{AB} = \int_0^1 dx \frac{1}{[xA + (1-x)B]^2}, \quad (2.61)$$

while the most general version for arbitrary powers is given in appendix A and can be proved recursively as an exercise in variable substitution.

We turn to the evaluation of the 1-scale 2-loop triangle

$$\begin{array}{c} p_1 \\ \diagup \quad \diagdown \\ \text{---} \quad \text{---} \\ \diagdown \quad \diagup \\ p_2 \end{array} \equiv \int \frac{d^d k}{(2\pi)^d} \frac{d^d l}{(2\pi)^d} \frac{1}{(k-p_1)^2 (k+p_2)^2 l^2 (l-k)^2}. \quad (2.62)$$

We will proceed as follows:

1. Introduce a Feynman parameter for the two propagators involving the loop momentum l according to the formula (2.61)
2. Integrate over the loop momentum l using the standard formula (A.4)
3. Introduce Feynman parameters for the propagators containing the loop momentum k according to the formula (A.3)
4. Perform the integration over all the Feynman parameters introduced

In the case at hand we can readily identify the bubble integral and Feynman-parametrize it:

$$B(k^2) \equiv \int \frac{d^d l}{(2\pi)^d} \frac{1}{l^2 (l-k)^2} \stackrel{(2.61)}{=} \int_0^1 dx \int \frac{d^d l}{(2\pi)^d} \frac{1}{[l^2 - 2xk \cdot l + xk^2]^2}. \quad (2.63)$$

Performing the shift $l \mapsto l + xk$, and using formula (A.4) with $n = 2$ and $d = 4 - 2\varepsilon$, we get

$$B(k^2) = \int_0^1 dx \int \frac{d^d l}{(2\pi)^d} \frac{1}{[l^2 - x(x-1)k^2]^2} \stackrel{(A.4)}{=} \frac{i\Gamma(\varepsilon)}{(4\pi)^{2-\varepsilon}} \int_0^1 dx [x(x-1)k^2]^{-\varepsilon} \equiv \frac{B_\varepsilon}{(k^2)^\varepsilon}. \quad (2.64)$$

We now plug this in

$$\begin{array}{c} p_1 \\ \diagup \quad \diagdown \\ \text{---} \quad \text{---} \\ \diagdown \quad \diagup \\ p_2 \end{array} \text{---} p_{34} = B_\varepsilon \int \frac{d^d k}{(2\pi)^d} \frac{1}{(k^2)^\varepsilon (k-p_1)^2 (k+p_2)^2} \quad (2.65)$$

$$= B_\varepsilon \frac{\Gamma(2+\varepsilon)}{\Gamma(\varepsilon)} \int_0^1 dy dz \int \frac{d^d k}{(2\pi)^d} \frac{(1-y-z)^{\varepsilon-1}}{[k^2 + 2yk \cdot p_1 - 2zk \cdot p_2]^{2+\varepsilon}}, \quad (2.66)$$

where we have already made use of the δ -function to eliminate one of the Feynman parameters. We now perform the shift $k \mapsto k - yp_1 + zp_2$, and writing $s_{34} = 2p_1 \cdot p_2$ using again formula (A.4) with $n = 2 + \varepsilon$, we end up with

$$\begin{array}{c} p_1 \\ \diagup \quad \diagdown \\ \text{---} \quad \text{---} \\ \diagdown \quad \diagup \\ p_2 \end{array} \text{---} p_{34} = B_\varepsilon \frac{(-1)^{2+\varepsilon} i \Gamma(2\varepsilon)}{(4\pi)^{d/2} \Gamma(\varepsilon)} (-s_{34})^{-2\varepsilon} \int_0^1 dy dz y^{-2\varepsilon} z^{-2\varepsilon} (1-y-z)^{\varepsilon-1}. \quad (2.67)$$

Performing the integration over the Feynman parameters y and z ,⁷ the final result reads

$$\begin{array}{c} p_1 \\ \diagup \quad \diagdown \\ \text{---} \quad \text{---} \\ \diagdown \quad \diagup \\ p_2 \end{array} \text{---} p_{34} = A_4 (-s_{34})^{-2\varepsilon}, \quad (2.68)$$

where A_4 is a ratio of products of Γ -functions with different argument that originate from the evaluation of the hypergeometric functions ${}_pF_q$ evaluated at argument 1. Its explicit value can be found in reference [99].

2.7.3 Multiple polylogarithms

In practice, the brute force integration of integrals involving many Feynman parameters, as in the case of multi-loop integrals with more than one external momentum, especially when they are not massless, is a formidably difficult task. When many scales are involved (be it kinematical invariants or masses) one will end up with complicated functions of a myriad of ratios of these scales. However, performing the integration “one step at a time” with recursively defined functions as those we will discuss in this section allows for a more transparent and algorithmic method.

⁷This involves some tricks like inversion relations and change of variables that are not completely straightforward.

At 1-loop, logarithms and classical polylogarithms, defined recursively through

$$\text{Li}_n(z) \equiv \begin{cases} \int_0^z \frac{dt}{t} \text{Li}_{n-1}(t), & n > 1 \\ -\ln(1-z), & n = 1 \end{cases} \quad (2.69)$$

suffice to express the results when only a few scales are involved. For instance, the 1-loop $H \rightarrow b\bar{b}$ amplitude involves only two scales (m_H and m_b) and can be expressed with the use of logarithms and dilogarithms up to the finite part (chapter 4).

At higher-loop orders and in many-scale problems, new transcendental functions appear such as multiple polylogarithms (MPLs) [111, 112]. Although it is known that they do not cover all cases [113], the latter are sufficient to cover a large number of the phenomenologically relevant ones. An MPL of *weight* n is defined recursively via

$$G(a_1, \dots, a_n; z) \equiv \int_0^z \frac{dt}{t - a_1} G(a_2, \dots, a_n; t), \quad n > 1, \quad (2.70)$$

with $G(; z) \equiv 1$ (i.e. when no coefficients are left), and $a_i, z \in \mathbb{C}$. They contain the classical (poly)logarithms:

$$G(\underbrace{0, \dots, 0}_n; z) = \frac{1}{n!} \ln^n z \quad (2.71a)$$

$$G(\underbrace{0, \dots, 0}_{n-1}, 1; z) = -\text{Li}_n(z) \quad (2.71b)$$

Using this definition, the problem of computing integrals over Feynman parameters is solved recursively. After the k -th integration yielding an MPL, one performs the variable substitutions and partial fractions necessary to bring the integral in the form where equation (2.70) can be used to perform the $(k+1)$ -th integration and so on. Most of the effort is now shifted to finding the suited variable transformations of variables and bringing the variable one wishes to integrate upon next in the last entry of the MPL. For a more detailed presentation of the computational tools we refer the reader to reference [114].

This method has been applied for the computation of the 3-mass 2-loop triangle master integrals in reference [115] and in the computation of the master integrals we will need in chapter 8 [2].

MPLs exhibit a *shuffle algebra* [116]: the product of two MPLs of weight n_1 and n_2 with the same argument is the sum of the MPLs with coefficient obtained through all shuffle combinations of the coefficients, which are the permutation of the coefficient list of both functions that preserve the order of the elements of each list of coefficient separately. Expressed in formula, this reads

$$G(a_1, \dots, a_{n_1}; z) G(a_{n_1+1}, \dots, a_{n_1+n_2}; z) = \sum_{\sigma \in \Sigma(n_1, n_2)} G(a_{\sigma(1)}, \dots, a_{\sigma(n_1+n_2)}; z), \quad (2.72)$$

where $\Sigma(n_1, n_2)$ denotes the set of all shuffles of $n_1 + n_2$ elements, i.e. the subset of the symmetric group $S_{n_1+n_2}$ defined by

$$\Sigma(n_1, n_2) = \{\sigma \in S_{n_1+n_2} \mid \sigma^{-1}(1) < \dots < \sigma^{-1}(n_1) \ \& \ \sigma^{-1}(n_1 + 1) < \dots < \sigma^{-1}(n_1 + n_2)\}. \quad (2.73)$$

For example, for a product of two weight 2 MPLs $G(a, b; z)$ and $G(c, d; z)$ we need to consider all permutations of (a, b, c, d) which have a before b and c before d :

$$\begin{aligned} G(a, b; z)G(c, d; z) &= G(a, b, c, d; z) + G(a, c, b, d; z) \\ &\quad + G(c, a, b, d; z) + G(c, a, d, b; z) + G(c, d, a, b; z). \end{aligned} \quad (2.74)$$

2.7.4 Symbol and coproducts

We present here a very short introduction to the technology used to organize and simplify the computation of multi-loop Feynman integrals following the presentation made in [117].

MPLs are not independent and exhibit many functional relations among themselves, which can obscure the form of the results, for example by making cancellations not explicit.

The symbol method and its refined version, the coproduct method, allow to show equality of two functions up to some pieces without having to make explicit use of the functional identities (which are not all known in the general case). Although the computation of the symbol or coproduct of a given expression is algorithmic, the inverse problem – i.e. finding a simpler function having the same symbol/coproduct – is highly non trivial and is still an open problem. There are however some guidelines regarding what types of function can be expected [118].

Leaving aside a completely rigorous treatment, we will now illustrate the main computational steps needed to use the coproduct. First, the coproduct of a product of MPLs is the product of the coproducts:

$$\Delta(F(w) \cdot G(z)) = \Delta(F(w)) \cdot \Delta(G(z)). \quad (2.75)$$

Second, the coproduct can be written as sum,

$$\Delta = \sum_{p+q=n} \Delta_{p,q} \quad (2.76)$$

where $\Delta_{p,q}$ maps MPLs of weight n to a tensor product of functions with weight p resp. q . Third, the coproduct can be iterated on each component of the tensor separately and the order in which this is achieved is not important. Finally, in order to account for the fact that even zeta values ζ_{2n} are proportional over the rational number to the n -th power of $\zeta_2 = \pi^2/6$ the coproduct treats the real number π in a special way⁸ (conjecture from [117]) by defining:

$$\Delta(\pi) \equiv \pi \otimes 1. \quad (2.77)$$

⁸The symbol of any function proportional to $i\pi$ or ζ_n will vanish, whereas the coproduct will retain part of the information.

The definition of the coproduct allows to show that for an MPL $G(z)$ of weight n

$$\mathcal{S}(G(z)) = \Delta_{\underbrace{1, \dots, 1}_n}(G(z)) \pmod{\pi}, \quad (2.78)$$

where $\pmod{\pi}$ means that the coproducts of π are set to zero.

As an example of the application of the coproduct, we will ‘find’ the inversion relation for Li_3 (in what follows z stands for $z + i0$ to avoid making the notation too cumbersome):

$$\text{Li}_3(1/z) = \text{Li}_3(z) + \frac{1}{6} \ln^3 z - \frac{i\pi}{2} \ln^2 z - \frac{\pi^2}{3} \ln z \quad (2.79)$$

We will use without proof, the formulae,

$$\Delta(\ln z) = 1 \otimes \ln z + \ln z \otimes 1 \quad (2.80)$$

$$\Delta(\text{Li}_n(z)) = 1 \otimes \text{Li}_n(z) + \text{Li}_n(z) \otimes 1 + \sum_{k=1}^{n-1} \underbrace{\frac{1}{k!} \text{Li}_{n-k}(z) \otimes \ln^k z}_{=\Delta_{n-k,k}(\text{Li}_n(z))} \quad (2.81)$$

We first compute

$$\Delta_{2,1}(\text{Li}_3(1/z)) = \text{Li}_2(1/z) \otimes \ln(1/z) \quad (2.82)$$

$$\Delta_{1,2}(\text{Li}_3(1/z)) = \frac{1}{2} \underbrace{\text{Li}_1(1/z)}_{=-\ln(1-1/z)} \otimes \ln^2(1/z). \quad (2.83)$$

Then from either one of these, say the second one, we compute

$$\Delta_{1,1,1}(\text{Li}_3(1/z)) = -\ln(1-1/z) \otimes \ln(1/z) \otimes \ln(1/z). \quad (2.84)$$

We then use the fact that

$$-\ln(1-1/z) = -\ln \frac{1-z}{-z} = -\ln(1-z) + \ln(-z) = -\ln(1-z) + \ln z - i\pi, \quad (2.85)$$

to rewrite (2.84) as

$$\Delta_{1,1,1}(\text{Li}_3(1/z)) = -\ln(1-z) \otimes \ln z \otimes \ln z + \ln z \otimes \ln z \otimes \ln z - i\pi \otimes \ln z \otimes \ln z \quad (2.86)$$

$$= \Delta_{1,1,1}(\text{Li}_3(z)) + \frac{1}{6} \Delta_{1,1,1}(\ln^3 z) + \frac{i}{2} \Delta_{1,1,1}(\pi \ln^2 z), \quad (2.87)$$

where in the last equation we identified each summand of (2.86) (note that we kept π in the coproduct, as it has weight 1⁹). Before we continue, let us define

$$X \equiv \text{Li}_3(1/z) - \left[\text{Li}_3(z) + \frac{1}{6} \ln^3 z + \frac{i\pi}{2} \ln^2 z \right]. \quad (2.88)$$

⁹We would like to point out at this stage that with the symbol, the last term would be missing, illustrating the bigger loss of information that symbol calculus bears with it.

Once more we compute the coproducts

$$\Delta_{1,2}(X) = 0 \tag{2.89}$$

$$\Delta_{2,1}(X) = -\frac{1}{3}\pi^2 \otimes \ln z = -\frac{1}{3}\Delta_{2,1}(\pi^2 \ln z) \tag{2.90}$$

The first coproduct did not give us more information, whereas the second did catch a missing piece of the identity (2.79). Now the only terms that can still be missing are real numbers of weight 3: π^3 and ζ_3 . By evaluating the both side of the identity at a given point, say $z = 1$, we see that they do not appear.

The treatment we just presented shows the philosophy behind the coproduct calculus. Let us stress that the gymnastics we just went through in this example is artificial, and that the usual goal is to simplify expressions, for example by seeing how (2.79) makes various terms cancel each other, without having to explicitly use the identity.

For the renormalization of the parton density functions (PDFs), only a subclass of the MPLs it needed (see e.g. [81]), called *harmonic polylogarithms* (HPLs), for which the coefficients satisfy, $a_i \in \{-1, 0, 1\}$ and with a normalization that differs by a factor of $(-1)^{\#\{a_i=+1\}}$. The technology of symbol and coproduct can of course be used on these functions.

Part II

QCD corrections for WH production

Chapter 3

Introduction

Although the LHC has started its operation only a couple of years ago and at half the design energy, it has already provided plenty of information on the existence of a Standard Model (SM) Higgs boson. With the 5 fb^{-1} luminosity collected with $\sqrt{s} = 7\text{ TeV}$ at the end of 2011, ATLAS was able to exclude the presence of a SM Higgs boson in the range $133\text{ GeV} < m_H < 230\text{ GeV}$ and $260\text{ GeV} < m_H < 437\text{ GeV}$ [9], and CMS in the range $129\text{ GeV} < m_H < 525\text{ GeV}$ [10], in both cases at 99% confidence level. Furthermore, adding 6 fb^{-1} of the 2012 run at $\sqrt{s} = 8\text{ TeV}$, it has been possible to discover a new boson with mass around 125 GeV [119, 120] which has then been corroborated in different channels.

It remains in principle to establish whether this boson is indeed the SM Higgs by studying in detail all its decay modes. A light Higgs boson decays predominantly into a $b\bar{b}$ pair, see figure 1. If it is directly produced in gluon-gluon fusion (the process giving the largest cross section) this signal is overwhelmed by the huge QCD dijet background. This is why the decay modes that have led to the discovery are those which do not involve hadronic final states, like $H \rightarrow \gamma\gamma$ [121, 122], $H \rightarrow WW$ [123, 124] or $H \rightarrow ZZ$ [125–127]. Although they are suppressed with respect to the dominant $b\bar{b}$ mode, it is still possible to extract a signal from the background.

There is however another possibility to study the $b\bar{b}$ decay of the Higgs boson, namely when it is produced in association with a massive vector boson (W or Z boson): the Higgsstrahlung process. In this case there are various possibilities to disentangle the signal over the large $Vb\bar{b}$ background originating from other processes, some of which have been already used at the LHC [128–130]. Among them, one of the most promising strategies makes use of the fact that at the LHC, especially at $\sqrt{s} = 14\text{ TeV}$, it is possible to produce particles with transverse momenta well above their masses, $p_T \gg m$. This is the so-called *boosted* regime, in which one can reconstruct heavy particles decaying hadronically, because their decay products are likely to fall inside one jet with a large radius, a *fat jet*.

Recent proposals for finding a boosted Higgs boson decaying into a $b\bar{b}$ pair are based on the investigation of the substructure of each fat jet [131, 132]. Within these approaches the Higgs boson candidate is a multi-jet system which should contain not only the Higgs boson decay products, but also QCD radiation associated to them. It is therefore crucial

to have predictions for the Higgsstrahlung process that implement gluon radiation, both from the initial and final state which we will cover in the next chapters.

Higher-order corrections to the Higgsstrahlung process, where the Higgs boson decays into a $b\bar{b}$ pair, have been known since a long time. NLO QCD corrections to Higgs boson production in association with a vector boson have been computed in references [133–135] and implemented in the program MCFM [136]. NLO EW corrections are available as well [137] and implemented, together with NLO QCD corrections, in the program HAWK [138]. NNLO results exist for the total cross section [139] for both WH and ZH processes, while a fully differential code is available for WH up to NNLO QCD for the production only [140] and including NNLO QCD corrections both to production and decay in the case of massless bottom quarks [141]. In all but the last reference, the decay of the Higgs into a $b\bar{b}$ pair is implemented at LO only. Concerning decay into a $b\bar{b}$ pair, NLO corrections for massive bottom quarks have been computed in references [142, 143], while for massless bottom quarks a fully differential calculation is available at NNLO [144]. NLO corrections have been interfaced to parton showers in the MC@NLO framework in reference [145]. Furthermore, starting from version 2.5, Herwig++ [146] implements NLO corrections to Higgs boson production [147] and decay, both matched independently to parton shower.

This part of the thesis will be dedicated to the study of the Higgsstrahlung process at NLO in QCD in the case where the Higgs boson decays to a pair of massive bottom quarks. In chapter 4, we compute the fully differential decay rate of a Higgs boson to a pair of massive bottom quarks at NLO in QCD. This decay rate is then implemented in our event generator for Higgsstrahlung, which also takes into account the NLO QCD corrections related to the initial state. This event generator is then used to study the impact of the full NLO corrections on the fat-jet analysis in chapter 5.

Chapter 4

Higgs decay to bottom quarks

In this chapter, we present the computation of the fully differential decay rate of a Higgs boson to a pair of massive bottom quarks at NLO in QCD. Most computations of this chapter were performed as part of the author's Master's thesis project and the relevant pieces were taken from the Master's thesis [148].

Notations Throughout this chapter we work in DREG [52] with $d \equiv 4 - 2\varepsilon$ and we will use the following notations:

$$M \equiv m_H, \quad m \equiv m_b = m_{\bar{b}}, \quad \beta \equiv \sqrt{1 - \frac{4m^2}{M^2}}, \quad y \equiv \frac{m}{v}, \quad (4.1)$$

where $v = 246$ GeV is the vacuum expectation value of the Higgs field.

In the parametrization of phase space integrals, we use the notational shortcut $\bar{x} \equiv 1 - x$ for parameters in the unit interval.

4.1 Leading order

The phase space of the LO decay rate (as well as the one of the NLO virtual, that has the same kinematics) is the special case of equation (2.6) for two equal masses:

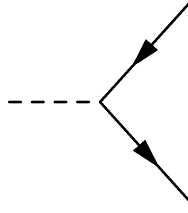
$$\Phi_2(M; m, m) = \frac{\Omega_{3-2\varepsilon}}{2^{5-4\varepsilon} \pi^{2-2\varepsilon}} \beta^{1-2\varepsilon} M^{-2\varepsilon}. \quad (4.2)$$

There is only one diagram for $H \rightarrow b\bar{b}$ at LO which is shown in figure 4.1. Using the corresponding Feynman rule (section 1.3.2), we obtain directly

$$|\mathcal{M}_T|^2 = 2N_c y^2 \mu^{2\varepsilon} M^2 \beta^2, \quad (4.3)$$

and obtain readily:

$$\Gamma_{H \rightarrow b\bar{b}}^{\text{LO}} \stackrel{(2.1)}{=} \frac{N_c y^2}{8\pi} \beta^3 M. \quad (4.4)$$

Figure 4.1: LO diagram of $H \rightarrow b\bar{b}$.

4.2 Next-to-leading order

At NLO, we have to take into account the emission of an extra gluon, as well as the virtual 1-loop contribution. Furthermore the couplings need to be renormalized in order to absorb the UV singularities that will appear (see section 2.3.1).

4.2.1 Real

Phase space

We now need to consider the phase space for one massless particle (the gluon, g) together with two equal-mass particles (the bottom quark b and antiquark \bar{b}). We work in the center-of-mass frame of the Higgs. Using the factorization property (equation (2.5)), we have,

$$d\Phi_3(M; 0, m, m) = \int_{Q_-^2}^{Q_+^2} \frac{dQ^2}{2\pi} d\Phi_2(M; 0, \sqrt{Q^2}) d\Phi_2(\sqrt{Q^2}; m, m) \quad (4.5)$$

The first term is easy to compute, since we are in the center of mass frame of the Higgs, and we get,

$$d\Phi_2(M; 0, \sqrt{Q^2}) = \frac{(2\pi)^{2-d} \Omega_{d-1}}{4M} E_g^{d-3}, \quad (4.6)$$

where

$$E_g = \frac{M^2 - Q^2}{2M},$$

is the energy of the gluon in this frame. We remark on the way that this part of the phase space vanishes in the soft limit¹:

$$E_g \rightarrow 0 \Leftrightarrow Q^2 \rightarrow M^2. \quad (4.7)$$

¹Actually, Q^2 is nothing else than the invariant mass squared of the $b\bar{b}$ system.

The other term is more involved since there is now an explicit dependence on an angle as we are interested in the differential phase space. We choose this angle to be the angle between the bottom quark and the gluon:

$$p_b \cdot p_g = E_b E_g - |\vec{b}| E_g t, \quad t = \cos \vartheta_{bg} \in [-1, 1] \quad (4.8)$$

Changing the integration over t to an integration over $s_{bg} \equiv (p_b + p_g)^2$ using the trick of multiplying by,

$$1 = \int_{s_{bg}^-}^{s_{bg}^+} ds_{bg} \delta(s_{bg} - (p_b + p_g)^2),$$

we get the relations,

$$t = \frac{m^2 - s_{bg} + 2E_b E_g}{2|\vec{b}| E_g}, \quad E_b = \frac{s + s_{bg} - m^2 - 2E_g M}{2M}, \quad (4.9)$$

by solving the δ -functions.

Focusing on the term $(1 - t^2)^{-\varepsilon}$, we see a polynomial of the second degree in s_{bg} ,

$$-Q^2 s_{bg}^2 + Q^2(2m^2 + M^2 - Q^2)s_{bg} - m^2(M^4 + m^2 Q^2 - M^2 Q^2). \quad (4.10)$$

Since we want to have a real solution for s_{bg} , we require the discriminant to be positive or zero. This defines the limit of the integration over Q^2 :

$$Q_-^2 = 4m^2, \quad Q_+^2 = M^2. \quad (4.11)$$

We can then factorize the polynomial (4.10) using its zeros in,

$$-Q^2(s_{bg} - s_{bg}^-(Q^2))(s_{bg} - s_{bg}^+(Q^2))$$

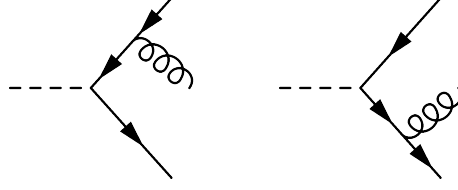
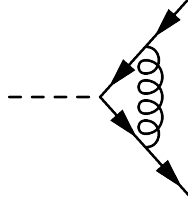
Making a linear parametrization (which we will use for the matrix element later on),

$$Q^2 = Q_-^2 + x_1(Q_+^2 - Q_-^2) = 4m^2 + x_1(M^2 - 4m^2), \quad (4.12a)$$

$$s_{bg} = s_{bg}^-(x_1) + x_2(s_{bg}^+(x_1) - s_{bg}^-(x_1)) \quad (4.12b)$$

and plugging it all in equation (4.5) we obtain the final result,

$$d\Phi_3(M; 0, m, m) = \frac{\Omega_{3-2\varepsilon} \Omega_{2-2\varepsilon}}{2^{10-6\varepsilon} \pi^{5-4\varepsilon}} \beta^{5-6\varepsilon} M^{2-4\varepsilon} \times \\ \times dx_1 dx_2 x_1^{1/2-\varepsilon} \bar{x}_1^{1-2\varepsilon} (x_2 \bar{x}_2)^{-\varepsilon} (1 - \bar{x}_1 \beta^2)^{-1/2}. \quad (4.13)$$

Figure 4.2: NLO diagrams of $H \rightarrow b\bar{b}g$.Figure 4.3: NLO 1-loop diagram of $H \rightarrow b\bar{b}$.

Matrix elements

Two diagrams contribute to $H \rightarrow b\bar{b}g$ at NLO. They are shown in figure 4.2. Using the corresponding Feynman rules (sections 1.3.2 and 1.2.1), we obtain $(s_{ij} = (p_i + p_j)^2$ and $Q^2 = s_{b\bar{b}})$

$$\begin{aligned}
 |\mathcal{M}_R|^2 &= 2^6 \pi^2 N_c C_F y^2 g_s^2 \mu^{4\epsilon} \times & (4.14) \\
 &\times \left[\frac{(s_{b\bar{b}} - 8m^2)s_{b\bar{b}} + M^4 - \epsilon(M^2 - s_{b\bar{b}})^2}{(s_{bg} - m^2)(s_{\bar{b}g} - m^2)} - \frac{2m^2(M^2 - 4m^2)(M^2 - s_{b\bar{b}})^2}{(s_{bg} - m^2)^2(s_{\bar{b}g} - m^2)^2} \right] \\
 &= 2^8 \pi^2 N_c C_F y^2 g_s^2 \mu^{4\epsilon} \frac{1 - \bar{x}_1 \beta^2}{\beta^2 \bar{x}_1^2} \left[\frac{2 - \bar{x}_1(1 + x_1 + \bar{x}_1 \epsilon)}{\kappa(x_1, x_2)} - \frac{2(1 - \beta^2)(1 - \bar{x}_1 \beta^2)}{\kappa(x_1, x_2)^2} \right], & (4.15)
 \end{aligned}$$

where we inserted the parametrization of the real emission phase space and defined

$$\kappa(x_1, x_2) \equiv 1 - (1 - 4x_1 x_2 \bar{x}_2) \beta^2. \quad (4.16)$$

We expect the real emission to become singular when the gluon becomes soft, $E_g(s_{b\bar{b}}(x_1)) = 0$, equation (4.6), i.e. at $x_1 = 1$. We see that indeed the expression (4.15) is singular for $\bar{x}_1 = 0$. This singularity is factorized and can thus be extracted with the method of +-distributions (see section 2.3.2).

4.2.2 Virtual

The phase space of the NLO virtual process is the same as for the LO.

There is only one 1-loop diagram contributing to $H \rightarrow b\bar{b}$ at NLO, see figure 4.3. This time we need only the interference term between the LO and the NLO 1-loop:

$$|\mathcal{M}_T + \mathcal{M}_V|^2 = \underbrace{|\mathcal{M}_T|^2}_{\mathcal{O}(1) \rightarrow \text{LO}} + \underbrace{\mathcal{M}_V \mathcal{M}_T^* + \mathcal{M}_T \mathcal{M}_V^*}_{\mathcal{O}(\alpha_s) \rightarrow \text{NLO}} + \underbrace{|\mathcal{M}_V|^2}_{\mathcal{O}(\alpha_s^2) \rightarrow \text{NNLO}} \quad (4.17)$$

Again, using the Feynman rules (sections 1.3.2 and 1.2.1) and performing the traces in d dimensions using FORM [60, 61], we get,

$$\begin{aligned} \mathcal{M}_V \mathcal{M}_T^* &= i2^{1+2\varepsilon} \pi^{-2+2\varepsilon} N_c C_F y^2 g_s^2 \mu^{4\varepsilon} \left[\beta^2 (1 + \beta^2) M^4 I_{0,m,m}^{1,1,1}(0, p_b, -p_{\bar{b}}) \right. \\ &\quad \left. - (1 + \beta^2) M^2 (I_{0,m}^{1,1}(0, p_b) + I_{0,m}^{1,1}(0, -p_{\bar{b}})) + 2(1 - \beta^2 + \varepsilon\beta^2) M^2 I_{m,m}^{1,1}(p_b, -p_{\bar{b}}) \right], \end{aligned} \quad (4.18)$$

where we introduced the shorthand notation for the scalar loops,

$$I_{m_1, \dots, m_n}^{\nu_1, \dots, \nu_n}(p_1, \dots, p_n) = \int d^d k \left[\prod_{i=1}^n ((k + p_i)^2 - m_i^2 + i0)^{\nu_i} \right]^{-1}. \quad (4.19)$$

At this stage, we need to make a remark concerning the $+i0$ prescription: it is taken as an infinitesimal imaginary number in the upper complex plane. It allows to select the poles within the integration contour unambiguously: we shift the pole over or under the real axis in a consistent way by imposing $m^2 \rightarrow m^2 - i0$. In our case it amounts to take $\beta^2 \rightarrow \beta^2 + i0$. At the end of the calculation, when it is no longer needed, we can forget it. The essential point is its sign, so we do not need to worry about the rest of the expression: e.g. $\sqrt{\beta^2 + i0} = \sqrt{\beta^2} + i0 \times (\text{something positive}) \rightarrow \sqrt{\beta^2} + i0$.

This prescription also settles the issue of how to deal with a logarithm of a negative number (branch choice):

$$a > 0 : \quad \ln(-a \pm i0) = \ln(a) \pm i\pi. \quad (4.20)$$

The other part is,

$$\begin{aligned} \mathcal{M}_T \mathcal{M}_V^* &= i2^{1+2\varepsilon} \pi^{-2+2\varepsilon} N_c C_F y^2 g_s^2 \mu^{4\varepsilon} \left[\beta^2 (1 + \beta^2) M^4 I_{0,m,m}^{1,1,1}(0, p_b, -p_{\bar{b}})^* \right. \\ &\quad \left. - (1 + \beta^2) M^2 (I_{0,m}^{1,1}(0, p_b)^* + I_{0,m}^{1,1}(0, -p_{\bar{b}})^*) + 2(1 - \beta^2 + \varepsilon\beta^2) M^2 I_{m,m}^{1,1}(p_b, -p_{\bar{b}})^* \right]. \end{aligned} \quad (4.21)$$

With the above in mind it becomes clear that,

$$(I_{m_1, \dots, m_n}^{\nu_1, \dots, \nu_n})^* = I_{m_1, \dots, m_n}^{\nu_1, \dots, \nu_n} (+i0 \rightarrow -i0). \quad (4.22)$$

Since,

$$\mathcal{M}_V \mathcal{M}_T^* + \mathcal{M}_T \mathcal{M}_V^* = 2\text{Re}(\mathcal{M}_V \mathcal{M}_T^*), \quad (4.23)$$

we finally obtain,

$$\begin{aligned} 2\text{Re}(\mathcal{M}_V \mathcal{M}_T^*) &= 2\text{Re} \left\{ i2^{1+2\varepsilon} \pi^{-2+2\varepsilon} N_c C_F y^2 g_s^2 \mu^{4\varepsilon} \left[\beta^2 (1 + \beta^2) M^4 I_{0,m,m}^{1,1,1}(0, p_b, -p_{\bar{b}}) \right. \right. \\ &\quad \left. - (1 + \beta^2) M^2 (I_{0,m}^{1,1}(0, p_b) + I_{0,m}^{1,1}(0, -p_{\bar{b}})) \right. \\ &\quad \left. \left. + 2(1 - \beta^2 + \varepsilon\beta^2) M^2 I_{m,m}^{1,1}(p_b, -p_{\bar{b}}) \right] \right\}. \end{aligned} \quad (4.24)$$

We now turn to the evaluation of the scalar loops: To evaluate $I_{0,m,m}^{1,1,1}(0, p_b, -p_{\bar{b}})$, we use an IBP, equation (2.50), coming from,

$$f(k) = \frac{k^\mu}{k^2((p_b + k)^2 - m^2)((p_{\bar{b}} - k)^2 - m^2)}, \quad (4.25)$$

which leads to,

$$(d-4)I_{0,m,m}^{1,1,1}(0, p_b, -p_{\bar{b}}) - 2I_{m,m}^{2,1}(p_b, -p_{\bar{b}}) = 0. \quad (4.26)$$

The evaluation of the three bubble integrals using Feynman parametrization (section 2.7.2), equations (A.3) and (A.4), yields,²

$$I_{m,m}^{2,1}(p_b, -p_{\bar{b}}) = -i\pi^{2-\varepsilon}\Gamma(1+\varepsilon)M^{-2-2\varepsilon} \int_0^1 dx x K(x)^{-1-\varepsilon} \quad (4.27a)$$

$$I_{0,m}^{1,1}(0, p_b) = I_{0,m}^{1,1}(0, -p_{\bar{b}}) = i\pi^{2-\varepsilon}\Gamma(\varepsilon)m^{-2\varepsilon} \frac{1}{1-2\varepsilon} \quad (4.27b)$$

$$I_{m,m}^{1,1}(p_b, -p_{\bar{b}}) = i\pi^{2-\varepsilon}\Gamma(\varepsilon)M^{-2\varepsilon} \int_0^1 dx K(x)^{-\varepsilon}, \quad (4.27c)$$

where,

$$K(x) \equiv x(x-1) + \frac{1-\beta^2}{4} - i0.$$

Putting everything together, equation (4.24) becomes finally,

$$\begin{aligned} 2\text{Re}(\mathcal{M}_V \mathcal{M}_T^*) &= 2^2 N_c C_F y^2 g_s^2 \mu^{4\varepsilon} M^{2-2\varepsilon} (4\pi)^\varepsilon \Gamma(\varepsilon) \text{Re} \left[-\beta^2(1+\beta^2) \int_0^1 dx x K(x)^{-1-\varepsilon} \right. \\ &\quad \left. + 2(1+\beta^2) \left(\frac{1-\beta^2}{4} \right)^{-\varepsilon} \frac{1}{1-2\varepsilon} - 2(1-\beta^2 + \varepsilon\beta^2) \int_0^1 dx K(x)^{-\varepsilon} \right] \quad (4.28) \end{aligned}$$

4.2.3 Renormalization

Renormalization consists in absorbing the UV divergences arising from higher order corrections into the physical parameters of the theory (section 2.3.1). We follow here a line similar to reference [149].

The fermion propagator is modified to the dressed one (by resummation of the 1-particle-irreducible diagrams) and finally to the field-strength renormalized propagator,

$$\frac{i}{\not{p} - m_0} \rightarrow \frac{i}{\not{p} - m_0 - \Sigma(\not{p})} = \frac{iZ_\psi}{\not{p} - m} \quad (4.29)$$

²The integral $I_{m,m}^{2,1}$ is actually still reducible to tadpole and bubble master integrals, but we computed it directly.

where $\Sigma(\not{p})$ is the self-energy of the quark, to be computed in section 4.2.3. From the last term, we see that $\Sigma(m)$ can be understood as the mass difference between the bare and the physical masses, when the fermion is on-shell:

$$\Sigma(m) = m - m_0. \quad (4.30)$$

Expanding the self energy around $\not{p} = m$, we have,

$$\Sigma(\not{p}) \simeq \Sigma(m) + (\not{p} - m) \left. \frac{d\Sigma}{d\not{p}} \right|_{\not{p}=m}, \quad (4.31)$$

which implies,

$$\not{p} - m_0 - \Sigma(\not{p}) \simeq \not{p} - m_0 - \left(m - m_0 + (\not{p} - m) \left. \frac{d\Sigma}{d\not{p}} \right|_{\not{p}=m} \right) \quad (4.32)$$

$$= (\not{p} - m) \left(1 - \left. \frac{d\Sigma}{d\not{p}} \right|_{\not{p}=m} \right), \quad (4.33)$$

which in turn implies, using equation (4.29),

$$Z_\psi^{-1} = 1 - \left. \frac{d\Sigma}{d\not{p}} \right|_{\not{p}=m} \quad (4.34)$$

The most often used renormalization scheme is the modified minimal subtraction ($\overline{\text{MS}}$) scheme where only the $\frac{1}{\varepsilon}$ -pole and finite part of,

$$(4\pi)^\varepsilon \Gamma(\varepsilon) = \frac{1}{\varepsilon} - \gamma_E + \ln 4\pi + \mathcal{O}(\varepsilon), \quad (4.35)$$

is subtracted. This results in a pole of the propagator not lying at the physical mass m and with residue different from 1, which makes the interpretation of the propagator difficult. We decided to use the on-shell (OS) scheme instead, where the whole finite part is taken. We now turn to the computation of the self-energy.

Bottom quark self-energy

The quark self-energy is described in QCD at $\mathcal{O}(\alpha_s)$ by the diagram of figure 4.4. Using

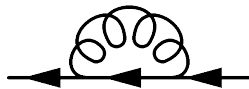


Figure 4.4: Quark self-energy at $\mathcal{O}(\alpha_s)$.

the Feynman rules (section 1.2.1, there is no external propagator!), we obtain for a massive quark,

$$\begin{aligned}\Sigma(\not{p}) &= -iC_F g_s^2 \mu^{2\varepsilon} \int \frac{d^d k}{(2\pi)^d} \frac{\gamma_\mu(\not{p} + \not{k} + m)\gamma^\mu}{k^2 [(p+k)^2 - m^2]} \\ &= mA(p^2) + \not{p}B(p^2)\end{aligned}\quad (4.36a)$$

$$A(p^2) \equiv C_F \frac{\alpha_s}{4\pi} \mu^{2\varepsilon} (4\pi)^\varepsilon \Gamma(\varepsilon) (4-2\varepsilon) \int_0^1 dx [m^2 x - p^2 x(1-x)]^{-\varepsilon} \quad (4.36b)$$

$$B(p^2) \equiv C_F \frac{\alpha_s}{4\pi} \mu^{2\varepsilon} (4\pi)^\varepsilon \Gamma(\varepsilon) (-2+2\varepsilon) \int_0^1 dx (1-x) [m^2 x - p^2 x(1-x)]^{-\varepsilon}, \quad (4.36c)$$

where we used the basic properties of γ -matrices [35].

We will need the derivative of $\Sigma(\not{p})$ for $\not{p} = m$:

$$\left. \frac{d}{d\not{p}} p^2 \right|_{\not{p}=m} = 2m, \quad \left. \frac{d}{d(p^2)} [m^2 x - p^2 x(1-x)] \right|_{p^2=m^2} = \varepsilon m^{-2} [m^2 x^2]^{-\varepsilon} \frac{1-x}{x}. \quad (4.37)$$

Higgs boson wave function Since the Higgs has no color charge and thus cannot couple directly to gluons, we can only have corrections through quark loops and these do not appear at NLO. We can thus set

$$Z_H = 1. \quad (4.38)$$

Gluon wave function The gluon wave function gets corrections through quark, gluon and ghost loops.

$$Z_g = 1 + \mathcal{O}(g_s^2). \quad (4.39)$$

Since the presence of a gluon already implies a factor g_s^2 , the correction will be of $\mathcal{O}(g_s^4)$ and we can forget them at NLO. We shall set $Z_g = 1$ throughout the computation.

Bottom quark wave function

We start with the evaluation of Z_ψ . Equation (4.34) tells us that,

$$Z_\psi = 1 + \left. \frac{d\Sigma}{d\not{p}} \right|_{\not{p}=m} = B(m^2) + 2m^2 \left. \frac{d}{d(p^2)} [A(p^2) + B(p^2)] \right|_{p^2=m^2} \quad (4.40a)$$

$$= 1 + 2C_F g_s^2 \left(\frac{m}{\mu}\right)^{-2\varepsilon} (4\pi)^\varepsilon \Gamma(\varepsilon) \int_0^1 dx x^{-2\varepsilon} \left[-1 + x + \left(\frac{2}{x} + 1 - 3x\right) \varepsilon \right] + \mathcal{O}(g_s^4) \quad (4.40b)$$

Bottom quark mass and Yukawa coupling

We proceed by evaluating Z_m from equation (4.30), which gives us,

$$m_0 = m - \Sigma(m) = [1 - A(m^2) - B(m^2)] m \quad (4.41)$$

so that we can read out,

$$Z_m = 1 - A(m^2) - B(m^2) \quad (4.42a)$$

$$= 1 + 2C_F \frac{\alpha_s}{4\pi} \left(\frac{m}{\mu}\right)^{-2\varepsilon} (4\pi)^\varepsilon \Gamma(\varepsilon) \int_0^1 dx x^{-2\varepsilon} [-1 - x + x\varepsilon] + \mathcal{O}(g_s^4). \quad (4.42b)$$

As for the Yukawa coupling since $y = m/v$ we expect that $Z_y = Z_m$.

At N^kLO, diagrams of order g_s^{2k} do not need to be renormalized since any corrections would be of order g_s^{2k+2} . For our NLO computation, we thus only need to renormalize the tree-level amplitude.

4.2.4 Total decay rate

Putting all the pieces together, we obtain the differential decay rate for the $H \rightarrow b\bar{b}$ at NLO in QCD. The renormalization cancels the UV divergence of the virtual diagram. Upon integration over the phase space of the real emission, the IR divergence of the real is equal and opposite to the IR divergence of the virtual leaving only a finite decay rate, that is independent of the renormalization scale μ :

$$\begin{aligned} \frac{\Gamma_{H \rightarrow b\bar{b}}^{\text{NLO}}}{\Gamma_{H \rightarrow b\bar{b}}^{\text{LO}}} = 1 + C_F \frac{\alpha_s}{\pi} \left\{ \int dx_1 dx_2 \frac{r(x_1, x_2) - r(1, x_2)}{\bar{x}_1} - 1 - 3\beta L - \ln\left(\frac{4\beta^4}{1 - \beta^2}\right) \right. \\ \left. + \frac{1 + \beta^2}{2\beta} \left[\frac{L^2}{2} + 2L(2L + \ln \beta) + \frac{2\pi^2}{3} + \text{Li}_2\left(\frac{-2\beta}{1 - \beta}\right) \right. \right. \\ \left. \left. - \text{Li}_2\left(\frac{2\beta}{1 + \beta}\right) + \text{Li}_2\left(\frac{1 - \beta}{1 + \beta}\right) \right] \right\}, \quad (4.43) \end{aligned}$$

with

$$r(x_1, x_2) \equiv 2\sqrt{x_1(1 - \bar{x}_1\beta^2)} \frac{1 + x_1^2 + 2x_1(1 - 2x_2)^2 + \beta^2\bar{x}_1(1 - x_1(1 - 2x_2)^2 + 4x_1^2x_2\bar{x}_2)}{\kappa(x_1, x_2)^2}, \quad (4.44)$$

and κ as defined in equation (4.16).

The total decay rate (4.43) is found to be in excellent numerical agreement with the result available in the literature [142,143] although the parametrization we have used makes the integration somewhat cumbersome.

Chapter 5

Higgsstrahlung at NLO

We present here our implementation of an event generator to investigate the effect of NLO QCD corrections to both production and decay on present and future Higgs searches. The corrections to production and decay are treated separately in the code: first a Higgs and a vector boson (decaying to leptons) are produced, and then the Higgs boson decays to bottom quarks. We lose no information about spin correlations as the Higgs boson is a scalar particle. Having our own fully differential code give us the opportunity to study NLO QCD corrections to production and decay separately and assess their relative importance. We stick to a fixed-order calculation since its outcome can be interpreted more easily than the corresponding one from Monte Carlo event generators.

5.1 Setup

The production process was computed up to NLO in the following fashion: we generated the relevant matrix elements for the process depicted in figure 5.1 with QGRAF [59] and interpreted these with the Feynman rules (sections 1.3.2 and 1.2.1) using a housemade set of routines coded in FORM [60, 61]. The finite width of the vector boson has been taken into account by allowing the mass of the decaying vector boson to follow a Breit-Wigner distribution centered around m_V of width Γ_V . These were checked against the results in the literature. For the decay, we implemented the differential decay rate whose computation has been detailed in chapter 4

For definiteness, we present the results in the case of Higgs boson production in association with a W boson. The adaptation to the production in association with a Z boson is straightforward in that it just amounts to change some parameters like the vector boson mass and couplings, as well as the PDFs that are needed as the initial state has two identical quarks (section 1.3.2).

Denoting by $d\sigma_{pp \rightarrow WH}$ the differential cross section for WH production and by $d\Gamma_{H \rightarrow b\bar{b}}$ the differential decay rate for a Higgs boson decaying into a $b\bar{b}$ pair we have the perturbative expansions

$$d\sigma_{pp \rightarrow WH} = d\sigma_{pp \rightarrow WH}^{(0)} + d\sigma_{pp \rightarrow WH}^{(1)}, \quad d\Gamma_{H \rightarrow b\bar{b}} = d\Gamma_{H \rightarrow b\bar{b}}^{(0)} + d\Gamma_{H \rightarrow b\bar{b}}^{(1)}, \quad (5.1)$$

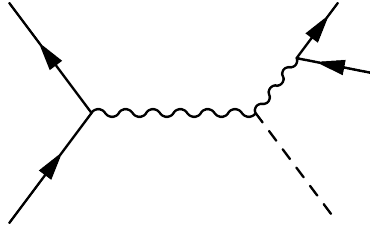


Figure 5.1: LO diagram for the Higgstrahlung process with the vector boson decaying leptonically.

where $d\sigma_{pp \rightarrow WH}^{(1)}$ is of relative order α_s with respect to $d\sigma_{pp \rightarrow WH}^{(0)}$ (and similarly $d\Gamma_{H \rightarrow b\bar{b}}^{(1)}$ with respect to $d\Gamma_{H \rightarrow b\bar{b}}^{(0)}$). Using the narrow width approximation, which is reasonable for a light SM Higgs, we can combine NLO corrections to production and decay as follows

$$d\sigma_{pp \rightarrow (H \rightarrow b\bar{b})W} = \left(d\sigma_{pp \rightarrow WH}^{(0)} \times \frac{d\Gamma_{H \rightarrow b\bar{b}}^{(0)} + d\Gamma_{H \rightarrow b\bar{b}}^{(1)}}{\Gamma_{H \rightarrow b\bar{b}}^{(0)} + \Gamma_{H \rightarrow b\bar{b}}^{(1)}} + d\sigma_{pp \rightarrow WH}^{(1)} \times \frac{d\Gamma_{H \rightarrow b\bar{b}}^{(0)}}{\Gamma_{H \rightarrow b\bar{b}}^{(0)}} \right) \times \text{Br}(H \rightarrow b\bar{b}), \quad (5.2)$$

where $\Gamma_{H \rightarrow b\bar{b}}^{(0)}$ is the LO total $H \rightarrow b\bar{b}$ decay rate (equation (4.4)), $\Gamma_{H \rightarrow b\bar{b}}^{(1)}$ the corresponding NLO correction (equation (4.43)) and $\text{Br}(H \rightarrow b\bar{b})$ is the branching ratio for the decay $H \rightarrow b\bar{b}$.

Before describing the phenomenology we briefly give some details of the calculation. To handle IR divergences of the production we use a fully local subtraction method both for production and decay. We first compute real and virtual matrix elements in $d = 4 - 2\varepsilon$ dimensions. We then suitably parametrize the phase space for the emission of a single real gluon, expand each denominator occurring in the real matrix element in powers of ε using the expansion in $+$ -distributions (section 2.3.2), and cancel all the resulting $1/\varepsilon^2$ and $1/\varepsilon$ poles point by point in phase space either against virtual corrections, or against the PDF counterterm provided by the $\overline{\text{MS}}$ factorization scheme (section 1.2.2).

For the production process, we use, depending on the computation order, the LO or NLO MSTW2008 PDFs [150] interfaced through the library LHAPDF [88], the latter corresponding to $\alpha_s(m_Z) = 0.120179$, which is evolved up to the relevant scale for the NLO corrections. We consider both W^+ and W^- production, keeping the full spin correlations when letting them decay into a lepton and a neutrino. Concerning the Higgs boson decay, all matrix elements for $H \rightarrow b\bar{b}$ are computed for massive bottom quarks, using the OS renormalization scheme with a pole mass $m_b = 4.24 \text{ GeV}$ (the detailed treatment is presented in chapter 4). We have checked that our production code agrees with MCFM for both total numbers and differential distributions. Furthermore, in the following we will consider the production of a SM Higgs boson of mass $m_H = 125 \text{ GeV}$, with $\text{Br}(H \rightarrow b\bar{b}) = 0.578$ taken from references [11, 151, 152].¹

¹In fact, since we will be concerned mainly on K-factors and shapes of distributions, the actual value of $\text{Br}(H \rightarrow b\bar{b})$ will not be relevant for the main issues discussed here.

5.2 Higgs searches with the fat-jet method

Proton-proton collisions at the LHC with $\sqrt{s} = 14$ TeV at high luminosity are a natural place to look for a boosted Higgs boson: one has the possibility to cut on a high-transverse momentum Higgs boson, and still have a number of events that makes it possible to significantly distinguish the signal from the background. Therefore, we first give theoretical predictions for observables that are of use at the LHC with $\sqrt{s} = 14$ TeV when searching for a boosted Higgs boson associated to a W boson, using the strategy of reference [131].

In the following we describe the set of kinematical cuts we employ for this analysis. First of all, we put some basic constraints on the decay products of the W boson, namely that the charged lepton has a transverse momentum $p_T^l > 30$ GeV and a pseudorapidity $|\eta_l| < 2.5$, and that the total missing transverse momentum fulfils $p_T^{\text{miss}} > 30$ GeV. We then require that the reconstructed W boson have large transverse momentum $p_T^W > 210$ GeV. This value is approximately equal to the minimum transverse momentum that a boosted Higgs boson recoiling against a W boson must have, at tree level, so that the $b\bar{b}$ pair resulting from its decay falls into a cone of radius $R = 1.2$. The latter is the value of jet radius R considered in reference [131].

Specifically, a Higgs boson decaying into a $b\bar{b}$ pair is searched for by clustering each event into fat jets using the Cambridge/Aachen algorithm [92, 93] (section 2.5) from the software package **FastJet** [95] with $R = 1.2$, and examining the substructure of each jet to see if it contains the Higgs boson decay products.

Once we have identified a fat jet j , in order to establish whether it can be considered a Higgs candidate, we follow the procedure proposed in reference [131], which we briefly recall:

1. Undo the last clustering inside the fat jet j , thus identifying two subjets j_1 and j_2 ordered according to their invariant mass, $m_{j_1}^2 > m_{j_2}^2$;
2. Require a significant mass drop $m_{j_1}^2 < \mu m_j^2$ and impose $\max\{p_{T,1}^2, p_{T,2}^2\} \Delta R_{j_1, j_2}^2 > y_{\text{cut}} m_j^2$, in order to suppress asymmetric splittings.

If both conditions are fulfilled then j is a candidate Higgs jet and the procedure terminates. Otherwise set $j = j_1$ and we go back to step 1. The fat jet is then kept as a Higgs candidate only if both j_1 and j_2 have b-tags.

Finally, again following reference [131], one should apply a filtering procedure, which consists in reclustering the candidate Higgs jet with a radius $R_{\text{filt}} < R$, and then choosing the candidate Higgs mass as the invariant mass of the hardest (i.e. with the highest p_T) n_{filt} subjets. Since our calculation is pure NLO for both production and decay, a fat jet will contain at most three subjets. As suggested in reference [131], we choose $n_{\text{filt}} = 3$, and therefore we can skip the filtering step at this stage.

The first relevant observable we consider is the transverse momentum $p_{T,j}$ of the candidate Higgs jet. In particular, we wish to perform an analogous study as the one done in reference [140], including NLO corrections to both Higgs boson production and decay.

As in reference [140], we require the candidate Higgs jet to be the one with the highest transverse momentum and to be central, $|\eta_j| < 2.5$.

In figure 5.2 we show plots for the fat-jet p_T -spectrum corresponding to two different event selection procedures. In the first case no constraint is imposed on any extra jet, whilst in the second case we impose a jet-veto condition, requiring that there are no further jets with $p_T > p_{T,\text{veto}} \equiv 30 \text{ GeV}$ and $|\eta| < \eta_{\text{veto}} \equiv 3$ (again according to what is done in reference [131]).

The perturbative stability of our predictions is investigated by simultaneous variation of renormalization and factorization scales for the production process in the interval

$$\frac{m_H + m_W}{2} \leq \mu_R^{(p)} \stackrel{!}{=} \mu_F^{(p)} \leq 2(m_H + m_W). \quad (5.3)$$

Since we know from the study of reference [153] that, for the fat-jet analysis described above, no infrared problems are expected from QCD corrections to the decay process, we have decided to fix the renormalization scale for the decay at $\mu_R^{(d)} = m_H$.

At LO the distributions with and without an extra-jet veto obviously coincide. On the contrary, as observed already in reference [140], there are substantial differences for NLO distributions. Without a veto on an extra jet, if one excludes the lowest p_T -bin, NLO corrections to production are positive, giving roughly a constant K-factor of about 1.3 at large $p_{T,j}$. The addition of NLO corrections to decay does not alter significantly this K-factor, reducing it to 1.2 (see figure 5.2, red and dark-blue bands). The fact that the K-factor is only slightly decreased when adding NLO corrections to decay suggests that the observable we consider is sufficiently inclusive with respect to extra gluon radiation from the $b\bar{b}$ system. In other words, in the boosted regime we are considering, final-state QCD radiation is well contained inside the fat jet, and therefore we observe no large virtual corrections unbalanced by real radiation. After imposing the jet veto, NLO corrections become negative, and increase in size when the jet transverse momentum increases. This is due to virtual contributions that do not cancel fully against initial-state real radiation, giving a (negative) logarithmic left-over as large as $\alpha_s \ln^2(p_{T,j}/p_{T,\text{veto}})$. We observe that, also in this case, the addition of NLO corrections to decay causes only a mild reduction of the K-factor, around 10% and roughly constant over the whole fat-jet p_T -range (see figure 5.2, purple and light-blue bands).

A remark is in order concerning the behaviour of the fat-jet p_T -spectrum in the lowest p_T -bin. There one notices a significant decrease in the cross section in going from LO to NLO, as well as a larger variation when varying renormalization and factorization scales. This bin corresponds in fact to the situation in which one imposes symmetric p_T cuts on both the Higgs boson and the W boson. As observed in references [154, 155] and explained in reference [156], symmetric cuts can cause instabilities in the QCD perturbative series. However, such instabilities could be removed by performing a resummation of large logarithms appearing in the distribution in the transverse momentum of the HW system [156]. The physics underlying such resummation is implemented in all parton shower Monte Carlo's, which should then be used for Higgs searches including the symmetric-cut region. Performing such a resummation is beyond the scope of this work and we restrict our

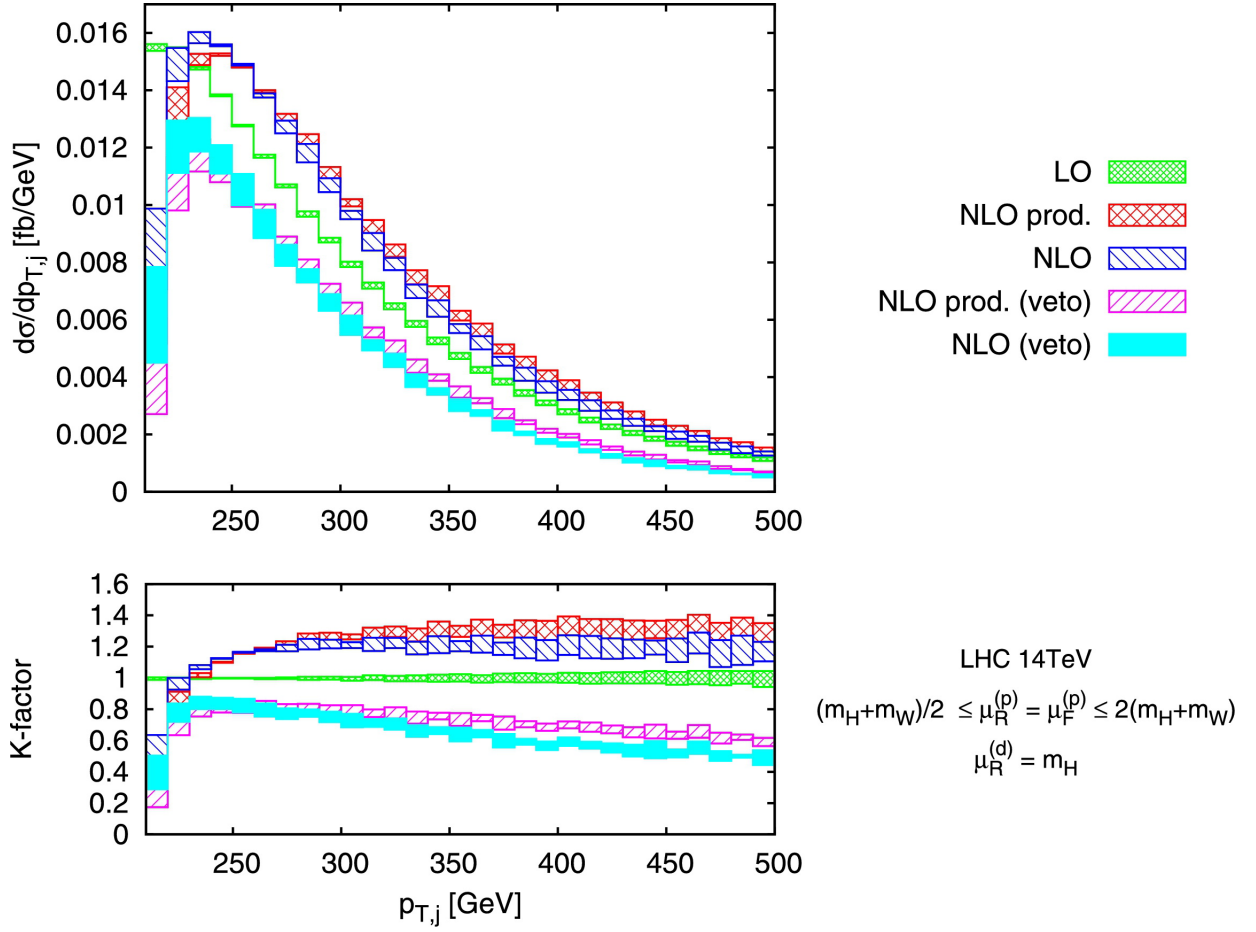


Figure 5.2: The transverse momentum distribution of the candidate Higgs fat jet at the LHC with $\sqrt{s} = 14$ TeV, corresponding to the kinematical cuts described in the text.

	LO	NLO (prod.)	NLO
σ_{inc} [fb]	$1.53^{+0.02}_{-0.03}$	$1.87^{+0.05}_{-0.05}$	$1.80^{+0.06}_{-0.07}$
$\sigma_{0\text{-jet}}$ [fb]	$1.53^{+0.02}_{-0.03}$	$1.19^{+0.04}_{-0.06}$	$1.12^{+0.06}_{-0.08}$

Table 5.1: Cross section for Higgs boson production in association to a high- p_T W boson selected according to the cuts described in the main text, for $230 \text{ GeV} < p_{T,j} < 500 \text{ GeV}$, with ($\sigma_{0\text{-jet}}$) and without (σ_{inc}) a veto on an extra jet.

subsequent analyses to the asymmetric-cut region $p_{T,j} > 230 \text{ GeV}$, where our fixed-order predictions seem to be reliable. Finally, table 5.1 lists an example of the cross sections we obtain for the integrated p_T spectrum for $\mu_R^{(p)} = \mu_F^{(p)} = m_H + m_W$ and of $\mu_R^{(d)} = m_H$, together with the corresponding renormalization and factorization scale uncertainties.

From the plots in figure 5.2 it looks like the net effect of QCD corrections to Higgs boson decay is just that of reducing the production rate of a candidate Higgs fat jet. However, the fat jet considered there can have an arbitrary invariant mass, whilst in general one measures the fat-jet invariant mass distribution, given a set of kinematical cuts, and looks for a mass peak. Therefore, it is useful to investigate the impact of NLO corrections to Higgs boson production and decay over the reconstruction of a mass peak based on the fat-jet analysis described above. At NLO there are two effects that can potentially spoil this reconstruction. The first is the emission of a parton from the initial state that is subsequently clustered within the fat jet. The second is the loss of gluon radiation from the $b\bar{b}$ pair originating from the decay of the Higgs boson that does not get caught in the fat jet. Both effects are studied through the plots shown in figure 5.3 where the differential distribution $d\sigma/dm_j$ in the invariant mass of the fat jet is plotted. The renormalization and factorization scales are fixed to their central value $\mu_R^{(p)} = \mu_F^{(p)} = m_H + m_W$ and $\mu_R^{(d)} = m_H$. The first NLO curve in figure 5.3 (green, dashed) corresponds to the fully inclusive situation in which the only selection requirement is that there is a candidate Higgs jet, with no cut whatsoever on the jet transverse momentum. This curve is shown to illustrate how the fat-jet selection technique works in practice. We first observe that the fat-jet method is pretty robust under radiative corrections, in that, even without requiring a high- p_T W boson, only around 30% of candidate Higgs events fall outside the mass window $110 \text{ GeV} < m_j < 140 \text{ GeV}$ (a typical bin size for boosted Higgs searches at the LHC, see [128]). The region to the right of the peak corresponds to situations in which initial-state radiation is clustered inside the fat jet, thus artificially increasing the invariant mass of the latter. To the left of the peak we see a long tail corresponding to events in which a gluon emitted from the $b\bar{b}$ system originating from Higgs boson decay escapes the fat jet. This effect is entirely due to NLO corrections to Higgs boson decay, and its contribution to degrading the resolution of the mass peak is comparable to that coming from NLO corrections to the production process. In fact, most events outside the mass window $110 \text{ GeV} < m_j < 140 \text{ GeV}$ have $m_j < 110 \text{ GeV}$. These events extend down to $m_j = 2m_b$, corresponding to the situation in which the $b\bar{b}$ pair recoils against a hard gluon. The other two curves correspond to events

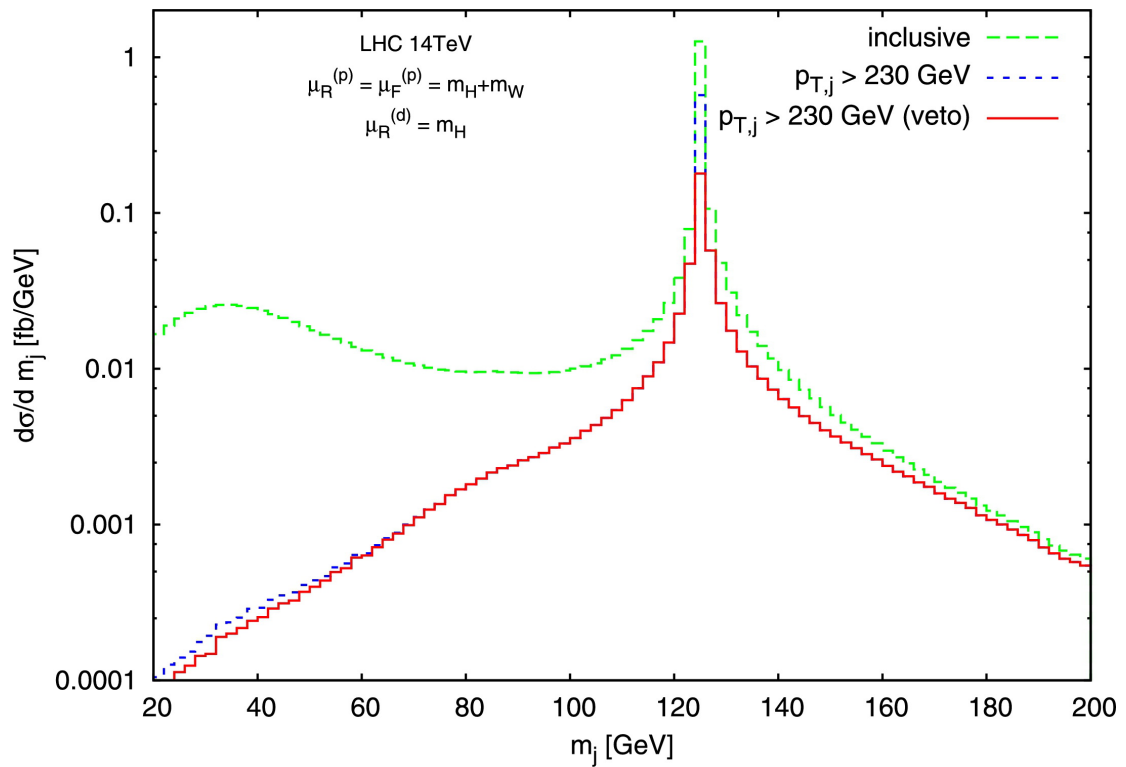


Figure 5.3: The distribution in the invariant mass of the candidate Higgs jet, without any kinematical cuts (green, dashed), fully inclusive with respect to all other jets (blue, dashed), and with a jet-veto condition (red, solid).

passing the same kinematical cuts as in figure 5.2, and with an additional cut on the fat-jet transverse momentum $p_{T,j} > 230$ GeV. We first observe that this cut reduces considerably the fraction of events with $m_j < 110$ GeV which is around 10% both with and without the jet veto. A further remark is in order concerning the curve (solid, red) obtained by imposing the additional constraint of vetoing all extra jets with $p_T > 30$ GeV and rapidity $|\eta| < 3$. In this case, as expected from the study of reference [140] and figure 5.2, the peak height is reduced because of the suppression of real emission and the dominance of negative uncanceled virtual corrections. Among the effects of the jet veto there is also that of eliminating events in which a gluon emitted by the $b\bar{b}$ system escapes the fat jet. For the red solid curve this is visible in the figure for $m_j < 60$ GeV and has a negligible impact on the resolution of the mass peak. We finally remark that the fact that the mass peak survives depends crucially on both the jet-veto condition and the procedure used to identify a candidate Higgs jet. We have observed that decreasing $p_{T,\text{veto}}$ can lower the number of selected events in such a way that a peak is not visible any more. The same remark holds for alternative procedures for defining a candidate Higgs jet, which need to be tested against final-state QCD radiation as well. An example of how the latter can affect significantly the outcome of a Higgs search analysis is discussed in the next section.

5.3 Higgs searches at the LHC with $\sqrt{s} = 8$ TeV

In this section we shall present our analysis on the impact of QCD radiative corrections to production and decay for the search strategy described by CMS to look for a high- p_T Higgs radiated off a vector boson at the LHC with $\sqrt{s} = 8$ TeV.

Rather than performing a fat-jet analysis, CMS uses a simplified procedure aimed at identifying a boosted hadronic system that could be considered as a Higgs candidate [128], which we summarize shortly. First, they impose cuts on the decay products of the W boson. For a W boson decaying into a muon and its associated neutrino (the case we consider in the following), they require $p_T^l > 20$ GeV and $|\eta_l| < 2.4$, together with a constraint on the missing transverse energy $p_T^{\text{miss}} > 35$ GeV. The Higgs candidate is a dijet system consisting of two central ($|\eta| < 2.5$) b -tagged jets with $p_T > 30$ GeV, reconstructed with the anti- k_t algorithm [157] with $R = 0.5$. Then, high- p_T events are selected by imposing a cut both on the transverse momentum of the reconstructed W boson $p_T^W > 160$ GeV and on that of the dijet system $p_{T,j} > 165$ GeV, and requiring the latter to be central ($|\eta_j| < 2.5$). Finally, the W boson and the Higgs candidate are required to be almost back-to-back in the transverse plane, by imposing $\Delta\phi_{W,j} \equiv |\phi_W - \phi_j| > 3$, where ϕ_i denotes the azimuthal angle of i , and no extra jets are allowed with $p_T > 20$ GeV and $|\eta| < 2.4$.

Among these conditions, the requirement on $\Delta\phi_{W,j}$, is particularly sensitive to initial-state radiation, in particular soft and collinear gluon emissions along the beam. We wish therefore to investigate if our predictions for the $\Delta\phi_{W,j}$ distribution are stable against higher-order corrections. We do this via simultaneous variations of renormalization and

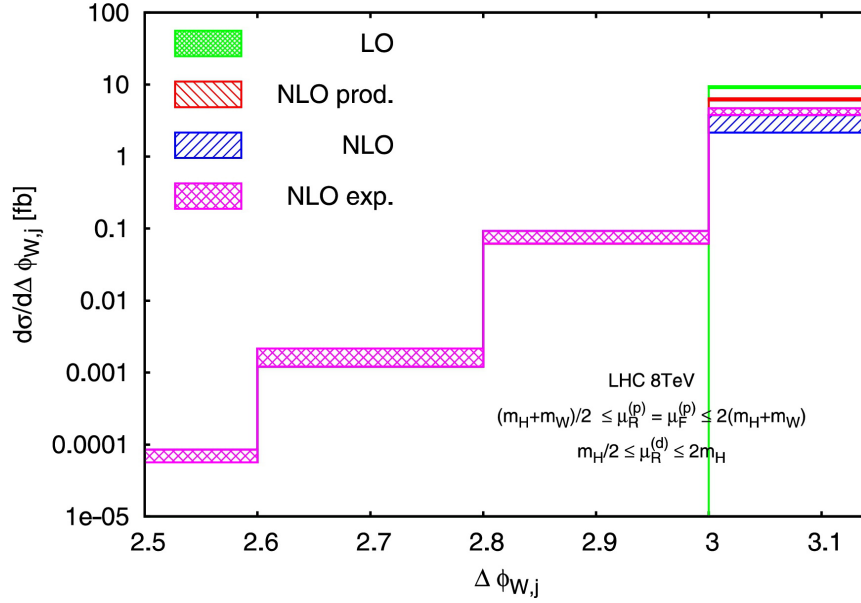


Figure 5.4: The differential distribution in the azimuthal angle $\Delta\phi_{W,j}$ between the reconstructed W boson and the candidate Higgs jet, corresponding to the selection cuts described in the text.

factorization scales for the production process

$$\frac{m_H + m_W}{2} \leq \mu_R^{(p)} \stackrel{!}{=} \mu_F^{(p)} \leq 2(m_H + m_W), \quad (5.4)$$

and independent variation of the renormalization scale for the decay

$$\frac{m_H}{2} \leq \mu_R^{(d)} \leq 2m_H. \quad (5.5)$$

Figure 5.4 shows the $\Delta\phi_{W,j}$ distribution, obtained after imposing the cuts described above. First of all, one notices that most events are concentrated in the bin $\Delta\phi_{W,j} > 3$, so that we expect that bin to be wide enough to ensure a sufficiently inclusive cancellation of large real and virtual corrections arising from the region close to $\Delta\phi_{W,j} = \pi$. This is confirmed by the fact that, if one considers production only (the histogram labelled “NLO prod.”), the K-factor we observe in that bin is moderate (around 0.8). Indeed, the cut on $\Delta\phi_{W,j}$ is only one of the effects that are responsible for this K-factor, the others being the cut on the jet p_T and the jet-veto condition, which can also put constraints on initial-state radiation. We remark that, if the constraint on $\Delta\phi_{W,j}$ were moved closer to π while keeping all other cuts fixed, one would expect large logarithmic contributions $\alpha_s^n \ln^m(\pi - \Delta\phi_{W,j})$ arising from multiple initial-state soft-collinear emissions. These could be resummed, either analytically, or using Monte Carlo event generators. When adding final-state radiation, one observes that the height of the distribution in the rightmost bin is further depleted. However, due to the fact that, for $\Delta\phi_{W,j} < 3$ the NLO distributions for corrections to production only and production and decay basically coincide, this depletion cannot be ascribed to a restriction

on final-state radiation imposed indirectly through the cut on $\Delta\phi_{W,j}$. The reduction of the cross section is mainly due to the loss of QCD radiation from the $b\bar{b}$ system. Due to the jet-veto condition, any gluon that is not clustered inside the two b-jets that constitute the Higgs candidate is likely to be soft, and therefore $\Delta\phi_{W,j}$ will be close to π . It is this restriction on final-state radiation that causes an imbalance between real and virtual corrections, giving a large negative contribution.

A further source of large virtual corrections, which contribute significantly to the size of the observed K-factor, is the presence of a term $\alpha_s \ln(m_b/m_H)$ in the virtual corrections, coming from the OS renormalization of the coupling of the bottom quark to the Higgs. To investigate the impact of this term, we use a different prescription to combine NLO corrections to production and decay, by strictly expanding equation (5.2) at order α_s :

$$d\sigma_{pp \rightarrow (H \rightarrow b\bar{b})W}^{\text{exp}} = \left\{ d\sigma_{pp \rightarrow WH}^{(0)} \times \left[\frac{d\Gamma_{H \rightarrow b\bar{b}}^{(0)}}{\Gamma_{H \rightarrow b\bar{b}}^{(0)}} \left(1 - \frac{\Gamma_{H \rightarrow b\bar{b}}^{(1)}}{\Gamma_{H \rightarrow b\bar{b}}^{(0)}} \right) + \frac{d\Gamma_{H \rightarrow b\bar{b}}^{(1)}}{\Gamma_{H \rightarrow b\bar{b}}^{(0)}} \right] + d\sigma_{pp \rightarrow WH}^{(1)} \times \frac{d\Gamma_{H \rightarrow b\bar{b}}^{(0)}}{\Gamma_{H \rightarrow b\bar{b}}^{(0)}} \right\} \times \text{Br}(H \rightarrow b\bar{b}). \quad (5.6)$$

We see that the curve corresponding to this last prescription (purple, labelled ‘‘NLO exp.’’) is significantly higher than the curve corresponding to equation (5.2) (blue, labelled ‘‘NLO’’). The difference between the two prescriptions can be understood as an indication on the convergence of perturbation theory. In this respect, we have checked that all the results we have obtained in the previous section using the fat-jet procedure are, within scale uncertainties, insensitive to a change of prescription, thus indicating that this procedure is inclusive enough with respect to final-state radiation to ensure good convergence of the perturbative expansion. In the following, whenever relevant, we will use both prescriptions.

We now present the distributions studied in the previous section, this time relative to the candidate Higgs selected according to the CMS procedure, and for LHC at $\sqrt{s} = 8 \text{ TeV}$.² For the mass distribution, we will also compare the mass spectrum corresponding to the CMS analysis with that obtained with the fat-jet analysis described in section 5.2. In this case m_j will label the invariant mass of the fat jet.

Figure 5.5 contains distributions in the transverse momentum $p_{T,j}$ of the candidate Higgs dijet system. Each band corresponds to a simultaneous variation of renormalization and factorization scales for the production process

$$\frac{m_H + m_W}{2} \leq \mu_R^{(p)} \stackrel{!}{=} \mu_F^{(p)} \leq 2(m_H + m_W), \quad (5.7)$$

while renormalization scale for the decay is kept fixed at $\mu_R^{(d)} = m_H$. If one does not include NLO corrections to the decay, one observes a 20% reduction in the cross section with respect to LO. This reduction is driven mainly by the jet-veto condition, and as

²We have checked that our considerations do not change in the case of LHC at $\sqrt{s} = 7 \text{ TeV}$.

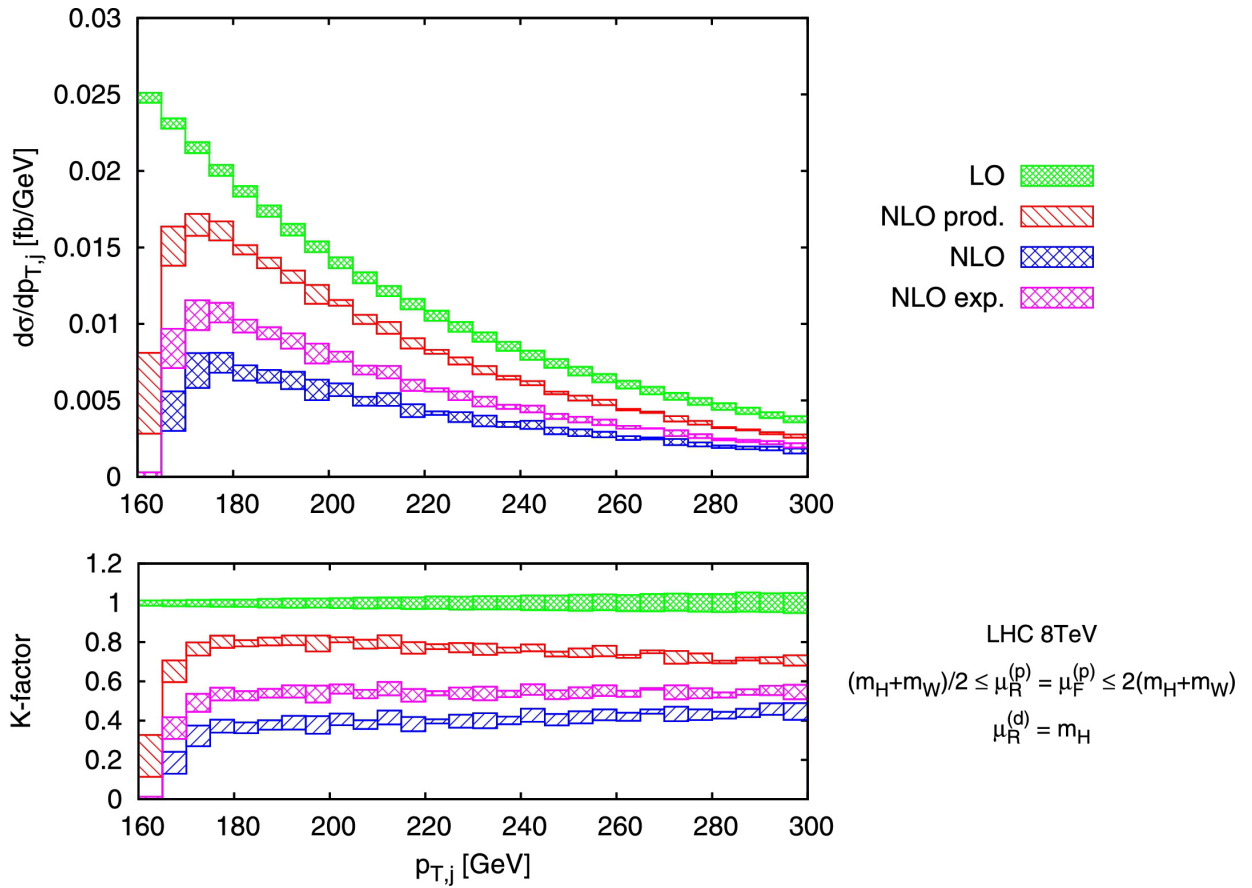


Figure 5.5: The distribution in the transverse momentum $p_{T,j}$ of the candidate Higgs dijet system, corresponding to the selection cuts described in the text.

expected gets mildly more pronounced as the dijet transverse momentum increases. The inclusion of NLO corrections to Higgs boson decay causes a further decrease of the cross section. We interpret this result as a sizable loss of QCD final-state radiation by the two jets that constitute the Higgs candidate system, likely due to the fact that the b -jets have a small radius and the typical perturbative jet p_T -loss increases with decreasing radius, as explained in reference [158], and the lost radiation undergoes a jet-veto constraint. This in turn causes a poor convergence of the perturbative series, as one observes by comparing the “NLO” (blue) and “NLO exp.” (purple) curves. We have checked that this does not happen if one performs a fat-jet analysis with the same parameters as in section 5.2, where one observes instead a K-factor of around 0.6 for $p_{T,j} > 250$ GeV, although in this case the $p_{T,j}$ distribution drops abruptly, as expected, for $p_{T,j} < 200$ GeV. We have also checked that for larger p_T values ($p_{T,j} > 350$ GeV) the CMS and fat-jet procedure give comparable $p_{T,j}$ spectra. Another remark concerns the first bin ($160 \text{ GeV} < p_{T,j} < 165 \text{ GeV}$), where the distribution is unstable against scale variations (it becomes even negative if one includes corrections to Higgs boson decay), again due to the fact that this bin corresponds to symmetric transverse momentum cuts, in which the W boson and the b -dijet system recoil against a soft-collinear gluon. This bin is not included in the CMS analysis, and will not be considered in all our subsequent studies.

We then present in figure 5.6 the distribution in the invariant mass of the candidate Higgs system $d\sigma/dm_j$. We consider here four distributions, the first (solid, red) obtained with the CMS selection procedure, the second (dashed, blue) corresponding to the fat-jet selection procedure explained at the beginning of section 5.2, with the same selection cuts as CMS for the leptons, the W boson and the candidate Higgs system, the third (dashed, green) corresponding to the CMS procedure but where only NLO corrections to the production process are considered, and the fourth (dotted, purple) again corresponding to the CMS procedure and obtained using equation (5.6).

From the plots we see that the mass distribution resulting from the CMS procedure (red, solid), catches more candidate Higgs events than the fat-jet one, as expected due to the lower p_T -cut on the selected b -jets. However, the mass distribution does not display a mass peak in the expected position. In fact the value of the distribution at $m_j = 125$ GeV is negative (see inset plot of figure 5.6) if one uses equation (5.2), and only slightly positive if one uses instead equation (5.6) (the purple dotted curve labelled “CMS exp.”). Regardless of the actual value of the distribution at $m_j = 125$ GeV, this clearly indicates that radiation from the $b\bar{b}$ pair originating from Higgs boson decay is not naturally included in the candidate Higgs system. On the contrary, the fat-jet procedure (blue, dashed) gives correctly a peak at $m_j = 125$ GeV, although with a reduced height with respect to that of the shifted peak resulting from the CMS procedure. This result does not change if one uses the alternative prescription of equation (5.6). The third curve (green, dashed) shows the mass distribution obtained by considering NLO corrections to production only.

We notice that the peak is in the expected position, with a height that is roughly five times larger than that of the peak corresponding to the fat-jet procedure. In this respect, we remark that the parameters we have chosen for the fat-jet analysis are identical to those of section 5.2. In principle one should redetermine their optimal value after a full

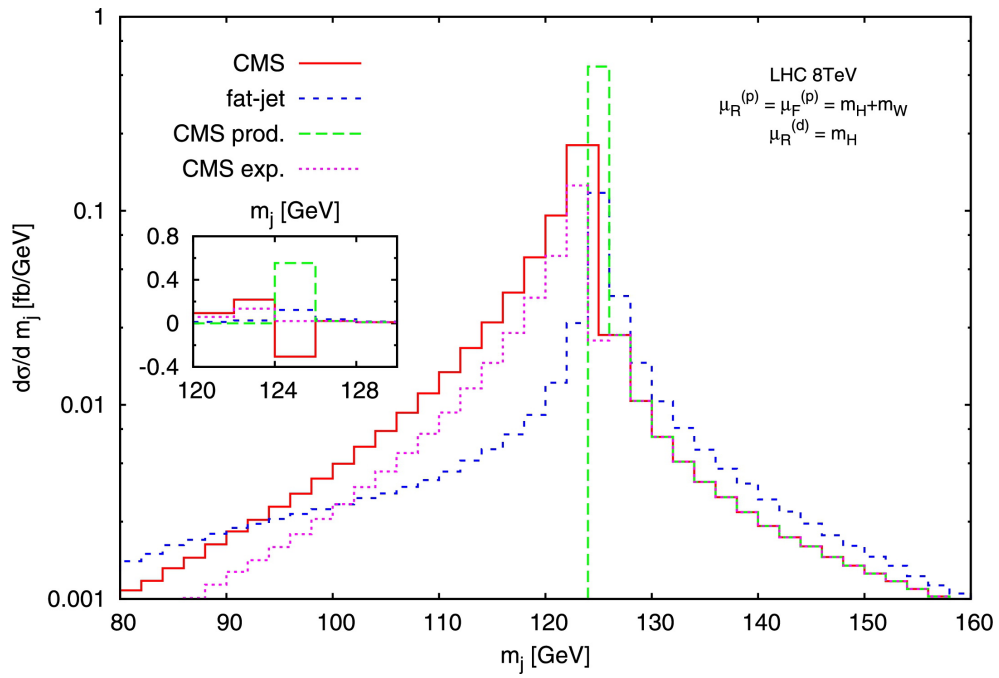


Figure 5.6: The distribution in the invariant mass m_j of the candidate Higgs jet obtained with the procedure adopted by CMS, with and without NLO corrections to Higgs decay, and with the fat-jet procedure described in section 5.2.

simulation of signal and background, including parton shower effects (for instance using the recent developments of reference [147]).

Chapter 6

Conclusion

We have implemented NLO corrections to Higgs boson production in association with a leptonically decaying W boson and to its subsequent decay into a bottom quark-antiquark pair, in a numerical code that returns weighted events, fully differential in the decay products of the Higgs boson and of the W boson. We have then looked at how NLO QCD corrections to Higgs boson decay affect various observables that are relevant for Higgs searches at the LHC. In particular, we have analyzed two different experimental setups, one with $\sqrt{s} = 14$ TeV and the other with $\sqrt{s} = 8$ TeV.

In the first case, the Higgs boson is produced in a boosted regime, with its transverse momentum larger than its mass, and detected using the fat-jet technique proposed in reference [131]. With our study in section 5.2, we assess that the Higgs candidate obtained with the fat-jet procedure is stable against radiative corrections. Its mass distribution is peaked at the expected value of the Higgs boson mass and the resolution of the peak is reasonably good (see figure 5.3). We remark that the height of the peak is sensitive to the jet-veto condition that one imposes on any jet besides the candidate Higgs fat jet, the stronger the veto the stronger the suppression of the peak. In our case the height of the peak obtained after imposing a jet-veto condition is roughly a third of that we get if we are fully inclusive with respect to all jets.

The second experimental setup we have considered corresponds to the event selection done at that point by the CMS experiment, but for the LHC current energy $\sqrt{s} = 8$ TeV. CMS chooses configurations in which both the Higgs boson and the W boson have high transverse momentum. Then they do not perform a full fat-jet analysis, but rather consider as a Higgs candidate a system of two b-jets satisfying a set of transverse momentum and rapidity cuts. Again we have checked how relevant distributions are influenced by QCD corrections to Higgs boson decay. We have found that such corrections have a big impact both on the candidate Higgs transverse momentum spectrum and on its invariant mass distribution. In particular, for the latter it turns out that the effect of an extra jet-veto and the loss of QCD radiation from the $b\bar{b}$ system give a displacement of the mass peak from its expected position, with a poor peak resolution. This suggests an instability of the CMS procedure against radiative corrections from the final state, and reveals how important it is to have NLO information on the Higgs boson decay as well. We remark

that the use of a parton shower event generator will give a smoother mass distribution, but will not significantly improve the mass resolution of the peak, which is mainly affected by the large p_T loss of the selected b-jets. For comparison we have also studied the jet-mass distribution for a candidate Higgs jet obtained with the same fat-jet procedure considered for the LHC at $\sqrt{s} = 14$ TeV. Also in this case the procedure seems stable under radiative corrections, and we are able to reconstruct a mass peak in the expected position.

The study we have performed gives some new information on the impact of higher-order corrections on the Higgsstrahlung process. An analogous study for the ZH production process can be achieved by changing the couplings and PDFs used.

More studies are needed both to improve the accuracy of the calculation, including for instance NNLO corrections to both production and decay, such as the one presented in reference [141]. Furthermore, it is necessary to devise procedures to cure the instabilities we have found in our analysis.

Part III

QCD corrections for $\gamma^*\gamma^*$ production

Chapter 7

Introduction

In this part, we shall present the investigation performed on the QCD corrections to the $\gamma^*\gamma^*$ production process. This is a first step towards the study of the general class of diboson processes which, as the name suggests, involve two EW vector bosons in the final state, that may be different. This process is interesting from the theoretical point of view because it can involve multiple scales: besides the kinematical invariants, the masses/virtualities of the final state bosons enter the game and make the treatment all the more challenging. It is also particularly relevant from the experimental point of view because it is a background process for Higgs searches for example in the “golden channel” where the Higgs decays to a pair of Z bosons or when looking for a Higgs decaying to a pair of W bosons as in both cases the vector bosons are kinematically driven to have different virtualities (one being in general on-shell due to the resonance enhancement). Therefore precise and reliable estimations of the contribution to the background of these processes including perturbative corrections beyond the LO in QCD constitute a priority.

Currently, the computation of this process are known differentially up to NLO in QCD [159–165]. The status of the NNLO corrections to diboson production is the following: The full result is known since a couple of years for $\gamma\gamma$ production [166]. For the equal-mass case, which is relevant for WW and ZZ production, the 2-loop master integrals have been computed in references [167, 168], and the inclusive ZZ production has just been published [169]. For unequal masses, which encompasses $W\gamma^{(*)}$, WW^* , $W^{(*)}Z^{(*)}$, $Z\gamma^{(*)}$, and ZZ^* production, the 2-loop master integrals have been published [170, 171] while this work was in progress, furthermore all the 2-loop QCD helicity amplitudes are also available [172, 173].

In the following chapters, we will present the ingredients entering the computation of the cross-section corrections at NNLO in QCD for a gauge invariant subset of the diagrams involved in the process $pp \rightarrow \gamma^*\gamma^*$, namely those coming from N_f massless quark flavors.

In chapter 8, we concentrate on the 2-loop virtual amplitudes and express these in terms of master integrals using established reduction methods. We shall present the organization of the reduction in the general case and then spell out the result for the N_f piece which consists of diagrams with a light quark loop. We evaluate the latter with direct integration methods along the lines of reference [115]. We tackle the corresponding piece for the double-

real radiation in chapter 9, where we shall present the implementation of a subtraction method after we parametrize the phase-space hierarchically which makes all IR singularities appear in a factorized form. Finally in chapter 10 we present some distributions obtained when combining both virtual and real corrections in an in-house event generator.

Chapter 8

Virtual corrections

In this chapter we present the steps of the computation of the 1- and a gauge-invariant subset of the full 2-loop correction to the $q\bar{q} \rightarrow \gamma^*\gamma^*$ process, where both photons are off-shell with non-related virtualities. We will detail the treatment of the 2-loop case: the one-loop computation goes along the same lines, but involves less subtleties.

We will focus on the computation of the unrenormalized 2-loop contribution. The renormalized 2-loop virtual contribution that has been implemented for the numerical results presented in chapter 10 can be written in terms of the bare one as

$$d\sigma_{VV}^{q\bar{q}} = d\sigma_{VV}^{U;q\bar{q}} - \frac{\beta_0|_{N_f}}{\varepsilon} a_s d\sigma_V^{q\bar{q}}. \quad (8.1)$$

After we present the generation and reduction framework in the general case, we will restrict the discussion to a subset of the full amplitude in the last section.

8.1 Generation

The diagrams relevant to the 0-, 1- and 2-loop amplitudes are generated using **QGRAF** [59]. The 1-loop diagrams contain one more internal gluon propagator than the tree-level process. Out of the 12 diagrams, 4 vanish due to color, leaving 8 diagrams. The 2-loop diagrams have one more loop and can thus have an extra (heavy or massless) fermion, gluon, or ghost loop. Out of the 198 diagrams, 54 vanish due to color (section 1.2.2), leaving 144 diagrams.

At NLO, the amplitude is obtained by computing the interference of the 1-loop diagrams with the 0-loop diagrams. At NNLO, the amplitude is obtained by computing the interference of the 2-loop diagrams with the 0-loop diagrams, and by the squared sum of the 1-loop diagrams. We map these expressions to integrals within standard topologies according to their propagator structure, we reduce each integral to a set of master integrals using the Laporta algorithm [100] and we evaluate the master integrals analytically. In what follows we describe these steps in more detail.

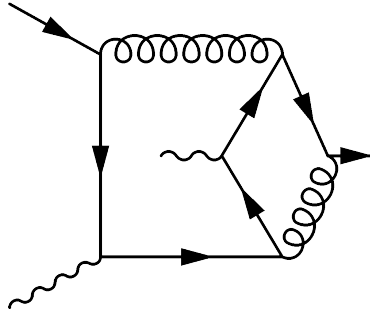


Figure 8.1: This diagram belongs to the \mathcal{X} topology class.

8.2 Mapping to topologies

In what follows, we will detail the treatment of the 2-loop case: the 1-loop computation goes along the same lines, but involves less subtleties.

The loop momenta k and l are assigned by QGRAF but we are free to transform them using transformations that do not alter the measure of the loop momenta, i.e. for which the determinant of the Jacobian is unity.

The invariance under such transformations is used to organize the calculation and classify the diagrams into topology classes that depend exclusively on the denominator structure. For each diagram, we generate the image under all authorized transformations and match the result with the standard form for each of the topology classes \mathcal{P} of planar diagrams or \mathcal{X} of non-planar diagrams. In the implementation, a diagram from the \mathcal{X} class as the one shown in figure 8.1 is characterized as follows: it is not possible to find a transformation of the loop momenta which reduces the number of propagators containing both k and l to one.

At this stage each diagram is written as (section 2.6):

$$\frac{N(\{k, l, q_1, q_2, q_3\})}{D_1^{n_1}(q_1, q_2, q_3) \cdots D_9^{n_9}(q_1, q_2, q_3)}$$

where for both classes ($q_{1\dots n} \equiv q_1 + \cdots + q_n$),

$$\begin{aligned} D_1 &= k^2, & D_2 &= (k + q_1)^2, & D_3 &= (k + q_{12})^2, & D_9 &= (k - l)^2. \\ D_5 &= l^2, & D_6 &= (l + q_1)^2, & D_7 &= (l + q_{12})^2, & D_8 &= (l + q_{123})^2, \end{aligned} \quad (8.2)$$

while, depending on the topology class,

$$\mathcal{P} : D_4 = (k + q_{123})^2, \quad \mathcal{X} : D_4 = (l - k + q_{123})^2. \quad (8.3)$$

and N is a polynomial of all the possible scalar products of independent external¹ and loop momenta which comes from the translation of the diagram with the Feynman rules of

¹We stress that the momenta q_1, \dots, q_3 can be any three of the four independent momenta.

QED and QCD (sections 1.2.1 and 1.3.2). We use the Feynman gauge $\xi = 1$ for the gluon propagator and the polarization sum for a photon with 4-momentum p reads

$$\sum_{\lambda} (\varepsilon_{\lambda}^{\mu})^*(p) \varepsilon_{\lambda}^{\nu}(p) = -g^{\mu\nu} + \frac{p^{\mu} p^{\nu}}{p^2}, \quad (8.4)$$

where the second piece does not contribute because of the Ward identity for the off-shell photon. We evaluate the chains of γ -matrices in $d = 4 - 2\varepsilon$ dimensions using a housemade set of routines coded in FORM [60, 61]. All the scalar products in N are expressed in terms of the denominators. The relation is obtained by inverting (8.2) and (8.3). For the class-independent products:

$$\begin{aligned} k^2 &= D_1, & l^2 &= D_5, \\ 2k \cdot q_1 &= D_2 - D_1 - q_1^2, & 2l \cdot q_1 &= D_6 - D_5 - q_1^2, \\ 2k \cdot q_2 &= D_3 - D_2 + q_1^2 - q_{12}^2, & 2l \cdot q_2 &= D_7 - D_6 + q_1^2 - q_{12}^2, \\ 2k \cdot l &= D_1 + D_5 - D_9, & 2l \cdot q_3 &= D_8 - D_7 + q_{12}^2 - q_{123}^2, \end{aligned}$$

while for class-dependent product:

$$\begin{aligned} \mathcal{P} : 2k \cdot q_3 &= D_4 - D_3 + q_{12}^2 - q_{123}^2, \\ \mathcal{X} : 2k \cdot q_3 &= D_1 - D_3 - D_4 - D_5 + D_8 + D_9 + q_{12}^2. \end{aligned}$$

which allows to rewrite N as a polynomial in the denominators and the invariants s, t, u, s_3, s_4 . Each term can then be expressed as a sum

$$\mathcal{T} : \sum_i f_i(s, t, u, s_3, s_4) T(n_{1,i}, \dots, n_{9,i}, q_1, q_2, q_3) \quad (8.5)$$

where for the topology class $\mathcal{T} \in \{\mathcal{P}, \mathcal{X}\}$ we have defined the *topology* T :

$$\mathcal{T} : T(n_1, \dots, n_9, q_1, q_2, q_3) \equiv \prod_{i=1}^9 D_i^{-n_i}(q_1, q_2, q_3). \quad (8.6)$$

We have now brought all terms into *scalar* integrals, which are characterized by integer indices and three independent momenta.

Before moving to the presentation of the reduction, we would like to stress that there is still in principle some level of arbitrariness with this setup due to the residual invariance of the result under transformations of the loop momenta (in particular swapping): different naming of the same inherent topology with different momenta can occur. For example,

$$P(n_1, \dots, n_9, p_1, p_2, p_3) = P(n_1, n_4, n_3, n_2, n_5, n_8, n_7, n_6, n_9, p_4, p_3, p_2),$$

as can be seen by substituting $p_1 = -p_2 - p_3 - p_4$ and applying the transformation $(k, l) \mapsto (-k, -l)$ in the left hand side expression. This has no influence on the final result, but can impair computational efficiency as it would make us reduce two equivalent off-shell classes (section 2.6.4). If two general off-shell classes are connected as in the example above, we only need to perform the reduction on one of them and we can get the other one by transformation.

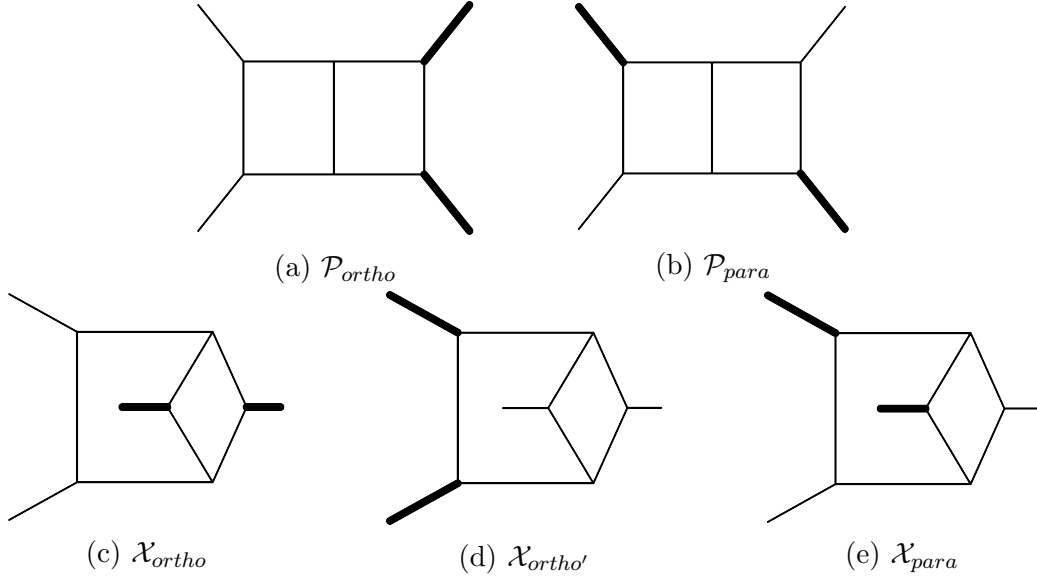


Figure 8.2: Mass classes of 2-loop 2-scale topologies. Thick external lines denote the non-light-like momenta.

8.3 Reduction with AIR

The reduction of the integrals to master integrals is performed with AIR [78] which is based on Laporta's algorithm [100]. The description of the ingredients necessary is done in section 2.6.5. We list here the specific ingredients needed for the case under study.

Off-shell classes The integrals are assigned to one of five off-shell topology classes relevant to our process:

$$\begin{aligned}
 q_1^2 = 0, q_2^2 = 0, q_3^2 \neq 0 &\Rightarrow P(\dots, q_1, q_2, q_3) \in \mathcal{P}_{ortho} \\
 q_1^2 = 0, q_2^2 \neq 0, q_3^2 = 0 &\Rightarrow P(\dots, q_1, q_2, q_3) \in \mathcal{P}_{para} \\
 q_1^2 = 0, q_2^2 = 0, q_3^2 \neq 0 &\Rightarrow X(\dots, q_1, q_2, q_3) \in \mathcal{X}_{ortho} \\
 q_1^2 \neq 0, q_2^2 \neq 0, q_3^2 = 0 &\Rightarrow X(\dots, q_1, q_2, q_3) \in \mathcal{X}_{ortho'} \\
 q_1^2 = 0, q_2^2 \neq 0, q_3^2 = 0 &\Rightarrow X(\dots, q_1, q_2, q_3) \in \mathcal{X}_{para}
 \end{aligned} \tag{8.7}$$

The off-shell classes are shown pictorially in figure 8.2, where the thick lines correspond to non-light-like external momenta.

The reduction of each off-shell class is performed separately, with the IBPs (and LIs) specific to this off-shell configuration.

Zero topologies Using the notation of section 2.6.4, a topology vanishes as soon as one of the constraints is fulfilled (note that when we use $\bar{\Theta}$, the condition requires also

$\Theta(n_5, n_6) = 0$):

$$\begin{aligned} Z[\mathcal{P}_{ortho}] = \{ & \Theta(n_1, \dots, n_9) < 3, \Theta(n_1, \dots, n_4, n_9) < 2, \Theta(n_5, \dots, n_9) < 2, \\ & \Theta(n_1, n_2, n_3, n_5, n_6, n_7) < 1, \Theta(n_2, n_3, n_4, n_6, n_7, n_8) < 1, \\ & \Theta(n_1, n_4, n_5, n_8) < 1, \Theta(n_3, n_4, n_7, n_8) < 1, \\ & \Theta(n_1, n_4, n_9) < 1, \Theta(n_3, n_4, n_9) < 1, \Theta(n_5, n_8, n_9) < 1, \Theta(n_7, n_8, n_9) < 1\}, \end{aligned} \quad (8.8)$$

$$\begin{aligned} Z[\mathcal{P}_{para}] = \{ & \Theta(n_1, \dots, n_9) < 3, \Theta(n_1, \dots, n_4, n_9) < 2, \Theta(n_5, \dots, n_9) < 2, \\ & \Theta(n_1, n_2, n_3, n_5, n_6, n_7) < 1, \Theta(n_2, n_3, n_4, n_6, n_7, n_8) < 1, \\ & \Theta(n_1, n_2, n_5, n_6) < 1, \Theta(n_3, n_4, n_7, n_8) < 1, \\ & \Theta(n_1, n_2, n_9) < 1, \Theta(n_3, n_4, n_9) < 1, \Theta(n_5, n_6, n_9) < 1, \Theta(n_7, n_8, n_9) < 1\}, \end{aligned} \quad (8.9)$$

$$\begin{aligned} Z[\mathcal{X}_{ortho}] = \{ & \Theta(n_1, \dots, n_9) < 3, \\ & \Theta(n_1, \dots, n_4, n_9) < 2, \Theta(n_1, n_2, n_3, n_5, \dots, n_8) < 2, \Theta(n_4, \dots, n_9) < 2, \\ & \Theta(n_4, n_5, n_8, n_9) < 1, \Theta(n_4, n_7, n_8, n_9) < 1, \\ & \bar{\Theta}(n_1, n_4, n_9) < 1, \bar{\Theta}(n_1, n_7, n_8) < 1, \bar{\Theta}(n_3, n_7, n_8) < 1, \bar{\Theta}(n_3, n_7, n_9) < 1\}, \end{aligned} \quad (8.10)$$

$$\begin{aligned} Z[\mathcal{X}_{ortho}'] = \{ & \Theta(n_1, \dots, n_9) < 3, \\ & \Theta(n_1, \dots, n_4, n_9) < 2, \Theta(n_1, n_2, n_3, n_5, \dots, n_8) < 2, \Theta(n_4, \dots, n_9) < 2, \\ & \Theta(n_3, n_4, n_7, n_8) < 1, \Theta(n_4, n_7, n_8, n_9) < 1, \\ & \bar{\Theta}(n_1, n_2, n_4, n_7) < 1, \bar{\Theta}(n_1, n_2, n_4, n_8) < 1, \bar{\Theta}(n_2, n_3, n_8, n_9) < 1, \\ & \bar{\Theta}(n_1, n_2, n_3) < 1, \bar{\Theta}(n_1, n_2, n_4) < 1, \bar{\Theta}(n_2, n_3, n_9) < 1, \bar{\Theta}(n_4, n_9) < 1\}, \end{aligned} \quad (8.11)$$

$$\begin{aligned} Z[\mathcal{X}_{para}] = \{ & \Theta(n_1, \dots, n_9) < 3, \\ & \Theta(n_1, \dots, n_4, n_9) < 2, \Theta(n_1, n_2, n_3, n_5, \dots, n_8) < 2, \Theta(n_4, \dots, n_9) < 2, \\ & \Theta(n_3, n_4, n_7, n_8) < 1, \Theta(n_3, n_4, n_9) < 1, \\ & \bar{\Theta}(n_1, n_2, n_4, n_7) < 1, \bar{\Theta}(n_1, n_2, n_4, n_8) < 1, \bar{\Theta}(n_2, n_3, n_8, n_9) < 1, \\ & \bar{\Theta}(n_1, n_2, n_3) < 1, \bar{\Theta}(n_1, n_2, n_4) < 1, \bar{\Theta}(n_2, n_3, n_9) < 1, \bar{\Theta}(n_4, n_9) < 1\}. \end{aligned} \quad (8.12)$$

Seeds The set of seeds should contain all the scalar topologies appearing in the process that have been obtained as discussed in the last section.

We find for the process at hand, that independently of the off-shell class, the maximum number of propagators is 7, while the minimum number of propagators is 3. Furthermore the sum of the absolute values of the negative indices ranges from 0 to 4 for all off-shell classes. Some integrals of the off-shell classes \mathcal{P}_{ortho} and \mathcal{X}_{ortho}' present one dotted propagator, while the other classes only have simple propagators. Finally, no integrals of the off-shell classes \mathcal{X}_{ortho} or \mathcal{X}_{para} have propagators in the fifth and sixth position. They can however have negative indices at these positions.

Once the reduction is completed, the amplitude can be written as a sum of rational coefficients of the invariants multiplying the master integrals.

In the next section, we present the results for a gauge-invariant subset of the full amplitude.

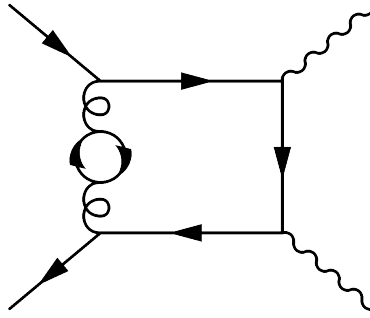


Figure 8.3: Diagram contributing to the 2-loop N_f -piece of the process $q\bar{q} \rightarrow \gamma^*\gamma^*$.

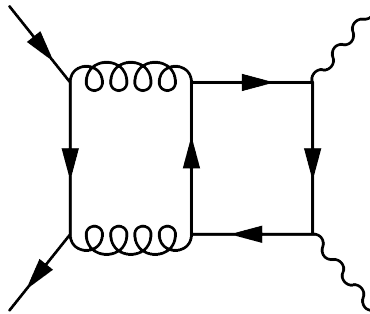


Figure 8.4: Diagram *not* contributing to the 2-loop N_f -piece of the process $q\bar{q} \rightarrow \gamma^*\gamma^*$.

8.4 Double-virtual N_f amplitude

We present in this section the first results for a gauge-invariant subset of the diagrams having an internal massless quark loop inserted, like the one shown in figure 8.3. These are in one-to-one correspondence with the 1-loop diagrams where the gluon propagator is replaced by its one-loop self energy diagram, and they are multiplied by a factor N_f , which denotes the number of massless quark flavors.

Note that diagrams involving a quark loop that is connected to one or both external photons – like the one shown in figure 8.4 – do not belong to the N_f -piece as they are proportional to the electromagnetic charge of the individual quarks in the fermion loop.

For the process under study, it is possible to bring all diagrams to integrals of the form

$$P(n_1, \dots, n_9, p_1, p_2, p_3), \quad \text{or} \quad P(n_1, \dots, n_9, p_1, p_2, p_4),$$

where the coefficients n_1 , n_3 and n_4 are negative or vanish. This defines a subclass of \mathcal{P}_{ortho} which is faster to reduce as it involves less propagators.

After reduction, we find that we can express the 2-loop N_f -piece through twelve master integrals. Six of them are:

$$P(0, 1, 0, 0, 0, 0, 0, 1, 1, p_1, p_2, p_4) = {}_{p_{24}} \text{---} \bigcirc \quad (8.13a)$$

$$P(0, 1, 0, 0, 1, 0, 1, 0, 1, p_1, p_2, p_4) = \text{Diagram (8.13b)} \quad (8.13b)$$

$$P(0, 1, 0, 0, 1, 0, 0, 1, 1, p_1, p_2, p_4) = \text{Diagram (8.13c)} \quad (8.13c)$$

$$P(0, 1, 0, 0, 0, 0, 1, 1, 1, p_1, p_2, p_4) = \text{Diagram (8.13d)} \quad (8.13d)$$

$$P(0, 1, 0, 0, 1, 0, 1, 1, 1, p_1, p_2, p_4) = \text{Diagram (8.13e)} \quad (8.13e)$$

$$P(0, 1, 0, 0, 1, 0, 1, 1, 2, p_1, p_2, p_4) = \text{Diagram (8.13f)} \quad (8.13f)$$

and the other six can be obtained by setting $p_4 \rightarrow p_3$ in the above.

The coefficients of the master integrals for the N_f -piece of the unrenormalized 2-loop amplitude can be found in the appendix B.

The integrals of interest depend on four scales, one of which can be factored out so that we can work with the ratios u, v, w :

$$\begin{aligned} p_1^2 = 0, \quad p_2^2 = 0, \quad p_3^2 = m_3^2, \quad p_4^2 = m_4^2, \\ s = (p_1 + p_2)^2, \quad t = (p_1 + p_3)^2, \\ u = \frac{p_3^2}{s}, \quad v = \frac{p_4^2}{s}, \quad w = \frac{t}{s}. \end{aligned} \quad (8.14)$$

It can be convenient to write u and v in terms of two new variables z, \bar{z} :

$$\begin{aligned} z, \bar{z} = \frac{1}{2} \left(1 + u - v \pm \sqrt{\lambda(u, v, 1)} \right), \\ u = z\bar{z}, \quad v = (1 - z)(1 - \bar{z}), \end{aligned} \quad (8.15)$$

where $\lambda(a, b, c) = a^2 + b^2 + c^2 - 2ab - 2ac - 2bc$ is the Källén function. The same parametrization was used for the three-mass triangle integrals in ref. [115], except that now there is one more scale (w). We work in the Euclidean region where $p_i^2 \leq 0$, $i = 1, \dots, 4$, and thus u, v, w are positive. Moreover, in analogy to the case of the three-mass triangles, we first compute the integrals in the region where $\lambda(1, u, v) < 0$ and thus z and \bar{z} are complex conjugate to each other. In this region the functions are well defined and have no branch cuts in the complex z plane.

The analytic expressions contain the functions $\mathcal{P}_w(z)$, $\mathcal{Q}_3^\pm(z)$ and \mathcal{R}_3^\pm , besides ordinary logarithms and classical polylogarithms. The full expressions of these functions and of the master integrals needed are given in reference [2].

8.4.1 Computation of the master integrals

In this section we describe briefly how we computed the master integrals using the techniques presented in section 2.7 and illustrate some of the steps with an example. From the computation philosophy point of view, the approach is the same as in reference [115], also known as symbolic integration. A more detailed treatment can be found in reference [114].

The general procedure is the following. We represent the integrals in the Feynman parametrization (section 2.7.2) and expand the integrand in the dimensional regularization parameter ε . Since the integrals diverge as $\varepsilon \rightarrow 0$ and in addition some of the singularities overlap, we will factorize these singularities with the method of non-linear mappings [79] and perform the expansion in ε with the help of +-distributions (section 2.3.2). We then perform the integration order by order working with multiple polylogarithms $G(a_1, \dots, a_n; t)$, which we have defined along with their main properties in section 2.7.3. After the (trivial) integration over the first Feynman parameter, we write all the gained (poly)logarithms in the integrand as (a sum of) multiple polylogarithms (MPLs) where the Feynman parameter which we want to integrate next has to be in the last argument, in order to be able to use the recursive definition (2.70). Note that all the denominators in the integral need to be linear, i.e. of the form $t \pm a$, where a is a linear function of the remaining integration variables. This is the case for the integrals we consider. Moreover, the MPLs in the numerator have to be written as a sum without products of MPLs left. This can be achieved using the shuffle algebra of MPLs (2.72) [116].

Using partial fractioning and the shuffle algebra, we can express the MPLs in the form where we can make use of equation (2.70). We then repeat these steps for each Feynman parameter of the integral. The main challenge in the later steps consists in rewriting the MPLs such that the next Feynman parameter we integrate is again the last argument. In order to find the functional equations among MPLs which allow us to perform this task, we make use of the Hopf algebra structure of these functions and its coproduct [117, 174]. An algorithm to obtain the right form is given in [175].

Let us illustrate the steps mentioned so far with one of the two boxes appearing in the N_f part of the two-loop amplitude as an example:

$$B_{2a} = \begin{array}{c} p_1 \text{---} \text{---} p_3 \\ \diagup \quad \diagdown \\ \bullet \\ \diagdown \quad \diagup \\ p_2 \text{---} \text{---} p_4 \end{array} = e^{2\gamma_E \varepsilon} \int \frac{d^d k d^d l}{(i\pi^{d/2})^2} \frac{1}{(k+l)^4 (k+p_1)^2 (k+p_{13})^2 (k+p_{134})^2 l^2}, \quad (8.16)$$

where $p_{i\dots j} = p_i + \dots + p_j$.

First we need to parametrize the integral and factorize the singularities. Note that the 2-loop integrals relevant for the N_f piece of the NNLO correction to $q\bar{q} \rightarrow \gamma^* \gamma^*$ are practically 1-loop boxes with inserted bubble integrals. We integrate the bubble sub-integral out using the formula

$$\int \frac{d^d l}{i\pi^{d/2}} \frac{1}{[l^2]^{\nu_a} [(k+l)^2]^{\nu_b}} = (-1)^{\frac{d}{2}} (k^2)^{\frac{d}{2} - \nu_a - \nu_b} \frac{\Gamma(\nu_a + \nu_b - \frac{d}{2}) \Gamma(\frac{d}{2} - \nu_a) \Gamma(\frac{d}{2} - \nu_b)}{\Gamma(\nu_a) \Gamma(\nu_b) \Gamma(d - \nu_a - \nu_b)}, \quad (8.17)$$

which is obtained using equations (A.3) and (A.4), and obtain one-loop boxes with one of the propagators raised to an ε -dependent power. More precisely, the 2-loop integrals can

be written as

$$(-1)^{\frac{d}{2}} e^{2\gamma_E \varepsilon} \frac{\Gamma(\nu_a + \nu_b - \frac{d}{2}) \Gamma(\frac{d}{2} - \nu_a) \Gamma(\frac{d}{2} - \nu_b)}{\Gamma(\nu_a) \Gamma(\nu_b) \Gamma(d - \nu_a - \nu_b)} \int_0^1 \left(\prod_{i=1}^4 dx_i \right) \text{fp}(\nu_1, \nu_2, \nu_3, \nu_4, d), \quad (8.18)$$

where ν_a and ν_b are the powers of the propagators of the bubble integral and $\text{fp}(\nu_1, \nu_2, \nu_3, \nu_4, d)$ is the usual Feynman parametrization of the 1-loop box integral for arbitrary powers ν_i of propagators in d dimensions

$$\begin{aligned} \text{fp}(\nu_1, \nu_2, \nu_3, \nu_4, d) &\equiv \frac{(-1)^{\frac{d}{2}} \Gamma(\nu - \frac{d}{2})}{\prod_i \Gamma(\nu_i)} \delta \left(1 - \sum_i x_i \right) x_1^{\nu_1-1} x_2^{\nu_2-1} x_3^{\nu_3-1} x_4^{\nu_4-1} \\ &\times (x_1 + x_2 + x_3 + x_4)^{\nu-d} (s x_2 x_4 + t x_1 x_3 + m_3^2 x_2 x_3 + m_4^2 x_3 x_4)^{\frac{d}{2}-\nu}. \end{aligned} \quad (8.19)$$

In the case of B_{2a} , the propagator between the legs p_1 and p_2 is raised to the power $1 + \varepsilon$:

$$\begin{aligned} \text{fp}(1 + \varepsilon, 1, 1, 1, 4 - 2\varepsilon) &= \frac{(-1)^{2-\varepsilon} \Gamma(2 + 2\varepsilon)}{\Gamma(1 + \varepsilon)} \delta \left(1 - \sum x_i \right) \left(\sum x_i \right)^{3\varepsilon} \\ &\times x_1^\varepsilon (m_4^2 x_3 x_4 + m_3^2 x_2 x_3 + x_1 x_3 t + x_2 x_4 s)^{-2-2\varepsilon}. \end{aligned} \quad (8.20)$$

Performing the following mapping,

$$x_i \mapsto \frac{x_i}{\sum_j x_j A_j}, \quad (8.21)$$

where the A_j are not specified for the moment, we obtain for the right hand side of equation (8.20),

$$\frac{(-1)^{2-\varepsilon} \Gamma(2 + 2\varepsilon)}{\Gamma(1 + \varepsilon)} \frac{\delta \left(1 - \sum x_i \right) A_1^{1+\varepsilon} A_2 A_3 A_4 \left(\sum x_i A_i \right)^{3\varepsilon} x_1^\varepsilon}{(s A_2 A_4 x_2 x_4 + t A_1 A_3 x_1 x_3 + m_3^2 A_2 A_3 x_2 x_3 + m_4^2 A_3 A_4 x_3 x_4)^{2+\varepsilon}}. \quad (8.22)$$

It is possible to remove all the kinematical dependencies from the denominator by solving the system of equations [176]

$$A_2 A_4 = 1/s, \quad A_1 A_3 = 1/t, \quad A_2 A_3 = 1/m_3^2, \quad A_3 A_4 = 1/m_4^2. \quad (8.23)$$

We obtain the solution for $s > 0$:

$$A_1 = \sqrt{\frac{m_3^2 m_4^2}{s t^2}}, \quad A_2 = \sqrt{\frac{m_4^2}{s m_3^2}}, \quad A_3 = \sqrt{\frac{s}{m_3^2 m_4^2}}, \quad A_4 = \sqrt{\frac{m_3^2}{s m_4^2}}, \quad (8.24)$$

and end up with

$$\frac{(-1)^{2-\varepsilon} \Gamma(2 + 2\varepsilon)}{\Gamma(1 + \varepsilon)} \frac{\delta \left(1 - \sum x_i \right) A_1^{1+\varepsilon} A_2 A_3 A_4 \left(\sum x_i A_i \right)^{3\varepsilon} x_1^\varepsilon}{(x_2 x_4 + x_3 (x_1 + x_2 + x_4))^{2+2\varepsilon}}. \quad (8.25)$$

The δ -distribution can be solved choosing for example

$$x_3 = y_1, \quad x_2 = (1 - y_1)y_2, \quad x_4 = (1 - y_1)(1 - y_2)y_3, \quad x_1 = (1 - y_1)(1 - y_2)(1 - y_3), \quad (8.26)$$

where the Jacobian of the transformation is $(1 - y_1)^2(1 - y_2)$. Writing $\bar{y}_i = 1 - y_i$ we arrive at

$$\frac{(-1)^{2-\varepsilon}\Gamma(2+2\varepsilon)}{\Gamma(1+\varepsilon)} \frac{A_1^{1+\varepsilon} A_2 A_3 A_4 (\sum x_i A_i)^{3\varepsilon} \bar{y}_1^{-\varepsilon} \bar{y}_2^{1+\varepsilon} \bar{y}_3^\varepsilon}{(\bar{y}_1 y_2 \bar{y}_2 y_3 + y_1)^{2+2\varepsilon}}, \quad (8.27)$$

where for the moment we did not make the change of variables in the sum $(\sum x_i A_i)^{3\varepsilon}$ for better readability. We obtain overlapping singularities for $y_1 = 0$ and either $y_2 = 0$, $y_2 = 1$ or $y_3 = 0$. These can be factorized completely by the following non-linear mapping

$$y_1 \mapsto \frac{y_1 y_2 \bar{y}_2 y_3}{y_1 y_2 \bar{y}_2 y_3 + \bar{y}_1}. \quad (8.28)$$

The Jacobian is cancelled entirely and we end up with an integral free of overlapping singularities. Putting everything together using equation (8.18) with $\nu_a = 2$ and $\nu_b = 1$, we obtain:

$$B_{2a} = -(-1)^{4-2\varepsilon} \frac{c_\Gamma^2}{\varepsilon} \frac{\Gamma(1-2\varepsilon)\Gamma(2+2\varepsilon)}{\Gamma(1-\varepsilon)^2\Gamma(1+\varepsilon)^2} \int_0^1 \left(\prod_{n=1}^3 dy_i \right) y_2^{-1-2\varepsilon} y_3^{-1-2\varepsilon} \times A_1^{1+\varepsilon} A_2 A_3 A_4 \bar{y}_1^{-\varepsilon} \bar{y}_2^{-\varepsilon} \bar{y}_3^\varepsilon (\bar{y}_1 y_2 A_2 + y_1 y_2 \bar{y}_2 y_3 A_3 + \bar{y}_1 \bar{y}_2 y_3 A_4 + \bar{y}_1 \bar{y}_2 \bar{y}_3 A_1)^{3\varepsilon}, \quad (8.29)$$

where

$$c_\Gamma \equiv e^{\gamma_E \varepsilon} \frac{\Gamma(1+\varepsilon)\Gamma(1-\varepsilon)^2}{\Gamma(1-2\varepsilon)}. \quad (8.30)$$

Substituting the expressions for the A_j 's (8.24) and using the variables u, v, w we obtain finally the following parametrization for B_{2a} :

$$B_{2a} = -\frac{c_\Gamma^2}{\varepsilon} \frac{\Gamma(1-2\varepsilon)\Gamma(2+2\varepsilon)}{\Gamma(1-\varepsilon)^2\Gamma(1+\varepsilon)^2} (-s)^{-2-2\varepsilon} u^{-\varepsilon} v^{-\varepsilon} w^{-1-4\varepsilon} \times \int_0^1 \left(\prod_{i=1}^3 dy_i \right) b_{2a}(y_1, y_2, y_3) y_2^{-1-2\varepsilon} y_3^{-1-2\varepsilon}, \quad (8.31)$$

where the function $b_{2a}(y_1, y_2, y_3)$ is free of singularities and given by

$$b_{2a}(y_1, y_2, y_3) \equiv \bar{y}_1^{-\varepsilon} \bar{y}_2^{-\varepsilon} \bar{y}_3^\varepsilon (w(u\bar{y}_1 \bar{y}_2 y_3 + v\bar{y}_1 y_2 + y_1 y_2 \bar{y}_2 y_3) + uv\bar{y}_1 \bar{y}_2 \bar{y}_3)^{3\varepsilon}. \quad (8.32)$$

The two singularities are located in the variables y_2 and y_3 in a factorized form as intended. We now perform the expansion in ε with the help of the $+$ -distribution, equation (A.10), and our integral becomes a sum of four finite integrals

$$\int_0^1 \left(\prod_{i=1}^3 dy_i \right) b_{2a}(y_1, y_2, y_3) y_2^{-1-2\varepsilon} y_3^{-1-2\varepsilon} = I_{2a}^{\delta\delta} + I_{2a}^{\delta+} + I_{2a}^{+\delta} + I_{2a}^{++}, \quad (8.33)$$

with

$$\begin{aligned} I_{2a}^{\delta\delta} &= \int_0^1 dy_1 \frac{b_{2a}(y_1, 0, 0)}{4\varepsilon^2}, \\ I_{2a}^{\delta+} &= - \int_0^1 dy_1 dy_3 \frac{b_{2a}(y_1, 0, y_3) - b_{2a}(y_1, 0, 0)}{2\varepsilon y_3^{1+2\varepsilon}}, \\ I_{2a}^{+\delta} &= - \int_0^1 dy_1 dy_2 \frac{b_{2a}(y_1, y_2, 0) - b_{2a}(y_1, 0, 0)}{2\varepsilon y_2^{1+2\varepsilon}}, \\ I_{2a}^{++} &= \int_0^1 dy_1 dy_2 dy_3 \frac{b_{2a}(y_1, y_2, y_3) - b_{2a}(y_1, 0, y_3) - b_{2a}(y_1, y_2, 0) + b_{2a}(y_1, 0, 0)}{y_2^{1+2\varepsilon} y_3^{1+2\varepsilon}}, \end{aligned} \quad (8.34)$$

which can be integrated order by order in ε .

Let us do some of the integrations explicitly to give a taste of the integration using MPLs. The integral $I_{2a}^{\delta\delta}$ is trivial and can be integrated directly without having to expand the integrand in ε . The integration over y_1 in $I_{2a}^{\delta+}$ can be performed without any trouble, but let us illustrate the use of MPLs. Using equations (2.71a) and (2.70), we find that the finite (ε^0) of $I_{2a}^{\delta+}$ is given by

$$\begin{aligned} I_{2a}^{\delta+}|_{\varepsilon^0} &= -\frac{1}{2} \int_0^1 dy_3 \frac{3 \ln(-vy_3 + wy_3 + v) + \ln(1 - y_3) - 3 \ln(v)}{y_3} \\ &= -\frac{1}{2} \int_0^1 dy_3 \frac{3 G\left(\frac{v}{v-w}; y_3\right) + G(1; y_3)}{y_3}, \\ &= -\frac{3}{2} G\left(0, \frac{v}{v-w}; 1\right) - \frac{1}{2} G(0, 1; 1). \end{aligned} \quad (8.35)$$

All the other integrals can be performed in the same manner. Note that at one point we will face a denominator of the form

$$ux - vx - x^2 - u + x \quad (8.36)$$

whose roots are given by z and \bar{z} defined by equation (8.15), allowing us to factorize them and to perform partial fraction with these.

The result will be a quite lengthy expression with many MPLs which are not all independent. With the help of the symbol or its enhanced extension, the coproduct, we can map the expressions into a tensor algebra, where all the functional equations are just simple algebraic identities, and simplify the expression significantly (section 2.7.4). Afterwards, we have to find an (simpler) expression with the same symbol. We will perform this step by constructing a priori a basis of functions in each weight and use this basis as an ansatz with arbitrary coefficients. By comparing the symbol of the integral with the symbol of our basis, we can determine values of the coefficients and obtain a result expressed through the functions of our basis.

The basis is not unique and we will use this freedom to construct the basis out of so-called single-valued polylogarithms. These functions are combinations of MPLs where all the individual discontinuities cancel. In reference [115] a single-valued basis was presented for the three-mass triangle integrals and a general algorithm for its construction. These functions will return as a subset of the basis functions for the integrals needed for this work.

The construction of a single valued basis was carried out following the procedure presented in [115]. The details of the computation can be found in references [2, 114].

8.4.2 Catani poles

Inserting the expressions for the master integrals in the amplitude we checked that the poles of the 1-loop (starting with ε^{-2}) and 2-loop N_f -piece (starting with ε^{-3}) amplitudes satisfy the results given by Catani [177]. We review here shortly the steps of this verification.

The renormalization of the coupling (section 2.3.1) consists only in replacing the bare QCD coupling constant $a_s = \frac{\alpha_s}{\pi}$ according to

$$a_s^b S_\varepsilon = a_s(\mu) \left[1 - \frac{\beta_0}{\varepsilon} a_s(\mu) + \mathcal{O}(a_s^2(\mu)) \right], \quad (8.37)$$

where

$$\beta_0 \equiv \frac{11C_A - 4T_R N_f}{12} \quad S_\varepsilon = (4\pi)^\varepsilon e^{-\varepsilon\gamma_E} \quad (8.38)$$

are respectively the first coefficient of the QCD β -function (of which only the N_f -piece is relevant to our study) and the typical phase-space volume factor in $d = 4 - 2\varepsilon$ dimensions and γ_E is the Euler-Masceroni constant. Corrections of higher order in the a_s are not needed for the 2-loop result as the underlying tree-level process does not involve QCD vertices. The renormalization of the bare 2-loop amplitude yields terms of $\mathcal{O}(a_s^3)$, that are beyond the order needed. The renormalization of the bare 1-loop amplitude however will contribute to $\mathcal{O}(a_s^2)$:

$$\mathcal{M}_{2\text{-loop}} = \mathcal{M}_{2\text{-loop}}^b - \frac{\beta_0}{\varepsilon} \mathcal{M}_{1\text{-loop}}^b \quad (8.39)$$

After this renormalization, the poles of each order are described by the operators I_1 (for the $\mathcal{O}(a_s)$ and $\mathcal{O}(a_s^2)$ coefficients) and I_2 (for the $\mathcal{O}(a_s^2)$) for which explicit results are given respectively in sections 3 and 5 of reference [177] for the problem at hand, of which we only need the piece that is proportional to N_f .

At $\mathcal{O}(a_s)$ we should have for the poles of the 1-loop renormalized,

$$\mathcal{M}_{1\text{-loop}}|_{poles} = a_s \mathcal{I}_1 \mathcal{M}_{0\text{-loop}}. \quad (8.40)$$

with²

$$\mathcal{I}_1 = -C_F \left[\frac{1}{\varepsilon^2} + \frac{3 + 2L}{2\varepsilon} \right] + \mathcal{O}(\varepsilon), \quad (8.41)$$

where

$$L \equiv \ln \left(\frac{\mu^2}{s} \right). \quad (8.42)$$

Picking the invariants³

$$t = -731.5762320546179, \quad u = -218.5257231465692, \quad s_3 = 1, \quad s_4 = 4, \quad (8.43)$$

discarding the couplings, setting $\mu^2 \stackrel{!}{=} s = s_3 + s_4 - t - u = 955.1019552011871$, $N_c = 3$ and computing with 32-digits precision with `Maple` [101], we obtain for the difference of the left- and right-hand side of equation (8.40)

$$\left(\frac{0.04}{\varepsilon^2} + \frac{1.81 + 3.71i}{\varepsilon} \right) \cdot 10^{-27}.$$

Repeating the same procedure at $\mathcal{O}(a_s^2)$ with the same phase-space point for the N_f part of the renormalized 2-loop matrix element, for which

$$\mathcal{M}_{2\text{-loop}, N_f}|_{poles} = a_s^2 \mathcal{I}_2|_{N_f} \mathcal{M}_{0\text{-loop}}. \quad (8.44)$$

with

$$\mathcal{I}_2|_{N_f} = -\frac{C_F N_f}{8} \left[\frac{1}{\varepsilon^3} + \frac{4 + 6L}{9\varepsilon^2} - \frac{65 + 9\pi^2 + 60L}{54\varepsilon} \right], \quad (8.45)$$

Using the same point and procedure as above the difference of the left- and right-hand side of equation (8.44) reads

$$\left(\frac{0.0009}{\varepsilon^3} - \frac{1.357 - 0.157i}{\varepsilon^2} + \frac{5.460 - 0.227i}{\varepsilon} \right) \cdot 10^{-26}.$$

The last numerical check shows that the numerical evaluation of complicated functions such as the master integrals (8.13) is not showing numerical instabilities.

²Note that Catani expands in $\frac{\alpha_s}{2\pi}$ instead of $a_s = \frac{\alpha_s}{\pi}$.

³We drop the units for this numerical check.

Chapter 9

Real corrections

In this chapter we will concentrate on the real-emission contributions at NLO and NNLO of the production of two off-shell photons with unrelated virtualities. The notations used are detailed in appendix A.

9.1 Single real amplitude

9.1.1 Quark-antiquark initial state channel

Let us now focus on the NLO real partonic cross section contribution from the sub-process $q\bar{q} \rightarrow g\gamma^*\gamma^*$. Although it is not proportional to N_f , it will contribute to the N_f part of the NNLO correction via the renormalization of α_s . The matrix element has IR singularities when the extra (potentially unresolved) gluon, g , becomes soft or collinear to one of the initial state partons p_1, p_2 . These singularities translate into ε -poles that have to be extracted analytically in order to achieve their cancellation among the different pieces of the computation.

The differential cross-section is given by

$$d\sigma_R^{q\bar{q}} = \frac{1}{2s_{12}} d\Phi_{12 \rightarrow g\gamma^*\gamma^*} |\mathcal{M}_{12 \rightarrow g\gamma^*\gamma^*}|^2, \quad (9.1)$$

where $|\mathcal{M}_{12 \rightarrow g\gamma^*\gamma^*}|^2$ is the $q\bar{q} \rightarrow g\gamma^*\gamma^*$ matrix element squared, summed over spin and colour and averaged over initial state quantum numbers. The phase space measure can be decomposed as

$$d\Phi_{12 \rightarrow g\gamma^*\gamma^*} = \frac{s_{12} dz}{2\pi} d\Phi_{12 \rightarrow gQ} d\Phi_{Q \rightarrow \gamma^*\gamma^*}, \quad (9.2)$$

where

$$Q \equiv p_1 + p_2 - p_g. \quad (9.3)$$

In order to control the collinear behavior of the gluon it is pertinent to parametrize its momentum as

$$p_g = \bar{z}\bar{\lambda} p_1 + \bar{z}\lambda p_2 + \bar{z}\sqrt{s_{12}\lambda\bar{\lambda}} e_T, \quad (9.4)$$

$$Q = (1 - \bar{z}\bar{\lambda})p_1 + (1 - \bar{z}\lambda)p_2 - \bar{z}\sqrt{s_{12}\lambda\bar{\lambda}} e_T, \quad (9.5)$$

where e_T is the unit vector transverse to p_1, p_2 in $d = 4 - 2\varepsilon$ dimensions.

Using parametrization (9.4) we obtain

$$d\Phi_{12 \rightarrow gQ} = \frac{1}{8\pi} \frac{d\Omega_{d-2}}{(2\pi)^{d-2}} \bar{z} d\lambda (s_{12}\bar{z}^2\lambda\bar{\lambda})^{-\varepsilon}, \quad (9.6)$$

where we use $d\Omega_{d-2}$ to denote the differential solid angle generating e_T . The collinear limits of the matrix element squared are universal, in the sense that they are independent of the process under consideration and can be computed for any parametrization [178]. Here, the two collinear limits $p_g \parallel p_1$ and $p_g \parallel p_2$ correspond to $\lambda \rightarrow 0$ and $\lambda \rightarrow 1$ respectively, and in these limits the matrix element squared diverges and has the following asymptotic behavior

$$|\mathcal{M}_{12 \rightarrow g\gamma^*\gamma^*}|^2 \sim \frac{-2g_s^2}{z} \frac{P_{qq}(z)}{-s_{12}\bar{z}\lambda} B_1(z) + \mathcal{O}(\lambda^0), \quad \text{as } \lambda \rightarrow 0, \quad (9.7)$$

$$|\mathcal{M}_{12 \rightarrow g\gamma^*\gamma^*}|^2 \sim \frac{-2g_s^2}{z} \frac{P_{qq}(z)}{-s_{12}\bar{z}\lambda} B_2(z) + \mathcal{O}(\bar{\lambda}^0), \quad \text{as } \lambda \rightarrow 1, \quad (9.8)$$

where the splitting kernel is given by

$$P_{qq}(z) = C_F \left(\frac{2z}{\bar{z}} + (1 - \varepsilon)\bar{z} \right), \quad (9.9)$$

and

$$B_1(z) \equiv B(zp_1, p_2), \quad B_2(z) \equiv B(p_1, zp_2), \quad (9.10)$$

are the shifted Born matrix element squared. The soft limit is also universal and commutes trivially with the collinear limits. As can be checked explicitly, subtracting the soft limit is not necessary in the present case, as the sum of (9.7) and (9.8) reproduces the universal soft limit as $z \rightarrow 1$.

We thus obtain a simple subtraction procedure at NLO which allows us to separate the hard and collinear terms

$$d\sigma_R^{q\bar{q}} = d\sigma_H^{q\bar{q}} + d\sigma_{C_1}^{q\bar{q}} + d\sigma_{C_2}^{q\bar{q}}, \quad (9.11a)$$

with

$$d\sigma_H^{q\bar{q}} = \frac{1}{2s_{12}} d\Phi_{12 \rightarrow g\gamma^*\gamma^*} \left[|\mathcal{M}_{12 \rightarrow g\gamma^*\gamma^*}|^2 - 2g_s^2 \frac{P_{qq}(z)}{s_{12}\bar{z}\lambda} \frac{B_1(z)}{z} - 2g_s^2 \frac{P_{qq}(z)}{s_{12}\bar{z}\lambda} \frac{B_2(z)}{z} \right], \quad (9.11b)$$

$$d\sigma_{C_{1,2}}^{q\bar{q}} = \frac{1}{2s_{12}} d\Phi_{12 \rightarrow g\gamma^*\gamma^*} \left[2g_s^2 \frac{P_{qq}(z)}{s_{12}\bar{z}\lambda} \frac{B_{1,2}(z)}{z} \right]. \quad (9.11c)$$

The integral over the hard differential cross section $d\sigma_H^{q\bar{q}}$ is finite, and can therefore be taken in $d = 4$ dimensions. Note that the massive phase space $d\Phi_{Q \rightarrow \gamma^* \gamma^*}$ implicitly depends on λ and z via the definition of Q , see equation (9.3), and has also to be taken at $\lambda = 0, 1$ in the counter-terms. It follows that the momenta of the off-shell photons entering the subtraction terms are different from those entering the real matrix element squared. Explicitly writing the full dependence on the photon momenta, we have

$$d\Phi_{12 \rightarrow g \gamma^* \gamma^*} B_1(z) \equiv \frac{s_{12} dz d\Omega_{d-2}}{16 (2\pi)^d} \bar{z} d\lambda (s_{12} \bar{z}^2 \lambda \bar{\lambda})^{-\varepsilon} d\Phi_{Q|\lambda=0 \rightarrow \gamma^* \gamma^*} B(z p_1, p_2, p_{\gamma_1^*}, p_{\gamma_2^*}),$$

with $p_{\gamma_1^*} + p_{\gamma_2^*} = Q|_{\lambda=0}$. We will use this shorthand notation for all subsequent limits.

The integrals over the collinear counter terms $d\sigma_{C_1}^{q\bar{q}}$ and $d\sigma_{C_2}^{q\bar{q}}$ contain all the ε -poles. But since the shifted born matrix elements squared $B_1(z)$ and $B_2(z)$ and their respective massive phase spaces do not depend on λ , the integration over λ can be carried out analytically, extracting the ε -poles

$$\int_{\lambda} d\sigma_{C_{1,2}}^{q\bar{q}} = -\frac{1}{\varepsilon} a_s \left(\frac{\mu^2}{s_{12}} \right)^{\varepsilon} C_{\varepsilon} \frac{B_{1,2}(z)}{2z s_{12}} d\Phi_{Q \rightarrow \gamma^* \gamma^*} dz \bar{z}^{-2\varepsilon} P_{qq}(z), \quad (9.12)$$

where

$$C_{\varepsilon} \equiv \frac{e^{\varepsilon \gamma_E} \Gamma(1 - \varepsilon)}{\Gamma(1 - 2\varepsilon)}. \quad (9.13)$$

However, the resulting integrated counter terms are still singular at the $z \rightarrow 1$ (soft) limit, see (9.9). In order to extract this last singularity we use an expansion in $+$ -distributions (section 2.3.2), which leads to the result

$$\int_{\lambda} d\sigma_{C_{1,2}}^{q\bar{q}} = a_s \left(\frac{\mu^2}{s_{12}} \right)^{\varepsilon} G_{qq}^{NLO}(z) d\sigma_{B_{1,2}}(z) dz, \quad (9.14)$$

where the shifted Born differential cross section is defined as

$$d\sigma_{B_i}(z) \equiv \frac{B_i(z)}{2z s_{12}} d\Phi_{Q \rightarrow \gamma^* \gamma^*}, \quad (9.15)$$

and the integrated NLO splitting kernel is

$$G_{qq}^{NLO}(z) = C_{\varepsilon} C_F \left[\left(\frac{1}{\varepsilon^2} + \frac{3}{2\varepsilon} \right) \delta(\bar{z}) + 4\mathcal{D}_1(\bar{z}) + \bar{z} - 2(1+z) \ln \bar{z} \right] - \frac{P_{qq}^{(0)}(z)}{\varepsilon},$$

with $P_{qq}^{(0)}(z)$ being the Altarelli-Parisi splitting kernel

$$P_{qq}^{(0)}(z) = C_F \left[2\mathcal{D}_0(\bar{z}) - (1+z) + \frac{3}{2} \delta(\bar{z}) \right]. \quad (9.16)$$

Note that this splitting kernel is related to $P_{qq}(z)$ but not identical. This form makes manifest the cancellation of the ε -poles against the PDF counter term (2.34b) and the 1-loop virtual amplitude (section 8.4.2).

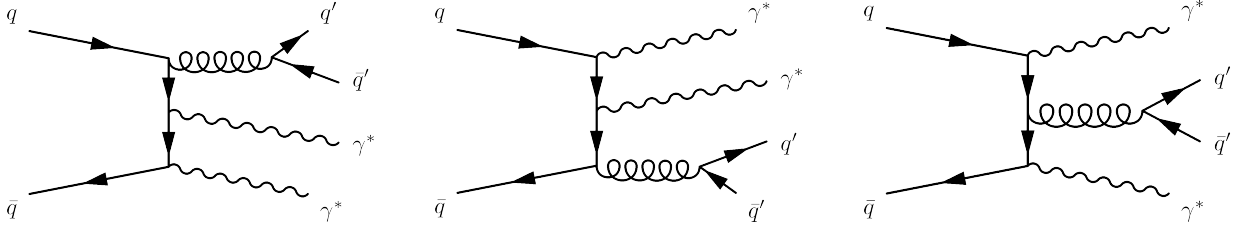


Figure 9.1: Three of the six diagrams contributing to the double-real in the large N_f limit. The other three diagrams can be obtained by crossing the two photons.

9.1.2 Quark-gluon initial state channels

The sub-processes that contribute to the NLO real hadronic cross section $qg \rightarrow q\gamma^*\gamma^*$, $gq \rightarrow q\gamma^*\gamma^*$, $\bar{q}g \rightarrow \bar{q}\gamma^*\gamma^*$, $g\bar{q} \rightarrow \bar{q}\gamma^*\gamma^*$, are treated in a similar fashion. For example, looking at the sub-process $qg \rightarrow q\gamma^*\gamma^*$ we parametrize, as before,

$$p_q = \bar{z}\bar{\lambda} p_1 + \bar{z}\lambda p_2 + \bar{z}\sqrt{s_{12}\lambda\bar{\lambda}} e_T. \quad (9.17)$$

The matrix element squared is finite at the soft limit ($z \rightarrow 1$) and the limit $p_1 \parallel p_q$ ($\lambda \rightarrow 0$). It is only singular at $\lambda \rightarrow 1$, with the asymptotic behavior

$$|\mathcal{M}_{12 \rightarrow q\gamma^*\gamma^*}|^2 \sim \frac{-g_s^2 P_{qg}(z)}{z - s\bar{z}\lambda} B_2(z) + \mathcal{O}(\bar{\lambda}^0), \quad \text{as } \lambda \rightarrow 1 \quad (9.18)$$

where the corresponding splitting-kernel is

$$P_{qg}(z) = \frac{z^2 + \bar{z}^2 - \varepsilon}{4(1 - \varepsilon)}. \quad (9.19)$$

This leads to an integrated collinear counter term

$$\int_{\lambda} d\sigma_C^{qg} = a_s \left(\frac{\mu^2}{s_{12}} \right)^\varepsilon G_{qg}^{NLO}(z) d\sigma_{B_2}(z) dz \quad (9.20)$$

with

$$G_{qg}^{NLO}(z) = -\frac{P_{qg}^{(0)}(z)}{\varepsilon} - 2z\bar{z} - 2(z^2 + \bar{z}^2) \ln \bar{z}, \quad (9.21)$$

where the Altarelli-Parisi splitting kernel is given by

$$P_{qg}^{(0)}(z) = \frac{1}{4} (z^2 + \bar{z}^2). \quad (9.22)$$

For these channels, the cancellation of the ε -poles only involves the PDF counter terms (2.34b), and not the virtual contributions.

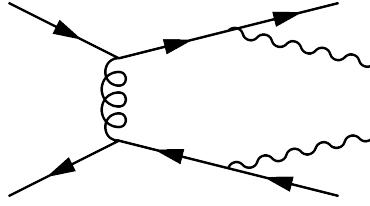


Figure 9.2: Example of a diagram that is *not* included for the double-real N_f amplitude.

9.2 Double-real N_f amplitude

We now consider the double-real contributions to the total cross-section in the large N_f limit. Among all the double-real corrections, only $q\bar{q} \rightarrow \gamma^*\gamma^*q'\bar{q}'$, with the $q'\bar{q}'$ -pair being attached to an intermediate gluon, is proportional to N_f , via explicit summation over the flavor of the $q'\bar{q}'$ -pair. In particular, all diagrams where the $q'\bar{q}'$ -pair is attached to a γ^* will not be proportional to N_f , because of the different charges of the different quark flavors. The only matrix element squared we need to consider has a structure similar to the NLO one, excepted that the gluon is now off-shell and attached to the current $g^* \rightarrow q'\bar{q}'$, see figure 9.1. In particular, we are not considering diagrams where quarks from the initial state end up in the final state, such as the one depicted in figure 9.2.

First note that the NLO corrections described in the previous section will also contribute to the double-real differential cross-section $d\sigma_{RR}$, via the renormalization of the strong coupling constant. However, only the $q\bar{q}$ channel will contribute, as the renormalization of α_s cancels exactly the β_0 term of the PDF counter-terms in the case of the quark-gluon channels.

The double-real differential cross section is then given by

$$d\sigma_{RR} = d\sigma_{RR}^U - a_s \frac{\beta_0|_{N_f}}{\varepsilon} (d\sigma_H^{q\bar{q}} + d\sigma_{C_1}^{q\bar{q}} + d\sigma_{C_2}^{q\bar{q}}), \quad (9.23)$$

where the unrenormalized double-real cross section is

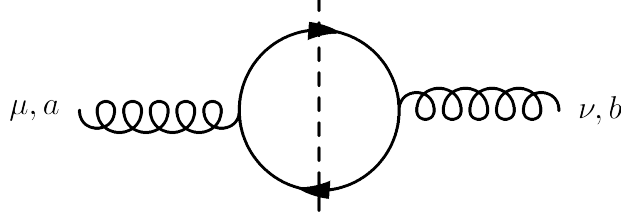
$$d\sigma_{RR}^U = \frac{1}{2s_{12}} d\Phi_{12 \rightarrow q\bar{q}\gamma^*\gamma^*} |\mathcal{M}_{12 \rightarrow q\bar{q}\gamma^*\gamma^*}|^2, \quad (9.24)$$

and the NLO hard and collinear counter terms are defined in the previous section. We drop the $q\bar{q}$ in the definition of NNLO quantities, since only this channel contributes in the large N_f limit. Furthermore, we will also drop the primes from the final state quark-antiquark pair.

In what follows, we will integrate over the phase space of the final state quarks. This simplifies the extraction of limits, at the cost of losing differential information on the final state quarks. In particular, the spin correlations in the final state collinear singularity will be integrated out.

We factorize the phase space as follows:

$$d\Phi_{12 \rightarrow q\bar{q}\gamma^*\gamma^*} = \frac{s_{12}}{2\pi} \frac{dz ds_g}{2\pi} d\Phi_{12 \rightarrow g^*Q} d\Phi_{g^* \rightarrow q\bar{q}} d\Phi_{Q \rightarrow \gamma^*\gamma^*}. \quad (9.25)$$

Figure 9.3: Integration over the $q\bar{q}$ phase space.

with $s_g = p_g^2$ being the 4-momentum squared of the parent off-shell gluon, $p_g = p_q + p_{\bar{q}}$, and $Q^2 = z s_{12}$. Performing the $d\Phi_{g \rightarrow q\bar{q}}$ integration, hence losing differential information on the final state quarks, we can write

$$\int d\Phi_{g^* \rightarrow q\bar{q}} |\mathcal{M}_{12 \rightarrow q\bar{q}\gamma^*\gamma^*}|^2 = \frac{A(\varepsilon)}{s_g^{1+\varepsilon}} |\mathcal{M}_{12 \rightarrow g^*\gamma^*\gamma^*}|^2, \quad (9.26)$$

where $\mathcal{M}_{12 \rightarrow g^*\gamma^*\gamma^*}$ is the matrix element for the production of two off-shell photons and an off-shell gluon, and $A(\varepsilon)$ is given by

$$A(\varepsilon) = 2g_s^2 N_f \frac{d-2}{d-1} \frac{1}{2} \frac{\Omega_{d-1}}{(4\pi)^{d-2}}. \quad (9.27)$$

Note that the computation of $A(\varepsilon)$ goes along the same lines as the Passarino-Veltman reduction of section 2.6.1: we make an ansatz from the Lorentz structure possible for the integral shown in figure 9.3, with the metric $g^{\mu\nu}$ and the gluon momentum $p_g^\mu p_g^\nu$ and we contract to find the coefficients, the only difference being that we are dealing this time with a phase space integral, but this has no effect on the computation itself.

Hence in the following section we will consider

$$d\sigma_{RR}^U = \frac{1}{2s_{12}} \frac{s_{12}}{2\pi} \frac{dz}{2\pi} \frac{ds_g}{2\pi} d\Phi_{12 \rightarrow g^*Q} d\Phi_{Q \rightarrow \gamma^*\gamma^*} \frac{A(\varepsilon)}{s_g^{1+\varepsilon}} |\mathcal{M}_{12 \rightarrow g^*\gamma^*\gamma^*}|^2. \quad (9.28)$$

9.2.1 Subtraction in the hierarchical parametrization

In this section, we present a subtraction procedure for $d\sigma_{RR}^U$. We parametrize the momentum of the off-shell gluon hierarchically as

$$p_g = \bar{z}\bar{\lambda}p_1 + \bar{z}\lambda \frac{1 - \rho\bar{z}\bar{\lambda}}{1 - \bar{z}\bar{\lambda}} p_2 + \bar{z}\sqrt{s_{12}\rho\lambda\bar{\lambda}} e_T, \quad (9.29)$$

where e_T is again the unit vector transverse to p_1 and p_2 in $d = 4 - 2\varepsilon$ dimensions. We have the invariants

$$s_{1g} \equiv (p_1 - p_g)^2 = -s_{12}\bar{z}\lambda \quad (9.30a)$$

$$s_{2g} \equiv (p_2 - p_g)^2 = -s_{12}\bar{z}\bar{\lambda} \left(1 - \frac{\bar{z}\lambda\rho}{1 - \bar{\lambda}\bar{z}}\right) \quad (9.30b)$$

$$s_g \equiv p_g^2 = (p_q + p_{\bar{q}})^2 = s_{12} \frac{\bar{z}^2\lambda\bar{\lambda}\bar{\rho}}{1 - \bar{z}\bar{\lambda}}. \quad (9.30c)$$

Using this parametrization, the phase space measure reads

$$d\Phi_{12 \rightarrow g^* Q} = \rho^{-\varepsilon} \frac{1}{8\pi} \frac{d\Omega_{d-2}}{(2\pi)^{d-2}} \bar{z} d\lambda (s_{12} \bar{z}^2 \lambda \bar{\lambda})^{-\varepsilon}, \quad (9.31)$$

where $d\Omega_{d-2}$ denotes the integral over e_T , and (9.28) becomes

$$d\sigma_{RR}^U = \frac{1}{2s_{12}} \frac{s_{12}}{2\pi} \frac{dz}{2\pi} \frac{ds_g}{2\pi} \frac{A(\varepsilon)}{s_g^{1+\varepsilon}} \rho^{-\varepsilon} d\Phi_{12 \rightarrow gQ} d\Phi_{Q \rightarrow \gamma^* \gamma^*} |\mathcal{M}_{12 \rightarrow g^* \gamma^* \gamma^*}|^2. \quad (9.32)$$

The singular limits of the double real matrix element squared are once again universal but are asymmetric as a consequence of the asymmetry of the hierarchical parametrization under the exchange $p_1 \leftrightarrow p_2$. We have to consider the following singular limits:

- $p_g = p_q + p_{\bar{q}} \parallel p_1$: This corresponds to $\lambda \rightarrow 0$, such that $p_g \rightarrow \bar{z}p_1$, and the matrix element squared has the asymptotic behavior

$$|\mathcal{M}_{12 \rightarrow g^* \gamma^* \gamma^*}|^2 \sim \frac{-4g_s^2 B_1(z)}{\tilde{s}_{1g}} \frac{1}{z} P_{qq;1}(z, \rho) + \mathcal{O}(\lambda^0), \quad \text{as } \lambda \rightarrow 0, \quad (9.33)$$

with

$$P_{qq;1}(z, \rho) = C_F \left[\frac{2}{\bar{z}} - 2 + (1 - \varepsilon) \bar{z} \rho \right], \quad (9.34)$$

and

$$\tilde{s}_{1g} \equiv -s_{12} \bar{z} \lambda. \quad (9.35)$$

- $p_g = p_q + p_{\bar{q}} \parallel p_2$: This corresponds to $\lambda \rightarrow 1$, such that $p_g \rightarrow \bar{z}p_2$, and the matrix element squared has the asymptotic behavior

$$|\mathcal{M}_{12 \rightarrow g^* \gamma^* \gamma^*}|^2 \sim \frac{-4g_s^2 B(p_1, zp_2)}{\tilde{s}_{2g}} \frac{1}{z} P_{qq;2}(z, \rho) + \mathcal{O}(\bar{\lambda}^0), \quad \text{as } \lambda \rightarrow 1, \quad (9.36)$$

with

$$P_{qq;2}(z, \rho) = C_F \left[\frac{2}{\bar{z}} - 2 + (1 - \varepsilon) \bar{z} \left(1 - \frac{z\bar{\rho}}{1 - \bar{z}\bar{\rho}} \right) \right], \quad (9.37)$$

and

$$\tilde{s}_{2g} \equiv -s_{12} \bar{z} \bar{\lambda} (1 - \bar{\rho} \bar{z}). \quad (9.38)$$

- $p_q \parallel p_{\bar{q}}$: This is the final state collinear singularity, when the gluon becomes on-shell ($s_g \rightarrow 0$), but remains in the hard region. It corresponds to $\rho \rightarrow 1$ and the double real matrix element trivially tends to the NLO matrix element

$$\lim_{\rho \rightarrow 1} |\mathcal{M}_{12 \rightarrow g^* \gamma^* \gamma^*}|^2 = |\mathcal{M}_{12 \rightarrow g \gamma^* \gamma^*}|^2. \quad (9.39)$$

The corresponding singularity does not come from the matrix element squared but from the factor s_g^{-1} in (9.32).

Note that both NNLO splitting kernels, (9.34) and (9.37), tend smoothly to the NLO splitting kernel (9.9) as $\rho \rightarrow 1$. It can be checked explicitly that no explicit subtraction of the soft limit is necessary in the case at hand.

We can separate the singularities of $d\sigma_{RR}^U$ from the hard part by writing

$$d\sigma_{RR}^U = d\sigma_{HH} + d\sigma_{R;C} + d\sigma_{CC_1} + d\sigma_{CC_2}, \quad (9.40a)$$

where the double-hard contribution to the differential cross-section, the two collinear counterterms and the remnant from the NLO renormalization are respectively

$$\begin{aligned} d\sigma_{HH} = & \frac{1}{2s_{12}} \frac{s_{12}}{2\pi} \frac{dz ds_g}{2\pi} \frac{A(\varepsilon)}{s_g^{1+\varepsilon}} \rho^{-\varepsilon} d\Phi_{12 \rightarrow gQ} d\Phi_{Q \rightarrow \gamma^* \gamma^*} \\ & \times \left[|\mathcal{M}_{12 \rightarrow g^* \gamma^* \gamma^*}|^2 - \frac{4g_s^2}{-\tilde{s}_{1g}} P_{qq;1}(z, \rho) \frac{B_1(z)}{z} - \frac{4g_s^2}{-\tilde{s}_{2g}} P_{qq;2}(z, \rho) \frac{B_2(z)}{z} \right. \\ & \left. - |\mathcal{M}_{12 \rightarrow g \gamma^* \gamma^*}|^2 + \frac{4g_s^2}{-\tilde{s}_{1g}^*} P_{qq}(z) \frac{B_1(z)}{z} + \frac{4g_s^2}{-\tilde{s}_{2g}^*} P_{qq}(z) \frac{B_2(z)}{z} \right], \end{aligned} \quad (9.40b)$$

$$d\sigma_{CC_1} = \frac{1}{2s_{12}} \frac{s_{12}}{2\pi} \frac{dz ds_g}{2\pi} \frac{A(\varepsilon)}{s_g^{1+\varepsilon}} \rho^{-\varepsilon} d\Phi_{12 \rightarrow gQ} d\Phi_{Q \rightarrow \gamma^* \gamma^*} \frac{4g_s^2}{-\tilde{s}_{1g}} P_{qq;1}(z, \rho) \frac{B_1(z)}{z}, \quad (9.40c)$$

$$d\sigma_{CC_2} = \frac{1}{2s_{12}} \frac{s_{12}}{2\pi} \frac{dz ds_g}{2\pi} \frac{A(\varepsilon)}{s_g^{1+\varepsilon}} \rho^{-\varepsilon} d\Phi_{12 \rightarrow gQ} d\Phi_{Q \rightarrow \gamma^* \gamma^*} \frac{4g_s^2}{-\tilde{s}_{2g}} P_{qq;2}(z, \rho) \frac{B_2(z)}{z}, \quad (9.40d)$$

$$\begin{aligned} d\sigma_{R;C} = & \frac{1}{2s_{12}} \frac{s_{12}}{2\pi} \frac{dz ds_g}{2\pi} \frac{A(\varepsilon)}{s_g^{1+\varepsilon}} \rho^{-\varepsilon} d\Phi_{12 \rightarrow gQ} d\Phi_{Q \rightarrow \gamma^* \gamma^*} \\ & \times \left[|\mathcal{M}_{12 \rightarrow g \gamma^* \gamma^*}|^2 + \frac{4g_s^2}{-\tilde{s}_{1g}^*} P_{qq}(z) \frac{B_1(z)}{z} + \frac{4g_s^2}{-\tilde{s}_{2g}^*} P_{qq}(z) \frac{B_2(z)}{z} \right]. \end{aligned} \quad (9.40e)$$

For the $d\sigma_{R;C}$ we have also defined the limits of s_{1g} and s_{2g} as $\rho \rightarrow 1$ as

$$\tilde{s}_{1g}^* = -s_{12} \bar{z} \lambda, \quad \tilde{s}_{2g}^* = -s_{12} \bar{z} \bar{\lambda}. \quad (9.41)$$

Note that the content of the bracket is identical to the subtracted single-real matrix element squared (9.11b).

9.2.2 Integrating the collinear counterterms

As for NLO, the shifted Born matrix elements squared $B_{1,2}(z)$ do not depend on λ and ρ anymore, and hence those variables can be integrated over, giving rise to the ε -poles.

Spelling out the triple collinear counterterms (9.40c) and (9.40d), we get

$$\begin{aligned} d\sigma_{CC_i} = & dz d\lambda \frac{d\bar{\rho}}{\bar{\rho}^{1+\varepsilon}} \rho^{-\varepsilon} (\bar{z}^4 \lambda^2 \bar{\lambda}^2)^{-\varepsilon} (1 - \bar{z} \bar{\lambda})^\varepsilon a_s^2 \left(\frac{\mu^2}{s_{12}} \right)^{2\varepsilon} \frac{N_f}{4} \frac{(1 - \varepsilon) e^{2\varepsilon \gamma_E}}{(3 - 2\varepsilon) \Gamma(2 - 2\varepsilon)} \\ & \times d\Phi_{Q \rightarrow \gamma^* \gamma^*} \frac{\bar{z}}{-\tilde{s}_{ig}} P_{qq;i}(z, \rho) \frac{B_i(z)}{z}. \end{aligned} \quad (9.42)$$

The integration over λ and ρ is slightly more complicated than at NLO but the result can be written in terms of hypergeometric functions ${}_2F_1(a, b, c; \bar{z})$, where a and b are ε -dependent. We have used the `HypExp` [106] package to expand them in ε and then performed a $+$ -distribution expansion over \bar{z} to extract the double soft singularity. We note here that the part of $d\sigma_{CC_{1,2}}$ that is singular at the soft ($z \rightarrow 1$) limit is symmetric, such that the asymmetry due to the parametrization between $d\sigma_{CC_1}$ and $d\sigma_{CC_2}$ is limited to the regular coefficients and doesn't affect the δ - and $+$ -distribution terms. As at NLO, we can write the results as

$$\int_{\lambda, \rho} d\sigma_{CC_{1,2}} = a_s^2 \left(\frac{\mu^2}{s_{12}} \right)^{2\varepsilon} G_{1,2}^{NNLO}(z) d\sigma_{B_{1,2}}(z) dz, \quad (9.43)$$

where the integrated splitting kernels are

$$\begin{aligned} G_1^{NNLO}(z) = & \frac{C_F N_f}{48} \left\{ -\frac{\delta(\bar{z})}{\varepsilon^3} + \frac{1}{\varepsilon^2} \left[4\mathcal{D}_0(\bar{z}) - \frac{5}{3}\delta(\bar{z}) - 2(1+z) \right] \right. \\ & + \frac{1}{\varepsilon} \left[-16\mathcal{D}_1(\bar{z}) + \frac{20}{3}\mathcal{D}_0(\bar{z}) - \frac{1}{18}(56 - 21\pi^2)\delta(\bar{z}) \right. \\ & \left. \left. - \frac{10}{3}(1+z) + 8(1+z)\ln\bar{z} + 2(1+z^2)\frac{\ln z}{\bar{z}} \right] \right. \\ & + 32\mathcal{D}_2(\bar{z}) - \frac{80}{3}\mathcal{D}_1(\bar{z}) + \frac{2}{9}(56 - 21\pi^2)\mathcal{D}_0(\bar{z}) \\ & - \frac{1}{54}(328 - 105\pi^2 - 1116\zeta_3)\delta(\bar{z}) \\ & - 4(1+z^2)\frac{\text{Li}_2(\bar{z})}{\bar{z}} - 16(1+z)\ln^2\bar{z} - (1+z^2)\frac{\ln^2 z}{\bar{z}} - 8(1+z^2)\frac{\ln z \ln \bar{z}}{\bar{z}} \\ & + \frac{40}{3}(1+z)\ln\bar{z} + \frac{10}{3}(1+z^2)\frac{\ln z}{\bar{z}} \\ & \left. \left. - \frac{1}{9}(38 + 74z + (1+z)(-21\pi^2)) \right\} + \mathcal{O}(\varepsilon), \quad (9.44) \end{aligned}$$

$$G_2^{NNLO}(z) = G_1^{NNLO}(z) + \frac{C_F N_f}{48} \left(4(1+z^2)\frac{\text{Li}_2(\bar{z})}{\bar{z}} - 4\ln z - 4\bar{z} \right) + \mathcal{O}(\varepsilon). \quad (9.45)$$

The poles of the integrated collinear counter-terms cancel against (i) those of the renormalized 2-loop virtual contribution (section 8.4.2), (ii) those of the PDF counter-terms (2.34c) and (iii) those of the NLO integrated counter-terms (9.14) contributing to NNLO due to renormalization, see equation (9.23). The N_f -part of the Altarelli-Parisi splitting kernel is

$$P_{qq}^{(1)}|_{N_f} = -\frac{N_f C_F}{18} \left(\delta(\bar{z}) \left(\pi^2 + \frac{3}{4} \right) + 10\mathcal{D}_0(\bar{z}) + 3\ln(z)\frac{1+z^2}{\bar{z}} - 11z + 1 \right), \quad (9.46)$$

and enters together with the N_f -part of β_0 to give the PDF counterterm we need, i.e. $\Delta_{qq}^{(2)}|_{N_f}$ given by equation (2.34c).

The single hard collinear counter term $d\sigma_{R;C}$, equation (9.40e), can be integrated over ρ analytically to expose the final state singularity. Using

$$\int \frac{1}{2\pi} \frac{ds_g}{s_g^{1+\varepsilon}} \rho^{-\varepsilon} A(\varepsilon) = -\frac{N_f}{6\varepsilon} a_s \left[1 + \frac{5}{3}\varepsilon - \varepsilon \ln \left(\frac{s_{12} \bar{z}^2 \lambda \bar{\lambda}}{\mu^2 (1 - \bar{z} \lambda)} \right) + \mathcal{O}(\varepsilon^2) \right], \quad (9.47)$$

it can be easily shown that the singularity arising from the integral over ρ cancels against the renormalization of the strong coupling constant acting on the hard differential cross section, leaving the finite contribution

$$d\sigma_{\bar{H}} \equiv \int_{\rho} d\sigma_{R;C} - a_s \frac{\beta_0|_{N_f}}{\varepsilon} d\sigma_H^{q\bar{q}} = a_s \frac{N_f}{6} \left[-\frac{5}{3} + \ln \left(\frac{s_{12} \bar{z}^2 \lambda \bar{\lambda}}{\mu^2 (1 - \bar{z} \lambda)} \right) \right] d\sigma_H^{q\bar{q}}. \quad (9.48)$$

Chapter 10

Numerical results

The various contributions to the differential cross section for the N_f part of the process $pp \rightarrow \gamma^* \gamma^* + X$ up to the NNLO in the strong coupling expansion that we presented in chapters 8 and 9 have been implemented in two different programs. The virtual contributions are written in terms of master integrals (chapter 8) which in turn are evaluated in terms of HPLs. In order to ensure the correct implementation of the master integrals various analytic and numerical checks were performed against published results in the literature. We have used the program `CHAPLIN` [110] for the numerical evaluation of the necessary harmonic polylogarithms in the physical region. The poles of the 1- and 2-loop virtual amplitudes, as predicted by [177] were checked both analytically and numerically, at the implementation level (section 8.4.2). The NLO contribution was checked against the `MCFM` [136] implementation.¹

The double real contributions were implemented in two different ways, according to the hierarchical and the symmetric hierarchical parametrizations, see sections 9.2.1 and reference [2] respectively. Due to the different double-real counter terms, the numerical results for the double-hard, the single-hard and the integrated triple-collinear counterterm cross sections are individually different. Only the sum of these contributions is physical, which provides a strong numerical check of our two implementations.

In the following we present indicatively some differential distributions of interest, including their factorization and renormalization scale dependence.

We use the central grid of the MSTW08 PDFs [150] at the appropriate QCD order, ignoring the uncertainties due to PDFs and the strong coupling constant. The strong coupling constant is run at the appropriate QCD order (section 2.3.1) while the electromagnetic coupling constant is kept fixed to its value at m_Z .

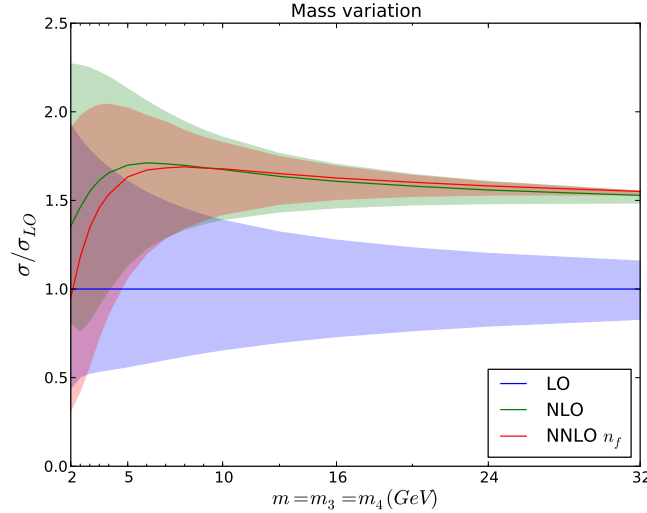


Figure 10.1: Scale variation at LO, NLO and NNLO as a function of the photon virtualities, here taken to be equal.

10.1 Equal virtualities

The total cross section obviously depends on the virtualities of the off-shell photons. As a first study, we set the virtualities to be equal and study the scale uncertainty of the NLO and NNLO K -factors as a function of the common photon virtuality, in figure 10.1. The renormalization and factorization scales are set to be equal and varied in the interval

$$\frac{m}{2} \leq \mu_R \stackrel{!}{=} \mu_F \leq 2m \quad (10.1)$$

where $m = \sqrt{s_3} = \sqrt{s_4}$. For photons that are widely off-shell, i.e. with $\sqrt{s_{3,4}} > 10$ GeV, the NNLO N_f cross section lies within a percent of the NLO cross section and the NNLO N_f scale uncertainty is reduced, implying a satisfactory perturbative convergence for the process. As the limit of on-shell photons $m \rightarrow 0$ is approached the cross-section blows up and so does its scale uncertainty, as expected since we do not impose any final state cuts on the two photons. The result should not be taken seriously for low virtualities as large cancellations are expected originating from the IBPs of the reduction that can yield numerical instabilities, and the evolution of the PDFs and couplings at low energy takes the finite bottom-quark mass into account.

¹The $pp \rightarrow \gamma^* \gamma^*$ without photon decays is not an out-of-the-box process in MCFM, but it was possible to compare our result with $\sqrt{s_3} = \sqrt{s_4} = m_Z$ against MCFM's $pp \rightarrow ZZ$ with modified couplings of the Z boson to quarks.

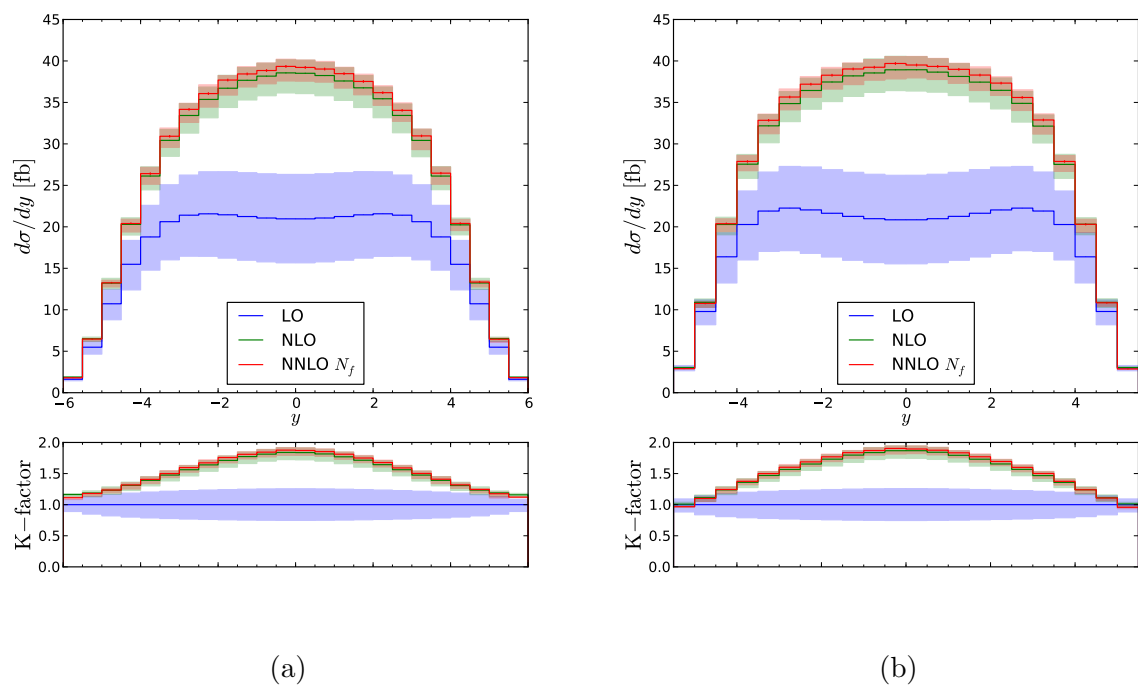


Figure 10.2: Rapidity distribution of the two off-shell photons with virtualities 30 GeV (a) and 15 GeV (b). The bottom plots show the bin-by-bin ratio to the LO.

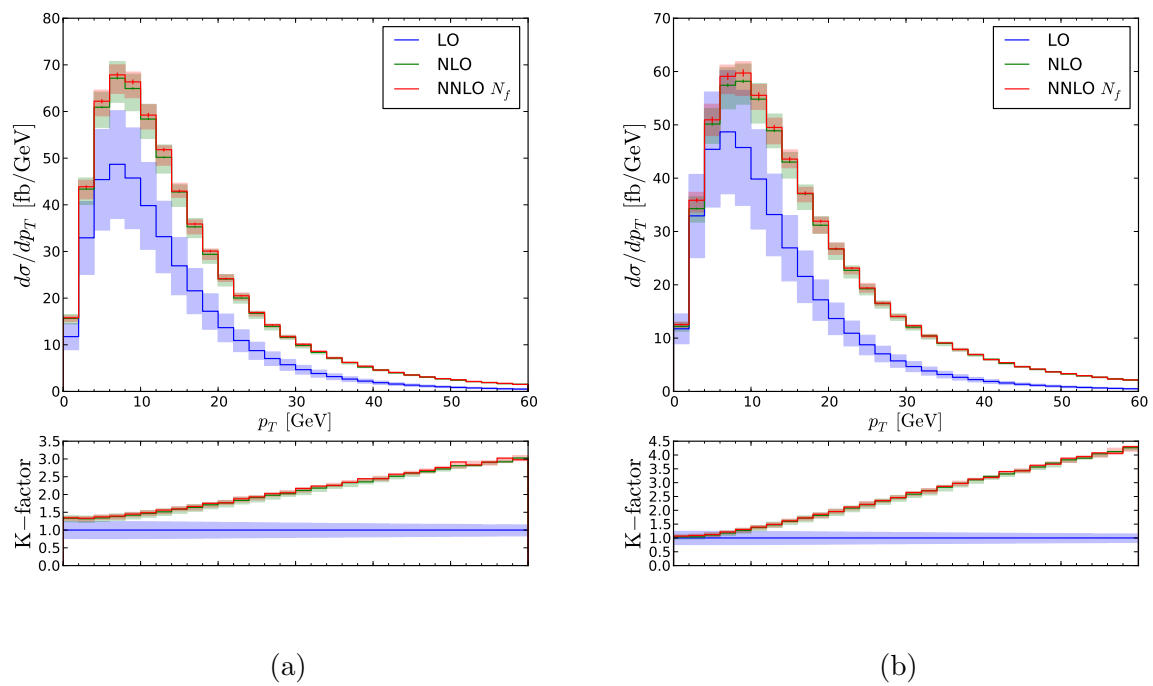


Figure 10.3: Transverse momentum distribution of the two off-shell photons with virtualities 30 GeV (a) and 15 GeV (b). The bottom plots show the bin-by-bin ratio to the LO.

10.2 Unequal virtualities

Next we turn to differential distributions for unequal photon virtualities. We set

$$\sqrt{s_3} = 15 \text{ GeV}, \quad \sqrt{s_4} = 30 \text{ GeV}. \quad (10.2)$$

In figure 10.2 we present the rapidity distributions of the two photons at each order in α_s . The transverse momentum distributions for the two photons are shown in figure 10.3. The scale uncertainties are shown as shaded regions in the figures. The renormalization and factorization scales are kept equal to each other and varied in the interval

$$10 \text{ GeV} \leq \mu_R \stackrel{!}{=} \mu_F \leq 40 \text{ GeV}. \quad (10.3)$$

We note that the NNLO N_f contribution does not alter the shape of the transverse momentum distribution apart from a small upward shift of the central value. The rapidity distributions at NNLO follow the NLO pattern and again the central value is slightly shifted upwards. Note that for both distributions, the scale variation of the NNLO is reduced and for the most part completely contained within the NLO scale variation which shows the improvement of the perturbative expansion. Table 10.1 lists the inclusive cross sections we obtain by varying the renormalization and factorization scales around the central values (10.3). The number in parenthesis indicates the Monte-Carlo error on the last digit after letting the program run for a couple of minutes on a standard personal computer. These numbers can be recovered by summing the bins of the transverse-momentum or rapidity distributions.

LO	NLO	NNLO N_f
401.12(4) $^{+89.59}_{-91.55}$ pb	637.25(15) $^{+26.21}_{-39.61}$ pb	648.32(44) $^{+15.03}_{-28.48}$ pb

Table 10.1: Inclusive cross sections for $\gamma^*\gamma^*$ production with fixed virtualities 30 GeV and 15 GeV together with the effect of scale variations as described in the text.

Off-shell diphoton production contributes as a background, along with Z pair production, to the Higgs boson measurements in the golden channel $pp \rightarrow H \rightarrow ZZ^* \rightarrow 4l$. In that case the invariant mass of the photon pair must be in a window of several GeV around the Higgs mass of 125 GeV. We therefore set the virtualities of the photons to

$$\sqrt{s_3} = 91.19 \text{ GeV}, \quad \sqrt{s_4} = 27 \text{ GeV}, \quad (10.4)$$

and obtain the invariant mass distribution of the photon pair shown in figure 10.4. The renormalization and factorization scales are kept equal to each other and varied in the interval

$$29.55 \text{ GeV} \leq \mu_R \stackrel{!}{=} \mu_F \leq 118.19 \text{ GeV}, \quad (10.5)$$

around the central scale $\frac{1}{2}(91.19 + 27) \text{ GeV}$.

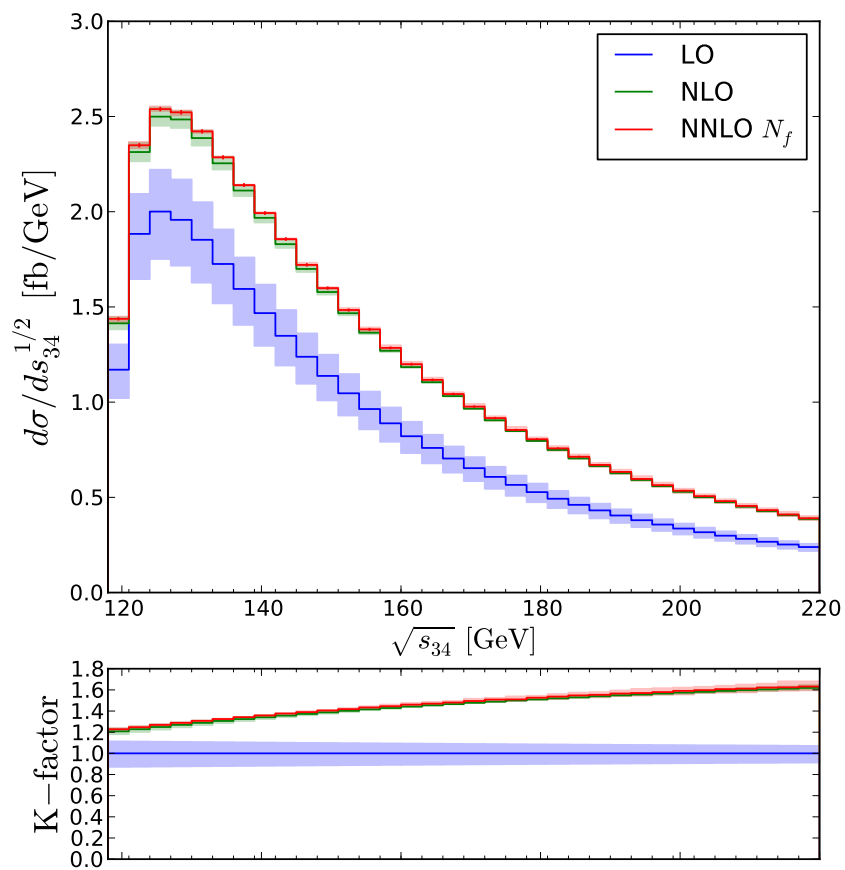


Figure 10.4: Invariant mass distribution of the photon pair with virtualities 91.19 GeV and 27 GeV.

We note that the uncertainty that is given by scale variation shrinks as we go from NLO to NNLO and lies within the NLO scale uncertainty, showing a better convergence behavior. Although the process we compute is $\gamma^*\gamma^*$ and not ZZ^* direct production, our choice of masses is motivated by the fact that the distribution of the invariant mass of the photon pair varies sharply in the region where $\sqrt{s_{34}} \approx 125$ GeV and thus a reliable perturbative computation needs to be precise enough not to be spoiled by the scale uncertainty, as is the case for the NNLO N_f distribution.

Chapter 11

Conclusion

We presented the computation of the NNLO QCD real and virtual corrections of a gauge-invariant subset of the process $pp \rightarrow \gamma^* \gamma^*$, namely the contribution due to N_f massless quark loops. On the one hand, the relevant double-virtual diagrams were generated and reduced to master integrals which were then computed and simplified using the modern coproduct technique. On the other hand the double-real diagrams were computed, their phase space parametrized and singularities extracted. The singularities from the virtual and real diagrams and the PDF counterterms were computed independently and checked to cancel each other, which gives us confidence in the computation. The implementation is differential in the momentum of the off-shell photons and was performed in two independent codes.

The preliminary study of the effect of this N_f piece on the differential distribution is mostly the improvement of the behavior under scale variations. We do not observe a significant alteration of the shape of distribution relative to the NLO result.

The next steps will consist in extending the result to the full NNLO QCD corrections including gluon and ghost loops. The reduction to master integrals of the full 2-loop amplitude is well under way and most necessary master integrals have been identified. The remaining steps lie in the computation of the master integrals needed for this process using the same techniques as those presented here.

Furthermore, the implementation of processes like direct production of WW , WZ , $Z\gamma^*$ that are genuinely interesting in their own right, but are also specifically directly relevant for backgrounds to Higgs searches, can be achieved in this framework by taking into account the different vector and axial couplings and combining them with the relevant PDFs.

Outlook

Two years ago the history of high-energy physics came to a climax with the announcement of the discovery of a new boson at CERN. We need to go back to 1983 and the announcement of the discovery of the W and Z bosons to see such an electrifying event happen.

There is a growing evidence that the boson is *a* Higgs boson, i.e. that it is related to the mechanism of electroweak symmetry breaking. But the journey is far from over. The study of the properties of this Higgs boson, to assess or discard its SM-like behavior will require the comparison of experimental data with theoretical predictions. We can estimate ourselves to be lucky, because the Higgs lies in a domain where many decay branching ratios are in principle accessible (figure 1). As the time of a new high-energy lepton collider still lies far in the future, the efforts are focused on extracting the most information in a hadronic environment, which is a challenge both experimentally and theoretically. In this context, the computation of cross sections for signal as well as background processes with fully resolved kinematics to an order in QCD where the theoretical uncertainty can be safely assumed under control is critical.

In this thesis we have focused on two different aspects that are of direct relevance for the investigation of the properties of the Higgs boson observed at the LHC. In the case of the Higgsstrahlung process, the straightforward outlook is the study of the effect at NNLO in QCD and the implementation of a fat-jet strategy on the experimental analysis side. For the $\gamma^*\gamma^*$ production process, the extension to include the fully differential dependence on the final state quarks is on the way, and the full NNLO computation should be possible in a near future, with the evaluation of the necessary master integrals using modern refined techniques like the coproduct. Adapting the couplings, the implementation of a fully differential diboson production code with corrections up to NNLO QCD lies within reach.

So far, there has been no surprise discovery of new particles (like supersymmetric partners, or a new vector boson) and the SM seems to provide an excellent description of the phenomenology we observe at high-energy colliders. Even in the eventuality of nature being “boring”, higher-order computations reveal very beautiful mathematical structures that are not yet fully understood, which might hint that the language of Feynman diagrams might hide superior principles and maybe some work needs to be done on the more formal side.

Appendices

Appendix A

Notations and useful formulae

Units We work in the whole thesis in units where $\hbar = c = 1$. In these units we can express cross sections through the conversion

$$1\text{fb} = 2,568 \cdot 10^{-12} \text{GeV}^{-2}.$$

QCD The number of colors is N_c . C_F and C_A denote the color factor for the fundamental and adjoint representation respectively. We always use the normalization $T_F = 1/2$.

We define

$$\beta_0 \equiv \frac{11N_c - 2N_f}{12}, \quad a_s \equiv \frac{\alpha_s(\mu)}{\pi} \quad (\text{A.1})$$

DREG The metric tensor is denoted $g^{\mu\nu}$ and we use the most-plus sign convention which is the common choice in high-energy physics. With this metric, the mass such that $p^2 = p_\mu p_\nu g^{\mu\nu} = m^2$. When dealing with divergences in DREG [35, 52, 53], the following quantities are used:

$$d \equiv 4 - 2\varepsilon, \quad \Omega_d \equiv \frac{2\pi^{d/2}}{\Gamma(d/2)}, \quad S_\varepsilon \equiv (4\pi)^\varepsilon \exp(-\gamma_E \varepsilon), \quad (\text{A.2})$$

where $\gamma_E \approx 0.5772156649$ is the Euler-Mascheroni constant.

Loop integrals In the evaluation of loop integrals with Feynman parameters, the following formulae are useful [17],

$$\frac{1}{A_1^{\nu_1} \cdots A_n^{\nu_n}} = \frac{\Gamma(\sum \nu_i)}{\prod \Gamma(\nu_i)} \int_0^1 dx_1 \cdots dx_n \frac{\delta(\sum x_i - 1) \prod x_i^{\nu_i - 1}}{[\sum x_i A_i]^{\sum \nu_i}}, \quad (\text{A.3})$$

$$\int \frac{d^d l}{(2\pi)^d} \frac{1}{[l^2 - \Delta]^n} = \frac{(-1)^n i \Gamma(n - d/2)}{(4\pi)^{d/2} \Gamma(n)} \Delta^{d/2 - n}. \quad (\text{A.4})$$

We note that,

$$\Gamma(\varepsilon) = \frac{1}{\varepsilon} - \gamma_E + \mathcal{O}(\varepsilon), \quad \Gamma(1 + \varepsilon) = \varepsilon \Gamma(\varepsilon). \quad (\text{A.5})$$

PDFs We define the convolution of two functions through

$$[f \otimes g](z) \equiv \int_0^1 dx dy f(x) g(y) \delta(z - xy), \quad (\text{A.6})$$

and we will make use of the following straightforward identity:

$$\int_0^1 dz [f \otimes g](z) \sigma(z) = \int_0^1 dx dy f(x) g(y) \sigma(xy). \quad (\text{A.7})$$

For the extraction of singularities, we use $+$ -distributions which are defined via

$$\int_0^1 dx \left[\frac{f(x)}{x} \right]_+ g(x) = \int_0^1 dx \frac{f(x)}{x} (g(x) - g(0)), \quad (\text{A.8})$$

and we introduce the shorthand notation

$$\mathcal{D}_n(x) \equiv \left[\frac{\ln^n x}{x} \right]_+. \quad (\text{A.9})$$

Using this notation we can write the following expansion in $+$ -distributions:

$$\frac{1}{\bar{z}^{1+n\varepsilon}} \equiv -\frac{\delta(\bar{z})}{n\varepsilon} + \sum_{k=0}^{\infty} \frac{(-n\varepsilon)^k}{k!} \mathcal{D}_k(\bar{z}). \quad (\text{A.10})$$

Appendix B

Coefficients of the master integrals for the N_f -piece of the 2-loop amplitude of $q\bar{q} \rightarrow \gamma^* \gamma^*$

```
# coefficients_masters_2LNf.mpl
#
# This file contains the coefficient of each master integral for the
# Nf-piece of the *unrenormalized* 2-loop amplitude.
#
# The naming follows the notation from the publication, i.e. cpbox0011p1p2p3
# is the coefficient of the master Pbox(0,0,1,1,p1,p2,p3).
#
# The functions are given as a rational function of the invariants s, t, u,
# s3 and s4, that are subject to the condition s + t + u = s3 + s4.
#
# We have factored out Nf*CF*Nc*(asu*Sepsilon)^2

cpbox010000011p1p2p3 := 4*(e-1)*(32*e^5*s3^5*s4^5*t+32*e^5*s3^5*s4^5*u+32*e^5*
s3^5*s4^4*t*u+32*e^5*s3^5*s4^4*u^2-64*e^5*s3^5*s4^3*t*u^2-64*e^5*s3^5*s4^3*u^3
+32*e^5*s3^4*s4^5*t*u+32*e^5*s3^4*s4^5*u^2-16*e^5*s3^4*s4^4*t^3-80*e^5*s3^4*s4
^4*t^2*u-192*e^5*s3^4*s4^4*t*u^2-128*e^5*s3^4*s4^4*u^3-16*e^5*s3^4*s4^3*t^3*u
-80*e^5*s3^4*s4^3*t^2*u^2-144*e^5*s3^4*s4^3*t*u^3-80*e^5*s3^4*s4^3*u^4+32*e^5*
s3^4*s4^2*t^3*u^2+160*e^5*s3^4*s4^2*t^2*u^3+304*e^5*s3^4*s4^2*t*u^4+176*e^5*s3
^4*s4^2*u^5-64*e^5*s3^3*s4^5*t*u^2-64*e^5*s3^3*s4^5*u^3-16*e^5*s3^3*s4^4*t^3*u
-80*e^5*s3^3*s4^4*t^2*u^2-144*e^5*s3^3*s4^4*t*u^3-80*e^5*s3^3*s4^4*u^4+2*e^5*
s3^3*s4^3*t^5+26*e^5*s3^3*s4^3*t^4*u+124*e^5*s3^3*s4^3*t^3*u^2+492*e^5*s3^3*s4
^3*t^2*u^3+866*e^5*s3^3*s4^3*t*u^4+474*e^5*s3^3*s4^3*u^5+2*e^5*s3^3*s4^2*t^5*u
+26*e^5*s3^3*s4^2*t^4*u^2+100*e^5*s3^3*s4^2*t^3*u^3-60*e^5*s3^3*s4^2*t^2*u^4
-390*e^5*s3^3*s4^2*t*u^5-254*e^5*s3^3*s4^2*u^6-4*e^5*s3^3*s4*t^5*u^2-52*e^5*s3^
3*s4*t^4*u^3-208*e^5*s3^3*s4*t^3*u^4-352*e^5*s3^3*s4*t^2*u^5-268*e^5*s3^3*s4*t
*u^6-76*e^5*s3^3*s4*u^7+32*e^5*s3^2*s4^4*t^3*u^2+160*e^5*s3^2*s4^4*t^2*u^3+304
```


$2*s^4^2*t^u^6-150*e^4*s^3^2*s^4^2*u^7-4*e^4*s^3^2*s^4*t^6*u^2-14*e^4*s^3^2*s^4*t^5*u^3-62*e^4*s^3^2*s^4*t^4*u^4+32*e^4*s^3^2*s^4*t^3*u^5+476*e^4*s^3^2*s^4*t^2*u^6+654*e^4*s^3^2*s^4*t^u^7+262*e^4*s^3^2*s^4*u^8+e^4*s^3^2*t^6*u^3+16*e^4*s^3^2*t^5*u^4+84*e^4*s^3^2*t^4*u^5+202*e^4*s^3^2*t^3*u^6+247*e^4*s^3^2*t^2*u^7+150*e^4*s^3^2*t^u^8+36$
 $*e^4*s^3^2*u^9-24*e^4*s^3*s^4^5*t^u^4-24*e^4*s^3*s^4^5*u^5+20*e^4*s^3*s^4^4*t^3*u^3+52*e^4*s^3*s^4^4*t^2*u^4+92*e^4*s^3*s^4^4*t^u^5+60*e^4*s^3*s^4^4*u^6-4*e^4*s^3*s^4^3*t^5*u^2-32*e^4*s^3*s^4^3*t^4*u^3-132*e^4*s^3*s^4^3*t^3*u^4-348*e^4*s^3*s^4^3*t^2*u^5$
 $-432*e^4*s^3*s^4^3*t^u^6-188*e^4*s^3*s^4^3*u^7-4*e^4*s^3*s^4^2*t^6*u^2-14*e^4*s^3*s^4^2*t^5*u^3-62*e^4*s^3*s^4^2*t^4*u^4+32*e^4*s^3*s^4^2*t^3*u^5+476*e^4*s^3*s^4^2*t^2*u^6$
 $+654*e^4*s^3*s^4^2*t^u^7+262*e^4*s^3*s^4^2*u^8-4*e^4*s^3*s^4*t^6*u^3+6*e^4*s^3*s^4*t^5*u^4+152*e^4*s^3*s^4*t^4*u^5+304*e^4*s^3*s^4*t^3*u^6+128*e^4*s^3*s^4*t^2*u^7-102*e^4$
 $*s^3*s^4*t^u^8-68*e^4*s^3*s^4*u^9+4*e^4*s^3*t^6*u^4-8*e^4*s^3*t^5*u^5-114*e^4*s^3*t^4*u^6-296*e^4*s^3*t^3*u^7-344*e^4*s^3*t^2*u^8-192*e^4*s^3*t^u^9-42*e^4*s^3*u^10+6*e$
 $^4*s^4^4*t^3*u^4+18*e^4*s^4^4*t^2*u^5+18*e^4*s^4^4*t^u^6+6*e^4*s^4^4*u^7-4*e^4*s^4^3*t^5*u^3-22*e^4*s^4^3*t^4*u^4-60*e^4*s^4^3*t^3*u^5-88*e^4*s^4^3*t^2*u^6-64*e^4*s$
 $^4^3*t^u^7-18*e^4*s^4^3*u^8+e^4*s^4^2*t^6*u^3+16*e^4*s^4^2*t^5*u^4+84*e^4*s^4^2*t^4*u^5+202*e^4*s^4^2*t^3*u^6+247*e^4*s^4^2*t^2*u^7+150*e^4*s^4^2*t^u^8+36$
 $*e^4*s^4^2*u^9+4*e^4*s^4*t^6*u^4-8*e^4*s^4*t^5*u^5-114*e^4*s^4*t^4*u^6-296*e^4*s^4*t^3*u^7-344*e^4*s^4*t^2*u^8-192*e^4*s^4*t^u^9-42*e^4*s^4*u^10-3*e^4*t^6*u^5+4*e^4*t^5*u^6$
 $+64*e^4*t^4*u^7+156*e^4*t^3*u^8+169*e^4*t^2*u^9+88*e^4*t^u^10+18*e^4*u^11-192*$
 $e^3*s^3^6*s^4^4*u+448*e^3*s^3^6*s^4^3*u^2-288*e^3*s^3^6*s^4^2*u^3+544*e^3*s^3^5*s^4^5*$
 $t-32*e^3*s^3^5*s^4^5*u-1024*e^3*s^3^5*s^4^4*t^u+448*e^3*s^3^5*s^4^4*u^2+96*e^3*s^3^5*$
 $s^4^3*t^2*u+328*e^3*s^3^5*s^4^3*t^u^2-1104*e^3*s^3^5*s^4^3*u^3-224*e^3*s^3^5*s^4^2*t^2$
 $*u^2-48*e^3*s^3^5*s^4^2*t^u^3+640*e^3*s^3^5*s^4^2*u^4+144*e^3*s^3^5*s^4*t^2*u^3+296$
 $*e^3*s^3^5*s^4*t^u^4+128*e^3*s^3^5*s^4*u^5-192*e^3*s^3^4*s^4^6*u-1024*e^3*s^3^4*s^4^5*$
 $t^u+448*e^3*s^3^4*s^4^5*u^2-272*e^3*s^3^4*s^4^4*t^3-640*e^3*s^3^4*s^4^4*t^2*u+1136*e$
 $^3*s^3^4*s^4^4*t^u^2-1184*e^3*s^3^4*s^4^4*u^3+512*e^3*s^3^4*s^4^3*t^3*u+1232*e^3*s^3^4$
 $*s^4^3*t^2*u^2+1224*e^3*s^3^4*s^4^3*t^u^3+2248*e^3*s^3^4*s^4^3*u^4-12*e^3*s^3^4*s^4^2$
 $*t^4*u-110*e^3*s^3^4*s^4^2*t^3*u^2+60*e^3*s^3^4*s^4^2*t^2*u^3-574*e^3*s^3^4*s^4^2*t$
 $*u^4-1052*e^3*s^3^4*s^4^2*u^5+28*e^3*s^3^4*s^4*t^4*u^2-100*e^3*s^3^4*s^4*t^3*u^3-688$
 $*e^3*s^3^4*s^4*t^2*u^4-924*e^3*s^3^4*s^4*t^u^5-316*e^3*s^3^4*s^4*u^6-18*e^3*s^3^4*t^4$
 $*u^3-70*e^3*s^3^4*t^3*u^4-104*e^3*s^3^4*t^2*u^5-70*e^3*s^3^4*t^u^6-18*e^3*s^3^4*u^7$
 $+448*e^3*s^3^3*s^4^6*u^2+96*e^3*s^3^3*s^4^5*t^2*u+328*e^3*s^3^3*s^4^5*t^u^2-1104*e^3$
 $*s^3^3*s^4^5*u^3+512*e^3*s^3^3*s^4^4*t^3*u+1232*e^3*s^3^3*s^4^4*t^2*u^2+1224*e^3*s^3$
 $^3*s^4^4*t^u^3+2248*e^3*s^3^3*s^4^4*u^4+34*e^3*s^3^3*s^4^3*t^5+190*e^3*s^3^3*s^4^3*t^4$
 $*u-360*e^3*s^3^3*s^4^3*t^3*u^2-1876*e^3*s^3^3*s^4^3*t^2*u^3-3090*e^3*s^3^3*s^4^3*t^*$
 $u^4-2930*e^3*s^3^3*s^4^3*u^5-64*e^3*s^3^3*s^4^2*t^5*u-456*e^3*s^3^3*s^4^2*t^4*u^2$
 $-1354*e^3*s^3^3*s^4^2*t^3*u^3-1810*e^3*s^3^3*s^4^2*t^2*u^4-446*e^3*s^3^3*s^4^2*t^u^5+$
 $770*e^3*s^3^3*s^4^2*u^6+8*e^3*s^3^3*s^4*t^5*u^2+150*e^3*s^3^3*s^4*t^4*u^3+992*e^3*s^3$
 $^3*s^4*t^3*u^4+2232*e^3*s^3^3*s^4*t^2*u^5+1944*e^3*s^3^3*s^4*t^u^6+538*e^3*s^3^3*s^4*$
 $u^7+26*e^3*s^3^3*t^5*u^3+152*e^3*s^3^3*t^4*u^4+346*e^3*s^3^3*t^3*u^5+390*e^3*s^3^3$
 $*t^2*u^6+220*e^3*s^3^3*t^u^7+50*e^3*s^3^3*u^8-288*e^3*s^3^2*s^4^6*u^3-224*e^3*s^3^2$
 $*s^4^5*t^2*u^2-48*e^3*s^3^2*s^4^5*t^u^3+640*e^3*s^3^2*s^4^5*u^4-12*e^3*s^3^2*s^4^4*t^4$
 $*u-110*e^3*s^3^2*s^4^4*t^3*u^2+60*e^3*s^3^2*s^4^4*t^2*u^3-574*e^3*s^3^2*s^4^4*t^u^4$
 $-1052*e^3*s^3^2*s^4^4*u^5-64*e^3*s^3^2*s^4^3*t^5*u-456*e^3*s^3^2*s^4^3*t^4*u^2-1354*$

$$\begin{aligned}
& e^3 s^3 t^2 s^4 t^3 u^3 - 1810 e^3 s^3 t^2 s^4 t^2 u^4 - 446 e^3 s^3 t^2 s^4 t^3 u^5 + 770 e^3 s^3 t^2 s^4 t^3 u^6 - 7 e^3 s^3 t^2 s^4 t^2 t^6 u + 59 e^3 s^3 t^2 s^4 t^2 t^5 u^2 + 923 e^3 s^3 t^2 s^4 t^2 t^4 u^3 + 3438 e^3 s^3 t^2 s^4 t^2 t^3 u^4 + 5243 e^3 s^3 t^2 s^4 t^2 t^2 u^5 + 3495 e^3 s^3 t^2 s^4 t^2 t^2 u^6 + 577 e^3 s^3 t^2 s^4 t^2 u^7 + 28 e^3 s^3 t^2 s^4 t^6 u^2 + 182 e^3 s^3 t^2 s^4 t^5 u^3 + 90 e^3 s^3 t^2 s^4 t^4 u^4 - 1110 e^3 s^3 t^2 s^4 t^3 u^5 - 2522 e^3 s^3 t^2 s^4 t^2 u^6 - 2040 e^3 s^3 t^2 s^4 t^2 u^7 - 564 e^3 s^3 t^2 s^4 u^8 - 23 e^3 s^3 t^2 t^6 u^3 - 193 e^3 s^3 t^2 t^5 u^4 - 623 e^3 s^3 t^2 t^4 u^5 - 1024 e^3 s^3 t^2 t^3 u^6 - 921 e^3 s^3 t^2 t^2 u^7 - 435 e^3 s^3 t^2 t^2 u^8 - 85 e^3 s^3 t^2 u^9 + 144 e^3 s^3 s^4 t^5 t^2 u^3 + 296 e^3 s^3 s^4 t^5 t^2 u^4 + 128 e^3 s^3 s^4 t^5 u^5 + 28 e^3 s^3 s^4 t^4 t^4 u^2 - 100 e^3 s^3 s^4 t^4 t^3 u^3 - 688 e^3 s^3 s^4 t^4 t^2 u^4 - 924 e^3 s^3 s^4 t^4 t^2 u^5 - 316 e^3 s^3 s^4 t^4 u^6 + 8 e^3 s^3 s^4 t^3 t^5 u^2 + 150 e^3 s^3 s^4 t^3 t^4 u^3 + 992 e^3 s^3 s^4 t^3 t^3 u^4 + 2232 e^3 s^3 s^4 t^3 t^2 u^5 + 1944 e^3 s^3 s^4 t^3 t^2 u^6 + 538 e^3 s^3 s^4 t^3 u^7 + 28 e^3 s^3 s^4 t^2 t^6 u^2 + 182 e^3 s^3 s^4 t^2 t^5 u^3 + 90 e^3 s^3 s^4 t^2 t^4 u^4 - 1110 e^3 s^3 s^4 t^2 t^3 u^5 - 2522 e^3 s^3 s^4 t^2 t^2 u^6 - 2040 e^3 s^3 s^4 t^2 t^2 u^7 - 564 e^3 s^3 s^4 t^2 u^8 - 84 e^3 s^3 s^4 t^6 u^3 - 550 e^3 s^3 s^4 t^5 u^4 - 1222 e^3 s^3 s^4 t^4 u^5 - 1152 e^3 s^3 s^4 t^3 u^6 - 296 e^3 s^3 s^4 t^2 u^7 + 222 e^3 s^3 s^4 t^2 u^8 + 122 e^3 s^3 s^4 u^9 + 60 e^3 s^3 t^6 u^4 + 380 e^3 s^3 t^5 u^5 + 1010 e^3 s^3 t^4 u^6 + 1442 e^3 s^3 t^3 u^7 + 1166 e^3 s^3 t^2 u^8 + 506 e^3 s^3 t^2 u^9 + 92 e^3 s^3 t^2 u^{10} - 18 e^3 s^4 t^4 t^4 u^3 - 70 e^3 s^4 t^4 t^3 u^4 - 104 e^3 s^4 t^4 t^2 u^5 - 70 e^3 s^4 t^4 t^2 u^6 - 18 e^3 s^4 t^4 u^7 + 26 e^3 s^4 t^3 t^5 u^3 + 152 e^3 s^4 t^3 t^4 u^4 + 346 e^3 s^4 t^3 t^3 u^5 + 390 e^3 s^4 t^3 t^2 u^6 + 220 e^3 s^4 t^3 t^2 u^7 + 50 e^3 s^4 t^3 u^8 - 23 e^3 s^4 t^2 t^6 u^3 - 193 e^3 s^4 t^2 t^5 u^4 - 623 e^3 s^4 t^2 t^4 u^5 - 1024 e^3 s^4 t^2 t^3 u^6 - 921 e^3 s^4 t^2 t^2 u^7 - 435 e^3 s^4 t^2 t^2 u^8 - 85 e^3 s^4 t^2 u^9 + 60 e^3 s^4 t^6 u^4 + 380 e^3 s^4 t^5 u^5 + 1010 e^3 s^4 t^4 u^6 + 1442 e^3 s^4 t^3 u^7 + 1166 e^3 s^4 t^2 u^8 + 506 e^3 s^4 t^2 u^9 + 92 e^3 s^4 t^2 u^{10} - 39 e^3 t^6 u^5 - 221 e^3 t^5 u^6 - 533 e^3 t^4 u^7 - 702 e^3 t^3 u^8 - 533 e^3 t^2 u^9 - 221 e^3 t^2 u^{10} - 39 e^3 u^{11} + 352 e^2 s^3 t^6 s^4 t^4 u - 960 e^2 s^3 t^6 s^4 t^3 u^2 + 576 e^2 s^3 t^6 s^4 t^2 u^3 - 608 e^2 s^3 t^5 s^4 t^5 t + 448 e^2 s^3 t^5 s^4 t^5 u + 1120 e^2 s^3 t^5 s^4 t^4 t u - 2464 e^2 s^3 t^5 s^4 t^4 u^2 - 176 e^2 s^3 t^5 s^4 t^3 t^2 u - 124 e^2 s^3 t^5 s^4 t^3 t^2 u^2 + 3964 e^2 s^3 t^5 s^4 t^3 u^3 + 480 e^2 s^3 t^5 s^4 t^2 t^2 u^2 + 248 e^2 s^3 t^5 s^4 t^2 t^2 u^3 - 1656 e^2 s^3 t^5 s^4 t^2 u^4 - 288 e^2 s^3 t^5 s^4 t^2 u^3 - 540 e^2 s^3 t^5 s^4 t^2 u^4 - 212 e^2 s^3 t^5 s^4 u^5 + 352 e^2 s^3 t^4 s^4 t^6 u + 1120 e^2 s^3 t^4 s^4 t^5 t u - 2464 e^2 s^3 t^4 s^4 t^5 u^2 + 304 e^2 s^3 t^4 s^4 t^4 t^3 + 528 e^2 s^3 t^4 s^4 t^4 t^2 u - 1064 e^2 s^3 t^4 s^4 t^4 t^2 u^2 + 6520 e^2 s^3 t^4 s^4 t^4 u^3 - 560 e^2 s^3 t^4 s^4 t^3 t^3 u - 568 e^2 s^3 t^4 s^4 t^3 t^2 u^2 - 1056 e^2 s^3 t^4 s^4 t^3 t^2 u^3 - 6760 e^2 s^3 t^4 s^4 t^3 u^4 + 22 e^2 s^3 t^4 s^4 t^2 t^4 u - 24 e^2 s^3 t^4 s^4 t^2 t^3 u^2 - 1592 e^2 s^3 t^4 s^4 t^2 t^2 u^3 - 1224 e^2 s^3 t^4 s^4 t^2 t^2 u^4 + 1602 e^2 s^3 t^4 s^4 t^2 u^5 - 60 e^2 s^3 t^4 s^4 t^4 u^2 + 112 e^2 s^3 t^4 s^4 t^3 u^3 + 1320 e^2 s^3 t^4 s^4 t^2 u^4 + 1888 e^2 s^3 t^4 s^4 t^2 u^5 + 660 e^2 s^3 t^4 s^4 u^6 + 36 e^2 s^3 t^4 t^4 u^3 + 128 e^2 s^3 t^4 t^3 u^4 + 172 e^2 s^3 t^4 t^2 u^5 + 104 e^2 s^3 t^4 t^2 u^6 + 24 e^2 s^3 t^4 u^7 - 960 e^2 s^3 t^3 s^4 t^6 u^2 - 176 e^2 s^3 t^3 s^4 t^5 t^2 u - 124 e^2 s^3 t^3 s^4 t^5 t^2 u^2 + 3964 e^2 s^3 t^3 s^4 t^5 u^3 - 560 e^2 s^3 t^3 s^4 t^4 t^3 u - 568 e^2 s^3 t^3 s^4 t^4 t^2 u^2 - 1056 e^2 s^3 t^3 s^4 t^4 t^2 u^3 - 6760 e^2 s^3 t^3 s^4 t^4 u^4 - 38 e^2 s^3 t^3 s^4 t^3 t^5 - 196 e^2 s^3 t^3 s^4 t^3 t^4 u + 208 e^2 s^3 t^3 s^4 t^3 t^3 u^2 - 228 e^2 s^3 t^3 s^4 t^3 t^2 u^3 + 222 e^2 s^3 t^3 s^4 t^3 t^2 u^4 + 4512 e^2 s^3 t^3 s^4 t^3 u^5 + 70 e^2 s^3 t^3 s^4 t^2 t^5 u + 470 e^2 s^3 t^3 s^4 t^2 t^4 u^2 + 1906 e^2 s^3 t^3 s^4 t^2 t^3 u^3 + 4702 e^2 s^3 t^3 s^4 t^2 t^2 u^4 + 4384 e^2 s^3 t^3 s^4 t^2 t^2 u^5 + 212 e^2 s^3 t^3 s^4 t^2 u^6 + 12 e^2 s^3 t^3 s^4 t^5 u^2 + 22 e^2 s^3 t^3 s^4 t^4 u^3 - 808 e^2 s^3 t^3 s^4 t^3 u^4 - 2788 e^2 s^3 t^3 s^4 t^2 u^5 - 2880 e^2 s^3 t^3 s^4 t^2 u^6 - 870 e^2 s^3 t^3 s^4 u^7 - 40 e^2 s^3 t^3
\end{aligned}$$

$$\begin{aligned}
 & *s^4 \cdot 2t^4 \cdot u^2 - 940 \cdot e \cdot s^3 \cdot s^4 \cdot 2t^2 \cdot u^3 - 3468 \cdot e \cdot s^3 \cdot s^4 \cdot 2t^2 \cdot u^4 - 4150 \cdot e \cdot s^3 \cdot s^4 \cdot \\
 & 2t \cdot u^5 - 740 \cdot e \cdot s^3 \cdot s^4 \cdot 2u^6 - 16 \cdot e \cdot s^3 \cdot s^4 \cdot t^5 \cdot u^2 - 128 \cdot e \cdot s^3 \cdot s^4 \cdot t^4 \cdot u^3 + 76 \cdot e \cdot s^3 \cdot \\
 & ^3 \cdot s^4 \cdot t^3 \cdot u^4 + 1248 \cdot e \cdot s^3 \cdot s^4 \cdot t^2 \cdot u^5 + 1720 \cdot e \cdot s^3 \cdot s^4 \cdot t \cdot u^6 + 644 \cdot e \cdot s^3 \cdot s^4 \cdot u^7 + 22 \\
 & \cdot e \cdot s^3 \cdot 3t^5 \cdot u^3 + 160 \cdot e \cdot s^3 \cdot 3t^4 \cdot u^4 + 404 \cdot e \cdot s^3 \cdot 3t^3 \cdot u^5 + 476 \cdot e \cdot s^3 \cdot 3t^2 \cdot u^6 + 270 \cdot e \\
 & \cdot s^3 \cdot 3t \cdot u^7 + 60 \cdot e \cdot s^3 \cdot 3u^8 - 352 \cdot e \cdot s^3 \cdot 2s^4 \cdot u^3 - 320 \cdot e \cdot s^3 \cdot 2s^4 \cdot 5t^2 \cdot u^2 - 248 \cdot e \cdot s^3 \\
 & \cdot 2s^4 \cdot 5t \cdot u^3 + 1096 \cdot e \cdot s^3 \cdot 2s^4 \cdot 5u^4 - 16 \cdot e \cdot s^3 \cdot 2s^4 \cdot 4t^4 \cdot u + 72 \cdot e \cdot s^3 \cdot 2s^4 \cdot 4t^3 \cdot u^2 \\
 & + 1462 \cdot e \cdot s^3 \cdot 2s^4 \cdot 4t^2 \cdot u^3 + 1660 \cdot e \cdot s^3 \cdot 2s^4 \cdot 4t \cdot u^4 - 818 \cdot e \cdot s^3 \cdot 2s^4 \cdot 4u^5 - 30 \cdot e \cdot s^3 \cdot 2 \\
 & \cdot s^4 \cdot 3t^5 \cdot u - 176 \cdot e \cdot s^3 \cdot 2s^4 \cdot 3t^4 \cdot u^2 - 940 \cdot e \cdot s^3 \cdot 2s^4 \cdot 3t^3 \cdot u^3 - 3468 \cdot e \cdot s^3 \cdot 2s^4 \cdot 3t^2 \cdot \\
 & \cdot 2u^4 - 4150 \cdot e \cdot s^3 \cdot 2s^4 \cdot 3t \cdot u^5 - 740 \cdot e \cdot s^3 \cdot 2s^4 \cdot 3u^6 - 7 \cdot e \cdot s^3 \cdot 2s^4 \cdot 2t^6 \cdot u - 18 \cdot e \cdot s^3 \cdot \\
 & 2s^4 \cdot 2t^5 \cdot u^2 + 190 \cdot e \cdot s^3 \cdot 2s^4 \cdot 2t^4 \cdot u^3 + 1280 \cdot e \cdot s^3 \cdot 2s^4 \cdot 2t^3 \cdot u^4 + 3453 \cdot e \cdot s^3 \cdot 2s^4 \\
 & \cdot 2t^2 \cdot u^5 + 3834 \cdot e \cdot s^3 \cdot 2s^4 \cdot 2t \cdot u^6 + 1188 \cdot e \cdot s^3 \cdot 2s^4 \cdot 2u^7 + 22 \cdot e \cdot s^3 \cdot 2s^4 \cdot t^6 \cdot u^2 + \\
 & 186 \cdot e \cdot s^3 \cdot 2s^4 \cdot t^5 \cdot u^3 + 532 \cdot e \cdot s^3 \cdot 2s^4 \cdot t^4 \cdot u^4 + 588 \cdot e \cdot s^3 \cdot 2s^4 \cdot t^3 \cdot u^5 - 118 \cdot e \cdot s^3 \cdot 2s^4 \\
 & \cdot t^2 \cdot u^6 - 622 \cdot e \cdot s^3 \cdot 2s^4 \cdot t \cdot u^7 - 284 \cdot e \cdot s^3 \cdot 2s^4 \cdot u^8 - 13 \cdot e \cdot s^3 \cdot 2t^6 \cdot u^3 - 122 \cdot e \cdot s^3 \cdot 2t^5 \\
 & \cdot u^4 - 452 \cdot e \cdot s^3 \cdot 2t^4 \cdot u^5 - 840 \cdot e \cdot s^3 \cdot 2t^3 \cdot u^6 - 835 \cdot e \cdot s^3 \cdot 2t^2 \cdot u^7 - 426 \cdot e \cdot s^3 \cdot 2t \cdot u^8 - 88 \\
 & \cdot e \cdot s^3 \cdot 2u^9 + 176 \cdot e \cdot s^3 \cdot s^4 \cdot 5t^2 \cdot u^3 + 332 \cdot e \cdot s^3 \cdot s^4 \cdot 5t \cdot u^4 + 140 \cdot e \cdot s^3 \cdot s^4 \cdot 5u^5 + \\
 & 40 \cdot e \cdot s^3 \cdot s^4 \cdot 4t^4 \cdot u^2 - 32 \cdot e \cdot s^3 \cdot s^4 \cdot 4t^3 \cdot u^3 - 804 \cdot e \cdot s^3 \cdot s^4 \cdot 4t^2 \cdot u^4 - 1264 \cdot e \cdot s^3 \cdot s^4 \cdot 4 \\
 & \cdot t \cdot u^5 - 500 \cdot e \cdot s^3 \cdot s^4 \cdot 4u^6 - 16 \cdot e \cdot s^3 \cdot s^4 \cdot 3t^5 \cdot u^2 - 128 \cdot e \cdot s^3 \cdot s^4 \cdot 3t^4 \cdot u^3 + 76 \cdot e \cdot s^3 \cdot s^4 \\
 & \cdot 3t^3 \cdot u^4 + 1248 \cdot e \cdot s^3 \cdot s^4 \cdot 3t^2 \cdot u^5 + 1720 \cdot e \cdot s^3 \cdot s^4 \cdot 3t \cdot u^6 + 644 \cdot e \cdot s^3 \cdot s^4 \cdot 3u^7 + 22 \cdot e \cdot s^3 \\
 & \cdot s^4 \cdot 2t^6 \cdot u^2 + 186 \cdot e \cdot s^3 \cdot s^4 \cdot 2t^5 \cdot u^3 + 532 \cdot e \cdot s^3 \cdot s^4 \cdot 2t^4 \cdot u^4 + 588 \cdot e \cdot s^3 \cdot s^4 \cdot 2t^3 \cdot u^5 - 118 \\
 & \cdot e \cdot s^3 \cdot s^4 \cdot 2t^2 \cdot u^6 - 622 \cdot e \cdot s^3 \cdot s^4 \cdot 2t \cdot u^7 - 284 \cdot e \cdot s^3 \cdot s^4 \cdot 2u^8 - 60 \cdot e \cdot s^3 \cdot s^4 \cdot t^6 \cdot u^3 - 396 \\
 & \cdot e \cdot s^3 \cdot s^4 \cdot t^5 \cdot u^4 - 1044 \cdot e \cdot s^3 \cdot s^4 \cdot t^4 \cdot u^5 - 1500 \cdot e \cdot s^3 \cdot s^4 \cdot t^3 \cdot u^6 - 1212 \cdot e \cdot s^3 \cdot s^4 \cdot t^2 \cdot u^7 - 480 \\
 & \cdot e \cdot s^3 \cdot s^4 \cdot t \cdot u^8 - 60 \cdot e \cdot s^3 \cdot s^4 \cdot u^9 + 34 \cdot e \cdot s^3 \cdot t^6 \cdot u^4 + 206 \cdot e \cdot s^3 \cdot t^5 \cdot u^5 + 544 \cdot e \cdot s^3 \cdot t^4 \cdot u^6 + 796 \\
 & \cdot e \cdot s^3 \cdot t^3 \cdot u^7 + 674 \cdot e \cdot s^3 \cdot t^2 \cdot u^8 + 310 \cdot e \cdot s^3 \cdot t \cdot u^9 + 60 \cdot e \cdot s^3 \cdot u^{10} - 22 \cdot e \cdot s^4 \cdot 4t^4 \cdot u^3 - 80 \\
 & \cdot e \cdot s^4 \cdot 4t^3 \cdot u^4 - 110 \cdot e \cdot s^4 \cdot 4t^2 \cdot u^5 - 68 \cdot e \cdot s^4 \cdot 4t \cdot u^6 - 16 \cdot e \cdot s^4 \cdot 4u^7 + 22 \cdot e \cdot s^4 \cdot 3t^5 \cdot u^3 + 160 \\
 & \cdot e \cdot s^4 \cdot 3t^4 \cdot u^4 + 404 \cdot e \cdot s^4 \cdot 3t^3 \cdot u^5 + 476 \cdot e \cdot s^4 \cdot 3t^2 \cdot u^6 + 270 \cdot e \cdot s^4 \cdot 3t \cdot u^7 + 60 \cdot e \cdot s^4 \cdot 3u^8 - 13 \\
 & \cdot e \cdot s^4 \cdot 2t^6 \cdot u^3 - 122 \cdot e \cdot s^4 \cdot 2t^5 \cdot u^4 - 452 \cdot e \cdot s^4 \cdot 2t^4 \cdot u^5 - 840 \cdot e \cdot s^4 \cdot 2t^3 \cdot u^6 - 835 \cdot e \cdot s^4 \cdot 2t^2 \cdot u^7 - 426 \\
 & \cdot e \cdot s^4 \cdot 2t \cdot u^8 - 88 \cdot e \cdot s^4 \cdot 2u^9 + 34 \cdot e \cdot s^4 \cdot t^6 \cdot u^4 + 206 \cdot e \cdot s^4 \cdot t^5 \cdot u^5 + 544 \cdot e \cdot s^4 \cdot t^4 \cdot u^6 + 796 \\
 & \cdot e \cdot s^4 \cdot t^3 \cdot u^7 + 674 \cdot e \cdot s^4 \cdot t^2 \cdot u^8 + 310 \cdot e \cdot s^4 \cdot t \cdot u^9 + 60 \cdot e \cdot s^4 \cdot u^{10} - 19 \cdot e \cdot t^6 \cdot u^5 - 98 \cdot e \cdot t^5 \cdot u^6 - 218 \\
 & \cdot e \cdot t^4 \cdot u^7 - 272 \cdot e \cdot t^3 \cdot u^8 - 203 \cdot e \cdot t^2 \cdot u^9 - 86 \cdot e \cdot t \cdot u^{10} - 16 \cdot e \cdot u^{11} + 64 \cdot s^3 \cdot 6s^4 \cdot 4u - 128 \cdot s^3 \cdot 6s^4 \\
 & \cdot 3u^2 + 64 \cdot s^3 \cdot 6s^4 \cdot 2u^3 - 64 \cdot s^3 \cdot 5s^4 \cdot 5t + 128 \cdot s^3 \cdot 5s^4 \cdot 5u + 64 \cdot s^3 \cdot 5s^4 \cdot 4t \cdot u - 512 \cdot s^3 \cdot 5s^4 \\
 & \cdot 4u^2 - 32 \cdot s^3 \cdot 5s^4 \cdot 3t^2 \cdot u + 608 \cdot s^3 \cdot 5s^4 \cdot 3u^3 + 64 \cdot s^3 \cdot 5s^4 \cdot 2t^2 \cdot u^2 + 64 \cdot s^3 \cdot 5s^4 \cdot 2t \cdot u^3 - 192 \\
 & \cdot s^3 \cdot 5s^4 \cdot 2u^4 - 32 \cdot s^3 \cdot 5s^4 \cdot t^2 \cdot u^3 - 64 \cdot s^3 \cdot 5s^4 \cdot t \cdot u^4 - 32 \cdot s^3 \cdot 5s^4 \cdot u^5 + 64 \cdot s^3 \cdot 4s^4 \cdot 6u + 64 \\
 & \cdot s^3 \cdot 4s^4 \cdot 5t \cdot u - 512 \cdot s^3 \cdot 4s^4 \cdot 5u^2 + 32 \cdot s^3 \cdot 4s^4 \cdot 4t^3 \cdot u + 32 \cdot s^3 \cdot 4s^4 \cdot 4t^2 \cdot u^2 - 32 \cdot s^3 \cdot 4s^4 \cdot 4t \\
 & \cdot u^3 - 32 \cdot s^3 \cdot 4s^4 \cdot 4t^2 \cdot u^2 + 1152 \cdot s^3 \cdot 4s^4 \cdot 4u^3 - 32 \cdot s^3 \cdot 4s^4 \cdot 3t^3 \cdot u + 128 \cdot s^3 \cdot 4s^4 \cdot 3t^2 \cdot u^2 + 160 \\
 & \cdot s^3 \cdot 4s^4 \cdot 3t \cdot u^3 - 896 \cdot s^3 \cdot 4s^4 \cdot 3u^4 + 4 \cdot s^3 \cdot 4s^4 \cdot 2t^4 \cdot u - 16 \cdot s^3 \cdot 4s^4 \cdot 2t^3 \cdot u^2 - 328 \cdot s^3 \cdot 4s^4 \\
 & \cdot 2t^2 \cdot u^3 - 464 \cdot s^3 \cdot 4s^4 \cdot 2t \cdot u^4 + 68 \cdot s^3 \cdot 4s^4 \cdot 2u^5 - 8 \cdot s^3 \cdot 4s^4 \cdot s^4 \cdot t^4 \cdot u^2 + 144 \cdot s^3 \cdot 4s^4 \cdot t^2 \cdot u^4 + 256 \\
 & \cdot s^3 \cdot 4s^4 \cdot t \cdot u^5 + 120 \cdot s^3 \cdot 4s^4 \cdot u^6 + 4 \cdot s^3 \cdot 4t^4 \cdot u^3 + 16 \cdot s^3 \cdot 4t^3 \cdot u^4 + 24 \cdot s^3 \cdot 4t^2 \cdot u^5 + 16 \cdot s^3 \cdot 4t \\
 & \cdot u^6 + 4 \cdot s^3 \cdot 4u^7 - 128 \cdot s^3 \cdot 3s^4 \cdot 6u^2 - 32 \cdot s^3 \cdot 3s^4 \cdot 5t^2 \cdot u + 608 \cdot s^3 \cdot 3s^4 \cdot 5u^3 - 32 \cdot s^3 \cdot 3s^4 \cdot 4t^3 \cdot u + 128 \\
 & \cdot s^3 \cdot 3s^4 \cdot 4t^2 \cdot u^2 + 160 \cdot s^3 \cdot 3s^4 \cdot 4t \cdot u^3 - 896 \cdot s^3 \cdot 3s^4 \cdot 4u^4 - 4 \cdot s^3 \cdot 3s^4 \cdot 3t^5 \cdot u - 24 \cdot s^3 \cdot 3s^4 \cdot 3t^4 \cdot u^2 - 528 \\
 & \cdot s^3 \cdot 3s^4 \cdot 3t^3 \cdot u^3 - 772 \cdot s^3 \cdot 3s^4 \cdot 3t^2 \cdot u^4 + 296 \cdot s^3 \cdot 3s^4 \cdot 3t \cdot u^5 + 4 \cdot s^3 \cdot 3s^4 \cdot 2t^5 \cdot u + 16 \cdot s^3 \cdot 3s^4 \\
 & \cdot 2t^4 \cdot u^2 + 120 \cdot s^3 \cdot 3s^4 \cdot 2t^3 \cdot u^3 + 688 \cdot s^3 \cdot 3s^4 \cdot 2t^2 \cdot u^4 + 996 \cdot s^3 \cdot 3s^4 \cdot 2t \cdot u^5 + 288 \cdot s^3 \cdot 3s^4 \cdot 2u^6 + 4 \\
 & \cdot s^3 \cdot 3s^4 \cdot t^5 \cdot u^2 + 40 \cdot s^3 \cdot 3s^4 \cdot t^4 \cdot u^3 + 56 \cdot s^3 \cdot 3s^4 \cdot t^3 \cdot u^4 - 144 \cdot s^3 \cdot 3s^4 \cdot t^2 \cdot u^5 - 316 \cdot s^3 \cdot 3s^4 \cdot t \cdot u^6 - 152 \\
 & \cdot s^3 \cdot 3s^4 \cdot u^7 - 4 \cdot s^3 \cdot
 \end{aligned}$$

$*s^4u^8 - 27e^3t^6u^3 - 151e^3t^5u^4 - 373e^3t^4u^5 - 522e^3t^3u^6 - 433e^3t^2u^7 - 199e^3t^1u^8 - 39e^3u^9 + 256e^2s^3s^6s^4^2u - 416e^2s^3s^5s^4^3t + 352e^2s^3s^5s^4^3u - 176e^2s^3s^5s^4^2t^2u - 944e^2s^3s^5s^4^2u^2 - 104e^2s^3s^5s^4t^2u - 172e^2s^3s^5s^4t^2u^2 - 188e^2s^3s^5s^4u^3 + 256e^2s^3s^4s^4^4u + 944e^2s^3s^4s^4^3t^2u - 1424e^2s^3s^4s^4^3u^2 + 208e^2s^3s^4s^4^2t^3 + 248e^2s^3s^4s^4^2t^2u + 1064e^2s^3s^4s^4^2t^2u^2 + 1472e^2s^3s^4s^4^2u^3 + 112e^2s^3s^4s^4t^3u + 472e^2s^3s^4s^4t^2u^2 + 752e^2s^3s^4s^4t^3u^3 + 632e^2s^3s^4s^4u^4 - 4e^2s^3s^4t^4u + 24e^2s^3s^4t^3u^2 + 84e^2s^3s^4t^2u^3 + 80e^2s^3s^4t^1u^4 + 24e^2s^3s^4u^5 - 896e^2s^3s^3s^4^4u^2 - 128e^2s^3s^3s^4^3t^2u + 100e^2s^3s^3s^4^3t^2u^2 + 1676e^2s^3s^3s^4^3u^3 - 480e^2s^3s^3s^4^2t^3u - 904e^2s^3s^3s^4^2t^2u^2 - 1016e^2s^3s^3s^4^2t^1u^3 - 848e^2s^3s^3s^4^2u^4 - 26e^2s^3s^3s^4t^5 - 114e^2s^3s^3s^4t^4u - 688e^2s^3s^3s^4t^3u^2 - 1552e^2s^3s^3s^4t^2u^3 - 1762e^2s^3s^3s^4t^1u^4 - 930e^2s^3s^3s^4u^5 + 4e^2s^3s^3t^5u - 8e^2s^3s^3t^4u^2 - 150e^2s^3s^3t^3u^3 - 338e^2s^3s^3t^2u^4 - 278e^2s^3s^3t^1u^5 - 78e^2s^3s^3u^6 + 576e^2s^3s^2s^4^4u^3 + 448e^2s^3s^2s^4^3t^2u^2 + 104e^2s^3s^2s^4^3t^1u^3 - 360e^2s^3s^2s^4^3u^4 + 16e^2s^3s^2s^4^2t^4u - 96e^2s^3s^2s^4^2t^3u^2 - 452e^2s^3s^2s^4^2t^2u^3 - 784e^2s^3s^2s^4^2t^1u^4 - 188e^2s^3s^2s^4^2u^5 + 68e^2s^3s^2s^4t^5u + 544e^2s^3s^2s^4t^4u^2 + 1538e^2s^3s^2s^4t^3u^3 + 2182e^2s^3s^2s^4t^2u^4 + 1802e^2s^3s^2s^4t^1u^5 + 682e^2s^3s^2s^4u^6 - 3e^2s^3s^2t^6u + 20e^2s^3s^2t^5u^2 + 200e^2s^3s^2t^4u^3 + 576e^2s^3s^2t^3u^4 + 761e^2s^3s^2t^2u^5 + 476e^2s^3s^2t^1u^6 + 114e^2s^3s^2u^7 - 288e^2s^3s^4^3t^2u^3 - 540e^2s^3s^4^3t^1u^4 - 212e^2s^3s^4^3u^5 - 56e^2s^3s^4^2t^4u^2 + 160e^2s^3s^4^2t^3u^3 + 720e^2s^3s^4^2t^2u^4 + 728e^2s^3s^4^2t^1u^5 + 224e^2s^3s^4^2u^6 + 2e^2s^3s^4t^5u^2 - 190e^2s^3s^4t^4u^3 - 508e^2s^3s^4t^3u^4 - 604e^2s^3s^4t^2u^5 - 454e^2s^3s^4t^1u^6 - 166e^2s^3s^4u^7 - 30e^2s^3t^6u^2 - 192e^2s^3t^5u^3 - 560e^2s^3t^4u^4 - 918e^2s^3t^3u^5 - 864e^2s^3t^2u^6 - 434e^2s^3t^1u^7 - 90e^2s^3u^8 + 36e^2s^4^2t^4u^3 + 128e^2s^4^2t^3u^4 + 172e^2s^4^2t^2u^5 + 104e^2s^4^2t^1u^6 + 24e^2s^4^2u^7 - 36e^2s^4t^5u^3 - 176e^2s^4t^4u^4 - 342e^2s^4t^3u^5 - 330e^2s^4t^2u^6 - 158e^2s^4t^1u^7 - 30e^2s^4u^8 + 29e^2t^6u^3 + 152e^2t^5u^4 + 348e^2t^4u^5 + 452e^2t^3u^6 + 353e^2t^2u^7 + 156e^2t^1u^8 + 30e^2u^9 - 160e^2s^3s^6s^4^2u + 224e^2s^3s^5s^4^3t - 256e^2s^3s^5s^4^3u + 144e^2s^3s^5s^4^2t^2u + 688e^2s^3s^5s^4^2u^2 + 56e^2s^3s^5s^4t^2u + 124e^2s^3s^5s^4t^1u^2 + 116e^2s^3s^5s^4u^3 - 160e^2s^3s^4s^4^4u - 400e^2s^3s^4s^4^3t^2u + 1168e^2s^3s^4s^4^3u^2 - 112e^2s^3s^4s^4^2t^3 - 168e^2s^3s^4s^4^2t^2u - 680e^2s^3s^4s^4^2t^1u^2 - 1024e^2s^3s^4s^4^2u^3 - 64e^2s^3s^4s^4t^3u - 360e^2s^3s^4s^4t^2u^2 - 648e^2s^3s^4s^4t^1u^3 - 448e^2s^3s^4s^4u^4 + 2e^2s^3s^4t^4u - 16e^2s^3s^4t^3u^2 - 54e^2s^3s^4t^2u^3 - 52e^2s^3s^4t^1u^4 - 16e^2s^3s^4u^5 + 576e^2s^3s^3s^4^4u^2 + 80e^2s^3s^3s^4^3t^2u - 244e^2s^3s^3s^4^3t^1u^2 - 1396e^2s^3s^3s^4^3u^3 + 208e^2s^3s^3s^4^2t^3u + 264e^2s^3s^3s^4^2t^2u^2 + 192e^2s^3s^3s^4^2t^1u^3 + 328e^2s^3s^3s^4^2u^4 + 14e^2s^3s^3s^4t^5 + 80e^2s^3s^3s^4t^4u + 448e^2s^3s^3s^4t^3u^2 + 1120e^2s^3s^3s^4t^2u^3 + 1350e^2s^3s^3s^4t^1u^4 + 660e^2s^3s^3s^4u^5 - 2e^2s^3s^3t^5u + 16e^2s^3s^3t^4u^2 + 132e^2s^3s^3t^3u^3 + 268e^2s^3s^3t^2u^4 + 214e^2s^3s^3t^1u^5 + 60e^2s^3s^3u^6 - 352e^2s^3s^2s^4^4u^3 - 288e^2s^3s^2s^4^3t^2u^2 - 104e^2s^3s^2s^4^3t^1u^3 + 312e^2s^3s^2s^4^3u^4 - 10e^2s^3s^2s^4^2t^4u + 144e^2s^3s^2s^4^2t^3u^2 + 706e^2s^3s^2s^4^2t^2u^3 + 1060e^2s^3s^2s^4^2t^1u^4 + 396e^2s^3s^2s^4^2u^5 - 30e^2s^3s^2s^4t^5u - 260e^2s^3s^2s^4t^4u^2 - 764e^2s^3s^2s^4t^3u^3 - 1176e^2s^3s^2s^4t^2u^4 - 1046e^2s^3s^2s^4t^1u^5 - 404e^2s^3s^2s^4u^6 - e^2s^3s^2t^6u - 26e^2s^3s^2t^5u^2 - 164e^2s^3s^2t^4u^3$

$$\begin{aligned}
 & u^3 - 440 e s^3 t^2 u^4 - 575 e s^3 t^2 u^5 - 362 e s^3 t^2 u^6 - 88 e s^3 t^2 u^7 + 176 e s^3 s^4 t^3 u^3 + 332 e s^3 s^4 t^3 u^4 + 140 e s^3 s^4 t^3 u^5 + 36 e s^3 s^4 t^2 u^4 - 80 e s^3 s^4 t^2 u^3 - 476 e s^3 s^4 t^2 u^4 - 568 e s^3 s^4 t^2 u^5 - 208 e s^3 s^4 t^2 u^6 - 14 e s^3 s^4 t^5 u^2 + 24 e s^3 s^4 t^3 u^4 + 40 e s^3 s^4 t^2 u^5 + 78 e s^3 s^4 t u^6 + 48 e s^3 s^4 u^7 + 18 e s^3 t^6 u^2 + 114 e s^3 t^5 u^3 + 336 e s^3 t^4 u^4 + 564 e s^3 t^3 u^5 + 546 e s^3 t^2 u^6 + 282 e s^3 t u^7 + 60 e s^3 u^8 - 22 e s^4 t^2 u^3 - 80 e s^4 t^2 u^4 - 110 e s^4 t^2 u^5 - 68 e s^4 t^2 u^6 - 16 e s^4 t^2 u^7 + 22 e s^4 t^5 u^3 + 116 e s^4 t^4 u^4 + 244 e s^4 t^3 u^5 + 256 e s^4 t^2 u^6 + 134 e s^4 t u^7 + 28 e s^4 u^8 - 13 e t^6 u^3 - 70 e t^5 u^4 - 166 e t^4 u^5 - 224 e t^3 u^6 - 181 e t^2 u^7 - 82 e t u^8 - 16 e u^9 + 64 s^3 t^6 s^4 u^2 - 64 s^3 t^5 s^4 u^3 + 128 s^3 t^5 s^4 u^3 - 64 s^3 t^5 s^4 u^2 - 256 s^3 t^5 s^4 u^2 - 32 s^3 t^5 s^4 u^2 - 64 s^3 t^5 s^4 u^2 - 32 s^3 t^5 s^4 u^3 + 64 s^3 t^4 s^4 u^4 + 64 s^3 t^4 s^4 u^3 - 384 s^3 t^4 s^4 u^3 + 32 s^3 t^4 s^4 u^2 + 32 s^3 t^4 s^4 u^2 + 96 s^3 t^4 s^4 u^2 + 320 s^3 t^4 s^4 u^3 + 32 s^3 t^4 s^4 u^3 + 192 s^3 t^4 s^4 u^2 + 288 s^3 t^4 s^4 u^3 + 128 s^3 t^4 s^4 u^4 + 4 s^3 t^4 u^4 + 16 s^3 t^4 u^3 + 24 s^3 t^4 u^3 + 16 s^3 t^4 u^4 + 4 s^3 t^4 u^5 - 128 s^3 t^3 s^4 u^2 - 32 s^3 t^3 s^4 u^3 + 352 s^3 t^3 s^4 u^3 - 32 s^3 t^3 s^4 u^2 + 64 s^3 t^3 s^4 u^2 + 160 s^3 t^3 s^4 u^3 - 64 s^3 t^3 s^4 u^4 - 4 s^3 t^3 s^4 u^5 - 24 s^3 t^3 s^4 u^4 - 120 s^3 t^3 s^4 u^3 - 368 s^3 t^3 s^4 u^2 - 452 s^3 t^3 s^4 u^4 - 184 s^3 t^3 s^4 u^5 - 4 s^3 t^3 u^3 - 32 s^3 t^3 u^2 - 88 s^3 t^3 u^3 - 112 s^3 t^3 u^4 - 68 s^3 t^3 u^5 - 16 s^3 t^3 u^6 + 64 s^3 t^2 s^4 u^3 + 64 s^3 t^2 s^4 u^3 + 64 s^3 t^2 s^4 u^3 - 64 s^3 t^2 s^4 u^3 + 4 s^3 t^2 s^4 u^2 - 16 s^3 t^2 s^4 u^2 - 200 s^3 t^2 s^4 u^2 - 336 s^3 t^2 s^4 u^2 - 124 s^3 t^2 s^4 u^5 + 4 s^3 t^2 s^4 u^4 + 24 s^3 t^2 s^4 u^4 + 88 s^3 t^2 s^4 u^3 + 224 s^3 t^2 s^4 u^4 + 260 s^3 t^2 s^4 u^5 + 104 s^3 t^2 s^4 u^6 + 2 s^3 t^2 u^6 + 20 s^3 t^2 u^5 + 84 s^3 t^2 u^4 + 176 s^3 t^2 u^4 + 194 s^3 t^2 u^5 + 108 s^3 t^2 u^6 + 24 s^3 t^2 u^7 - 32 s^3 s^4 t^3 u^3 - 64 s^3 s^4 t^3 u^4 - 32 s^3 s^4 t^3 u^5 - 8 s^3 s^4 t^2 u^4 + 80 s^3 s^4 t^2 u^4 + 128 s^3 s^4 t^2 u^5 + 56 s^3 s^4 t^2 u^6 + 4 s^3 s^4 t^2 u^7 + 24 s^3 s^4 t^2 u^8 + 56 s^3 s^4 t^3 u^4 + 48 s^3 s^4 t^2 u^5 + 4 s^3 s^4 t u^6 - 8 s^3 s^4 u^7 - 4 s^3 t^6 u^2 - 28 s^3 t^5 u^3 - 88 s^3 t^4 u^4 - 152 s^3 t^3 u^5 - 148 s^3 t^2 u^6 - 76 s^3 t u^7 - 16 s^3 u^8 + 4 s^4 t^2 u^3 + 16 s^4 t^2 u^4 + 24 s^4 t^2 u^5 + 16 s^4 t^2 u^6 + 4 s^4 t^2 u^7 - 4 s^4 t^5 u^3 - 24 s^4 t^4 u^4 - 56 s^4 t^3 u^5 - 64 s^4 t^2 u^6 - 36 s^4 t u^7 - 8 s^4 u^8 + 2 t^6 u^3 + 12 t^5 u^4 + 32 t^4 u^5 + 48 t^3 u^6 + 42 t^2 u^7 + 20 t u^8 + 4 u^9) / u^2 / (3 e - 2) / (-3 + 2 e) / (-4 s^3 s^4 t^2 + 2 t^2 u + u^2)^2 / (u - s)^2 / e / t; \\
\text{cpbox010010011p1p2p3} & := -2 * (e - 1) * (192 e^5 s^3 t^3 s^4 u^5 + 192 e^5 s^3 t^3 s^4 u^5 - 192 e^5 s^3 t^3 s^4 u^4 + 192 e^5 s^3 t^3 s^4 u^4 - 192 e^5 s^3 t^3 s^4 u^3 - 96 e^5 s^3 t^2 s^4 u^4 + 48 e^5 s^3 t^2 s^4 u^4 - 480 e^5 s^3 t^2 s^4 u^4 + 480 e^5 s^3 t^2 s^4 u^3 - 336 e^5 s^3 t^2 s^4 u^3 + 48 e^5 s^3 t^2 s^4 u^3 + 96 e^5 s^3 t^2 s^4 u^3 + 480 e^5 s^3 t^2 s^4 u^3 + 192 e^5 s^3 t^2 s^4 u^3 - 192 e^5 s^3 t^2 s^4 u^3 + 144 e^5 s^3 t^2 s^4 u^3 + 144 e^5 s^3 t^2 s^4 u^3 + 12 e^5 s^3 t^2 s^4 u^3 + 156 e^5 s^3 t^2 s^4 u^3 + 336 e^5 s^3 t^2 s^4 u^3 + 192 e^5 s^3 t^2 s^4 u^3 - 60 e^5 s^3 t^2 s^4 u^3 - 60 e^5 s^3 t^2 s^4 u^3 + 336 e^5 s^3 t^2 s^4 u^3 - 12 e^5 s^3 t^2 s^4 u^3 - 156 e^5 s^3 t^2 s^4 u^3 - 264 e^5 s^3 t^2 s^4 u^3 + 24 e^5 s^3 t^2 s^4 u^3 + 276 e^5 s^3 t^2 s^4 u^3 + 132 e^5 s^3 t^2 s^4 u^3 - 72 e^5 s^3 t^2 s^4 u^3 + 216 e^5 s^3 t^2 s^4 u^3 - 216 e^5 s^3 t^2 s^4 u^3 - 72 e^5 s^3 t^2 s^4 u^3 + 12 e^5 s^3 t^2 s^4 u^3 - 51 e^5 s^3 t^2 s^4 u^3 - 75 e^5 s^3 t^2 s^4 u^3 - 30 e^5 s^3 t^2 s^4 u^3 + 30 e^5 s^3 t^2 s^4 u^3 + 33 e^5 s^3 t^2 s^4 u^3 + 9 e^5 s^3 t^2 s^4 u^3 + 12 e^5 s^3 t^2 s^4 u^3 + 42 e^5 s^3 t^2 s^4 u^3 + 30 e^5 s^3 t^2 s^4 u^3 - 60 e^5 s^3 t^2 s^4 u^3 - 120 e^5 s^3 t^2 s^4 u^3 - 78 e^5 s^3 t^2 s^4 u^3 - 18 e^5 s^3 t^2 s^4 u^3 + 9 e^5 s^3 t^2 s^4 u^3 + 45 e^5 s^3 t^2 s^4 u^3 + 90 e^5 s^3 t^2 s^4 u^3 + 90 e^5 s^3 t^2 s^4 u^3 + 45 e^5 s^3 t^2 s^4 u^3 + 9 e^5 s^3 t^2 s^4 u^3 + 192 e^4 s^3 t^4 s^4 u - 128 e^4 s^3 t^4 s^4 u - 544 e^4 s^3 t^4 s^4 u +
 \end{aligned}$$

$32e^4s^3s^4^5u+736e^4s^3s^4^4t^*u+224e^4s^3s^4^4u^2-96e^4s^3s^4^3t^*u-632e^4s^3s^4^3t^*u^2-280e^4s^3s^4^3u^3+64e^4s^3s^4^2t^*u^2+272e^4s^3s^4^2t^*u^3+16e^4s^3s^4^2u^4-24e^4s^3s^4t^*u^4-24e^4s^3s^4u^5+192e^4s^3s^4^6u-288e^4s^3s^4^5t^*u-480e^4s^3s^4^5u^2+272e^4s^3s^4^4t^*u^3+880e^4s^3s^4^4t^*u^2+672e^4s^3s^4^4t^*u^2+656e^4s^3s^4^4u^3-344e^4s^3s^4^3t^*u-1184e^4s^3s^4^3t^*u^2-952e^4s^3s^4^3t^*u^3-784e^4s^3s^4^3u^4+12e^4s^3s^4^2t^*u^4+214e^4s^3s^4^2t^*u^2+586e^4s^3s^4^2t^*u^3+626e^4s^3s^4^2t^*u^4+386e^4s^3s^4^2u^5-8e^4s^3s^4^2s^4t^*u^2-68e^4s^3s^4^2s^4t^*u^3-84e^4s^3s^4^2s^4t^*u^4+4e^4s^3s^4^2s^4t^*u^5+28e^4s^3s^4^2s^4u^6+6e^4s^3s^4^2t^*u^4+18e^4s^3s^4^2t^*u^5+18e^4s^3s^4^2t^*u^6+6e^4s^3s^4^2u^7-144e^4s^3s^4^5t^*u^2-216e^4s^3s^4^5t^*u^2-72e^4s^3s^4^5u^3+168e^4s^3s^4^4t^*u^3+672e^4s^3s^4^4t^*u^2+696e^4s^3s^4^4t^*u^3+192e^4s^3s^4^4u^4-34e^4s^3s^4^3t^*u^5-322e^4s^3s^4^3t^*u^4-848e^4s^3s^4^3t^*u^2-1248e^4s^3s^4^3t^*u^3-998e^4s^3s^4^3t^*u^4-310e^4s^3s^4^3u^5+40e^4s^3s^4^2t^*u^5+390e^4s^3s^4^2t^*u^2+968e^4s^3s^4^2t^*u^3+1276e^4s^3s^4^2t^*u^4+1008e^4s^3s^4^2t^*u^5+350e^4s^3s^4^2u^6-14e^4s^3s^4^2s^4t^*u^2-126e^4s^3s^4^2s^4t^*u^3-376e^4s^3s^4^2s^4t^*u^4-584e^4s^3s^4^2s^4t^*u^5-474e^4s^3s^4^2s^4t^*u^6-154e^4s^3s^4^2s^4u^7-6e^4s^3s^4^2t^*u^4-24e^4s^3s^4^2t^*u^5-36e^4s^3s^4^2t^*u^6-24e^4s^3s^4^2t^*u^7-6e^4s^3s^4^2u^8+24e^4s^4^4t^*u^4+78e^4s^4^4t^*u^3+90e^4s^4^4t^*u^3+42e^4s^4^4t^*u^4+6e^4s^4^4u^5-24e^4s^4^4t^*u^5-150e^4s^4^4t^*u^2-324e^4s^4^4t^*u^3-312e^4s^4^4t^*u^4-132e^4s^4^4t^*u^5-18e^4s^4^4t^*u^6+25e^4s^4^4t^*u^6+142e^4s^4^4t^*u^2+372e^4s^4^4t^*u^3+550e^4s^4^4t^*u^4+463e^4s^4^4t^*u^5+204e^4s^4^4t^*u^6+36e^4s^4^4t^*u^7-30e^4s^4^4t^*u^2-156e^4s^4^4t^*u^3-366e^4s^4^4t^*u^4-504e^4s^4^4t^*u^5-426e^4s^4^4t^*u^6-204e^4s^4^4t^*u^7-42e^4s^4^4u^8+9e^4t^*u^6+54e^4t^*u^5+144e^4t^*u^5+216e^4t^*u^6+189e^4t^*u^7+90e^4t^*u^8+18e^4u^9-352e^3s^3s^4^4u+576e^3s^3s^4^4s^4^3u^2-288e^3s^3s^4^4s^4^2u^3+608e^3s^3s^4^4s^4^5t-448e^3s^3s^4^4s^4^5u-1152e^3s^3s^4^4t^*u+672e^3s^3s^4^4u^2+176e^3s^3s^4^4t^*u+776e^3s^3s^4^4s^4^3t^*u^2-352e^3s^3s^4^4s^4^3u^3-288e^3s^3s^4^4t^*u^2-336e^3s^3s^4^4t^*u^3+32e^3s^3s^4^4s^4^2u^4+144e^3s^3s^4^4t^*u^3+296e^3s^3s^4^4s^4^4t^*u^4+128e^3s^3s^4^4s^4^5u-352e^3s^3s^4^4s^4^6u+320e^3s^3s^4^4s^4^5t^*u+992e^3s^3s^4^4s^4^5u^2-304e^3s^3s^4^4s^4^4t^*u-480e^3s^3s^4^4s^4^4t^*u-688e^3s^3s^4^4s^4^4t^*u^2-1376e^3s^3s^4^4s^4^4u^3+552e^3s^3s^4^4s^4^3t^*u+1176e^3s^3s^4^4s^4^3t^*u^2+1152e^3s^3s^4^4s^4^3t^*u^3+1328e^3s^3s^4^4s^4^3u^4-22e^3s^3s^4^4s^4^2t^*u-246e^3s^3s^4^4s^4^2t^*u^3+592e^3s^3s^4^4s^4^2t^*u^3-550e^3s^3s^4^4s^4^2t^*u^4-502e^3s^3s^4^4s^4^2u^5+36e^3s^3s^4^4s^4^4t^*u^2-12e^3s^3s^4^4s^4^4t^*u^3-216e^3s^3s^4^4s^4^4t^*u^4-244e^3s^3s^4^4s^4^4t^*u^5-76e^3s^3s^4^4s^4^4u^6-18e^3s^3s^4^4s^4^4t^*u^3-70e^3s^3s^4^4s^4^4t^*u^4-104e^3s^3s^4^4s^4^4t^*u^5-70e^3s^3s^4^4s^4^4t^*u^6-18e^3s^3s^4^4s^4^4t^*u^7+224e^3s^3s^4^4s^4^4t^*u^2+328e^3s^3s^4^4s^4^4t^*u^2+176e^3s^3s^4^4s^4^4t^*u^3-232e^3s^3s^4^4s^4^4t^*u^3-936e^3s^3s^4^4s^4^4t^*u^2-1056e^3s^3s^4^4s^4^4t^*u^3-496e^3s^3s^4^4s^4^4t^*u^4+38e^3s^3s^4^4s^4^4t^*u^5+216e^3s^3s^4^4s^4^4t^*u+832e^3s^3s^4^4s^4^3t^*u^2+1736e^3s^3s^4^4s^4^3t^*u^3+1770e^3s^3s^4^4s^4^3t^*u^4+760e^3s^3s^4^4s^4^3u^5-70e^3s^3s^4^4s^4^2t^*u-520e^3s^3s^4^4s^4^2t^*u^2-1446e^3s^3s^4^4s^4^2t^*u^3-2246e^3s^3s^4^4s^4^2t^*u^4-2004e^3s^3s^4^4s^4^2t^*u^5-754e^3s^3s^4^4s^4^2u^6+22e^3s^3s^4^4s^4^4t^*u^2+280e^3s^3s^4^4s^4^4t^*u^3+788e^3s^3s^4^4s^4^4t^*u^4+1124e^3s^3s^4^4s^4^4t^*u^5+894e^3s^3s^4^4s^4^4t^*u^6+300e^3s^3s^4^4s^4^4t^*u^7+18e^3s^3s^4^4s^4^4t^*u^3+88e^$

$$\begin{aligned}
 & 3s^3t^4u^4+170e^3s^3t^3u^5+162e^3s^3t^2u^6+76e^3s^3t^1u^7+14e^3s^3u^8-26e^3s^4t^4u-102e^3s^4t^3u^2-144e^3s^4t^2u^3-86e^3s^4t^1u^4-18e^3s^4t^0u^5+26e^3s^4t^3u^5+172e^3s^4t^2u^6+422e^3s^4t^1u^7+482e^3s^4t^0u^8+256e^3s^4t^3u^5+50e^3s^4t^2u^6-11e^3s^4t^1u^7-107e^3s^4t^0u^8-415e^3s^4t^2u^6-804e^3s^4t^1u^7-821e^3s^4t^0u^8-421e^3s^4t^2u^6-85e^3s^4t^1u^7+34e^3s^4t^0u^8+216e^3s^4t^2u^6+618e^3s^4t^1u^7+92e^3s^4t^0u^8-27e^3t^6u^3-151e^3t^5u^4-373e^3t^4u^5-522e^3t^3u^6-433e^3t^2u^7-199e^3t^1u^8-39e^3u^9+256e^2s^3t^4s^4u-896e^2s^3t^3s^4u^2+576e^2s^3t^2s^4u^3-416e^2s^3t^1s^4u^4+352e^2s^3t^0s^4u^5+944e^2s^3t^3s^4t^4u-1424e^2s^3t^2s^4t^3u^2-128e^2s^3t^1s^4t^2u+100e^2s^3t^0s^4t^1u^2+1676e^2s^3t^3s^4t^3u^3+448e^2s^3t^2s^4t^2u^2+104e^2s^3t^1s^4t^1u^3-360e^2s^3t^0s^4t^0u^4-288e^2s^3t^3s^4t^2u^3-540e^2s^3t^2s^4t^1u^4-212e^2s^3t^1s^4t^0u^5+256e^2s^3t^2s^4t^6u-176e^2s^3t^2s^4t^5u-944e^2s^3t^2s^4t^4u^2+208e^2s^3t^2s^4t^3u^3+248e^2s^3t^2s^4t^2u+1064e^2s^3t^2s^4t^1u^2+1472e^2s^3t^2s^4t^0u^3-480e^2s^3t^2s^4t^3t^3u-904e^2s^3t^2s^4t^2t^2u-1016e^2s^3t^2s^4t^1t^1u^3-848e^2s^3t^2s^4t^0t^4u+16e^2s^3t^2s^4t^2t^4u-96e^2s^3t^2s^4t^1t^3u-452e^2s^3t^2s^4t^0t^2u^3-784e^2s^3t^2s^4t^2t^4u-188e^2s^3t^2s^4t^1t^5u-56e^2s^3t^2s^4t^0t^4u^2+160e^2s^3t^2s^4t^3t^3u+720e^2s^3t^2s^4t^2t^2u^4+728e^2s^3t^2s^4t^1t^1u^5+224e^2s^3t^2s^4t^0t^6u+36e^2s^3t^2t^4u^3+128e^2s^3t^2t^3u^4+172e^2s^3t^2t^2u^5+104e^2s^3t^2t^1u^6+24e^2s^3t^2u^7-104e^2s^3s^4t^5t^2u-172e^2s^3s^4t^5t^1u^2-188e^2s^3s^4t^5u^3+112e^2s^3s^4t^4t^3u+472e^2s^3s^4t^4t^2u^2+752e^2s^3s^4t^4t^1u^3+632e^2s^3s^4t^4u^4-26e^2s^3s^4t^3t^5u-114e^2s^3s^4t^3t^4u-688e^2s^3s^4t^3t^3u^2-1552e^2s^3s^4t^3t^2u^3-1762e^2s^3s^4t^3t^1u^4-930e^2s^3s^4t^3u^5+68e^2s^3s^4t^2t^5u+544e^2s^3s^4t^2t^4u^2+1538e^2s^3s^4t^2t^3u^3+2182e^2s^3s^4t^2t^2u^4+1802e^2s^3s^4t^2t^1u^5+682e^2s^3s^4t^2u^6+2e^2s^3s^4t^1t^5u^2-190e^2s^3s^4t^4u^3-508e^2s^3s^4t^3u^4-604e^2s^3s^4t^2u^5-454e^2s^3s^4t^1u^6-166e^2s^3s^4u^7-36e^2s^3t^5u^3-176e^2s^3t^4u^4-342e^2s^3t^3u^5-330e^2s^3t^2u^6-158e^2s^3t^1u^7-30e^2s^3u^8-4e^2s^4t^4t^4u+24e^2s^4t^4t^3u^2+84e^2s^4t^4t^2u^3+80e^2s^4t^4t^1u^4+24e^2s^4t^4u^5+4e^2s^4t^3t^5u-8e^2s^4t^3t^4u^2-150e^2s^4t^3t^3u^3-338e^2s^4t^3t^2u^4-278e^2s^4t^3t^1u^5-78e^2s^4t^3u^6-3e^2s^4t^2t^6u+20e^2s^4t^2t^5u^2+200e^2s^4t^2t^4u^3+576e^2s^4t^2t^3u^4+761e^2s^4t^2t^2u^5+476e^2s^4t^2t^1u^6+114e^2s^4t^2u^7-30e^2s^4t^1t^6u^2-192e^2s^4t^1t^5u^3-560e^2s^4t^1t^4u^4-918e^2s^4t^1t^3u^5-864e^2s^4t^1t^2u^6-434e^2s^4t^1t^1u^7-90e^2s^4u^8+29e^2t^6u^3+152e^2t^5u^4+348e^2t^4u^5+452e^2t^3u^6+353e^2t^2u^7+156e^2t^1u^8+30e^2u^9-160e^3s^4s^4u+576e^3s^4s^4t^3u^2-352e^3s^4s^4t^2u^3+224e^3s^4s^4t^1u^4-256e^3s^4s^4t^0u^5-400e^3s^4s^4t^3t^1u+1168e^3s^4s^4t^2u^2+80e^3s^4s^4t^1t^2u-244e^3s^4s^4t^0t^3u^2-1396e^3s^4s^4t^3u^3-288e^3s^4s^4t^2t^1u^2-104e^3s^4s^4t^1t^2u^3+312e^3s^4s^4t^0t^4u+176e^3s^4s^4t^3t^2u^3+332e^3s^4s^4t^2t^3u^4+140e^3s^4s^4t^1t^4u^5-160e^3s^4s^4t^0t^5u+144e^3s^4s^4t^2t^5u+688e^3s^4s^4t^1t^5u^2-112e^3s^4s^4t^0t^6u+168e^3s^4s^4t^3t^4u^2-680e^3s^4s^4t^2t^4u^3-1024e^3s^4s^4t^1t^4u^4+208e^3s^4s^4t^0t^4u^5+264e^3s^4s^4t^3t^3u^2+192e^3s^4s^4t^2t^3u^3+328e^3s^4s^4t^1t^3u^4-10e^3s^4s^4t^0t^4u+144e^3s^4s^4t^2t^3u^2+706e^3s^4s^4t^1t^2u^3+1060e^3s^4s^4t^0t^2u^4+396e^3s^4s^4t^2t^2u^5+36e^3s^4s^4t^1t^4u^6
 \end{aligned}$$

$$\begin{aligned}
& u^2-80e^3s^2s^4t^3u^3-476e^3s^2s^4t^2u^4-568e^3s^2s^4t^2u^5-208e^3s^2s^4u^6-22e^3s^2t^4u^3-80e^3s^2t^3u^4-110e^3s^2t^2u^5-68e^3s^2t^2u^6 \\
& -16e^3s^2u^7+56e^3s^3s^4^5t^2u+124e^3s^3s^4^5t^2u+116e^3s^3s^4^5u^3-64e^3s^3s^4^4t^3u-360e^3s^3s^4^4t^2u^2-648e^3s^3s^4^4t^2u^3-448e^3s^3s^4^4u^4+14e^3s^3s^4^3t^5+80e^3s^3s^4^3t^4u+448e^3s^3s^4^3t^3u^2+1120e^3s^3s^4^3t^2u^3+ \\
& 1350e^3s^3s^4^3t^2u^4+660e^3s^3s^4^3u^5-30e^3s^3s^4^2t^5u-260e^3s^3s^4^2t^4u^2-764e^3s^3s^4^2t^3u^3-1176e^3s^3s^4^2t^2u^4-1046e^3s^3s^4^2t^2u^5-404e^3s^3s^4^2u^6-14e^3s^3s^4t^5u^2+24e^3s^3s^4t^3u^4+40e^3s^3s^4t^2u^5+78e^3s^3s^4t^2u^6+48e^3s^3s^4u^7+22e^3s^3t^5u^3+116e^3s^3t^4u^4+244e^3s^3t^3u^5+256e^3s^3t^2u^6+134e^3s^3t^2u^7+28e^3s^3u^8+2e^3s^4^4t^4u-16e^3s^4^4t^3u^2-54e^3s^4^4t^2u^3-52e^3s^4^4t^2u^4-16e^3s^4^4u^5-2e^3s^4^3t^5u+16e^3s^4^3t^4u^2+132e^3s^4^3t^3u^3+268e^3s^4^3t^2u^4+214e^3s^4^3t^2u^5+60e^3s^4^3u^6-e^3s^4^2t^6u-26e^3s^4^2t^5u^2-164e^3s^4^2t^4u^3-440e^3s^4^2t^3u^4-575e^3s^4^2t^2u^5-362e^3s^4^2t^2u^6-88e^3s^4^2u^7+18e^3s^4t^6u^2+114e^3s^4t^5u^3+336e^3s^4t^4u^4+564e^3s^4t^3u^5+546e^3s^4t^2u^6+282e^3s^4t^2u^7+60e^3s^4u^8-13e^3t^6u^3-70e^3t^5u^4-166e^3t^4u^5-224e^3t^3u^6-181e^3t^2u^7-82e^3t^2u^8-16e^3u^9+64s^3^4s^4^4u-128s^3^4s^4^3u^2+64s^3^4s^4^2u^3-64s^3^3s^4^5t+128s^3^3s^4^5u+64s^3^3s^4^4t^2u-384s^3^3s^4^4u^2-32s^3^3s^4^3t^2u+352s^3^3s^4^3u^3+64s^3^3s^4^2t^2u^2+64s^3^3s^4^2t^2u^3-64s^3^3s^4^2u^4-32s^3^3s^4t^2u^3-64s^3^3s^4t^2u^4-32s^3^3s^4u^5+64s^3^2s^4^6u-64s^3^2s^4^5t^2u-256s^3^2s^4^5u^2+32s^3^2s^4^4t^3+32s^3^2s^4^4t^2u+96s^3^2s^4^4t^2u+320s^3^2s^4^4u^3-32s^3^2s^4^3t^3u+64s^3^2s^4^3t^2u^2+160s^3^2s^4^3t^2u^3-64s^3^2s^4^3u^4+4s^3^2s^4^2t^4u-16s^3^2s^4^2t^3u^2-200s^3^2s^4^2t^2u^3-336s^3^2s^4^2t^2u^4-124s^3^2s^4^2u^5-8s^3^2s^4t^4u^2+80s^3^2s^4t^2u^4+128s^3^2s^4t^2u^5+56s^3^2s^4u^6+4s^3^2t^4u^3+16s^3^2t^3u^4+24s^3^2t^2u^5+16s^3^2t^2u^6+4s^3^2u^7-32s^3s^4^5t^2u-64s^3s^4^5t^2u^2-32s^3s^4^5u^3+32s^3s^4^4t^3u+192s^3s^4^4t^2u^2+288s^3s^4^4t^2u^3+128s^3s^4^4u^4-4s^3s^4^3t^5-24s^3s^4^3t^4u-120s^3s^4^3t^3u^2-368s^3s^4^3t^2u^3-452s^3s^4^3t^2u^4-184s^3s^4^3u^5+4s^3s^4^2t^5u+24s^3s^4^2t^4u^2+88s^3s^4^2t^3u^3+224s^3s^4^2t^2u^4+260s^3s^4^2t^2u^5+104s^3s^4^2u^6+4s^3s^4t^5u^2+24s^3s^4t^4u^3+56s^3s^4t^3u^4+48s^3s^4t^2u^5+4s^3s^4t^2u^6-8s^3s^4u^7-4s^3t^5u^3-24s^3t^4u^4-56s^3t^3u^5-64s^3t^2u^6-36s^3t^2u^7-8s^3u^8+4s^4^4t^4u+16s^4^4t^3u^2+24s^4^4t^2u^3+16s^4^4t^2u^4+4s^4^4u^5-4s^4^3t^5u-32s^4^3t^4u^2-88s^4^3t^3u^3-112s^4^3t^2u^4-68s^4^3t^2u^5-16s^4^3u^6+2s^4^2t^6u+20s^4^2t^5u^2+84s^4^2t^4u^3+176s^4^2t^3u^4+194s^4^2t^2u^5+108s^4^2t^2u^6+24s^4^2u^7-4s^4t^6u^2-28s^4t^5u^3-88s^4t^4u^4-152s^4t^3u^5-148s^4t^2u^6-76s^4t^2u^7-16s^4u^8+2t^6u^3+12t^5u^4+32t^4u^5+48t^3u^6+42t^2u^7+20t^2u^8+4u^9)/(u-s4)^2/t/(-4s3s4+t^2+2t^2u+u^2)^2/(3e-2)/(-3+2e)/e/u^2; \\
\text{cpbox010010101p1p2p3} & := 2*(e-1)*(144e^5s^3^2s^4^2t^2u+144e^5s^3^2s^4^2u^2-72e^5s^3s^4t^3u-216e^5s^3s^4t^2u^2-216e^5s^3s^4t^2u^3-72e^5s^3s^4u^4+9e^5t^5u+45e^5t^4u^2+90e^5t^3u^3+90e^5t^2u^4+45e^5t^2u^5+9e^5u^6-48e^4s^3^3s^4t^2-24e^4s^3^3s^4t^2u+24e^4s^3^3s^4u^2-240e^4s^3^2s^4^2t^2-48e^4s^3^2s^4^2t^2u+336e^4s^3^2s^4^2u^2+48e^4s^3^2s^4t^3+72e^4s^3^2s^4t^2u-24e^4s^3^2s^4u^3+12e^4s^3^2t^4+30e^4s^3^2t^3u+18e^4s^3^2t^2u^2-6e^4s^3^2t^2u^3-6e^4s^3^2u^4-48e^4s^3s^4^3t^2-24e^4s^3s^4^3t^2u+24e
\end{aligned}$$

$$\begin{aligned}
 &^4s^3s^4^3u^2+48e^4s^3s^4^2t^3+72e^4s^3s^4^2t^2u-24e^4s^3s^4^2u^3+96e \\
 &^4s^3s^4t^4+204e^4s^3s^4t^3u-36e^4s^3s^4t^2u^2-300e^4s^3s^4t^2u^3-156e \\
 &e^4s^3s^4u^4-12e^4s^3t^5-42e^4s^3t^4u-48e^4s^3t^3u^2-12e^4s^3t^2u^3+12e^4s^3t^2u^4+6e^4s^3u^5+12e^4s^4^2t^4+30e^4s^4^2t^3u+18e^4s^4^2t^2u^2-6e^4s^4^2t^2u^3-6e^4s^4^2u^4-12e^4s^4t^5-42e^4s^4t^4u-48e^4s^4t^3u^2-12e^4s^4t^2u^3+12e^4s^4t^2u^4+6e^4s^4u^5-9e^4t^6-36e^4t^5u-36e^4t^4u^2+36e^4t^3u^3+99e^4t^2u^4+72e^4t^2u^5+18e^4u^6-128e^3s^3^3s^4^2t-64e^3s^3^3s^4^2u+48e^3s^3^3s^4t^2-24e^3s^3^3s^4t^2u-128e^3s^3^2s^4^3t-64e^3s^3^2s^4^3u+656e^3s^3^2s^4^2t^2+32e^3s^3^2s^4^2t^2u-624e^3s^3^2s^4^2u^2-48e^3s^3^2s^4t^3+136e^3s^3^2s^4t^2u+200e^3s^3^2s^4t^2u^2+16e^3s^3^2s^4u^3-4e^3s^3^2t^4-14e^3s^3^2t^3u-12e^3s^3^2t^2u^2+2e^3s^3^2t^2u^3+4e^3s^3^2u^4+48e^3s^3s^4^3t^2-24e^3s^3s^4^3t^2u-48e^3s^3s^4^2t^3+136e^3s^3s^4^2t^2u+200e^3s^3s^4^2t^2u^2+16e^3s^3s^4^2u^3-224e^3s^3s^4t^4-564e^3s^3s^4t^3u-120e^3s^3s^4t^2u^2+556e^3s^3s^4t^2u^3+336e^3s^3s^4u^4+4e^3s^3t^5+2e^3s^3t^4u-26e^3s^3t^3u^2-50e^3s^3t^2u^3-34e^3s^3t^2u^4-8e^3s^3u^5-4e^3s^4^2t^4-14e^3s^4^2t^3u-12e^3s^4^2t^2u^2+2e^3s^4^2t^2u^3+4e^3s^4^2u^4+4e^3s^4t^5+2e^3s^4t^4u-26e^3s^4t^3u^2-50e^3s^4t^2u^3-34e^3s^4t^2u^4-8e^3s^4u^5+27e^3t^6+117e^3t^5u+159e^3t^4u^2+6e^3t^3u^3-171e^3t^2u^4-147e^3t^2u^5-39e^3u^6+32e^2s^3^3s^4^2u+24e^2s^3^3s^4t^2+84e^2s^3^3s^4t^2u-60e^2s^3^3s^4u^2+32e^2s^3^2s^4^3u-416e^2s^3^2s^4^2t^2+168e^2s^3^2s^4^2t^2u+232e^2s^3^2s^4^2u^2+32e^2s^3^2s^4t^3-192e^2s^3^2s^4t^2u-120e^2s^3^2s^4t^2u^2+104e^2s^3^2s^4u^3-20e^2s^3^2t^4-40e^2s^3^2t^3u-12e^2s^3^2t^2u^2+16e^2s^3^2t^2u^3+8e^2s^3^2u^4+24e^2s^3s^4^3t^2+84e^2s^3s^4^3t^2u-60e^2s^3s^4^3u^2+32e^2s^3s^4^2t^3-192e^2s^3s^4^2t^2u-120e^2s^3s^4^2t^2u^2+104e^2s^3s^4^2u^3+136e^2s^3s^4t^4+396e^2s^3s^4t^3u+164e^2s^3s^4t^2u^2-316e^2s^3s^4t^2u^3-220e^2s^3s^4u^4+20e^2s^3t^5+72e^2s^3t^4u+82e^2s^3t^3u^2+14e^2s^3t^2u^3-30e^2s^3t^2u^4-14e^2s^3u^5-20e^2s^4^2t^4-40e^2s^4^2t^3u-12e^2s^4^2t^2u^2+16e^2s^4^2t^2u^3+8e^2s^4^2u^4+20e^2s^4t^5+72e^2s^4t^4u+82e^2s^4t^3u^2+14e^2s^4t^2u^3-30e^2s^4t^2u^4-14e^2s^4u^5-29e^2t^6-126e^2t^5u-184e^2t^4u^2-56e^2t^3u^3+111e^2t^2u^4+110e^2t^2u^5+30e^2u^6+64e*s^3^3s^4^2t+96e*s^3^3s^4^2u-24e*s^3^3s^4t^2-36e*s^3^3s^4t^2u+36e*s^3^3s^4u^2+64e*s^3^2s^4^3t+96e*s^3^2s^4^3u+96e*s^3^2s^4^2t^2-232e*s^3^2s^4^2t^2u-88e*s^3^2s^4^2u^2-16e*s^3^2s^4t^3-8e*s^3^2s^4t^2u-112e*s^3^2s^4t^2u^2-120e*s^3^2s^4u^3+12e*s^3^2t^4+24e*s^3^2t^3u+6e*s^3^2t^2u^2-12e*s^3^2t^2u^3-6e*s^3^2u^4-24e*s^3s^4^3t^2-36e*s^3s^4^3t^2u+36e*s^3s^4^3u^2-16e*s^3s^4^2t^3-8e*s^3s^4^2t^2u-112e*s^3s^4^2t^2u^2-120e*s^3s^4^2u^3-40e*s^3s^4t^4-52e*s^3s^4t^3u+120e*s^3s^4t^2u^2+236e*s^3s^4t^2u^3+104e*s^3s^4u^4-12e*s^3t^5-30e*s^3t^4u+60e*s^3t^2u^3+60e*s^3t^2u^4+18e*s^3u^5+12e*s^4^2t^4+24e*s^4^2t^3u+6e*s^4^2t^2u^2-12e*s^4^2t^2u^3-6e*s^4^2u^4-12e*s^4t^5-30e*s^4t^4u+60e*s^4t^2u^3+60e*s^4t^2u^4+18e*s^4u^5+13e*t^6+46e*t^5u+38e*t^4u^2-48e*t^3u^3-107e*t^2u^4-70e*t^2u^5-16e*u^6-64*s^3^3s^4^2u-64*s^3^2s^4^3u-32*s^3^2s^4^2t^2+64*s^3^2s^4^2t^2u+64*s^3^2s^4^2u^2+32*s^3^2s^4t^2u+64*s^3^2s^4t^2u^2+32*s^3^2s^4u^3+32*s^3s^4^2t^2u+64*s^3s^4^2t^2u^2+32*s^3s^4^2u^3+16*s^3s^4t^4-80*s^3s^4t^2u^2-96*s^3s^4t^2u^3-32*s^3s^4u^4-4*s^3t^4u-16*s^3t^3
 \end{aligned}$$

$$\begin{aligned}
& s^3 s^4 u^3 + 304 e^2 s^3 s^4 t + 736 e^2 s^3 s^4 u - 368 e^2 s^3 s^4 t^2 - 1008 e^2 s^3 s^4 t^3 u - 1216 e^2 s^3 s^4 t^3 u^2 + 888 e^2 s^3 s^4 t^2 t^3 + 1248 e^2 s^3 s^4 t^2 t^2 u + 1352 e^2 s^3 s^4 t^2 t u^2 + 992 e^2 s^3 s^4 t^2 u^3 + 108 e^2 s^3 s^4 t^4 + 996 e^2 s^3 s^4 t^3 u + 1964 e^2 s^3 s^4 t^2 u^2 + 1372 e^2 s^3 s^4 t u^3 + 296 e^2 s^3 s^4 u^4 + 36 e^2 s^3 t^5 + 164 e^2 s^3 t^4 u + 300 e^2 s^3 t^3 u^2 + 276 e^2 s^3 t^2 u^3 + 128 e^2 s^3 t u^4 + 24 e^2 s^3 u^5 - 156 e^2 s^3 s^4 t^3 - 768 e^2 s^3 s^4 t^2 u - 828 e^2 s^3 s^4 t^3 u^2 - 216 e^2 s^3 s^4 t^3 u^3 + 108 e^2 s^3 s^4 t^2 t^4 + 996 e^2 s^3 s^4 t^2 t^3 u + 1964 e^2 s^3 s^4 t^2 t^2 u^2 + 1372 e^2 s^3 s^4 t^2 t u^3 + 296 e^2 s^3 s^4 t^2 u^4 - 196 e^2 s^3 s^4 t^5 - 990 e^2 s^3 s^4 t^4 u - 2088 e^2 s^3 s^4 t^3 u^2 - 2284 e^2 s^3 s^4 t^2 u^3 - 1284 e^2 s^3 s^4 t u^4 - 294 e^2 s^3 s^4 u^5 - 36 e^2 s^3 t^6 - 212 e^2 s^3 t^5 u - 518 e^2 s^3 t^4 u^2 - 672 e^2 s^3 t^3 u^3 - 488 e^2 s^3 t^2 u^4 - 188 e^2 s^3 t u^5 - 30 e^2 s^3 u^6 + 36 e^2 s^4 t^2 t^5 + 164 e^2 s^4 t^2 t^4 u + 300 e^2 s^4 t^2 t^3 u^2 + 276 e^2 s^4 t^2 t^2 u^3 + 128 e^2 s^4 t^2 t u^4 + 24 e^2 s^4 t^2 u^5 - 36 e^2 s^4 t^6 - 212 e^2 s^4 t^5 u - 518 e^2 s^4 t^4 u^2 - 672 e^2 s^4 t^3 u^3 - 488 e^2 s^4 t^2 u^4 - 188 e^2 s^4 t u^5 - 30 e^2 s^4 u^6 + 29 e^2 t^7 + 181 e^2 t^6 u + 500 e^2 t^5 u^2 + 800 e^2 t^4 u^3 + 805 e^2 t^3 u^4 + 509 e^2 t^2 u^5 + 186 e^2 t u^6 + 30 e^2 u^7 - 120 e s^3 s^4 s^4 t^2 - 552 e s^3 s^4 s^4 t^2 u + 240 e s^3 s^4 s^4 t^3 - 912 e s^3 s^4 s^4 t^3 u + 96 e s^3 s^4 s^4 t^2 t^2 + 784 e s^3 s^4 s^4 t^2 t u + 1040 e s^3 s^4 s^4 t^2 u^2 + 80 e s^3 s^4 s^4 t^3 + 468 e s^3 s^4 s^4 t^2 u + 552 e s^3 s^4 s^4 t u^2 + 164 e s^3 s^4 s^4 u^3 - 120 e s^3 s^4 s^4 t^4 - 552 e s^3 s^4 s^4 u + 96 e s^3 s^4 s^4 t^3 t^2 + 784 e s^3 s^4 s^4 t^3 t u + 1040 e s^3 s^4 s^4 t^3 u^2 - 264 e s^3 s^4 s^4 t^2 t^3 - 56 e s^3 s^4 s^4 t^2 t u^2 - 320 e s^3 s^4 s^4 t^2 u^3 - 36 e s^3 s^4 s^4 t^4 - 620 e s^3 s^4 s^4 t^3 u - 1428 e s^3 s^4 s^4 t^2 u^2 - 1140 e s^3 s^4 s^4 t u^3 - 296 e s^3 s^4 s^4 u^4 - 22 e s^3 s^4 t^5 - 102 e s^3 s^4 t^4 u - 190 e s^3 s^4 t^3 u^2 - 178 e s^3 s^4 t^2 u^3 - 84 e s^3 s^4 t u^4 - 16 e s^3 s^4 u^5 + 80 e s^3 s^4 s^4 t^3 t^3 + 468 e s^3 s^4 s^4 t^2 t^2 u + 552 e s^3 s^4 s^4 t^3 t u^2 + 164 e s^3 s^4 s^4 t^3 u^3 - 36 e s^3 s^4 s^4 t^2 t^4 - 620 e s^3 s^4 s^4 t^2 t^3 u - 1428 e s^3 s^4 s^4 t^2 t^2 u^2 - 1140 e s^3 s^4 s^4 t^2 t u^3 - 296 e s^3 s^4 s^4 t^2 u^4 + 46 e s^3 s^4 s^4 t^5 + 300 e s^3 s^4 s^4 t^4 u + 768 e s^3 s^4 s^4 t^3 u^2 + 964 e s^3 s^4 s^4 t^2 u^3 + 594 e s^3 s^4 s^4 t u^4 + 144 e s^3 s^4 s^4 u^5 + 22 e s^3 t^6 + 138 e s^3 t^5 u + 360 e s^3 t^4 u^2 + 500 e s^3 t^3 u^3 + 390 e s^3 t^2 u^4 + 162 e s^3 t u^5 + 28 e s^3 u^6 - 22 e s^4 t^2 t^5 - 102 e s^4 t^2 t^4 u - 190 e s^4 t^2 t^3 u^2 - 178 e s^4 t^2 t^2 u^3 - 84 e s^4 t^2 t u^4 - 16 e s^4 t^2 u^5 + 22 e s^4 t^6 + 138 e s^4 t^5 u + 360 e s^4 t^4 u^2 + 500 e s^4 t^3 u^3 + 390 e s^4 t^2 u^4 + 162 e s^4 t u^5 + 28 e s^4 u^6 - 13 e t^7 - 83 e t^6 u - 236 e t^5 u^2 - 390 e t^4 u^3 - 405 e t^3 u^4 - 263 e t^2 u^5 - 98 e t u^6 - 16 e u^7 + 24 s^3 s^4 s^4 t^2 + 120 s^3 s^4 s^4 t^2 u - 16 s^3 s^4 s^4 t^3 + 240 s^3 s^4 s^4 t^3 u - 16 s^3 s^4 s^4 t^2 t^2 - 192 s^3 s^4 s^4 t^2 t u - 240 s^3 s^4 s^4 t^2 u^2 - 16 s^3 s^4 s^4 t^3 - 96 s^3 s^4 s^4 t^2 u - 120 s^3 s^4 s^4 t u^2 - 40 s^3 s^4 s^4 u^3 + 24 s^3 s^4 s^4 t^4 + 120 s^3 s^4 s^4 u - 16 s^3 s^4 s^4 t^3 t^2 - 192 s^3 s^4 s^4 t^3 t u - 240 s^3 s^4 s^4 t^3 u^2 + 24 s^3 s^4 s^4 t^2 t^3 - 56 s^3 s^4 s^4 t^2 t^2 u - 40 s^3 s^4 s^4 t^2 t u^2 + 40 s^3 s^4 s^4 t^2 u^3 + 8 s^3 s^4 s^4 t^4 + 136 s^3 s^4 s^4 t^3 u + 328 s^3 s^4 s^4 t^2 u^2 + 280 s^3 s^4 s^4 t u^3 + 80 s^3 s^4 s^4 u^4 + 4 s^3 s^4 t^5 + 20 s^3 s^4 t^4 u + 40 s^3 s^4 t^3 u^2 + 40 s^3 s^4 t^2 u^3 + 20 s^3 s^4 t u^4 + 4 s^3 s^4 u^5 - 16 s^3 s^4 t^3 t^3 - 96 s^3 s^4 s^4 t^3 t^2 u - 120 s^3 s^4 s^4 t^3 t u^2 - 40 s^3 s^4 s^4 t^3 u^3 + 8 s^3 s^4 s^4 t^2 t^4 + 136 s^3 s^4 s^4 t^2 t^3 u + 328 s^3 s^4 s^4 t^2 t^2 u^2 + 280 s^3 s^4 s^4 t^2 t u^3 + 80 s^3 s^4 s^4 t^2 u^4 - 4 s^3 s^4 s^4 t^5 - 40 s^3 s^4 s^4 t^4 u - 128 s^3 s^4 s^4 t^3 u^2 - 184 s^3 s^4 s^4 t^2 u^3 - 124 s^3 s^4 s^4 t u^4 - 32 s^3 s^4 s^4 u^5 - 4 s^3 t^6 - 28 s^3 t^5 u - 80 s^3 t^4 u^2 - 120 s^3 t^3 u^3 - 100 s^3 t^2 u^4 - 44 s^3 t u^5 - 8 s^3 u^6 + 4 s^4 t^2 t^5 + 20 s^4 t^2 t^4 u + 40 s^4 t^2 t^3 u^2 + 40 s^4 t^2 t^2 u^3 + 20 s^4 t^2 t u^4 + 4 s^4 t^2 u^5 - 4 s^4 t^6 - 28 s^4 t^5 u - 80 s^4 t^4 u^2 - 120 s^4 t^3 u^3 - 100 s^4 t^2 u^4 - 44 s^4 t u^5 - 8 s^4 u^6 + 2 t^7 + 14 t^6 u + 44 t^5 u^2 + 80 t^4 u^3 +
\end{aligned}$$

$90t^3u^4+62t^2u^5+24tu^6+4u^7)/u/(-3+2e)/(3e-2)/(-4s3s4+t^2+2tu+u^2)^2/t/(3e-1);$
 $cpbox010010112p1p2p3 := -4*(u-s3+t-s4)*(e-1)*(144e^5s3^2s4^2t^2u^2+144e^5s3^2s4^2u^3-72e^5s3s4t^3u^2-216e^5s3s4t^2u^3-216e^5s3s4t^2u^4-72e^5s3s4u^5+9e^5t^5u^2+45e^5t^4u^3+90e^5t^3u^4+90e^5t^2u^5+45e^5t^2u^6+9e^5u^7-288e^4s3^3s4^3t^3u-288e^4s3^3s4^3u-24e^4s3^3s4t^3u^2-24e^4s3^3s4u^3+144e^4s3^2s4^2t^3+576e^4s3^2s4^2t^2u+672e^4s3^2s4^2t^2u^2+384e^4s3^2s4^2u^3+24e^4s3^2s4t^2u^2+48e^4s3^2s4t^2u^3+24e^4s3^2s4u^4+6e^4s3^2t^3u^2+18e^4s3^2t^2u^3+18e^4s3^2t^2u^4+6e^4s3^2u^5-24e^4s3s4^3t^2u^2-24e^4s3s4^3u^3+24e^4s3s4^2t^2u^2+48e^4s3s4^2t^2u^3+24e^4s3s4^2u^4-18e^4s3s4t^5-162e^4s3s4t^4u-456e^4s3s4t^3u^2-648e^4s3s4t^2u^3-486e^4s3s4t^2u^4-150e^4s3s4u^5-6e^4s3t^4u^2-24e^4s3t^3u^3-36e^4s3t^2u^4-24e^4s3t^2u^5-6e^4s3u^6+6e^4s4^2t^3u^2+18e^4s4^2t^2u^3+18e^4s4^2t^2u^4+6e^4s4^2u^5-6e^4s4t^4u^2-24e^4s4t^3u^3-36e^4s4t^2u^4-24e^4s4t^2u^5-6e^4s4u^6+9e^4t^6u+54e^4t^5u^2+144e^4t^4u^3+216e^4t^3u^4+189e^4t^2u^5+90e^4t^2u^6+18e^4u^7-288e^3s3^4s4^2u+864e^3s3^3s4^3t+288e^3s3^3s4^2t^2u+288e^3s3^3s4^2u^2+144e^3s3^3s4t^2u+296e^3s3^3s4t^2u^2+128e^3s3^3s4u^3-288e^3s3^2s4^4u+288e^3s3^2s4^3t^2u+288e^3s3^2s4^3u^2-432e^3s3^2s4^2t^3-1296e^3s3^2s4^2t^2u-1104e^3s3^2s4^2t^2u^2-720e^3s3^2s4^2u^3-144e^3s3^2s4t^3u-456e^3s3^2s4t^2u^2-408e^3s3^2s4t^2u^3-96e^3s3^2s4u^4-18e^3s3^2t^4u-70e^3s3^2t^3u^2-104e^3s3^2t^2u^3-70e^3s3^2t^2u^4-18e^3s3^2u^5+144e^3s3s4^3t^2u+296e^3s3s4^3t^2u^2+128e^3s3s4^3u^3-144e^3s3s4^2t^3u-456e^3s3s4^2t^2u^2-408e^3s3s4^2t^2u^3-96e^3s3s4^2u^4+54e^3s3s4t^5+432e^3s3s4t^4u+1120e^3s3s4t^3u^2+1472e^3s3s4t^2u^3+1042e^3s3s4t^2u^4+312e^3s3s4u^5+18e^3s3t^5u+88e^3s3t^4u^2+170e^3s3t^3u^3+162e^3s3t^2u^4+76e^3s3t^2u^5+14e^3s3u^6-18e^3s4^2t^4u-70e^3s4^2t^3u^2-104e^3s4^2t^2u^3-70e^3s4^2t^2u^4-18e^3s4^2u^5+18e^3s4t^5u+88e^3s4t^4u^2+170e^3s4t^3u^3+162e^3s4t^2u^4+76e^3s4t^2u^5+14e^3s4u^6-27e^3t^6u-151e^3t^5u^2-373e^3t^4u^3-522e^3t^3u^4-433e^3t^2u^5-199e^3t^2u^6-39e^3u^7+576e^2s3^4s4^2u-928e^2s3^3s4^3t+800e^2s3^3s4^3u-576e^2s3^3s4^2t^2u-864e^2s3^3s4^2u^2-288e^2s3^3s4t^2u-540e^2s3^3s4t^2u^2-212e^2s3^3s4u^3+576e^2s3^2s4^4u-576e^2s3^2s4^3t^2u-864e^2s3^2s4^3u^2+464e^2s3^2s4^2t^3+992e^2s3^2s4^2t^2u+408e^2s3^2s4^2t^2u^2+424e^2s3^2s4^2u^3+288e^2s3^2s4t^3u+976e^2s3^2s4t^2u^2+968e^2s3^2s4t^2u^3+280e^2s3^2s4u^4+36e^2s3^2t^4u+128e^2s3^2t^3u^2+172e^2s3^2t^2u^3+104e^2s3^2t^2u^4+24e^2s3^2u^5-288e^2s3s4^3t^2u-540e^2s3s4^3t^2u^2-212e^2s3s4^3u^3+288e^2s3s4^2t^3u+976e^2s3s4^2t^2u^2+968e^2s3s4^2t^2u^3+280e^2s3s4^2u^4-58e^2s3s4t^5-414e^2s3s4t^4u-984e^2s3s4t^3u^2-1192e^2s3s4t^2u^3-798e^2s3s4t^2u^4-234e^2s3s4u^5-36e^2s3t^5u-176e^2s3t^4u^2-342e^2s3t^3u^3-330e^2s3t^2u^4-158e^2s3t^2u^5-30e^2s3u^6+36e^2s4^2t^4u+128e^2s4^2t^3u^2+172e^2s4^2t^2u^3+104e^2s4^2t^2u^4+24e^2s4^2u^5-36e^2s4t^5u-176e^2s4t^4u^2-342e^2s4t^3u^3-330e^2s4t^2u^4-158e^2s4t^2u^5-30e$

$$\begin{aligned}
& \sim 2*s4*u^6+29*e^2*t^6*u+152*e^2*t^5*u^2+348*e^2*t^4*u^3+452*e^2*t^3*u^4+353*e^2 \\
& *t^2*u^5+156*e^2*t*u^6+30*e^2*u^7-352*e*s3^4*s4^2*u+416*e*s3^3*s4^3*t-640*e*s3 \\
& ^3*s4^3*u+352*e*s3^3*s4^2*t*u+640*e*s3^3*s4^2*u^2+176*e*s3^3*s4*t^2*u+332*e*s3 \\
& ^3*s4*t*u^2+140*e*s3^3*s4*u^3-352*e*s3^2*s4^4*u+352*e*s3^2*s4^3*t*u+640*e*s3^2 \\
& *s4^3*u^2-208*e*s3^2*s4^2*t^3-304*e*s3^2*s4^2*t^2*u+40*e*s3^2*s4^2*t*u^2-104*e \\
& *s3^2*s4^2*u^3-176*e*s3^2*s4*t^3*u-648*e*s3^2*s4*t^2*u^2-720*e*s3^2*s4*t*u^3 \\
& -248*e*s3^2*s4*u^4-22*e*s3^2*t^4*u-80*e*s3^2*t^3*u^2-110*e*s3^2*t^2*u^3-68*e*s3 \\
& ^2*t*u^4-16*e*s3^2*u^5+176*e*s3*s4^3*t^2*u+332*e*s3*s4^3*t*u^2+140*e*s3*s4^3*u \\
& ^3-176*e*s3*s4^2*t^3*u-648*e*s3*s4^2*t^2*u^2-720*e*s3*s4^2*t*u^3-248*e*s3*s4^2 \\
& *u^4+26*e*s3*s4*t^5+168*e*s3*s4*t^4*u+392*e*s3*s4*t^3*u^2+496*e*s3*s4*t^2*u^3+ \\
& 358*e*s3*s4*t*u^4+112*e*s3*s4*u^5+22*e*s3*t^5*u+116*e*s3*t^4*u^2+244*e*s3*t^3* \\
& u^3+256*e*s3*t^2*u^4+134*e*s3*t*u^5+28*e*s3*u^6-22*e*s4^2*t^4*u-80*e*s4^2*t^3* \\
& u^2-110*e*s4^2*t^2*u^3-68*e*s4^2*t*u^4-16*e*s4^2*u^5+22*e*s4*t^5*u+116*e*s4*t^ \\
& 4*u^2+244*e*s4*t^3*u^3+256*e*s4*t^2*u^4+134*e*s4*t*u^5+28*e*s4*u^6-13*e*t^6*u \\
& -70*e*t^5*u^2-166*e*t^4*u^3-224*e*t^3*u^4-181*e*t^2*u^5-82*e*t*u^6-16*e*u^7+64* \\
& s3^4*s4^2*u-64*s3^3*s4^3*t+128*s3^3*s4^3*u-64*s3^3*s4^2*t*u-128*s3^3*s4^2*u^2 \\
& -32*s3^3*s4*t^2*u-64*s3^3*s4*t*u^2-32*s3^3*s4*u^3+64*s3^2*s4^4*u-64*s3^2*s4^3*t \\
& *u-128*s3^2*s4^3*u^2+32*s3^2*s4^2*t^3+32*s3^2*s4^2*t^2*u-32*s3^2*s4^2*t*u^2+32 \\
& *s3^2*s4*t^3*u+128*s3^2*s4*t^2*u^2+160*s3^2*s4*t*u^3+64*s3^2*s4*u^4+4*s3^2*t^4 \\
& *u+16*s3^2*t^3*u^2+24*s3^2*t^2*u^3+16*s3^2*t*u^4+4*s3^2*u^5-32*s3*s4^3*t^2*u \\
& -64*s3*s4^3*t*u^2-32*s3*s4^3*u^3+32*s3*s4^2*t^3*u+128*s3*s4^2*t^2*u^2+160*s3*s4 \\
& ^2*t*u^3+64*s3*s4^2*u^4-4*s3*s4*t^5-24*s3*s4*t^4*u-56*s3*s4*t^3*u^2-80*s3*s4*t \\
& ^2*u^3-68*s3*s4*t*u^4-24*s3*s4*u^5-4*s3*t^5*u-24*s3*t^4*u^2-56*s3*t^3*u^3-64* \\
& s3*t^2*u^4-36*s3*t*u^5-8*s3*u^6+4*s4^2*t^4*u+16*s4^2*t^3*u^2+24*s4^2*t^2*u^3+ \\
& 16*s4^2*t*u^4+4*s4^2*u^5-4*s4*t^5*u-24*s4*t^4*u^2-56*s4*t^3*u^3-64*s4*t^2*u^4 \\
& -36*s4*t*u^5-8*s4*u^6+2*t^6*u+12*t^5*u^2+32*t^4*u^3+48*t^3*u^4+42*t^2*u^5+20*t* \\
& u^6+4*u^7)/(-3+2*e)/(3*e-2)/(-4*s3*s4+t^2+2*t*u+u^2)^2/t/u/(3*e-1)/(-1+2*e); \\
\text{cpbox010000011p1p2p4} & := 4*(e-1)*(32*e^5*s3^5*s4^5*t+32*e^5*s3^5*s4^5*u+32*e^5* \\
& s3^5*s4^4*t^2+32*e^5*s3^5*s4^4*t*u-64*e^5*s3^5*s4^3*t^3-64*e^5*s3^5*s4^3*t^2*u \\
& +32*e^5*s3^4*s4^5*t^2+32*e^5*s3^4*s4^5*t*u-128*e^5*s3^4*s4^4*t^3-192*e^5*s3^4* \\
& s4^4*t^2*u-80*e^5*s3^4*s4^4*t*u^2-16*e^5*s3^4*s4^4*u^3-80*e^5*s3^4*s4^3*t^4 \\
& -144*e^5*s3^4*s4^3*t^3*u-80*e^5*s3^4*s4^3*t^2*u^2-16*e^5*s3^4*s4^3*t*u^3+176*e^ \\
& 5*s3^4*s4^2*t^5+304*e^5*s3^4*s4^2*t^4*u+160*e^5*s3^4*s4^2*t^3*u^2+32*e^5*s3^4* \\
& s4^2*t^2*u^3-64*e^5*s3^3*s4^5*t^3-64*e^5*s3^3*s4^5*t^2*u-80*e^5*s3^3*s4^4*t^4 \\
& -144*e^5*s3^3*s4^4*t^3*u-80*e^5*s3^3*s4^4*t^2*u^2-16*e^5*s3^3*s4^4*t*u^3+474*e^ \\
& 5*s3^3*s4^3*t^5+866*e^5*s3^3*s4^3*t^4*u+492*e^5*s3^3*s4^3*t^3*u^2+124*e^5*s3^3 \\
& *s4^3*t^2*u^3+26*e^5*s3^3*s4^3*t*u^4+2*e^5*s3^3*s4^3*u^5-254*e^5*s3^3*s4^2*t^6 \\
& -390*e^5*s3^3*s4^2*t^5*u-60*e^5*s3^3*s4^2*t^4*u^2+100*e^5*s3^3*s4^2*t^3*u^3+26 \\
& *e^5*s3^3*s4^2*t^2*u^4+2*e^5*s3^3*s4^2*t*u^5-76*e^5*s3^3*s4*t^7-268*e^5*s3^3* \\
& s4*t^6*u-352*e^5*s3^3*s4*t^5*u^2-208*e^5*s3^3*s4*t^4*u^3-52*e^5*s3^3*s4*t^3*u^ \\
& 4-4*e^5*s3^3*s4*t^2*u^5+176*e^5*s3^2*s4^4*t^5+304*e^5*s3^2*s4^4*t^4*u+160*e^5* \\
& s3^2*s4^4*t^3*u^2+32*e^5*s3^2*s4^4*t^2*u^3-254*e^5*s3^2*s4^3*t^6-390*e^5*s3^2* \\
& s4^3*t^5*u-60*e^5*s3^2*s4^3*t^4*u^2+100*e^5*s3^2*s4^3*t^3*u^3+26*e^5*s3^2*s4^3 \\
& *t^2*u^4+2*e^5*s3^2*s4^3*t*u^5-71*e^5*s3^2*s4^2*t^7-485*e^5*s3^2*s4^2*t^6*u \\
& -928*e^5*s3^2*s4^2*t^5*u^2-682*e^5*s3^2*s4^2*t^4*u^3-183*e^5*s3^2*s4^2*t^3*u^4
\end{aligned}$$

$-17e^5s^3^2s^4^2t^2u^5-2e^5s^3^2s^4^2t^2u^6+140e^5s^3^2s^4t^8+522e^5s^3^2s^4t^7u+718e^5s^3^2s^4t^6u^2+420e^5s^3^2s^4t^5u^3+72e^5s^3^2s^4t^4u^4-14e^5s^3^2s^4t^3u^5-2e^5s^3^2s^4t^2u^6+9e^5s^3^2t^9+49e^5s^3^2t^8u+110e^5s^3^2t^7u^2+130e^5s^3^2t^6u^3+85e^5s^3^2t^5u^4+29e^5s^3^2t^4u^5+4e^5s^3^2t^3u^6-76e^5s^3s^4^3t^7-268e^5s^3s^4^3t^6u-352e^5s^3s^4^3t^5u^2-208e^5s^3s^4^3t^4u^3-52e^5s^3s^4^3t^3u^4-4e^5s^3s^4^3t^2u^5+140e^5s^3s^4^2t^8+522e^5s^3s^4^2t^7u+718e^5s^3s^4^2t^6u^2+420e^5s^3s^4^2t^5u^3+72e^5s^3s^4^2t^4u^4-14e^5s^3s^4^2t^3u^5-2e^5s^3s^4^2t^2u^6-46e^5s^3s^4t^9-150e^5s^3s^4t^8u-116e^5s^3s^4t^7u^2+108e^5s^3s^4t^6u^3+210e^5s^3s^4t^5u^4+106e^5s^3s^4t^4u^5+16e^5s^3s^4t^3u^6-18e^5s^3t^10-104e^5s^3t^9u-250e^5s^3t^8u^2-320e^5s^3t^7u^3-230e^5s^3t^6u^4-88e^5s^3t^5u^5-14e^5s^3t^4u^6+9e^5s^4^2t^9+49e^5s^4^2t^8u+110e^5s^4^2t^7u^2+130e^5s^4^2t^6u^3+85e^5s^4^2t^5u^4+29e^5s^4^2t^4u^5+4e^5s^4^2t^3u^6-18e^5s^4t^10-104e^5s^4t^9u-250e^5s^4t^8u^2-320e^5s^4t^7u^3-230e^5s^4t^6u^4-88e^5s^4t^5u^5-14e^5s^4t^4u^6+9e^5t^11+55e^5t^10u+140e^5t^9u^2+190e^5t^8u^3+145e^5t^7u^4+59e^5t^6u^5+10e^5t^5u^6+32e^4s^3^6s^4^4t-128e^4s^3^5s^4^5t-224e^4s^3^5s^4^5u+384e^4s^3^5s^4^4t^2+288e^4s^3^5s^4^4t^2u-360e^4s^3^5s^4^3t^3-120e^4s^3^5s^4^3t^2u-16e^4s^3^5s^4^3t^2u^2+48e^4s^3^5s^4^2t^4-16e^4s^3^5s^4^2t^3u-24e^4s^3^5s^4t^5-24e^4s^3^5s^4t^4u+32e^4s^3^4s^4^6t+384e^4s^3^4s^4^5t^2+288e^4s^3^4s^4^5t^2u-912e^4s^3^4s^4^4t^3-192e^4s^3^4s^4^4t^2u+368e^4s^3^4s^4^4t^2u^2+112e^4s^3^4s^4^4u^3+232e^4s^3^4s^4^3t^4-304e^4s^3^4s^4^3t^3u-520e^4s^3^4s^4^3t^2u^2-144e^4s^3^4s^4^3t^2u^3+264e^4s^3^4s^4^2t^5+330e^4s^3^4s^4^2t^4u+222e^4s^3^4s^4^2t^3u^2+46e^4s^3^4s^4^2t^2u^3+2e^4s^3^4s^4^2t^2u^4+60e^4s^3^4s^4t^6+92e^4s^3^4s^4t^5u+52e^4s^3^4s^4t^4u^2+20e^4s^3^4s^4t^3u^3+6e^4s^3^4t^7+18e^4s^3^4t^6u+18e^4s^3^4t^5u^2+6e^4s^3^4t^4u^3-360e^4s^3^3s^4^5t^3-120e^4s^3^3s^4^5t^2u-16e^4s^3^3s^4^5t^2u^2+232e^4s^3^3s^4^4t^4-304e^4s^3^3s^4^4t^3u-520e^4s^3^3s^4^4t^2u^2-144e^4s^3^3s^4^4t^2u^3+772e^4s^3^3s^4^3t^5+1030e^4s^3^3s^4^3t^4u+580e^4s^3^3s^4^3t^3u^2+8e^4s^3^3s^4^3t^2u^3-104e^4s^3^3s^4^3t^2u^4-14e^4s^3^3s^4^3u^5-458e^4s^3^3s^4^2t^6-290e^4s^3^3s^4^2t^5u+128e^4s^3^3s^4^2t^4u^2+192e^4s^3^3s^4^2t^3u^3+122e^4s^3^3s^4^2t^2u^4+18e^4s^3^3s^4^2t^2u^5-188e^4s^3^3s^4t^7-432e^4s^3^3s^4t^6u-348e^4s^3^3s^4t^5u^2-132e^4s^3^3s^4t^4u^3-32e^4s^3^3s^4t^3u^4-4e^4s^3^3s^4t^2u^5-18e^4s^3^3t^8-64e^4s^3^3t^7u-88e^4s^3^3t^6u^2-60e^4s^3^3t^5u^3-22e^4s^3^3t^4u^4-4e^4s^3^3t^3u^5+48e^4s^3^2s^4^5t^4-16e^4s^3^2s^4^5t^3u+264e^4s^3^2s^4^4t^5+330e^4s^3^2s^4^4t^4u+222e^4s^3^2s^4^4t^3u^2+46e^4s^3^2s^4^4t^2u^3+2e^4s^3^2s^4^4t^2u^4-458e^4s^3^2s^4^3t^6-290e^4s^3^2s^4^3t^5u+128e^4s^3^2s^4^3t^4u^2+192e^4s^3^2s^4^3t^3u^3+122e^4s^3^2s^4^3t^2u^4+18e^4s^3^2s^4^3t^2u^5-150e^4s^3^2s^4^2t^7-780e^4s^3^2s^4^2t^6u-899e^4s^3^2s^4^2t^5u^2-312e^4s^3^2s^4^2t^4u^3-68e^4s^3^2s^4^2t^3u^4-4e^4s^3^2s^4^2t^2u^5+5e^4s^3^2s^4^2t^2u^6+262e^4s^3^2s^4t^8+654e^4s^3^2s^4t^7u+476e^4s^3^2s^4t^6u^2+32e^4s^3^2s^4t^5u^3-62e^4s^3^2s^4t^4u^4-14e^4s^3^2s^4t^3u^5-4e^4s^3^2s^4t^2u^6+36e^4s^3^2t^9+150e^4s^3^2t^8u+247e^4s^3^2t^7u^2+202e^4s^3^2t^6u^3+84e^4s^3^2t^5u^4+16e^4s^3^2t^4u^5+e$

$s4t^7u - 2522e^3s3^2s4t^6u^2 - 1110e^3s3^2s4t^5u^3 + 90e^3s3^2s4t^4u^4 + 182e^3s3^2s4t^3u^5 + 28e^3s3^2s4t^2u^6 - 85e^3s3^2t^9 - 435e^3s3^2t^8u - 921e^3s3^2t^7u^2 - 1024e^3s3^2t^6u^3 - 623e^3s3^2t^5u^4 - 193e^3s3^2t^4u^5 - 23e^3s3^2t^3u^6 + 128e^3s3s4^5t^5 + 296e^3s3s4^5t^4u + 144e^3s3s4^5t^3u^2 - 316e^3s3s4^4t^6 - 924e^3s3s4^4t^5u - 688e^3s3s4^4t^4u^2 - 100e^3s3s4^4t^3u^3 + 28e^3s3s4^4t^2u^4 + 538e^3s3s4^3t^7 + 1944e^3s3s4^3t^6u + 2232e^3s3s4^3t^5u^2 + 992e^3s3s4^3t^4u^3 + 150e^3s3s4^3t^3u^4 + 8e^3s3s4^3t^2u^5 - 564e^3s3s4^2t^8 - 2040e^3s3s4^2t^7u - 2522e^3s3s4^2t^6u^2 - 1110e^3s3s4^2t^5u^3 + 90e^3s3s4^2t^4u^4 + 182e^3s3s4^2t^3u^5 + 28e^3s3s4^2t^2u^6 + 122e^3s3s4t^9 + 222e^3s3s4t^8u - 296e^3s3s4t^7u^2 - 1152e^3s3s4t^6u^3 - 1222e^3s3s4t^5u^4 - 550e^3s3s4t^4u^5 - 84e^3s3s4t^3u^6 + 92e^3s3t^10 + 506e^3s3t^9u + 1166e^3s3t^8u^2 + 1442e^3s3t^7u^3 + 1010e^3s3t^6u^4 + 380e^3s3t^5u^5 + 60e^3s3t^4u^6 - 18e^3s4^4t^7 - 70e^3s4^4t^6u - 104e^3s4^4t^5u^2 - 70e^3s4^4t^4u^3 - 18e^3s4^4t^3u^4 + 50e^3s4^3t^8 + 220e^3s4^3t^7u + 390e^3s4^3t^6u^2 + 346e^3s4^3t^5u^3 + 152e^3s4^3t^4u^4 + 26e^3s4^3t^3u^5 - 85e^3s4^2t^9 - 435e^3s4^2t^8u - 921e^3s4^2t^7u^2 - 1024e^3s4^2t^6u^3 - 623e^3s4^2t^5u^4 - 193e^3s4^2t^4u^5 - 23e^3s4^2t^3u^6 + 92e^3s4t^10 + 506e^3s4t^9u + 1166e^3s4t^8u^2 + 1442e^3s4t^7u^3 + 1010e^3s4t^6u^4 + 380e^3s4t^5u^5 + 60e^3s4t^4u^6 - 39e^3t^11 - 221e^3t^10u - 533e^3t^9u^2 - 702e^3t^8u^3 - 533e^3t^7u^4 - 221e^3t^6u^5 - 39e^3t^5u^6 + 352e^2s3^6s4^4t - 960e^2s3^6s4^3t^2 + 576e^2s3^6s4^2t^3 + 448e^2s3^5s4^5t - 608e^2s3^5s4^5u - 2464e^2s3^5s4^4t^2 + 1120e^2s3^5s4^4t^2u + 3964e^2s3^5s4^3t^3 - 124e^2s3^5s4^3t^2u - 176e^2s3^5s4^3t^2u^2 - 1656e^2s3^5s4^2t^4 + 248e^2s3^5s4^2t^3u + 480e^2s3^5s4^2t^2u^2 - 212e^2s3^5s4t^5 - 540e^2s3^5s4t^4u - 288e^2s3^5s4t^3u^2 + 352e^2s3^4s4^6t - 2464e^2s3^4s4^5t^2 + 1120e^2s3^4s4^5t^2u + 6520e^2s3^4s4^4t^3 - 1064e^2s3^4s4^4t^2u + 528e^2s3^4s4^4t^2u^2 + 304e^2s3^4s4^4u^3 - 6760e^2s3^4s4^3t^4 - 1056e^2s3^4s4^3t^3u - 568e^2s3^4s4^3t^2u^2 - 560e^2s3^4s4^3t^2u^3 + 1602e^2s3^4s4^2t^5 - 1224e^2s3^4s4^2t^4u - 1592e^2s3^4s4^2t^3u^2 - 24e^2s3^4s4^2t^2u^3 + 22e^2s3^4s4^2t^2u^4 + 660e^2s3^4s4t^6 + 1888e^2s3^4s4t^5u + 1320e^2s3^4s4t^4u^2 + 112e^2s3^4s4t^3u^3 - 60e^2s3^4s4t^2u^4 + 24e^2s3^4t^7 + 104e^2s3^4t^6u + 172e^2s3^4t^5u^2 + 128e^2s3^4t^4u^3 + 36e^2s3^4t^3u^4 - 960e^2s3^3s4^6t^2 + 3964e^2s3^3s4^5t^3 - 124e^2s3^3s4^5t^2u - 176e^2s3^3s4^5t^2u^2 - 6760e^2s3^3s4^4t^4 - 1056e^2s3^3s4^4t^3u - 568e^2s3^3s4^4t^2u^2 - 560e^2s3^3s4^4t^2u^3 + 4512e^2s3^3s4^3t^5 + 222e^2s3^3s4^3t^4u - 228e^2s3^3s4^3t^3u^2 + 208e^2s3^3s4^3t^2u^3 - 196e^2s3^3s4^3t^2u^4 - 38e^2s3^3s4^3u^5 + 212e^2s3^3s4^2t^6 + 4384e^2s3^3s4^2t^5u + 4702e^2s3^3s4^2t^4u^2 + 1906e^2s3^3s4^2t^3u^3 + 470e^2s3^3s4^2t^2u^4 + 70e^2s3^3s4^2t^2u^5 - 870e^2s3^3s4t^7 - 2880e^2s3^3s4t^6u - 2788e^2s3^3s4t^5u^2 - 808e^2s3^3s4t^4u^3 + 22e^2s3^3s4t^3u^4 + 12e^2s3^3s4t^2u^5 - 78e^2s3^3t^8 - 366e^2s3^3t^7u - 678e^2s3^3t^6u^2 - 610e^2s3^3t^5u^3 - 260e^2s3^3t^4u^4 - 40e^2s3^3t^3u^5 + 576e^2s3^2s4^6t^3 - 1656e^2s3^2s4^5t^4 + 248e^2s3^2s4^5t^3u + 480e^2s3^2s4^5t^2u^2 + 1602e^2s3^2s4^4t^5 - 1224e^2s3^2s4^4t^4u - 1592e^2s3^2s4^4t^3u^2 - 24e^2s3^2s4^4t^2*$

$$\begin{aligned}
 & u^3 + 22e^2 s^3 s^4 t^4 u^4 + 212e^2 s^3 s^4 t^3 u^6 + 4384e^2 s^3 s^4 t^5 u^4 + 4702 \\
 & e^2 s^3 s^4 t^4 u^2 + 1906e^2 s^3 s^4 t^3 u^3 + 470e^2 s^3 s^4 t^2 u^4 + 70 \\
 & e^2 s^3 s^4 t^3 u^5 - 1366e^2 s^3 s^4 t^2 u^7 - 5806e^2 s^3 s^4 t^6 u - 6883e^2 s^3 s^4 t^2 u^5 \\
 & - 3824e^2 s^3 s^4 t^4 u^3 - 912e^2 s^3 s^4 t^3 u^4 - 34e^2 s^3 s^4 t^2 u^5 + 9e^2 s^3 s^4 t^2 u^6 \\
 & + 516e^2 s^3 s^4 t^8 + 1754e^2 s^3 s^4 t^7 u + 1846e^2 s^3 s^4 t^6 u^2 + 374e^2 s^3 s^4 t^5 u^3 \\
 & - 498e^2 s^3 s^4 t^4 u^4 - 304e^2 s^3 s^4 t^3 u^5 - 40e^2 s^3 s^4 t^2 u^6 + 114e^2 s^3 s^4 t^9 + 596e^2 s^3 s^4 t^8 u \\
 & + 1273e^2 s^3 s^4 t^7 u^2 + 1408e^2 s^3 s^4 t^6 u^3 + 840e^2 s^3 s^4 t^5 u^4 + 252e^2 s^3 s^4 t^4 u^5 \\
 & + 29e^2 s^3 s^4 t^3 u^6 - 212e^2 s^3 s^4 t^5 u^5 - 540e^2 s^3 s^4 t^4 u - 288 \\
 & e^2 s^3 s^4 t^3 u^2 + 660e^2 s^3 s^4 t^6 + 1888e^2 s^3 s^4 t^5 u + 1320e^2 s^3 s^4 t^4 u^2 \\
 & + 112e^2 s^3 s^4 t^3 u^3 - 60e^2 s^3 s^4 t^2 u^4 - 870e^2 s^3 s^4 t^7 - 2880e^2 s^3 s^4 t^6 u \\
 & - 2788e^2 s^3 s^4 t^5 u^2 - 808e^2 s^3 s^4 t^4 u^3 + 22e^2 s^3 s^4 t^3 u^4 + 12e^2 s^3 s^4 t^2 u^5 \\
 & + 516e^2 s^3 s^4 t^8 + 1754e^2 s^3 s^4 t^7 u + 1846e^2 s^3 s^4 t^6 u^2 + 374e^2 s^3 s^4 t^5 u^3 \\
 & - 498e^2 s^3 s^4 t^4 u^4 - 304e^2 s^3 s^4 t^3 u^5 - 40e^2 s^3 s^4 t^2 u^6 - 4e^2 s^3 s^4 t^9 + 290e^2 s^3 s^4 t^8 u \\
 & + 1160e^2 s^3 s^4 t^7 u^2 + 1968e^2 s^3 s^4 t^6 u^3 + 1760e^2 s^3 s^4 t^5 u^4 + 782e^2 s^3 s^4 t^4 u^5 \\
 & + 124e^2 s^3 s^4 t^3 u^6 - 90e^2 s^3 s^4 t^{10} - 508e^2 s^3 s^4 t^9 u - 1214e^2 s^3 s^4 t^8 u^2 \\
 & - 1574e^2 s^3 s^4 t^7 u^3 - 1168e^2 s^3 s^4 t^6 u^4 - 470e^2 s^3 s^4 t^5 u^5 - 80e^2 s^3 s^4 t^4 u^6 \\
 & + 24e^2 s^4 t^7 + 104e^2 s^4 t^6 u + 172e^2 s^4 t^5 u^2 + 128e^2 s^4 t^4 u^3 + 36e^2 s^4 t^3 u^4 \\
 & - 78e^2 s^4 t^8 - 366e^2 s^4 t^7 u - 678e^2 s^4 t^6 u^2 - 610e^2 s^4 t^5 u^3 - 260e^2 s^4 t^4 u^4 \\
 & - 40e^2 s^4 t^3 u^5 + 114e^2 s^4 t^2 u^6 + 596e^2 s^4 t^8 u + 1273e^2 s^4 t^7 u^2 + 1408e^2 s^4 t^6 u^3 + 840 \\
 & e^2 s^4 t^5 u^4 + 252e^2 s^4 t^4 u^5 + 29e^2 s^4 t^3 u^6 - 90e^2 s^4 t^{10} - 508e^2 s^4 t^9 u \\
 & - 1214e^2 s^4 t^8 u^2 - 1574e^2 s^4 t^7 u^3 - 1168e^2 s^4 t^6 u^4 - 470e^2 s^4 t^5 u^5 - 80e^2 s^4 t^4 u^6 \\
 & + 30e^2 s^4 t^{11} + 174e^2 s^4 t^{10} u + 445e^2 s^4 t^9 u^2 + 640e^2 s^4 t^8 u^3 + 540e^2 s^4 t^7 u^4 \\
 & + 250e^2 s^4 t^6 u^5 + 49e^2 s^4 t^5 u^6 - 256e^2 s^4 t^6 s^4 t^4 + 640e^2 s^4 t^5 s^4 t^3 \\
 & - 352e^2 s^4 t^2 s^4 t^3 - 448e^2 s^4 t^5 s^4 t^5 + 320e^2 s^4 t^5 s^4 t^5 u + 2112e^2 s^4 t^4 s^4 t^2 \\
 & - 480e^2 s^4 t^5 s^4 t^4 u - 2980e^2 s^4 t^5 s^4 t^3 - 20e^2 s^4 t^5 s^4 t^3 u^2 + 128e^2 s^4 t^5 s^4 t^3 u^2 \\
 & + 1096e^2 s^4 t^5 s^4 t^2 - 248e^2 s^4 t^5 s^4 t^2 u - 320e^2 s^4 t^5 s^4 t^2 u^2 + 140e^2 s^4 t^5 s^4 t^2 u^2 \\
 & + 332e^2 s^4 t^5 s^4 t^4 u + 176e^2 s^4 t^5 s^4 t^3 u^2 - 256e^2 s^4 t^5 s^4 t^3 u^2 + 2112e^2 s^4 t^5 s^4 t^3 u^2 \\
 & - 480e^2 s^4 t^5 s^4 t^3 u^2 - 480e^2 s^4 t^5 s^4 t^3 u^2 - 5320e^2 s^4 t^5 s^4 t^4 t^3 + 344e^2 s^4 t^5 s^4 t^4 t^2 u \\
 & - 208e^2 s^4 t^5 s^4 t^4 t^2 u - 160e^2 s^4 t^5 s^4 t^4 u^3 + 4864e^2 s^4 t^5 s^4 t^4 s^4 t^3 t^4 + 40e^2 s^4 t^5 s^4 t^3 t^3 u \\
 & - 200e^2 s^4 t^5 s^4 t^3 t^2 u^2 + 240e^2 s^4 t^5 s^4 t^3 t^2 u^3 - 818e^2 s^4 t^5 s^4 t^2 t^5 + 1660e^2 s^4 t^5 s^4 t^2 t^4 u \\
 & + 1462e^2 s^4 t^5 s^4 t^2 t^3 u^2 + 72e^2 s^4 t^5 s^4 t^2 t^2 u^3 - 16e^2 s^4 t^5 s^4 t^2 t^2 u^4 - 500e^2 s^4 t^5 s^4 t^2 t^6 u \\
 & - 1264e^2 s^4 t^5 s^4 t^2 t^5 u - 804e^2 s^4 t^5 s^4 t^2 t^4 u^2 - 32e^2 s^4 t^5 s^4 t^2 t^3 u^3 + 40e^2 s^4 t^5 s^4 t^2 t^2 u^4 \\
 & - 16e^2 s^4 t^5 s^4 t^2 t^7 u - 68e^2 s^4 t^5 s^4 t^2 t^6 u - 110e^2 s^4 t^5 s^4 t^2 t^5 u^2 - 80e^2 s^4 t^5 s^4 t^2 t^4 u^3 \\
 & - 22e^2 s^4 t^5 s^4 t^2 t^3 u^4 + 640e^2 s^4 t^5 s^4 t^2 t^3 s^4 t^6 t^2 - 2980e^2 s^4 t^5 s^4 t^2 t^3 s^4 t^5 t^2 u \\
 & + 128e^2 s^4 t^5 s^4 t^2 t^3 s^4 t^5 t^2 u^2 + 4864e^2 s^4 t^5 s^4 t^2 t^3 s^4 t^4 t^4 + 40e^2 s^4 t^5 s^4 t^2 t^3 s^4 t^4 t^3 u \\
 & - 200e^2 s^4 t^5 s^4 t^2 t^3 s^4 t^4 t^2 u^2 + 240e^2 s^4 t^5 s^4 t^2 t^3 s^4 t^4 t^2 u^3 - 2508e^2 s^4 t^5 s^4 t^2 t^3 s^4 t^3 t^5 \\
 & + 1960e^2 s^4 t^5 s^4 t^2 t^3 s^4 t^3 t^4 u + 1552e^2 s^4 t^5 s^4 t^2 t^3 s^4 t^3 t^3 u^2 + 84e^2 s^4 t^5 s^4 t^2 t^3 s^4 t^3 t^2 u^3 \\
 & + 108e^2 s^4 t^5 s^4 t^2 t^3 s^4 t^3 t^2 u^4 + 20e^2 s^4 t^5 s^4 t^2 t^3 s^4 t^3 t^5 u - 740e^2 s^4 t^5 s^4 t^2 t^3 s^4 t^2 t^6 \\
 & - 4150e^2 s^4 t^5 s^4 t^2 t^3 s^4 t^2 t^4 u^2 - 940e^2 s^4 t^5 s^4 t^2 t^3 s^4 t^2 t^3 u^3 - 176e^2 s^4 t^5 s^4 t^2 t^3 s^4 t^2 t^2 u^4 \\
 & - 30e^2 s^4 t^5 s^4 t^2 t^3 s^4 t^2 t^5 u + 644e^2 s^4 t^5 s^4 t^2 t^3 s^4 t^2 t^7 u + 1720e^2 s^4 t^5 s^4 t^2 t^3 s^4 t^2 t^6 u \\
 & + 1248e^2 s^4 t^5 s^4 t^2 t^3 s^4 t^2 t^5 u^2 + 76e^2 s^4 t^5 s^4 t^2 t^3 s^4 t^2 t^4 u^3 - 128e^2 s^4 t^5 s^4 t^2 t^3 s^4 t^2 t^3 u^4 \\
 & - 16e^2 s^4 t^5 s^4 t^2 t^3 s^4 t^2 t^2 u^5 + 60e^2 s^4 t^5 s^4 t^2 t^3 s^4 t^2 t^8 u + 270e^2 s^4 t^5 s^4 t^2 t^3 s^4 t^2 t^7 u \\
 & + 476e^2 s^4 t^5 s^4 t^2 t^3 s^4 t^2 t^6 u^2 + 404e^2 s^4 t^5 s^4 t^2 t^3 s^4 t^2 t^5 u^3
 \end{aligned}$$

$3+160e^{s^3}t^4u^4+22e^{s^3}t^3u^5-352e^{s^2}t^4s^6t^3+1096e^{s^2}t^4s^5t^4-248e^{s^2}t^4s^5t^3u-320e^{s^2}t^4s^5t^2u^2-818e^{s^2}t^4s^4t^5+1660e^{s^2}t^4s^4t^4u+1462e^{s^2}t^4s^4t^3u^2+72e^{s^2}t^4s^4t^2u^3-16e^{s^2}t^4s^4t^2u^4-740e^{s^2}t^4s^4t^3u^3-176e^{s^2}t^4s^4t^2u^4-30e^{s^2}t^4s^4t^3u^5+1188e^{s^2}t^4s^4t^2u^7+3834e^{s^2}t^4s^4t^2u^6+3453e^{s^2}t^4s^4t^2u^5+1280e^{s^2}t^4s^4t^2u^4+190e^{s^2}t^4s^4t^2u^3-18e^{s^2}t^4s^4t^2u^5-7e^{s^2}t^4s^4t^2u^6-284e^{s^2}t^4s^4t^2u^8-622e^{s^2}t^4s^4t^2u^7-118e^{s^2}t^4s^4t^2u^6+588e^{s^2}t^4s^4t^2u^5+532e^{s^2}t^4s^4t^2u^4+186e^{s^2}t^4s^4t^2u^3+22e^{s^2}t^4s^4t^2u^6-88e^{s^2}t^4s^4t^2u^9-426e^{s^2}t^4s^4t^2u^8-835e^{s^2}t^4s^4t^2u^7-840e^{s^2}t^4s^4t^2u^6-452e^{s^2}t^4s^4t^2u^5-122e^{s^2}t^4s^4t^2u^4-13e^{s^2}t^4s^4t^2u^3+140e^{s^2}t^4s^4t^2u^6+332e^{s^2}t^4s^4t^2u^5+176e^{s^2}t^4s^4t^2u^3-500e^{s^2}t^4s^4t^2u^6-1264e^{s^2}t^4s^4t^2u^5-804e^{s^2}t^4s^4t^2u^4-32e^{s^2}t^4s^4t^2u^3+40e^{s^2}t^4s^4t^2u^4+644e^{s^2}t^4s^4t^2u^3+1720e^{s^2}t^4s^4t^2u^6+1248e^{s^2}t^4s^4t^2u^5+76e^{s^2}t^4s^4t^2u^3-128e^{s^2}t^4s^4t^2u^4-16e^{s^2}t^4s^4t^2u^5-284e^{s^2}t^4s^4t^2u^8-622e^{s^2}t^4s^4t^2u^7-118e^{s^2}t^4s^4t^2u^6+588e^{s^2}t^4s^4t^2u^5+532e^{s^2}t^4s^4t^2u^4+186e^{s^2}t^4s^4t^2u^3+22e^{s^2}t^4s^4t^2u^6-60e^{s^2}t^4s^4t^2u^9-480e^{s^2}t^4s^4t^2u^8-1212e^{s^2}t^4s^4t^2u^7-1500e^{s^2}t^4s^4t^2u^6-1044e^{s^2}t^4s^4t^2u^5-396e^{s^2}t^4s^4t^2u^4-60e^{s^2}t^4s^4t^2u^6+60e^{s^2}t^4s^4t^2u^10+310e^{s^2}t^4s^4t^2u^9+674e^{s^2}t^4s^4t^2u^8+796e^{s^2}t^4s^4t^2u^7+544e^{s^2}t^4s^4t^2u^6-16e^{s^2}t^4s^4t^2u^11-86e^{s^2}t^4s^4t^2u^10-203e^{s^2}t^4s^4t^2u^9-272e^{s^2}t^4s^4t^2u^8-218e^{s^2}t^4s^4t^2u^7-98e^{s^2}t^4s^4t^2u^6-19e^{s^2}t^4s^4t^2u^5+64e^{s^2}t^4s^4t^2u^6+64e^{s^2}t^4s^4t^2u^3+128e^{s^2}t^4s^4t^2u^5-64e^{s^2}t^4s^4t^2u^4-512e^{s^2}t^4s^4t^2u^3+64e^{s^2}t^4s^4t^2u^6+608e^{s^2}t^4s^4t^2u^5-32e^{s^2}t^4s^4t^2u^4-192e^{s^2}t^4s^4t^2u^3+64e^{s^2}t^4s^4t^2u^5-64e^{s^2}t^4s^4t^2u^4-32e^{s^2}t^4s^4t^2u^3+64e^{s^2}t^4s^4t^2u^6-512e^{s^2}t^4s^4t^2u^5+64e^{s^2}t^4s^4t^2u^4+1152e^{s^2}t^4s^4t^2u^3-32e^{s^2}t^4s^4t^2u^4+32e^{s^2}t^4s^4t^2u^3-896e^{s^2}t^4s^4t^2u^4+160e^{s^2}t^4s^4t^2u^3+128e^{s^2}t^4s^4t^2u^2-32e^{s^2}t^4s^4t^2u^3+68e^{s^2}t^4s^4t^2u^5-464e^{s^2}t^4s^4t^2u^4-328e^{s^2}t^4s^4t^2u^3-16e^{s^2}t^4s^4t^2u^4+4e^{s^2}t^4s^4t^2u^3+120e^{s^2}t^4s^4t^2u^6+256e^{s^2}t^4s^4t^2u^5+144e^{s^2}t^4s^4t^2u^4-8e^{s^2}t^4s^4t^2u^4+4e^{s^2}t^4s^4t^2u^7+16e^{s^2}t^4s^4t^2u^6+24e^{s^2}t^4s^4t^2u^5+16e^{s^2}t^4s^4t^2u^4+4e^{s^2}t^4s^4t^2u^3-128e^{s^2}t^4s^4t^2u^6+608e^{s^2}t^4s^4t^2u^5-32e^{s^2}t^4s^4t^2u^4-896e^{s^2}t^4s^4t^2u^3+160e^{s^2}t^4s^4t^2u^4+128e^{s^2}t^4s^4t^2u^2-32e^{s^2}t^4s^4t^2u^3+296e^{s^2}t^4s^4t^2u^5-772e^{s^2}t^4s^4t^2u^4-528e^{s^2}t^4s^4t^2u^3-56e^{s^2}t^4s^4t^2u^3-24e^{s^2}t^4s^4t^2u^4-4e^{s^2}t^4s^4t^2u^5+288e^{s^2}t^4s^4t^2u^6+996e^{s^2}t^4s^4t^2u^5+688e^{s^2}t^4s^4t^2u^4+120e^{s^2}t^4s^4t^2u^3+16e^{s^2}t^4s^4t^2u^4+4e^{s^2}t^4s^4t^2u^5-152e^{s^2}t^4s^4t^2u^7-316e^{s^2}t^4s^4t^2u^6-144e^{s^2}t^4s^4t^2u^5+56e^{s^2}t^4s^4t^2u^4+40e^{s^2}t^4s^4t^2u^3+4e^{s^2}t^4s^4t^2u^5-16e^{s^2}t^4s^4t^2u^8-68e^{s^2}t^4s^4t^2u^7-112e^{s^2}t^4s^4t^2u^6-88e^{s^2}t^4s^4t^2u^5-32e^{s^2}t^4s^4t^2u^4-4e^{s^2}t^4s^4t^2u^3+64e^{s^2}t^4s^4t^2u^6-192e^{s^2}t^4s^4t^2u^5+64e^{s^2}t^4s^4t^2u^3+64e^{s^2}t^4s^4t^2u^5-464e^{s^2}t^4s^4t^2u^4-328e^{s^2}t^4s^4t^2u^3-16e^{s^2}t^4s^4t^2u^4+288e^{s^2}t^4s^4t^2u^6+996e^{s^2}t^4s^4t^2u^5+688e^{s^2}t^4s^4t^2u^4$

$$\begin{aligned}
& *u^2+192e^4*s3*s4^4*t^4+696e^4*s3*s4^4*t^3*u+672e^4*s3*s4^4*t^2*u^2+168e^4 \\
& *s3*s4^4*t*u^3-310e^4*s3*s4^3*t^5-998e^4*s3*s4^3*t^4*u-1248e^4*s3*s4^3*t^3* \\
& u^2-848e^4*s3*s4^3*t^2*u^3-322e^4*s3*s4^3*t*u^4-34e^4*s3*s4^3*u^5+350e^4* \\
& s3*s4^2*t^6+1008e^4*s3*s4^2*t^5*u+1276e^4*s3*s4^2*t^4*u^2+968e^4*s3*s4^2*t^ \\
& 3*u^3+390e^4*s3*s4^2*t^2*u^4+40e^4*s3*s4^2*t*u^5-154e^4*s3*s4*t^7-474e^4* \\
& s3*s4*t^6*u-584e^4*s3*s4*t^5*u^2-376e^4*s3*s4*t^4*u^3-126e^4*s3*s4*t^3*u^4 \\
& -14e^4*s3*s4*t^2*u^5-6e^4*s3*t^8-24e^4*s3*t^7*u-36e^4*s3*t^6*u^2-24e^4*s3* \\
& t^5*u^3-6e^4*s3*t^4*u^4+6e^4*s4^4*t^5+42e^4*s4^4*t^4*u+90e^4*s4^4*t^3*u^2+ \\
& 78e^4*s4^4*t^2*u^3+24e^4*s4^4*t*u^4-18e^4*s4^3*t^6-132e^4*s4^3*t^5*u-312e^ \\
& ^4*s4^3*t^4*u^2-324e^4*s4^3*t^3*u^3-150e^4*s4^3*t^2*u^4-24e^4*s4^3*t*u^5+36 \\
& *e^4*s4^2*t^7+204e^4*s4^2*t^6*u+463e^4*s4^2*t^5*u^2+550e^4*s4^2*t^4*u^3+372 \\
& *e^4*s4^2*t^3*u^4+142e^4*s4^2*t^2*u^5+25e^4*s4^2*t*u^6-42e^4*s4*t^8-204e^4 \\
& *s4*t^7*u-426e^4*s4*t^6*u^2-504e^4*s4*t^5*u^3-366e^4*s4*t^4*u^4-156e^4*s4* \\
& t^3*u^5-30e^4*s4*t^2*u^6+18e^4*t^9+90e^4*t^8*u+189e^4*t^7*u^2+216e^4*t^6* \\
& u^3+144e^4*t^5*u^4+54e^4*t^4*u^5+9e^4*t^3*u^6-352e^3*s3^4*s4^4*t+576e^3*s \\
& s3^4*s4^3*t^2-288e^3*s3^4*s4^2*t^3-448e^3*s3^3*s4^5*t+608e^3*s3^3*s4^5*u+ \\
& 672e^3*s3^3*s4^4*t^2-1152e^3*s3^3*s4^4*t*u-352e^3*s3^3*s4^3*t^3+776e^3*s3^ \\
& 3*s4^3*t^2*u+176e^3*s3^3*s4^3*t*u^2+32e^3*s3^3*s4^2*t^4-336e^3*s3^3*s4^2*t^ \\
& 3*u-288e^3*s3^3*s4^2*t^2*u^2+128e^3*s3^3*s4*t^5+296e^3*s3^3*s4*t^4*u+144e^ \\
& 3*s3^3*s4*t^3*u^2-352e^3*s3^2*s4^6*t+992e^3*s3^2*s4^5*t^2+320e^3*s3^2*s4^5* \\
& t*u-1376e^3*s3^2*s4^4*t^3-688e^3*s3^2*s4^4*t^2*u-480e^3*s3^2*s4^4*t*u^2-304 \\
& *e^3*s3^2*s4^4*u^3+1328e^3*s3^2*s4^3*t^4+1152e^3*s3^2*s4^3*t^3*u+1176e^3*s3 \\
& ^2*s4^3*t^2*u^2+552e^3*s3^2*s4^3*t*u^3-502e^3*s3^2*s4^2*t^5-550e^3*s3^2*s4^ \\
& 2*t^4*u-592e^3*s3^2*s4^2*t^3*u^2-246e^3*s3^2*s4^2*t^2*u^3-22e^3*s3^2*s4^2*t \\
& *u^4-76e^3*s3^2*s4*t^6-244e^3*s3^2*s4*t^5*u-216e^3*s3^2*s4*t^4*u^2-12e^3*s \\
& s3^2*s4*t^3*u^3+36e^3*s3^2*s4*t^2*u^4-18e^3*s3^2*t^7-70e^3*s3^2*t^6*u-104e^ \\
& ^3*s3^2*t^5*u^2-70e^3*s3^2*t^4*u^3-18e^3*s3^2*t^3*u^4+176e^3*s3*s4^5*t^3+ \\
& 328e^3*s3*s4^5*t^2*u+224e^3*s3*s4^5*t*u^2-496e^3*s3*s4^4*t^4-1056e^3*s3*s4 \\
& ^4*t^3*u-936e^3*s3*s4^4*t^2*u^2-232e^3*s3*s4^4*t*u^3+760e^3*s3*s4^3*t^5+ \\
& 1770e^3*s3*s4^3*t^4*u+1736e^3*s3*s4^3*t^3*u^2+832e^3*s3*s4^3*t^2*u^3+216e^ \\
& 3*s3*s4^3*t*u^4+38e^3*s3*s4^3*u^5-754e^3*s3*s4^2*t^6-2004e^3*s3*s4^2*t^5*u \\
& -2246e^3*s3*s4^2*t^4*u^2-1446e^3*s3*s4^2*t^3*u^3-520e^3*s3*s4^2*t^2*u^4-70e^ \\
& ^3*s3*s4^2*t*u^5+300e^3*s3*s4*t^7+894e^3*s3*s4*t^6*u+1124e^3*s3*s4*t^5*u^2+ \\
& 788e^3*s3*s4*t^4*u^3+280e^3*s3*s4*t^3*u^4+22e^3*s3*s4*t^2*u^5+14e^3*s3*t^8 \\
& +76e^3*s3*t^7*u+162e^3*s3*t^6*u^2+170e^3*s3*t^5*u^3+88e^3*s3*t^4*u^4+18e^ \\
& 3*s3*t^3*u^5-18e^3*s4^4*t^5-86e^3*s4^4*t^4*u-144e^3*s4^4*t^3*u^2-102e^3*s4 \\
& ^4*t^2*u^3-26e^3*s4^4*t*u^4+50e^3*s4^3*t^6+256e^3*s4^3*t^5*u+482e^3*s4^3*t \\
& ^4*u^2+422e^3*s4^3*t^3*u^3+172e^3*s4^3*t^2*u^4+26e^3*s4^3*t*u^5-85e^3*s4^2 \\
& *t^7-421e^3*s4^2*t^6*u-821e^3*s4^2*t^5*u^2-804e^3*s4^2*t^4*u^3-415e^3*s4^2 \\
& *t^3*u^4-107e^3*s4^2*t^2*u^5-11e^3*s4^2*t*u^6+92e^3*s4*t^8+450e^3*s4*t^7*u \\
& +912e^3*s4*t^6*u^2+990e^3*s4*t^5*u^3+618e^3*s4*t^4*u^4+216e^3*s4*t^3*u^5+ \\
& 34e^3*s4*t^2*u^6-39e^3*t^9-199e^3*t^8*u-433e^3*t^7*u^2-522e^3*t^6*u^3-373 \\
& *e^3*t^5*u^4-151e^3*t^4*u^5-27e^3*t^3*u^6+256e^2*s3^4*s4^4*t-896e^2*s3^4* \\
& s4^3*t^2+576e^2*s3^4*s4^2*t^3+352e^2*s3^3*s4^5*t-416e^2*s3^3*s4^5*u-1424e^ \\
& 2*s3^3*s4^4*t^2+944e^2*s3^3*s4^4*t*u+1676e^2*s3^3*s4^3*t^3+100e^2*s3^3*s4^3
\end{aligned}$$

$$\begin{aligned}
 & *t^2 u - 128 e^2 s^3 s^4^3 t^2 u^2 - 360 e^2 s^3 s^4^2 t^4 + 104 e^2 s^3 s^4^2 t^3 u + \\
 & 448 e^2 s^3 s^4^2 t^2 u^2 - 212 e^2 s^3 s^4 t^5 - 540 e^2 s^3 s^4 t^4 u - 288 e^2 s^3 \\
 & ^3 s^4 t^3 u^2 + 256 e^2 s^3^2 s^4^6 t - 944 e^2 s^3^2 s^4^5 t^2 - 176 e^2 s^3^2 s^4^5 t u + \\
 & 1472 e^2 s^3^2 s^4^4 t^3 + 1064 e^2 s^3^2 s^4^4 t^2 u + 248 e^2 s^3^2 s^4^4 t u^2 + 208 e^2 \\
 & 2 s^3^2 s^4^4 u^3 - 848 e^2 s^3^2 s^4^3 t^4 - 1016 e^2 s^3^2 s^4^3 t^3 u - 904 e^2 s^3^2 s^4^3 \\
 & ^3 t^2 u^2 - 480 e^2 s^3^2 s^4^3 t u^3 - 188 e^2 s^3^2 s^4^2 t^5 - 784 e^2 s^3^2 s^4^2 t^4 \\
 & u - 452 e^2 s^3^2 s^4^2 t^3 u^2 - 96 e^2 s^3^2 s^4^2 t^2 u^3 + 16 e^2 s^3^2 s^4^2 t u^4 + \\
 & 224 e^2 s^3^2 s^4 t^6 + 728 e^2 s^3^2 s^4 t^5 u + 720 e^2 s^3^2 s^4 t^4 u^2 + 160 e^2 s^3^2 \\
 & s^4 t^3 u^3 - 56 e^2 s^3^2 s^4 t^2 u^4 + 24 e^2 s^3^2 t^7 + 104 e^2 s^3^2 t^6 u + 172 e^2 s^3^2 \\
 & t^5 u^2 + 128 e^2 s^3^2 t^4 u^3 + 36 e^2 s^3^2 t^3 u^4 - 188 e^2 s^3 s^4^5 t^3 - 172 e^2 \\
 & s^3 s^4^5 t^2 u - 104 e^2 s^3 s^4^5 t u^2 + 632 e^2 s^3 s^4^4 t^4 + 752 e^2 s^3 s^4^4 t^3 \\
 & u + 472 e^2 s^3 s^4^4 t^2 u^2 + 112 e^2 s^3 s^4^4 t u^3 - 930 e^2 s^3 s^4^3 t^5 - 1762 e^2 \\
 & s^3 s^4^3 t^4 u - 1552 e^2 s^3 s^4^3 t^3 u^2 - 688 e^2 s^3 s^4^3 t^2 u^3 - 114 e^2 s^3 s^4^3 \\
 & t u^4 - 26 e^2 s^3 s^4^3 u^5 + 682 e^2 s^3 s^4^2 t^6 + 1802 e^2 s^3 s^4^2 t^5 u + 2182 e^2 \\
 & s^3 s^4^2 t^4 u^2 + 1538 e^2 s^3 s^4^2 t^3 u^3 + 544 e^2 s^3 s^4^2 t^2 u^4 + 68 e^2 s^3 s^4^2 \\
 & t u^5 - 166 e^2 s^3 s^4 t^7 - 454 e^2 s^3 s^4 t^6 u - 604 e^2 s^3 s^4 t^5 u^2 - 508 e^2 s^3 \\
 & s^4 t^4 u^3 - 190 e^2 s^3 s^4 t^3 u^4 + 2 e^2 s^3 s^4 t^2 u^5 - 30 e^2 s^3 t^8 - 158 e^2 s^3 \\
 & t^7 u - 330 e^2 s^3 t^6 u^2 - 342 e^2 s^3 t^5 u^3 - 176 e^2 s^3 t^4 u^4 - 36 e^2 s^3 t^3 \\
 & u^5 + 24 e^2 s^4^4 t^5 + 80 e^2 s^4^4 t^4 u + 84 e^2 s^4^4 t^3 u^2 + 24 e^2 s^4^4 t^2 u^3 - \\
 & 4 e^2 s^4^4 t u^4 - 78 e^2 s^4^3 t^6 - 278 e^2 s^4^3 t^5 u - 338 e^2 s^4^3 t^4 u^2 - 150 \\
 & e^2 s^4^3 t^3 u^3 - 8 e^2 s^4^3 t^2 u^4 + 4 e^2 s^4^3 t u^5 + 114 e^2 s^4^2 t^7 + 476 e^2 \\
 & s^4^2 t^6 u + 761 e^2 s^4^2 t^5 u^2 + 576 e^2 s^4^2 t^4 u^3 + 200 e^2 s^4^2 t^3 u^4 + 20 e^2 \\
 & s^4^2 t^2 u^5 - 3 e^2 s^4^2 t u^6 - 90 e^2 s^4 t^8 - 434 e^2 s^4 t^7 u - 864 e^2 s^4 t^6 \\
 & u^2 - 918 e^2 s^4 t^5 u^3 - 560 e^2 s^4 t^4 u^4 - 192 e^2 s^4 t^3 u^5 - 30 e^2 s^4 t^2 u^6 + \\
 & 30 e^2 t^9 + 156 e^2 t^8 u + 353 e^2 t^7 u^2 + 452 e^2 t^6 u^3 + 348 e^2 t^5 u^4 + \\
 & 152 e^2 t^4 u^5 + 29 e^2 t^3 u^6 - 160 e^2 s^3^4 s^4^4 t + 576 e^2 s^3^4 s^4^3 t^2 - 352 e^2 s^3^4 \\
 & s^4^2 t^3 - 256 e^2 s^3^3 s^4^5 t + 224 e^2 s^3^3 s^4^5 u + 1168 e^2 s^3^3 s^4^4 t^2 - 400 e^2 s^3^3 \\
 & s^4^4 t u - 1396 e^2 s^3^3 s^4^3 t^3 - 244 e^2 s^3^3 s^4^3 t^2 u + 80 e^2 s^3^3 s^4^3 t u^2 + 312 e^2 \\
 & s^3^3 s^4^2 t^4 - 104 e^2 s^3^3 s^4^2 t^3 u - 288 e^2 s^3^3 s^4^2 t^2 u^2 + 140 e^2 s^3^3 s^4 t^5 + \\
 & 332 e^2 s^3^3 s^4 t^4 u + 176 e^2 s^3^3 s^4 t^3 u^2 - 160 e^2 s^3^2 s^4^6 t + 688 e^2 s^3^2 s^4^5 t^2 + \\
 & 144 e^2 s^3^2 s^4^5 t u - 1024 e^2 s^3^2 s^4^4 t^3 - 680 e^2 s^3^2 s^4^4 t^2 u - 168 e^2 s^3^2 s^4^4 \\
 & t u^2 - 112 e^2 s^3^2 s^4^4 u^3 + 328 e^2 s^3^2 s^4^3 t^4 + 192 e^2 s^3^2 s^4^3 t^3 u + 264 e^2 \\
 & s^3^2 s^4^3 t^2 u^2 + 208 e^2 s^3^2 s^4^3 t u^3 + 396 e^2 s^3^2 s^4^2 t^5 + 1060 e^2 s^3^2 s^4^2 t^4 \\
 & u + 706 e^2 s^3^2 s^4^2 t^3 u^2 + 144 e^2 s^3^2 s^4^2 t^2 u^3 - 10 e^2 s^3^2 s^4^2 t u^4 - 208 \\
 & e^2 s^3^2 s^4 t^6 - 568 e^2 s^3^2 s^4 t^5 u - 476 e^2 s^3^2 s^4 t^4 u^2 - 80 e^2 s^3^2 s^4 t^3 u^3 + \\
 & 36 e^2 s^3^2 s^4 t^2 u^4 - 16 e^2 s^3^2 t^7 - 68 e^2 s^3^2 t^6 u - 110 e^2 s^3^2 t^5 u^2 - 80 e^2 s^3^2 \\
 & t^4 u^3 - 22 e^2 s^3^2 t^3 u^4 + 116 e^2 s^3 s^4^5 t^3 + 124 e^2 s^3 s^4^5 t^2 u + 56 e^2 s^3 s^4^5 \\
 & t u^2 - 448 e^2 s^3 s^4^4 t^4 - 648 e^2 s^3 s^4^4 t^3 u - 360 e^2 s^3 s^4^4 t^2 u^2 - 64 e^2 s^3 s^4^4 \\
 & t u^3 + 660 e^2 s^3 s^4^3 t^5 + 1350 e^2 s^3 s^4^3 t^4 u + 1120 e^2 s^3 s^4^3 t^3 u^2 + 448 e^2 s^3 \\
 & s^4^3 t^2 u^3 + 80 e^2 s^3 s^4^3 t u^4 + 14 e^2 s^3 s^4^3 u^5 - 404 e^2 s^3 s^4^2 t^6 - 1046 e^2 s^3 \\
 & s^4^2 t^5 u - 1176 e^2 s^3 s^4^2 t^4 u^2 - 764 e^2 s^3 s^4^2 t^3 u^3 - 260 e^2 s^3 s^4^2 t^2 u^4 - \\
 & 30 e^2 s^3 s^4^2 t u^5 + 48 e^2 s^3 s^4 t^7 + 78 e^2 s^3 s^4 t^6 u + 40 e^2 s^3 s^4 t^5 u^2 + 24 e^2 s^3 \\
 & s^4 t^4 u^3 - 14 e^2 s^3 s^4 t^2 u^5 + 28 e^2 s^3 t^8 + 134 e^2 s^3 t^7 u + 256 e^2 s^3 t^6 u^2 + 244 e^2 \\
 & s^3 t^5 u^3 + 116 e^2 s^3 t^4 u^4 + 22 e^2 s^3 t^3 u^5 - 16 e^2 s^4^4 t^5 - 52 e^2 s^4^4 t^4 u - 54 \\
 & e^2 s^4^4 t^3 u^2 - 16 e^2 s^4^4 t^2 u^3 + 2 e^2 s^4^4 t u^4 + 60 e^2 s^4^3 t^6 + 214 e^2 s^4^3 t^5 *
 \end{aligned}$$

$$\begin{aligned}
& u+268e^{s^4}t^4u^2+132e^{s^4}t^3u^3+16e^{s^4}t^2u^4-2e^{s^4}t^1u^5-88e^{s^4}t^0u^6 \\
& s^4-2t^7-362e^{s^4}t^6u-575e^{s^4}t^5u^2-440e^{s^4}t^4u^3-164e^{s^4}t^3u^4-26e^{s^4}t^2u^5 \\
& -e^{s^4}t^1u^6+60e^{s^4}t^0u^7+282e^{s^4}t^7u+546e^{s^4}t^6u^2+564e^{s^4}t^5u^3+336e^{s^4}t^4u^4 \\
& +114e^{s^4}t^3u^5+18e^{s^4}t^2u^6-16e^{s^4}t^1u^7-82e^{s^4}t^0u^8-181e^{s^4}t^7u^2-224e^{s^4}t^6u^3 \\
& -166e^{s^4}t^5u^4-70e^{s^4}t^4u^5-13e^{s^4}t^3u^6+64s^3t^4s^4-128s^3t^4s^4t^3 \\
& +64s^3t^4s^4t^2+64s^3t^4s^4t^3+128s^3t^3s^4t^5-64s^3t^3s^4t^5u-384s^3t^3s^4t^4 \\
& t^2+64s^3t^3s^4t^4t^2+352s^3t^3s^4t^3t^3-32s^3t^3s^4t^3t^2-64s^3t^3s^4t^2t^4 \\
& +64s^3t^3s^4t^2t^3+64s^3t^3s^4t^2t^2u^2-32s^3t^3s^4t^5-64s^3t^3s^4t^4u-32s^3t^3s^4t^3u^2 \\
& +64s^3t^2s^4t^6-256s^3t^2s^4t^5t^2-64s^3t^2s^4t^5t^2u+320s^3t^2s^4t^4t^3+96s^3t^2s^4t^4t^2u \\
& +32s^3t^2s^4t^4t^2+32s^3t^2s^4t^4u^3-64s^3t^2s^4t^3t^4+160s^3t^2s^4t^3t^3u+64s^3t^2s^4t^3t^2u^2 \\
& -32s^3t^2s^4t^3t^2u^3-124s^3t^2s^4t^2t^5-336s^3t^2s^4t^2t^4u-200s^3t^2s^4t^2t^3u^2-16s^3t^2s^4t^2t^2u^3 \\
& +4s^3t^2s^4t^2t^4+56s^3t^2s^4t^6+128s^3t^2s^4t^5u+80s^3t^2s^4t^4u^2-8s^3t^2s^4t^2u^4 \\
& +4s^3t^2t^7+16s^3t^2t^6u+24s^3t^2t^5u^2+16s^3t^2t^4u^3+4s^3t^2t^3u^4-32s^3t^3s^4t^5t^3 \\
& -64s^3t^3s^4t^5t^2u-32s^3t^3s^4t^5t^2u^2+128s^3t^3s^4t^4t^4+288s^3t^3s^4t^4t^3u \\
& +192s^3t^3s^4t^4t^2u^2+32s^3t^3s^4t^4t^2u^3-184s^3t^3s^4t^3t^5-452s^3t^3s^4t^3t^4u \\
& -368s^3t^3s^4t^3t^3u^2-120s^3t^3s^4t^3t^2u^3-24s^3t^3s^4t^3t^2u^4-4s^3t^3s^4t^3t^1u^5+104s^3t^3s^4t^2t^6 \\
& +260s^3t^3s^4t^2t^5u+224s^3t^3s^4t^2t^4u^2+88s^3t^3s^4t^2t^3u^3+24s^3t^3s^4t^2t^2u^4 \\
& +4s^3t^3s^4t^2t^1u^5-8s^3t^3s^4t^7+4s^3t^3s^4t^6u+48s^3t^3s^4t^5u^2+56s^3t^3s^4t^4u^3 \\
& +24s^3t^3s^4t^3u^4+4s^3t^3s^4t^2u^5-8s^3t^3s^4t^8-36s^3t^3s^4t^7u-64s^3t^3s^4t^6u^2-56s^3t^3s^4t^5u^3 \\
& -24s^3t^3s^4t^4u^4-4s^3t^3s^4t^3u^5+4s^4t^4t^5+16s^4t^4t^4u+24s^4t^4t^3u^2+16s^4t^4t^2u^3 \\
& +4s^4t^4t^1u^4-16s^4t^3t^6-68s^4t^3t^5u-112s^4t^3t^4u^2-88s^4t^3t^3u^3-32s^4t^3t^2u^4 \\
& -4s^4t^3t^1u^5+24s^4t^2t^7+108s^4t^2t^6u+194s^4t^2t^5u^2+176s^4t^2t^4u^3+84s^4t^2t^3u^4 \\
& +20s^4t^2t^2u^5+2s^4t^2t^1u^6-16s^4t^2t^8-76s^4t^1t^7u-148s^4t^1t^6u^2-152s^4t^1t^5u^3 \\
& -88s^4t^1t^4u^4-28s^4t^1t^3u^5-4s^4t^1t^2u^6+4t^9+20t^8u+42t^7u^2+48t^6u^3+32t^5u^4 \\
& +12t^4u^5+2t^3u^6)/t^2/e/(-3+2e)/(3e-2)/(-4s^3s^4+t^2+2t^2u+u^2)^2/u/(t-s)^2; \\
\text{cpbox010010011p1p2p4} & := 2*(e-1)*(-192e^5s^3t^5s^4t^3-192e^5s^3t^5s^4t^3u+192e^5s^3t^4s^4t^3 \\
& t^2+192e^5s^3t^4s^4t^3t^2+192e^5s^3t^4s^4t^3t^2u-48e^5s^3t^4s^4t^2t^3+336e^5s^3t^4s^4t^2t^2u \\
& +480e^5s^3t^4s^4t^2t^2u^2+96e^5s^3t^4s^4t^2u^3+192e^5s^3t^3s^4t^2t^4-192e^5s^3t^3s^4t^2t^3u \\
& -480e^5s^3t^3s^4t^2t^2u^2-96e^5s^3t^3s^4t^2t^2u^3+60e^5s^3t^3s^4t^2t^1u^4+60e^5s^3t^3s^4t^2t^0u^5 \\
& -192e^5s^3t^3s^4t^1u^6-336e^5s^3t^3s^4t^0u^7-156e^5s^3t^3s^4t^4u-12e^5s^3t^3s^4t^3u^2-336e^5s^3t^3s^4t^2u^3 \\
& -156e^5s^3t^3s^4t^1u^4-12e^5s^3t^3s^4t^0u^5-144e^5s^3t^2s^4t^2t^5-144e^5s^3t^2s^4t^2t^4u-132e^5s^3t^2s^4t^1t^6 \\
& -276e^5s^3t^2s^4t^1t^5u-24e^5s^3t^2s^4t^1t^4u^2+264e^5s^3t^2s^4t^1t^3u^3+156e^5s^3t^2s^4t^1t^2u^4 \\
& +12e^5s^3t^2s^4t^1t^1u^5-9e^5s^3t^2s^4t^1t^0u^6-33e^5s^3t^2s^4t^0u^7-30e^5s^3t^2s^4t^6u-30e^5s^3t^2s^4t^5u^2 \\
& +30e^5s^3t^2s^4t^4u^3+75e^5s^3t^2s^4t^3u^4+51e^5s^3t^2s^4t^2u^5+12e^5s^3t^2s^4t^1u^6+72e^5s^3t^2s^4t^0u^7 \\
& +216e^5s^3t^3s^4t^5u^2+72e^5s^3t^3s^4t^4u^3+18e^5s^3t^3s^4t^3u^4+78e^5s^3t^3s^4t^2u^5+120e^5s^3t^3s^4t^1u^6 \\
& +60e^5s^3t^3s^4t^0u^7-30e^5s^3t^4s^4t^4-42e^5s^3t^3s^4t^5-12e^5s^3t^2s^4t^6-9e^5s^3t^1s^4t^9-45e^5s^3t^0s^4t^8 \\
& -90e^5s^3t^0s^4t^7u^2-90e^5s^3t^0s^4t^6u^3-45e^5s^3t^0s^4t^5u^4-9e^5s^3t^0s^4t^4u^5-192e^4s^3t^6s^4t^2 \\
& -32e^4s^3t^5s^4t^3+544e^4s^3t^5s^4t^3u+480e^4s^3t^5s^4t^2t^2+288e^4s^3t^5s^4t^2t^1u+72e^4s^3t^5s^4t^1t^3 \\
& +216e^4s^3t^5s^4t^1t^2+144e^4s^3t^5s^4t^0t^4-192e^4s^3t^4s^4t^4t^2-224e^4s^3t^4s^4t^3t^2-736e^4s^3t^4s^4t^3t^1u \\
& -656e^4s^3t^4s^4t^2t^3-672e^4s^3t^4s^4t^2t^2u-880e^4s^3t^4s^4t^2t^1u^2-272e^4s^3t^4s^4t^1t^3-192e^4s^3t^4s^4t^0t^4 \\
& -696e^4s^3t^4s^4t^0t^3u-672e^4
\end{aligned}$$

$$\begin{aligned}
& *s^3^4*s^4*t^2*u^2-168*e^4*s^3^4*s^4*t*u^3-6*e^4*s^3^4*t^5-42*e^4*s^3^4*t^4*u-90*e^4 \\
& *s^3^4*t^3*u^2-78*e^4*s^3^4*t^2*u^3-24*e^4*s^3^4*t*u^4+128*e^4*s^3^3*s^4^4*t^2+280* \\
& e^4*s^3^3*s^4^3*t^3+632*e^4*s^3^3*s^4^3*t^2*u+96*e^4*s^3^3*s^4^3*t*u^2+784*e^4*s^3^3* \\
& s^4^2*t^4+952*e^4*s^3^3*s^4^2*t^3*u+1184*e^4*s^3^3*s^4^2*t^2*u^2+344*e^4*s^3^3*s^4^2* \\
& t*u^3+310*e^4*s^3^3*s^4*t^5+998*e^4*s^3^3*s^4*t^4*u+1248*e^4*s^3^3*s^4*t^3*u^2+848*e \\
& ^4*s^3^3*s^4*t^2*u^3+322*e^4*s^3^3*s^4*t*u^4+34*e^4*s^3^3*s^4*u^5+18*e^4*s^3^3*t^6+ \\
& 132*e^4*s^3^3*t^5*u+312*e^4*s^3^3*t^4*u^2+324*e^4*s^3^3*t^3*u^3+150*e^4*s^3^3*t^2* \\
& u^4+24*e^4*s^3^3*t*u^5-16*e^4*s^3^2*s^4^3*t^4-272*e^4*s^3^2*s^4^3*t^3*u-64*e^4*s^3^2 \\
& *s^4^3*t^2*u^2-386*e^4*s^3^2*s^4^2*t^5-626*e^4*s^3^2*s^4^2*t^4*u-586*e^4*s^3^2*s^4^2* \\
& t^3*u^2-214*e^4*s^3^2*s^4^2*t^2*u^3-12*e^4*s^3^2*s^4^2*t*u^4-350*e^4*s^3^2*s^4*t^6 \\
& -1008*e^4*s^3^2*s^4*t^5*u-1276*e^4*s^3^2*s^4*t^4*u^2-968*e^4*s^3^2*s^4*t^3*u^3-390*e^4 \\
& *s^3^2*s^4*t^2*u^4-40*e^4*s^3^2*s^4*t*u^5-36*e^4*s^3^2*t^7-204*e^4*s^3^2*t^6*u-463* \\
& e^4*s^3^2*t^5*u^2-550*e^4*s^3^2*t^4*u^3-372*e^4*s^3^2*t^3*u^4-142*e^4*s^3^2*t^2*u^ \\
& 5-25*e^4*s^3^2*t*u^6+24*e^4*s^3*s^4^3*t^5+24*e^4*s^3*s^4^3*t^4*u-28*e^4*s^3*s^4^2*t^6 \\
& -4*e^4*s^3*s^4^2*t^5*u+84*e^4*s^3*s^4^2*t^4*u^2+68*e^4*s^3*s^4^2*t^3*u^3+8*e^4*s^3*s^4 \\
& ^2*t^2*u^4+154*e^4*s^3*s^4*t^7+474*e^4*s^3*s^4*t^6*u+584*e^4*s^3*s^4*t^5*u^2+376*e^4 \\
& *s^3*s^4*t^4*u^3+126*e^4*s^3*s^4*t^3*u^4+14*e^4*s^3*s^4*t^2*u^5+42*e^4*s^3*t^8+204*e^ \\
& 4*s^3*t^7*u+426*e^4*s^3*t^6*u^2+504*e^4*s^3*t^5*u^3+366*e^4*s^3*t^4*u^4+156*e^4*s^3 \\
& *t^3*u^5+30*e^4*s^3*t^2*u^6-6*e^4*s^4^2*t^7-18*e^4*s^4^2*t^6*u-18*e^4*s^4^2*t^5*u^ \\
& 2-6*e^4*s^4^2*t^4*u^3+6*e^4*s^4*t^8+24*e^4*s^4*t^7*u+36*e^4*s^4*t^6*u^2+24*e^4*s^4* \\
& t^5*u^3+6*e^4*s^4*t^4*u^4-18*e^4*t^9-90*e^4*t^8*u-189*e^4*t^7*u^2-216*e^4*t^6*u \\
& ^3-144*e^4*t^5*u^4-54*e^4*t^4*u^5-9*e^4*t^3*u^6+352*e^3*s^3^6*s^4^2*t+448*e^3*s^3 \\
& ^5*s^4^3*t-608*e^3*s^3^5*s^4^3*u-992*e^3*s^3^5*s^4^2*t^2-320*e^3*s^3^5*s^4^2*t*u-176* \\
& e^3*s^3^5*s^4*t^3-328*e^3*s^3^5*s^4*t^2*u-224*e^3*s^3^5*s^4*t*u^2+352*e^3*s^3^4*s^4^4* \\
& t-672*e^3*s^3^4*s^4^3*t^2+1152*e^3*s^3^4*s^4^3*t*u+1376*e^3*s^3^4*s^4^2*t^3+688*e^3*s \\
& ^3^4*s^4^2*t^2*u+480*e^3*s^3^4*s^4^2*t*u^2+304*e^3*s^3^4*s^4^2*u^3+496*e^3*s^3^4*s^4* \\
& t^4+1056*e^3*s^3^4*s^4*t^3*u+936*e^3*s^3^4*s^4*t^2*u^2+232*e^3*s^3^4*s^4*t*u^3+18*e^ \\
& 3*s^3^4*t^5+86*e^3*s^3^4*t^4*u+144*e^3*s^3^4*t^3*u^2+102*e^3*s^3^4*t^2*u^3+26*e^3*s \\
& ^3^4*t*u^4-576*e^3*s^3^3*s^4^4*t^2+352*e^3*s^3^3*s^4^3*t^3-776*e^3*s^3^3*s^4^3*t^2*u \\
& -176*e^3*s^3^3*s^4^3*t*u^2-1328*e^3*s^3^3*s^4^2*t^4-1152*e^3*s^3^3*s^4^2*t^3*u-1176* \\
& e^3*s^3^3*s^4^2*t^2*u^2-552*e^3*s^3^3*s^4^2*t*u^3-760*e^3*s^3^3*s^4*t^5-1770*e^3*s^3^ \\
& 3*s^4*t^4*u-1736*e^3*s^3^3*s^4*t^3*u^2-832*e^3*s^3^3*s^4*t^2*u^3-216*e^3*s^3^3*s^4*t* \\
& u^4-38*e^3*s^3^3*s^4*u^5-50*e^3*s^3^3*t^6-256*e^3*s^3^3*t^5*u-482*e^3*s^3^3*t^4*u^2 \\
& -422*e^3*s^3^3*t^3*u^3-172*e^3*s^3^3*t^2*u^4-26*e^3*s^3^3*t*u^5+288*e^3*s^3^2*s^4^4 \\
& *t^3-32*e^3*s^3^2*s^4^3*t^4+336*e^3*s^3^2*s^4^3*t^3*u+288*e^3*s^3^2*s^4^3*t^2*u^2+ \\
& 502*e^3*s^3^2*s^4^2*t^5+550*e^3*s^3^2*s^4^2*t^4*u+592*e^3*s^3^2*s^4^2*t^3*u^2+246*e^ \\
& 3*s^3^2*s^4^2*t^2*u^3+22*e^3*s^3^2*s^4^2*t*u^4+754*e^3*s^3^2*s^4*t^6+2004*e^3*s^3^2* \\
& s^4*t^5*u+2246*e^3*s^3^2*s^4*t^4*u^2+1446*e^3*s^3^2*s^4*t^3*u^3+520*e^3*s^3^2*s^4*t^2 \\
& *u^4+70*e^3*s^3^2*s^4*t*u^5+85*e^3*s^3^2*t^7+421*e^3*s^3^2*t^6*u+821*e^3*s^3^2*t^5* \\
& u^2+804*e^3*s^3^2*t^4*u^3+415*e^3*s^3^2*t^3*u^4+107*e^3*s^3^2*t^2*u^5+11*e^3*s^3^2 \\
& *t*u^6-128*e^3*s^3*s^4^3*t^5-296*e^3*s^3*s^4^3*t^4*u-144*e^3*s^3*s^4^3*t^3*u^2+76*e^ \\
& 3*s^3*s^4^2*t^6+244*e^3*s^3*s^4^2*t^5*u+216*e^3*s^3*s^4^2*t^4*u^2+12*e^3*s^3*s^4^2*t^3 \\
& *u^3-36*e^3*s^3*s^4^2*t^2*u^4-300*e^3*s^3*s^4*t^7-894*e^3*s^3*s^4*t^6*u-1124*e^3*s^3* \\
& s^4*t^5*u^2-788*e^3*s^3*s^4*t^4*u^3-280*e^3*s^3*s^4*t^3*u^4-22*e^3*s^3*s^4*t^2*u^5-92 \\
& *e^3*s^3*t^8-450*e^3*s^3*t^7*u-912*e^3*s^3*t^6*u^2-990*e^3*s^3*t^5*u^3-618*e^3*s^3*
\end{aligned}$$

$t^4u^4 - 216e^3s^3t^3u^5 - 34e^3s^3t^2u^6 + 18e^3s^4^2t^7 + 70e^3s^4^2t^6u$
 $+ 104e^3s^4^2t^5u^2 + 70e^3s^4^2t^4u^3 + 18e^3s^4^2t^3u^4 - 14e^3s^4t^8 - 76$
 $e^3s^4t^7u - 162e^3s^4t^6u^2 - 170e^3s^4t^5u^3 - 88e^3s^4t^4u^4 - 18e^3s$
 $s^4t^3u^5 + 39e^3t^9 + 199e^3t^8u + 433e^3t^7u^2 + 522e^3t^6u^3 + 373e^3t^$
 $5u^4 + 151e^3t^4u^5 + 27e^3t^3u^6 - 256e^2s^3^6s^4^2t - 352e^2s^3^5s^4^3t +$
 $416e^2s^3^5s^4^3u + 944e^2s^3^5s^4^2t^2 + 176e^2s^3^5s^4^2tu + 188e^2s^3^5s$
 $s^4t^3 + 172e^2s^3^5s^4t^2u + 104e^2s^3^5s^4t^2u^2 - 256e^2s^3^4s^4^4t + 1424e^$
 $2s^3^4s^4^3t^2 - 944e^2s^3^4s^4^3tu - 1472e^2s^3^4s^4^2t^3 - 1064e^2s^3^4s^4^$
 $2t^2u - 248e^2s^3^4s^4^2t^2u^2 - 208e^2s^3^4s^4^2u^3 - 632e^2s^3^4s^4t^4 - 752e$
 $e^2s^3^4s^4t^3u - 472e^2s^3^4s^4t^2u^2 - 112e^2s^3^4s^4t^2u^3 - 24e^2s^3^4t^$
 $5 - 80e^2s^3^4t^4u - 84e^2s^3^4t^3u^2 - 24e^2s^3^4t^2u^3 + 4e^2s^3^4tu^4 +$
 $896e^2s^3^3s^4^4t^2 - 1676e^2s^3^3s^4^3t^3 - 100e^2s^3^3s^4^3t^2u + 128e^2s$
 $s^3^3s^4^3tu^2 + 848e^2s^3^3s^4^2t^4 + 1016e^2s^3^3s^4^2t^3u + 904e^2s^3^3s^4$
 $^2t^2u^2 + 480e^2s^3^3s^4^2tu^3 + 930e^2s^3^3s^4t^5 + 1762e^2s^3^3s^4t^4u +$
 $1552e^2s^3^3s^4t^3u^2 + 688e^2s^3^3s^4t^2u^3 + 114e^2s^3^3s^4tu^4 + 26e^2s$
 $s^3^3s^4u^5 + 78e^2s^3^3t^6 + 278e^2s^3^3t^5u + 338e^2s^3^3t^4u^2 + 150e^2s3$
 $^3t^3u^3 + 8e^2s^3^3t^2u^4 - 4e^2s^3^3tu^5 - 576e^2s^3^2s^4^4t^3 + 360e^2s$
 $s^3^2s^4^3t^4 - 104e^2s^3^2s^4^3t^3u - 448e^2s^3^2s^4^3t^2u^2 + 188e^2s^3^2s$
 $s^4^2t^5 + 784e^2s^3^2s^4^2t^4u + 452e^2s^3^2s^4^2t^3u^2 + 96e^2s^3^2s^4^2t^$
 $2u^3 - 16e^2s^3^2s^4^2tu^4 - 682e^2s^3^2s^4t^6 - 1802e^2s^3^2s^4t^5u - 2182e$
 $^2s^3^2s^4t^4u^2 - 1538e^2s^3^2s^4t^3u^3 - 544e^2s^3^2s^4t^2u^4 - 68e^2s^3^$
 $2s^4tu^5 - 114e^2s^3^2t^7 - 476e^2s^3^2t^6u - 761e^2s^3^2t^5u^2 - 576e^2s3$
 $^2t^4u^3 - 200e^2s^3^2t^3u^4 - 20e^2s^3^2t^2u^5 + 3e^2s^3^2tu^6 + 212e^2s$
 $s^3s^4^3t^5 + 540e^2s^3s^4^3t^4u + 288e^2s^3s^4^3t^3u^2 - 224e^2s^3s^4^2t^6$
 $- 728e^2s^3s^4^2t^5u - 720e^2s^3s^4^2t^4u^2 - 160e^2s^3s^4^2t^3u^3 + 56e^2s$
 $s^3s^4^2t^2u^4 + 166e^2s^3s^4t^7 + 454e^2s^3s^4t^6u + 604e^2s^3s^4t^5u^2 +$
 $508e^2s^3s^4t^4u^3 + 190e^2s^3s^4t^3u^4 - 2e^2s^3s^4t^2u^5 + 90e^2s^3t^8 +$
 $434e^2s^3t^7u + 864e^2s^3t^6u^2 + 918e^2s^3t^5u^3 + 560e^2s^3t^4u^4 + 192e$
 $e^2s^3t^3u^5 + 30e^2s^3t^2u^6 - 24e^2s^4^2t^7 - 104e^2s^4^2t^6u - 172e^2s^4$
 $^2t^5u^2 - 128e^2s^4^2t^4u^3 - 36e^2s^4^2t^3u^4 + 30e^2s^4t^8 + 158e^2s^4t$
 $^7u + 330e^2s^4t^6u^2 + 342e^2s^4t^5u^3 + 176e^2s^4t^4u^4 + 36e^2s^4t^3u^$
 $5 - 30e^2t^9 - 156e^2t^8u - 353e^2t^7u^2 - 452e^2t^6u^3 - 348e^2t^5u^4 - 152$
 $e^2t^4u^5 - 29e^2t^3u^6 + 160e^2s^3^6s^4^2t + 256e^2s^3^5s^4^3t - 224e^2s^3^5s^4^$
 $3u - 688e^2s^3^5s^4^2t^2 - 144e^2s^3^5s^4^2tu - 116e^2s^3^5s^4t^3 - 124e^2s^3^5s^4t^$
 $2u - 56e^2s^3^5s^4tu^2 + 160e^2s^3^4s^4^4t - 1168e^2s^3^4s^4^3t^2 + 400e^2s^3^4s^4^3s$
 $t^2u + 1024e^2s^3^4s^4^2t^3 + 680e^2s^3^4s^4^2t^2u + 168e^2s^3^4s^4^2tu^2 + 112e^2s^3^$
 $4s^4^2u^3 + 448e^2s^3^4s^4t^4 + 648e^2s^3^4s^4t^3u + 360e^2s^3^4s^4t^2u^2 + 64e^2s^3$
 $^4s^4tu^3 + 16e^2s^3^4t^5 + 52e^2s^3^4t^4u + 54e^2s^3^4t^3u^2 + 16e^2s^3^4t^2u^3$
 $- 2e^2s^3^4tu^4 - 576e^2s^3^3s^4^4t^2 + 1396e^2s^3^3s^4^3t^3 + 244e^2s^3^3s^4^3t^2u$
 $- 80e^2s^3^3s^4^3tu^2 - 328e^2s^3^3s^4^2t^4 - 192e^2s^3^3s^4^2t^3u - 264e^2s^3^3s^4^2$
 $t^2u^2 - 208e^2s^3^3s^4^2tu^3 - 660e^2s^3^3s^4t^5 - 1350e^2s^3^3s^4t^4u - 1120e^2s$
 $s^3^3s^4t^3u^2 - 448e^2s^3^3s^4t^2u^3 - 80e^2s^3^3s^4tu^4 - 14e^2s^3^3s^4u^5 - 60e$
 $s^3^3t^6 - 214e^2s^3^3t^5u - 268e^2s^3^3t^4u^2 - 132e^2s^3^3t^3u^3 - 16e^2s^3^3t^2$
 $u^4 + 2e^2s^3^3tu^5 + 352e^2s^3^2s^4^4t^3 - 312e^2s^3^2s^4^3t^4 + 104e^2s^3^2s^4^3t^$
 $3u + 288e^2s^3^2s^4^3t^2u^2 - 396e^2s^3^2s^4^2t^5 - 1060e^2s^3^2s^4^2t^4u - 706e^2$

$$\begin{aligned}
& s^3 \cdot 2s^4 \cdot t^2 \cdot u^2 - 144 \cdot e \cdot s^3 \cdot 2s^4 \cdot t^2 \cdot u^3 + 10 \cdot e \cdot s^3 \cdot 2s^4 \cdot t^2 \cdot u^4 + 404 \cdot e \cdot s^3 \cdot 2s^4 \cdot t^2 \cdot u^5 + 1046 \cdot e \cdot s^3 \cdot 2s^4 \cdot t^2 \cdot u^6 + 1176 \cdot e \cdot s^3 \cdot 2s^4 \cdot t^2 \cdot u^7 + 764 \cdot e \cdot s^3 \cdot 2s^4 \cdot t^2 \cdot u^8 + 260 \cdot e \cdot s^3 \cdot 2s^4 \cdot t^2 \cdot u^9 + 30 \cdot e \cdot s^3 \cdot 2s^4 \cdot t^2 \cdot u^{10} + 88 \cdot e \cdot s^3 \cdot 2s^4 \cdot t^2 \cdot u^{11} + 362 \cdot e \cdot s^3 \cdot 2s^4 \cdot t^2 \cdot u^{12} + 575 \cdot e \cdot s^3 \cdot 2s^4 \cdot t^2 \cdot u^{13} + 440 \cdot e \cdot s^3 \cdot 2s^4 \cdot t^2 \cdot u^{14} + 164 \cdot e \cdot s^3 \cdot 2s^4 \cdot t^2 \cdot u^{15} + 26 \cdot e \cdot s^3 \cdot 2s^4 \cdot t^2 \cdot u^{16} + e \cdot s^3 \cdot 2s^4 \cdot t^2 \cdot u^{17} - 140 \cdot e \cdot s^3 \cdot s^4 \cdot t^3 \cdot u^5 - 332 \cdot e \cdot s^3 \cdot s^4 \cdot t^3 \cdot u^6 - 176 \cdot e \cdot s^3 \cdot s^4 \cdot t^3 \cdot u^7 + 208 \cdot e \cdot s^3 \cdot s^4 \cdot t^2 \cdot u^6 + 568 \cdot e \cdot s^3 \cdot s^4 \cdot t^2 \cdot u^7 + 476 \cdot e \cdot s^3 \cdot s^4 \cdot t^2 \cdot u^8 + 80 \cdot e \cdot s^3 \cdot s^4 \cdot t^2 \cdot u^9 - 36 \cdot e \cdot s^3 \cdot s^4 \cdot t^2 \cdot u^{10} - 48 \cdot e \cdot s^3 \cdot s^4 \cdot t^7 - 78 \cdot e \cdot s^3 \cdot s^4 \cdot t^6 \cdot u - 40 \cdot e \cdot s^3 \cdot s^4 \cdot t^5 \cdot u^2 - 24 \cdot e \cdot s^3 \cdot s^4 \cdot t^4 \cdot u^3 + 14 \cdot e \cdot s^3 \cdot s^4 \cdot t^2 \cdot u^5 - 60 \cdot e \cdot s^3 \cdot t^8 - 282 \cdot e \cdot s^3 \cdot t^7 \cdot u - 546 \cdot e \cdot s^3 \cdot t^6 \cdot u^2 - 564 \cdot e \cdot s^3 \cdot t^5 \cdot u^3 - 336 \cdot e \cdot s^3 \cdot t^4 \cdot u^4 - 114 \cdot e \cdot s^3 \cdot t^3 \cdot u^5 - 18 \cdot e \cdot s^3 \cdot t^2 \cdot u^6 + 16 \cdot e \cdot s^4 \cdot t^2 \cdot u^7 + 68 \cdot e \cdot s^4 \cdot t^2 \cdot u^6 + 110 \cdot e \cdot s^4 \cdot t^2 \cdot u^5 + 80 \cdot e \cdot s^4 \cdot t^2 \cdot u^4 + 22 \cdot e \cdot s^4 \cdot t^2 \cdot u^3 - 28 \cdot e \cdot s^4 \cdot t^8 - 134 \cdot e \cdot s^4 \cdot t^7 \cdot u - 256 \cdot e \cdot s^4 \cdot t^6 \cdot u^2 - 244 \cdot e \cdot s^4 \cdot t^5 \cdot u^3 - 116 \cdot e \cdot s^4 \cdot t^4 \cdot u^4 - 22 \cdot e \cdot s^4 \cdot t^3 \cdot u^5 + 16 \cdot e \cdot t^9 + 82 \cdot e \cdot t^8 \cdot u + 181 \cdot e \cdot t^7 \cdot u^2 + 224 \cdot e \cdot t^6 \cdot u^3 + 166 \cdot e \cdot t^5 \cdot u^4 + 70 \cdot e \cdot t^4 \cdot u^5 + 13 \cdot e \cdot t^3 \cdot u^6 - 64 \cdot s^3 \cdot 6s^4 \cdot 2t - 128 \cdot s^3 \cdot 5s^4 \cdot 3t + 64 \cdot s^3 \cdot 5s^4 \cdot 3t \cdot u + 256 \cdot s^3 \cdot 5s^4 \cdot 2t^2 + 64 \cdot s^3 \cdot 5s^4 \cdot 2t \cdot u + 32 \cdot s^3 \cdot 5s^4 \cdot t^3 + 64 \cdot s^3 \cdot 5s^4 \cdot t^2 \cdot u + 32 \cdot s^3 \cdot 5s^4 \cdot t \cdot u^2 - 64 \cdot s^3 \cdot 4s^4 \cdot 4t + 384 \cdot s^3 \cdot 4s^4 \cdot 3t^2 - 64 \cdot s^3 \cdot 4s^4 \cdot 3t \cdot u - 320 \cdot s^3 \cdot 4s^4 \cdot 2t^3 - 96 \cdot s^3 \cdot 4s^4 \cdot 2t^2 \cdot u - 32 \cdot s^3 \cdot 4s^4 \cdot 2t \cdot u^2 - 32 \cdot s^3 \cdot 4s^4 \cdot 2t \cdot u^3 - 128 \cdot s^3 \cdot 4s^4 \cdot t^4 - 288 \cdot s^3 \cdot 4s^4 \cdot t^3 \cdot u - 192 \cdot s^3 \cdot 4s^4 \cdot t^2 \cdot u^2 - 32 \cdot s^3 \cdot 4s^4 \cdot t \cdot u^3 - 4 \cdot s^3 \cdot 4t^5 - 16 \cdot s^3 \cdot 4t^4 \cdot u - 24 \cdot s^3 \cdot 4t^3 \cdot u^2 - 16 \cdot s^3 \cdot 4t^2 \cdot u^3 - 4 \cdot s^3 \cdot 4t \cdot u^4 + 128 \cdot s^3 \cdot 3s^4 \cdot 4t^2 - 352 \cdot s^3 \cdot 3s^4 \cdot 3t^3 + 32 \cdot s^3 \cdot 3s^4 \cdot 3t \cdot u^2 + 64 \cdot s^3 \cdot 3s^4 \cdot 2t^4 - 160 \cdot s^3 \cdot 3s^4 \cdot 2t^3 \cdot u - 64 \cdot s^3 \cdot 3s^4 \cdot 2t^2 \cdot u^2 + 32 \cdot s^3 \cdot 3s^4 \cdot 2t \cdot u^3 + 184 \cdot s^3 \cdot 3s^4 \cdot t^5 + 452 \cdot s^3 \cdot 3s^4 \cdot t^4 \cdot u + 368 \cdot s^3 \cdot 3s^4 \cdot t^3 \cdot u^2 + 120 \cdot s^3 \cdot 3s^4 \cdot t^2 \cdot u^3 + 24 \cdot s^3 \cdot 3s^4 \cdot t \cdot u^4 + 4 \cdot s^3 \cdot 3s^4 \cdot u^5 + 16 \cdot s^3 \cdot 3t^6 + 68 \cdot s^3 \cdot 3t^5 \cdot u + 112 \cdot s^3 \cdot 3t^4 \cdot u^2 + 88 \cdot s^3 \cdot 3t^3 \cdot u^3 + 32 \cdot s^3 \cdot 3t^2 \cdot u^4 + 4 \cdot s^3 \cdot 3t \cdot u^5 - 64 \cdot s^3 \cdot 2s^4 \cdot 4t^3 + 64 \cdot s^3 \cdot 2s^4 \cdot 3t^4 - 64 \cdot s^3 \cdot 2s^4 \cdot 3t^3 \cdot u - 64 \cdot s^3 \cdot 2s^4 \cdot 3t^2 \cdot u^2 + 124 \cdot s^3 \cdot 2s^4 \cdot 2t^5 + 336 \cdot s^3 \cdot 2s^4 \cdot 2t^4 \cdot u + 200 \cdot s^3 \cdot 2s^4 \cdot 2t^3 \cdot u^2 + 16 \cdot s^3 \cdot 2s^4 \cdot 2t^2 \cdot u^3 - 4 \cdot s^3 \cdot 2s^4 \cdot 2t \cdot u^4 - 104 \cdot s^3 \cdot 2s^4 \cdot t^6 - 260 \cdot s^3 \cdot 2s^4 \cdot t^5 \cdot u - 224 \cdot s^3 \cdot 2s^4 \cdot t^4 \cdot u^2 - 88 \cdot s^3 \cdot 2s^4 \cdot t^3 \cdot u^3 - 24 \cdot s^3 \cdot 2s^4 \cdot t^2 \cdot u^4 - 4 \cdot s^3 \cdot 2s^4 \cdot t \cdot u^5 - 24 \cdot s^3 \cdot 2t^7 - 108 \cdot s^3 \cdot 2t^6 \cdot u - 194 \cdot s^3 \cdot 2t^5 \cdot u^2 - 176 \cdot s^3 \cdot 2t^4 \cdot u^3 - 84 \cdot s^3 \cdot 2t^3 \cdot u^4 - 20 \cdot s^3 \cdot 2t^2 \cdot u^5 - 2 \cdot s^3 \cdot 2t \cdot u^6 + 32 \cdot s^3 \cdot s^4 \cdot 3t^5 + 64 \cdot s^3 \cdot s^4 \cdot 3t^4 \cdot u + 32 \cdot s^3 \cdot s^4 \cdot 3t^3 \cdot u^2 - 56 \cdot s^3 \cdot s^4 \cdot 2t^6 - 128 \cdot s^3 \cdot s^4 \cdot 2t^5 \cdot u - 80 \cdot s^3 \cdot s^4 \cdot 2t^4 \cdot u^2 + 8 \cdot s^3 \cdot s^4 \cdot 2t^2 \cdot u^4 + 8 \cdot s^3 \cdot s^4 \cdot t^7 - 4 \cdot s^3 \cdot s^4 \cdot t^6 \cdot u - 48 \cdot s^3 \cdot s^4 \cdot t^5 \cdot u^2 - 56 \cdot s^3 \cdot s^4 \cdot t^4 \cdot u^3 - 24 \cdot s^3 \cdot s^4 \cdot t^3 \cdot u^4 - 4 \cdot s^3 \cdot s^4 \cdot t^2 \cdot u^5 + 16 \cdot s^3 \cdot t^8 + 76 \cdot s^3 \cdot t^7 \cdot u + 148 \cdot s^3 \cdot t^6 \cdot u^2 + 152 \cdot s^3 \cdot t^5 \cdot u^3 + 88 \cdot s^3 \cdot t^4 \cdot u^4 + 28 \cdot s^3 \cdot t^3 \cdot u^5 + 4 \cdot s^3 \cdot t^2 \cdot u^6 - 4 \cdot s^4 \cdot 2t^7 - 16 \cdot s^4 \cdot 2t^6 \cdot u - 24 \cdot s^4 \cdot 2t^5 \cdot u^2 - 16 \cdot s^4 \cdot 2t^4 \cdot u^3 - 4 \cdot s^4 \cdot 2t^3 \cdot u^4 + 8 \cdot s^4 \cdot t^8 + 36 \cdot s^4 \cdot t^7 \cdot u + 64 \cdot s^4 \cdot t^6 \cdot u^2 + 56 \cdot s^4 \cdot t^5 \cdot u^3 + 24 \cdot s^4 \cdot t^4 \cdot u^4 + 4 \cdot s^4 \cdot t^3 \cdot u^5 - 4 \cdot t^9 - 20 \cdot t^8 \cdot u - 42 \cdot t^7 \cdot u^2 - 48 \cdot t^6 \cdot u^3 - 32 \cdot t^5 \cdot u^4 - 12 \cdot t^4 \cdot u^5 - 2 \cdot t^3 \cdot u^6) / (s^3 - t)^2 / u / (-4 \cdot s^3 \cdot s^4 + t^2 + 2 \cdot t \cdot u + u^2)^2 / (3 \cdot e - 2) / (-3 + 2 \cdot e) / e / t^2; \\
\text{cpbox010010101p1p2p4} & := 2 \cdot (e - 1) \cdot (144 \cdot e^5 \cdot s^3 \cdot 2s^4 \cdot t^2 \cdot u^2 + 144 \cdot e^5 \cdot s^3 \cdot 2s^4 \cdot t^2 \cdot u^3 - 72 \cdot e^5 \cdot s^3 \cdot s^4 \cdot t^4 - 216 \cdot e^5 \cdot s^3 \cdot s^4 \cdot t^3 \cdot u - 216 \cdot e^5 \cdot s^3 \cdot s^4 \cdot t^2 \cdot u^2 - 72 \cdot e^5 \cdot s^3 \cdot s^4 \cdot t \cdot u^3 + 9 \cdot e^5 \cdot t^6 + 45 \cdot e^5 \cdot t^5 \cdot u + 90 \cdot e^5 \cdot t^4 \cdot u^2 + 90 \cdot e^5 \cdot t^3 \cdot u^3 + 45 \cdot e^5 \cdot t^2 \cdot u^4 + 9 \cdot e^5 \cdot t \cdot u^5 + 24 \cdot e^4 \cdot s^3 \cdot 3s^4 \cdot t^2 - 24 \cdot e^4 \cdot s^3 \cdot 3s^4 \cdot t \cdot u - 48 \cdot e^4 \cdot s^3 \cdot 3s^4 \cdot u^2 + 336 \cdot e^4 \cdot s^3 \cdot 2s^4 \cdot t^2 - 48 \cdot e^4 \cdot s^3 \cdot 2s^4 \cdot t \cdot u - 240 \cdot e^4 \cdot s^3 \cdot 2s^4 \cdot u^2 - 24 \cdot e^4 \cdot s^3 \cdot 2s^4 \cdot t^3 + 72 \cdot e^4 \cdot s^3 \cdot 2s^4 \cdot t \cdot u^2 + 48 \cdot e^4 \cdot s^3 \cdot 2s^4 \cdot u^3 - 6 \cdot e^4 \cdot s^3 \cdot 2t^4 - 6 \cdot e^4 \cdot s^3 \cdot 2t^3 \cdot u + 18 \cdot e^4 \cdot s^3 \cdot 2t^2 \cdot u^2 + 30 \cdot e^4 \cdot s^3 \cdot 2t \cdot u^3 + 12 \cdot e^4 \cdot s^3 \cdot 2u^4 + 24 \cdot e^4 \cdot s^3 \cdot s^4 \cdot 3t^2 - 24 \cdot e^4 \cdot s^3 \cdot s^4 \cdot 3t \cdot u - 48 \cdot e^4 \cdot s^3 \cdot s^4 \cdot 3u^2 - 24 \cdot e^4 \cdot s^3 \cdot s^4 \cdot 2t^3 + 72 \cdot e^4 \cdot s^3 \cdot s^4 \cdot 2t \cdot u^2 + 48 \cdot e^4 \cdot s^3 \cdot s^4 \cdot 2u^3 - 156 \cdot e^4 \cdot s^3 \cdot s^4 \cdot t^4 - 300 \cdot e^4 \cdot s^3 \cdot s^4 \cdot t^3 \cdot u - 36 \cdot e^4 \cdot s^3 \cdot s^4 \cdot t^2 \cdot u^2 + 204 \cdot e^4 \cdot s^3 \cdot s^4 \cdot t \cdot u^3 + 96 \cdot e^4 \cdot s^3 \cdot s^4 \cdot u^4 + 6 \cdot e^4 \cdot s^3 \cdot t^5 + 12 \cdot e^4 \cdot s^3 \cdot t^4 \cdot u - 12 \cdot e^4 \cdot s^3 \cdot t^3 \cdot u^2 - 48 \cdot e^4 \cdot s^3 \cdot t^2 \cdot u^3 - 42 \cdot e^4 \cdot s^3 \cdot t \cdot u^4 - 12 \cdot e^4 \cdot s^3 \cdot u^5 - 6 \cdot e^4 \cdot s^4 \cdot 2t^4 - 6 \cdot e^4 \cdot s^4 \cdot 2t^3 \cdot u + 18 \cdot e^4 \cdot s^4 \cdot 2t^2 \cdot u^2
\end{aligned}$$

$$\begin{aligned}
& u^2+30e^4s^4^2tu^3+12e^4s^4^2u^4+6e^4s^4t^5+12e^4s^4t^4u-12e^4s^4t^3u^2-48e^4s^4t^2u^3-42e^4s^4tu^4-12e^4s^4u^5+18e^4t^6+72e^4t^5u+99e^4t^4u^2+36e^4t^3u^3-36e^4t^2u^4-36e^4tu^5-9e^4u^6-64e^3s^3^3s^4^2t-128e^3s^3^3s^4^2u-24e^3s^3^3s^4t^2u+48e^3s^3^3s^4u^2-64e^3s^3^2s^4^3t-128e^3s^3^2s^4^3u-624e^3s^3^2s^4^2t^2+32e^3s^3^2s^4^2tu+656e^3s^3^2s^4^2u^2+16e^3s^3^2s^4t^3+200e^3s^3^2s^4t^2u+136e^3s^3^2s^4tu^2-48e^3s^3^2s^4u^3+4e^3s^3^2t^4+2e^3s^3^2t^3u-12e^3s^3^2t^2u^2-14e^3s^3^2tu^3-4e^3s^3^2u^4-24e^3s^3s^4^3t^2u+48e^3s^3s^4^3u^2+16e^3s^3s^4^2t^3+200e^3s^3s^4^2t^2u+136e^3s^3s^4^2tu^2-48e^3s^3s^4^2u^3+336e^3s^3s^4t^4+556e^3s^3s^4t^3u-120e^3s^3s^4t^2u^2-564e^3s^3s^4tu^3-224e^3s^3s^4u^4-8e^3s^3t^5-34e^3s^3t^4u-50e^3s^3t^3u^2-26e^3s^3t^2u^3+2e^3s^3tu^4+4e^3s^3u^5+4e^3s^4^2t^4+2e^3s^4^2t^3u-12e^3s^4^2t^2u^2-14e^3s^4^2tu^3-4e^3s^4^2u^4-8e^3s^4t^5-34e^3s^4t^4u-50e^3s^4t^3u^2-26e^3s^4t^2u^3+2e^3s^4t^2u^3+2e^3s^4tu^4+4e^3s^4u^5-39e^3t^6-147e^3t^5u-171e^3t^4u^2+6e^3t^3u^3+159e^3t^2u^4+117e^3tu^5+27e^3u^6+32e^2s^3^3s^4^2t-60e^2s^3^3s^4t^2+84e^2s^3^3s^4tu+24e^2s^3^3s^4u^2+32e^2s^3^2s^4^3t+232e^2s^3^2s^4^2t^2+168e^2s^3^2s^4^2tu-416e^2s^3^2s^4^2u^2+104e^2s^3^2s^4t^3-120e^2s^3^2s^4t^2u-192e^2s^3^2s^4tu^2+32e^2s^3^2s^4u^3+8e^2s^3^2t^4+16e^2s^3^2t^3u-12e^2s^3^2t^2u^2-40e^2s^3^2tu^3-20e^2s^3^2u^4-60e^2s^3s^4^3t^2+84e^2s^3s^4^3tu+24e^2s^3s^4^3u^2+104e^2s^3s^4^2t^3-120e^2s^3s^4^2t^2u-192e^2s^3s^4^2tu^2+32e^2s^3s^4^2u^3-220e^2s^3s^4t^4-316e^2s^3s^4t^3u+164e^2s^3s^4t^2u^2+396e^2s^3s^4tu^3+136e^2s^3s^4u^4-14e^2s^3t^5-30e^2s^3t^4u+14e^2s^3t^3u^2+82e^2s^3t^2u^3+72e^2s^3tu^4+20e^2s^3u^5+8e^2s^4^2t^4+16e^2s^4^2t^3u-12e^2s^4^2t^2u^2-40e^2s^4^2tu^3-20e^2s^4^2u^4-14e^2s^4t^5-30e^2s^4t^4u+14e^2s^4t^3u^2+82e^2s^4t^2u^3+72e^2s^4tu^4+20e^2s^4u^5+30e^2t^6+110e^2t^5u+111e^2t^4u^2-56e^2t^3u^3-184e^2t^2u^4-126e^2tu^5-29e^2u^6+96e^2s^3^3s^4^2t+64e^2s^3^3s^4^2u+36e^2s^3^3s^4t^2-36e^2s^3^3s^4tu-24e^2s^3^3s^4u^2+96e^2s^3^2s^4^3t+64e^2s^3^2s^4^3u-88e^2s^3^2s^4^2t^2-232e^2s^3^2s^4^2tu+96e^2s^3^2s^4^2u^2-120e^2s^3^2s^4t^3-112e^2s^3^2s^4t^2u-8e^2s^3^2s^4tu^2-16e^2s^3^2s^4u^3-6e^2s^3^2t^4-12e^2s^3^2t^3u+6e^2s^3^2t^2u^2+24e^2s^3^2tu^3+12e^2s^3^2u^4+36e^2s^3s^4^3t^2-36e^2s^3s^4^3tu-24e^2s^3s^4^3u^2-120e^2s^3s^4^2t^3-112e^2s^3s^4^2t^2u-8e^2s^3s^4^2tu^2-16e^2s^3s^4^2u^3+104e^2s^3s^4t^4+236e^2s^3s^4t^3u+120e^2s^3s^4t^2u^2-52e^2s^3s^4tu^3-40e^2s^3s^4u^4+18e^2s^3t^5+60e^2s^3t^4u+60e^2s^3t^3u^2-30e^2s^3tu^4-12e^2s^3u^5-6e^2s^4^2t^4-12e^2s^4^2t^3u+6e^2s^4^2t^2u^2+24e^2s^4^2tu^3+12e^2s^4^2u^4+18e^2s^4t^5+60e^2s^4t^4u+60e^2s^4t^3u^2-30e^2s^4tu^4-12e^2s^4u^5-16e^2t^6-70e^2t^5u-107e^2t^4u^2-48e^2t^3u^3+38e^2t^2u^4+46e^2tu^5+13e^2u^6-64s^3^3s^4^2t-64s^3^2s^4^3t+64s^3^2s^4^2t^2+64s^3^2s^4^2tu-32s^3^2s^4^2u^2+32s^3^2s^4t^3+64s^3^2s^4t^2u+32s^3^2s^4tu^2+32s^3s^4^2t^3+64s^3s^4^2t^2u+32s^3s^4^2tu^2-32s^3s^4t^4-96s^3s^4t^3u-80s^3s^4t^2u^2+16s^3s^4u^4-4s^3t^5-16s^3t^4u-24s^3t^3u^2-16s^3t^2u^3-4s^3tu^4-4s^4t^5-16s^4t^4u-24s^4t^3u^2-16s^4t^2u^3-4s^4tu^4+4t^6+20t^5u+38t^4u^2+32t^3u^3+8t^2u^4-4tu^5-2u^6)/t/(-4s^3s^4t^2+2tu^2)^2/(3e-2)/(-3+2e)/e/u;
\end{aligned}$$

cpbox010010111p1p2p4 := 4*(e-1)*(-288e^5s^3^3s^4^3t-288e^5s^3^3s^4^3u+288*

$$\begin{aligned}
& e^5 s^3^2 s^4^2 t^3 + 720 e^5 s^3^2 s^4^2 t^2 u + 576 e^5 s^3^2 s^4^2 t^2 u^2 + 144 e^5 s^3^2 s^4^2 u^3 - 90 e^5 s^3 s^4 t^5 - 378 e^5 s^3 s^4 t^4 u - 612 e^5 s^3 s^4 t^3 u^2 - 468 e^5 s^3 s^4 t^2 u^3 - 162 e^5 s^3 s^4 t u^4 - 18 e^5 s^3 s^4 u^5 + 9 e^5 t^7 + 54 e^5 t^6 u + 135 e^5 t^5 u^2 + 180 e^5 t^4 u^3 + 135 e^5 t^3 u^4 + 54 e^5 t^2 u^5 + 9 e^5 t u^6 - 96 e^4 s^3^4 s^4^2 t + 192 e^4 s^3^4 s^4^2 u - 1056 e^4 s^3^3 s^4^3 t - 192 e^4 s^3^3 s^4^3 u + 96 e^4 s^3^3 s^4^2 t^2 - 96 e^4 s^3^3 s^4^2 t u - 192 e^4 s^3^3 s^4^2 u^2 - 48 e^4 s^3^3 s^4 t^2 u - 96 e^4 s^3^3 s^4 t u^2 - 48 e^4 s^3^3 s^4 u^3 - 96 e^4 s^3^2 s^4^4 t + 192 e^4 s^3^2 s^4^4 u + 96 e^4 s^3^2 s^4^3 t^2 - 96 e^4 s^3^2 s^4^3 t u - 192 e^4 s^3^2 s^4^3 u^2 + 720 e^4 s^3^2 s^4^2 t^3 + 1632 e^4 s^3^2 s^4^2 t^2 u + 1248 e^4 s^3^2 s^4^2 t^2 u^2 + 336 e^4 s^3^2 s^4^2 u^3 + 48 e^4 s^3^2 s^4 t^3 u + 144 e^4 s^3^2 s^4 t^2 u^2 + 144 e^4 s^3^2 s^4 t u^3 + 48 e^4 s^3^2 s^4 u^4 + 6 e^4 s^3^2 t^5 + 24 e^4 s^3^2 t^4 u + 36 e^4 s^3^2 t^3 u^2 + 24 e^4 s^3^2 t^2 u^3 + 6 e^4 s^3^2 t u^4 - 48 e^4 s^3 s^4^3 t^2 u - 96 e^4 s^3 s^4^3 t u^2 - 48 e^4 s^3 s^4^3 u^3 + 48 e^4 s^3 s^4^2 t^3 u + 144 e^4 s^3 s^4^2 t^2 u^2 + 144 e^4 s^3 s^4^2 t u^3 + 48 e^4 s^3 s^4^2 u^4 - 186 e^4 s^3 s^4 t^5 - 780 e^4 s^3 s^4 t^4 u - 1332 e^4 s^3 s^4 t^3 u^2 - 1176 e^4 s^3 s^4 t^2 u^3 - 546 e^4 s^3 s^4 t u^4 - 108 e^4 s^3 s^4 u^5 - 6 e^4 s^3 t^6 - 30 e^4 s^3 t^5 u - 60 e^4 s^3 t^4 u^2 - 60 e^4 s^3 t^3 u^3 - 30 e^4 s^3 t^2 u^4 - 6 e^4 s^3 t u^5 + 6 e^4 s^4^2 t^5 + 24 e^4 s^4^2 t^4 u + 36 e^4 s^4^2 t^3 u^2 + 24 e^4 s^4^2 t^2 u^3 + 6 e^4 s^4^2 t u^4 - 6 e^4 s^4 t^6 - 30 e^4 s^4 t^5 u - 60 e^4 s^4 t^4 u^2 - 60 e^4 s^4 t^3 u^3 - 30 e^4 s^4 t^2 u^4 - 6 e^4 s^4 t u^5 + 18 e^4 t^7 + 108 e^4 t^6 u + 279 e^4 t^5 u^2 + 405 e^4 t^4 u^3 + 360 e^4 t^3 u^4 + 198 e^4 t^2 u^5 + 63 e^4 t u^6 + 9 e^4 u^7 - 208 e^3 s^3^4 s^4^2 t - 400 e^3 s^3^4 s^4^2 u + 1536 e^3 s^3^3 s^4^3 t + 864 e^3 s^3^3 s^4^3 u + 240 e^3 s^3^3 s^4^2 t^2 + 480 e^3 s^3^3 s^4^2 t u + 528 e^3 s^3^3 s^4^2 u^2 + 92 e^3 s^3^3 s^4 t^3 + 444 e^3 s^3^3 s^4 t^2 u + 492 e^3 s^3^3 s^4 t u^2 + 140 e^3 s^3^3 s^4 u^3 - 208 e^3 s^3^2 s^4^4 t - 400 e^3 s^3^2 s^4^4 u + 240 e^3 s^3^2 s^4^3 t^2 + 480 e^3 s^3^2 s^4^3 t u + 528 e^3 s^3^2 s^4^3 u^2 - 1512 e^3 s^3^2 s^4^2 t^3 - 3176 e^3 s^3^2 s^4^2 t^2 u - 2776 e^3 s^3^2 s^4^2 t^2 u^2 - 1112 e^3 s^3^2 s^4^2 u^3 - 52 e^3 s^3^2 s^4 t^4 - 488 e^3 s^3^2 s^4 t^3 u - 960 e^3 s^3^2 s^4 t^2 u^2 - 664 e^3 s^3^2 s^4 t u^3 - 140 e^3 s^3^2 s^4 u^4 - 18 e^3 s^3^2 t^5 - 88 e^3 s^3^2 t^4 u - 174 e^3 s^3^2 t^3 u^2 - 174 e^3 s^3^2 t^2 u^3 - 88 e^3 s^3^2 t u^4 - 18 e^3 s^3^2 u^5 + 92 e^3 s^3 s^4^3 t^3 + 444 e^3 s^3 s^4^3 t^2 u + 492 e^3 s^3 s^4^3 t u^2 + 140 e^3 s^3 s^4^3 u^3 - 52 e^3 s^3 s^4^2 t^4 - 488 e^3 s^3 s^4^2 t^3 u - 960 e^3 s^3 s^4^2 t^2 u^2 - 664 e^3 s^3 s^4^2 t u^3 - 140 e^3 s^3 s^4^2 u^4 + 390 e^3 s^3 s^4 t^5 + 1704 e^3 s^3 s^4 t^4 u + 3056 e^3 s^3 s^4 t^3 u^2 + 2844 e^3 s^3 s^4 t^2 u^3 + 1386 e^3 s^3 s^4 t u^4 + 284 e^3 s^3 s^4 u^5 + 14 e^3 s^3 t^6 + 90 e^3 s^3 t^5 u + 238 e^3 s^3 t^4 u^2 + 332 e^3 s^3 t^3 u^3 + 258 e^3 s^3 t^2 u^4 + 106 e^3 s^3 t u^5 + 18 e^3 s^3 u^6 - 18 e^3 s^4^2 t^5 - 88 e^3 s^4^2 t^4 u - 174 e^3 s^4^2 t^3 u^2 - 174 e^3 s^4^2 t^2 u^3 - 88 e^3 s^4^2 t u^4 - 18 e^3 s^4^2 u^5 + 14 e^3 s^4 t^6 + 90 e^3 s^4 t^5 u + 238 e^3 s^4 t^4 u^2 + 332 e^3 s^4 t^3 u^3 + 258 e^3 s^4 t^2 u^4 + 106 e^3 s^4 t u^5 + 18 e^3 s^4 u^6 - 39 e^3 t^7 - 238 e^3 t^6 u - 632 e^3 t^5 u^2 - 955 e^3 t^4 u^3 - 895 e^3 t^3 u^4 - 524 e^3 t^2 u^5 - 178 e^3 t u^6 - 27 e^3 u^7 + 736 e^2 s^3^4 s^4^2 t + 304 e^2 s^3^4 s^4^2 u + 352 e^2 s^3^3 s^4^3 t - 736 e^2 s^3^3 s^4^3 u - 1216 e^2 s^3^3 s^4^2 t^2 - 1008 e^2 s^3^3 s^4^2 t u - 368 e^2 s^3^3 s^4^2 u^2 - 216 e^2 s^3^3 s^4 t^3 - 828 e^2 s^3^3 s^4 t^2 u - 768 e^2 s^3^3 s^4 t u^2 - 156 e^2 s^3^3 s^4 u^3 + 736 e^2 s^3^2 s^4^4 t + 304 e^2 s^3^2 s^4^4 u - 1216 e^2 s^3^2 s^4^3 t^2 - 1008 e^2 s^3^2 s^4^3 t u - 368 e^2 s^3^2 s^4^3 u^2 + 992 e^2 s^3^2 s^4^2 t^3 + 1352 e^2 s^3^2 s^4^2 t^2 u + 1248 e^2 s^3^2 s^4^2 t u^2 + 888 e^2 s^3^2 s^4^2 u^3 + 296 e^2 s^3^2 s^4 t^4 + 1372 e^2 s^3^2 s^4 t^3 u + 1964 e^2 s^3^2 s^4 t^2 u^2 + 996 e^2 s^3^2 s^4 t u^3 + 108 e
\end{aligned}$$

$$\begin{aligned}
&^2*s3^2*s4*u^4+24*e^2*s3^2*t^5+128*e^2*s3^2*t^4*u+276*e^2*s3^2*t^3*u^2+300*e^2 \\
&*s3^2*t^2*u^3+164*e^2*s3^2*t*u^4+36*e^2*s3^2*u^5-216*e^2*s3*s4^3*t^3-828*e^2* \\
&s3*s4^3*t^2*u-768*e^2*s3*s4^3*t*u^2-156*e^2*s3*s4^3*u^3+296*e^2*s3*s4^2*t^4+ \\
&1372*e^2*s3*s4^2*t^3*u+1964*e^2*s3*s4^2*t^2*u^2+996*e^2*s3*s4^2*t*u^3+108*e^2* \\
&s3*s4^2*u^4-294*e^2*s3*s4*t^5-1284*e^2*s3*s4*t^4*u-2284*e^2*s3*s4*t^3*u^2-2088 \\
&*e^2*s3*s4*t^2*u^3-990*e^2*s3*s4*t*u^4-196*e^2*s3*s4*u^5-30*e^2*s3*t^6-188*e^2 \\
&*s3*t^5*u-488*e^2*s3*t^4*u^2-672*e^2*s3*t^3*u^3-518*e^2*s3*t^2*u^4-212*e^2*s3* \\
&t*u^5-36*e^2*s3*u^6+24*e^2*s4^2*t^5+128*e^2*s4^2*t^4*u+276*e^2*s4^2*t^3*u^2+ \\
&300*e^2*s4^2*t^2*u^3+164*e^2*s4^2*t*u^4+36*e^2*s4^2*u^5-30*e^2*s4*t^6-188*e^2* \\
&s4*t^5*u-488*e^2*s4*t^4*u^2-672*e^2*s4*t^3*u^3-518*e^2*s4*t^2*u^4-212*e^2*s4*t \\
&*u^5-36*e^2*s4*u^6+30*e^2*t^7+186*e^2*t^6*u+509*e^2*t^5*u^2+805*e^2*t^4*u^3+ \\
&800*e^2*t^3*u^4+500*e^2*t^2*u^5+181*e^2*t*u^6+29*e^2*u^7-552*e*s3^4*s4^2*t-120 \\
&*e*s3^4*s4^2*u-912*e*s3^3*s4^3*t+240*e*s3^3*s4^3*u+1040*e*s3^3*s4^2*t^2+784*e* \\
&s3^3*s4^2*t*u+96*e*s3^3*s4^2*u^2+164*e*s3^3*s4*t^3+552*e*s3^3*s4*t^2*u+468*e* \\
&s3^3*s4*t*u^2+80*e*s3^3*s4*u^3-552*e*s3^2*s4^4*t-120*e*s3^2*s4^4*u+1040*e*s3^2 \\
&*s4^3*t^2+784*e*s3^2*s4^3*t*u+96*e*s3^2*s4^3*u^2-320*e*s3^2*s4^2*t^3-56*e*s3^2 \\
&*s4^2*t^2*u-264*e*s3^2*s4^2*u^3-296*e*s3^2*s4*t^4-1140*e*s3^2*s4*t^3*u-1428*e* \\
&s3^2*s4*t^2*u^2-620*e*s3^2*s4*t*u^3-36*e*s3^2*s4*u^4-16*e*s3^2*t^5-84*e*s3^2*t \\
&^4*u-178*e*s3^2*t^3*u^2-190*e*s3^2*t^2*u^3-102*e*s3^2*t*u^4-22*e*s3^2*u^5+164* \\
&*e*s3*s4^3*t^3+552*e*s3*s4^3*t^2*u+468*e*s3*s4^3*t*u^2+80*e*s3*s4^3*u^3-296*e* \\
&s3*s4^2*t^4-1140*e*s3*s4^2*t^3*u-1428*e*s3*s4^2*t^2*u^2-620*e*s3*s4^2*t*u^3-36 \\
&*e*s3*s4^2*u^4+144*e*s3*s4*t^5+594*e*s3*s4*t^4*u+964*e*s3*s4*t^3*u^2+768*e*s3* \\
&s4*t^2*u^3+300*e*s3*s4*t*u^4+46*e*s3*s4*u^5+28*e*s3*t^6+162*e*s3*t^5*u+390*e* \\
&s3*t^4*u^2+500*e*s3*t^3*u^3+360*e*s3*t^2*u^4+138*e*s3*t*u^5+22*e*s3*u^6-16*e* \\
&s4^2*t^5-84*e*s4^2*t^4*u-178*e*s4^2*t^3*u^2-190*e*s4^2*t^2*u^3-102*e*s4^2*t*u^4 \\
&-22*e*s4^2*u^5+28*e*s4*t^6+162*e*s4*t^5*u+390*e*s4*t^4*u^2+500*e*s4*t^3*u^3+ \\
&360*e*s4*t^2*u^4+138*e*s4*t*u^5+22*e*s4*u^6-16*e*t^7-98*e*t^6*u-263*e*t^5*u^2 \\
&-405*e*t^4*u^3-390*e*t^3*u^4-236*e*t^2*u^5-83*e*t*u^6-13*e*u^7+120*s3^4*s4^2*t+ \\
&24*s3^4*s4^2*u+240*s3^3*s4^3*t-16*s3^3*s4^3*u-240*s3^3*s4^2*t^2-192*s3^3*s4^2* \\
&t*u-16*s3^3*s4^2*u^2-40*s3^3*s4*t^3-120*s3^3*s4*t^2*u-96*s3^3*s4*t*u^2-16*s3^3 \\
&*s4*u^3+120*s3^2*s4^4*t+24*s3^2*s4^4*u-240*s3^2*s4^3*t^2-192*s3^2*s4^3*t*u-16* \\
&s3^2*s4^3*u^2+40*s3^2*s4^2*t^3-40*s3^2*s4^2*t^2*u-56*s3^2*s4^2*t*u^2+24*s3^2* \\
&s4^2*u^3+80*s3^2*s4*t^4+280*s3^2*s4*t^3*u+328*s3^2*s4*t^2*u^2+136*s3^2*s4*t*u^ \\
&3+8*s3^2*s4*u^4+4*s3^2*t^5+20*s3^2*t^4*u+40*s3^2*t^3*u^2+40*s3^2*t^2*u^3+20*s3 \\
&^2*t*u^4+4*s3^2*u^5-40*s3*s4^3*t^3-120*s3*s4^3*t^2*u-96*s3*s4^3*t*u^2-16*s3*s4 \\
&^3*u^3+80*s3*s4^2*t^4+280*s3*s4^2*t^3*u+328*s3*s4^2*t^2*u^2+136*s3*s4^2*t*u^3+ \\
&8*s3*s4^2*u^4-32*s3*s4*t^5-124*s3*s4*t^4*u-184*s3*s4*t^3*u^2-128*s3*s4*t^2*u^3 \\
&-40*s3*s4*t*u^4-4*s3*s4*u^5-8*s3*t^6-44*s3*t^5*u-100*s3*t^4*u^2-120*s3*t^3*u^3 \\
&-80*s3*t^2*u^4-28*s3*t*u^5-4*s3*u^6+4*s4^2*t^5+20*s4^2*t^4*u+40*s4^2*t^3*u^2+ \\
&40*s4^2*t^2*u^3+20*s4^2*t*u^4+4*s4^2*u^5-8*s4*t^6-44*s4*t^5*u-100*s4*t^4*u^2 \\
&-120*s4*t^3*u^3-80*s4*t^2*u^4-28*s4*t*u^5-4*s4*u^6+4*t^7+24*t^6*u+62*t^5*u^2+90 \\
&*t^4*u^3+80*t^3*u^4+44*t^2*u^5+14*t*u^6+2*u^7)/u/(-3+2*e)/(3*e-2)/(-4*s3*s4+t^ \\
&2+2*t*u+u^2)^2/t/(3*e-1); \\
\text{cpbox010010112p1p2p4} := -4*(u-s3+t-s4)*(e-1)*(144*e^5*s3^2*s4^2*t^3+144*e^5*s3 \\
&^2*s4^2*t^2*u-72*e^5*s3*s4*t^5-216*e^5*s3*s4*t^4*u-216*e^5*s3*s4*t^3*u^2-72*e^
\end{aligned}$$

$$\begin{aligned}
& 5*s3*s4*t^2*u^3+9*e^5*t^7+45*e^5*t^6*u+90*e^5*t^5*u^2+90*e^5*t^4*u^3+45*e^5*t^3*u^4+9*e^5*t^2*u^5-288*e^4*s3^3*s4^3*t-288*e^4*s3^3*s4^3*u-24*e^4*s3^3*s4*t^3 \\
& -24*e^4*s3^3*s4*t^2*u+384*e^4*s3^2*s4^2*t^3+672*e^4*s3^2*s4^2*t^2*u+576*e^4*s3^2*s4^2*t*u^2+144*e^4*s3^2*s4^2*u^3+24*e^4*s3^2*s4*t^4+48*e^4*s3^2*s4*t^3*u+24 \\
& *e^4*s3^2*s4*t^2*u^2+6*e^4*s3^2*t^5+18*e^4*s3^2*t^4*u+18*e^4*s3^2*t^3*u^2+6*e^4*s3^2*t^2*u^3-24*e^4*s3*s4^3*t^3-24*e^4*s3*s4^3*t^2*u+24*e^4*s3*s4^2*t^4+48*e \\
& ^4*s3*s4^2*t^3*u+24*e^4*s3*s4^2*t^2*u^2-150*e^4*s3*s4*t^5-486*e^4*s3*s4*t^4*u-648*e^4*s3*s4*t^3*u^2-456*e^4*s3*s4*t^2*u^3-162*e^4*s3*s4*t*u^4-18*e^4*s3*s4*u \\
& ^5-6*e^4*s3*t^6-24*e^4*s3*t^5*u-36*e^4*s3*t^4*u^2-24*e^4*s3*t^3*u^3-6*e^4*s3*t^2*u^4+6*e^4*s4^2*t^5+18*e^4*s4^2*t^4*u+18*e^4*s4^2*t^3*u^2+6*e^4*s4^2*t^2*u^3 \\
& -6*e^4*s4*t^6-24*e^4*s4*t^5*u-36*e^4*s4*t^4*u^2-24*e^4*s4*t^3*u^3-6*e^4*s4*t^2*u^4+18*e^4*t^7+90*e^4*t^6*u+189*e^4*t^5*u^2+216*e^4*t^4*u^3+144*e^4*t^3*u^4+ \\
& 54*e^4*t^2*u^5+9*e^4*t*u^6-288*e^3*s3^4*s4^2*t+864*e^3*s3^3*s4^3*u+288*e^3*s3^3*s4^2*t^2+288*e^3*s3^3*s4^2*t*u+128*e^3*s3^3*s4*t^3+296*e^3*s3^3*s4*t^2*u+144 \\
& *e^3*s3^3*s4*t*u^2-288*e^3*s3^2*s4^4*t+288*e^3*s3^2*s4^3*t^2+288*e^3*s3^2*s4^3*t*u-720*e^3*s3^2*s4^2*t^3-1104*e^3*s3^2*s4^2*t^2*u-1296*e^3*s3^2*s4^2*t*u^2 \\
& -432*e^3*s3^2*s4^2*u^3-96*e^3*s3^2*s4*t^4-408*e^3*s3^2*s4*t^3*u-456*e^3*s3^2*s4*t^2*u^2-144*e^3*s3^2*s4*t*u^3-18*e^3*s3^2*t^5-70*e^3*s3^2*t^4*u-104*e^3*s3^2*t^3*u^2 \\
& -70*e^3*s3^2*t^2*u^3-18*e^3*s3^2*t*u^4+128*e^3*s3*s4^3*t^3+296*e^3*s3*s4^3*t^2*u+144*e^3*s3*s4^3*t*u^2-96*e^3*s3*s4^2*t^4-408*e^3*s3*s4^2*t^3*u-456* \\
& e^3*s3*s4^2*t^2*u^2-144*e^3*s3*s4^2*t*u^3+312*e^3*s3*s4*t^5+1042*e^3*s3*s4*t^4*u+1472*e^3*s3*s4*t^3*u^2+1120*e^3*s3*s4*t^2*u^3+432*e^3*s3*s4*t*u^4+54*e^3*s3 \\
& *s4*u^5+14*e^3*s3*t^6+76*e^3*s3*t^5*u+162*e^3*s3*t^4*u^2+170*e^3*s3*t^3*u^3+88*e^3*s3*t^2*u^4+18*e^3*s3*t*u^5-18*e^3*s4^2*t^5-70*e^3*s4^2*t^4*u-104*e^3*s4^2 \\
& *t^3*u^2-70*e^3*s4^2*t^2*u^3-18*e^3*s4^2*t*u^4+14*e^3*s4*t^6+76*e^3*s4*t^5*u+162*e^3*s4*t^4*u^2+170*e^3*s4*t^3*u^3+88*e^3*s4*t^2*u^4+18*e^3*s4*t*u^5-39*e^3 \\
& *t^7-199*e^3*t^6*u-433*e^3*t^5*u^2-522*e^3*t^4*u^3-373*e^3*t^3*u^4-151*e^3*t^2*u^5-27*e^3*t*u^6+576*e^2*s3^4*s4^2*t+800*e^2*s3^3*s4^3*t-928*e^2*s3^3*s4^3*u \\
& -864*e^2*s3^3*s4^2*t^2-576*e^2*s3^3*s4^2*t*u-212*e^2*s3^3*s4*t^3-540*e^2*s3^3*s4*t^2*u-288*e^2*s3^3*s4*t*u^2+576*e^2*s3^2*s4^4*t-864*e^2*s3^2*s4^3*t^2-576*e \\
& ^2*s3^2*s4^3*t*u+424*e^2*s3^2*s4^2*t^3+408*e^2*s3^2*s4^2*t^2*u+992*e^2*s3^2*s4^2*t*u^2+464*e^2*s3^2*s4^2*u^3+280*e^2*s3^2*s4*t^4+968*e^2*s3^2*s4*t^3*u+976*e \\
& ^2*s3^2*s4*t^2*u^2+288*e^2*s3^2*s4*t*u^3+24*e^2*s3^2*t^5+104*e^2*s3^2*t^4*u+172*e^2*s3^2*t^3*u^2+128*e^2*s3^2*t^2*u^3+36*e^2*s3^2*t*u^4-212*e^2*s3*s4^3*t^3 \\
& -540*e^2*s3*s4^3*t^2*u-288*e^2*s3*s4^3*t*u^2+280*e^2*s3*s4^2*t^4+968*e^2*s3*s4^2*t^3*u+976*e^2*s3*s4^2*t^2*u^2+288*e^2*s3*s4^2*t*u^3-234*e^2*s3*s4*t^5-798 \\
& *e^2*s3*s4*t^4*u-1192*e^2*s3*s4*t^3*u^2-984*e^2*s3*s4*t^2*u^3-414*e^2*s3*s4*t*u^4-58*e^2*s3*s4*u^5-30*e^2*s3*t^6-158*e^2*s3*t^5*u-330*e^2*s3*t^4*u^2-342*e^2 \\
& *s3*t^3*u^3-176*e^2*s3*t^2*u^4-36*e^2*s3*t*u^5+24*e^2*s4^2*t^5+104*e^2*s4^2*t^4*u+172*e^2*s4^2*t^3*u^2+128*e^2*s4^2*t^2*u^3+36*e^2*s4^2*t*u^4-30*e^2*s4*t^6 \\
& -158*e^2*s4*t^5*u-330*e^2*s4*t^4*u^2-342*e^2*s4*t^3*u^3-176*e^2*s4*t^2*u^4-36*e^2*s4*t*u^5+30*e^2*t^7+156*e^2*t^6*u+353*e^2*t^5*u^2+452*e^2*t^4*u^3+348*e^2*t^3 \\
& *u^4+152*e^2*t^2*u^5+29*e^2*t*u^6-352*e*s3^4*s4^2*t-640*e*s3^3*s4^3*t+416*e*s3^3*s4^3*u+640*e*s3^3*s4^2*t^2+352*e*s3^3*s4^2*t*u+140*e*s3^3*s4*t^3+332*e*s3^3 \\
& *s4*t^2*u+176*e*s3^3*s4*t*u^2-352*e*s3^2*s4^4*t+640*e*s3^2*s4^3*t^2+352*e*s3^2*s4^3*t^2+352*e*s3^2*s4^3*t*u+176*e*s3^2*s4^3*t*u^2-352*e*s3^2*s4^3*t^2+352*e*s3^2*s4^3*t^2
\end{aligned}$$

$$\begin{aligned}
& ^2*s4^3*t*u-104*e*s3^2*s4^2*t^3+40*e*s3^2*s4^2*t^2*u-304*e*s3^2*s4^2*t*u^2-208 \\
& *e*s3^2*s4^2*u^3-248*e*s3^2*s4*t^4-720*e*s3^2*s4*t^3*u-648*e*s3^2*s4*t^2*u^2 \\
& -176*e*s3^2*s4*t*u^3-16*e*s3^2*t^5-68*e*s3^2*t^4*u-110*e*s3^2*t^3*u^2-80*e*s3^2 \\
& *t^2*u^3-22*e*s3^2*t*u^4+140*e*s3*s4^3*t^3+332*e*s3*s4^3*t^2*u+176*e*s3*s4^3*t \\
& *u^2-248*e*s3*s4^2*t^4-720*e*s3*s4^2*t^3*u-648*e*s3*s4^2*t^2*u^2-176*e*s3*s4^2 \\
& *t*u^3+112*e*s3*s4*t^5+358*e*s3*s4*t^4*u+496*e*s3*s4*t^3*u^2+392*e*s3*s4*t^2*u \\
& ^3+168*e*s3*s4*t*u^4+26*e*s3*s4*u^5+28*e*s3*t^6+134*e*s3*t^5*u+256*e*s3*t^4*u^ \\
& 2+244*e*s3*t^3*u^3+116*e*s3*t^2*u^4+22*e*s3*t*u^5-16*e*s4^2*t^5-68*e*s4^2*t^4* \\
& u-110*e*s4^2*t^3*u^2-80*e*s4^2*t^2*u^3-22*e*s4^2*t*u^4+28*e*s4*t^6+134*e*s4*t^ \\
& 5*u+256*e*s4*t^4*u^2+244*e*s4*t^3*u^3+116*e*s4*t^2*u^4+22*e*s4*t*u^5-16*e*t^7 \\
& -82*e*t^6*u-181*e*t^5*u^2-224*e*t^4*u^3-166*e*t^3*u^4-70*e*t^2*u^5-13*e*t*u^6+ \\
& 64*s3^4*s4^2*t+128*s3^3*s4^3*t-64*s3^3*s4^3*u-128*s3^3*s4^2*t^2-64*s3^3*s4^2*t \\
& *u-32*s3^3*s4*t^3-64*s3^3*s4*t^2*u-32*s3^3*s4*t*u^2+64*s3^2*s4^4*t-128*s3^2*s4 \\
& ^3*t^2-64*s3^2*s4^3*t*u-32*s3^2*s4^2*t^2*u+32*s3^2*s4^2*t*u^2+32*s3^2*s4^2*u^3 \\
& +64*s3^2*s4*t^4+160*s3^2*s4*t^3*u+128*s3^2*s4*t^2*u^2+32*s3^2*s4*t*u^3+4*s3^2* \\
& t^5+16*s3^2*t^4*u+24*s3^2*t^3*u^2+16*s3^2*t^2*u^3+4*s3^2*t*u^4-32*s3*s4^3*t^3 \\
& -64*s3*s4^3*t^2*u-32*s3*s4^3*t*u^2+64*s3*s4^2*t^4+160*s3*s4^2*t^3*u+128*s3*s4^2 \\
& *t^2*u^2+32*s3*s4^2*t*u^3-24*s3*s4*t^5-68*s3*s4*t^4*u-80*s3*s4*t^3*u^2-56*s3* \\
& s4*t^2*u^3-24*s3*s4*t*u^4-4*s3*s4*u^5-8*s3*t^6-36*s3*t^5*u-64*s3*t^4*u^2-56*s3 \\
& *t^3*u^3-24*s3*t^2*u^4-4*s3*t*u^5+4*s4^2*t^5+16*s4^2*t^4*u+24*s4^2*t^3*u^2+16* \\
& s4^2*t^2*u^3+4*s4^2*t*u^4-8*s4*t^6-36*s4*t^5*u-64*s4*t^4*u^2-56*s4*t^3*u^3-24* \\
& s4*t^2*u^4-4*s4*t*u^5+4*t^7+20*t^6*u+42*t^5*u^2+48*t^4*u^3+32*t^3*u^4+12*t^2*u \\
& ^5+2*t*u^6)/(-3+2*e)/(3*e-2)/(-4*s3*s4+t^2+2*t*u+u^2)^2/t/u/(3*e-1)/(-1+2*e);
\end{aligned}$$

Bibliography

- [1] A. Banfi and J. Cancino, *Implications of QCD radiative corrections on high- p_T Higgs searches*, *Phys.Lett.* **B718** (2012) 499–506, [arXiv:1207.0674].
- [2] C. Anastasiou, J. Cancino, F. Chavez, C. Duhr, A. Lazopoulos, B. Mistlberger, and R. Mueller, *NNLO QCD corrections to $pp \rightarrow \gamma^* \gamma^*$ in the large N_F limit*, arXiv:1408.4546. Submitted to JHEP.
- [3] F. Englert and R. Brout, *Broken Symmetry and the Mass of Gauge Vector Mesons*, *Phys.Rev.Lett.* **13** (1964) 321–323.
- [4] P. W. Higgs, *Broken symmetries, massless particles and gauge fields*, *Phys.Lett.* **12** (1964) 132–133.
- [5] G. Guralnik, C. Hagen, and T. Kibble, *Global Conservation Laws and Massless Particles*, *Phys.Rev.Lett.* **13** (1964) 585–587.
- [6] P. W. Higgs, *Broken Symmetries and the Masses of Gauge Bosons*, *Phys.Rev.Lett.* **13** (1964) 508–509.
- [7] P. W. Higgs, *Spontaneous Symmetry Breakdown without Massless Bosons*, *Phys.Rev.* **145** (1966) 1156–1163.
- [8] T. Kibble, *Symmetry breaking in non-abelian gauge theories*, *Phys.Rev.* **155** (1967) 1554–1561.
- [9] **ATLAS Collaboration**, G. Aad *et al.*, *Combined search for the Standard Model Higgs boson using up to 4.9 fb⁻¹ of pp collision data at $\sqrt{s} = 7$ TeV with the ATLAS detector at the LHC*, *Phys.Lett.* **B710** (2012) 49–66, [arXiv:1202.1408].
- [10] **CMS Collaboration**, S. Chatrchyan *et al.*, *Combined results of searches for the standard model Higgs boson in pp collisions at $\sqrt{s} = 7$ TeV*, *Phys.Lett.* **B710** (2012) 26–48, [arXiv:1202.1488].
- [11] A. Djouadi, J. Kalinowski, and M. Spira, *HDECAY: A Program for Higgs boson decays in the standard model and its supersymmetric extension*, *Comput.Phys.Commun.* **108** (1998) 56–74, [hep-ph/9704448].

- [12] C. Collaboration, “Higgs physics results: Combined results for couplings.” <https://twiki.cern.ch/twiki/bin/view/CMSPublic/PhysicsResultsHIG>, 2014. [Online; accessed 24-May-2014].
- [13] **ATLAS Collaboration**, G. Aad *et al.*, *Measurements of Higgs boson production and couplings in diboson final states with the ATLAS detector at the LHC*, *Phys.Lett.* **B726** (2013) 88–119, [arXiv:1307.1427].
- [14] **CMS Collaboration**, S. Chatrchyan *et al.*, *Measurement of the properties of a Higgs boson in the four-lepton final state*, *Phys.Rev.* **D89** (2014) 092007, [arXiv:1312.5353].
- [15] F. Halzen and A. D. Martin, *Quarks and Leptons: An Introductory Course in Modern Particle Physics*. Wiley, 1984.
- [16] T.-P. Cheng and L.-F. Li, *Gauge theory of elementary particle physics*. Clarendon press Oxford, 1984.
- [17] M. E. Peskin and D. V. Schroeder, *An Introduction to Quantum Field Theory*. Westview, 1995.
- [18] S. Weinberg, *The quantum theory of fields: Foundations*, vol. 1. Cambridge university press, 1995.
- [19] S. Weinberg, *The quantum theory of fields: Modern applications*, vol. 2. Cambridge university press, 1996.
- [20] R. K. Ellis, W. J. Stirling, and B. R. Webber, *QCD and collider physics*, vol. 8. Cambridge University Press, 2003.
- [21] G. Dissertori, I. Knowles, and M. Schmelling, *Quantum Chromodynamics: High Energy Experiment and Theory*. Oxford University Press, 2003.
- [22] Wikipedia, “Standard model.” http://en.wikipedia.org/wiki/Standard_Model, 2014. [Online; accessed 20-June-2014].
- [23] **SNO Collaboration**, Q. Ahmad *et al.*, *Measurement of the rate of $\nu_e + d \rightarrow p + p + e^-$ interactions produced by 8B solar neutrinos at the Sudbury Neutrino Observatory*, *Phys.Rev.Lett.* **87** (2001) 071301, [nucl-ex/0106015].
- [24] **Planck Collaboration**, P. Ade *et al.*, *Planck 2013 results. XVI. Cosmological parameters*, arXiv:1303.5076.
- [25] **WMAP collaboration**, G. Hinshaw *et al.*, *Nine-Year Wilkinson Microwave Anisotropy Probe (WMAP) Observations: Cosmological Parameter Results*, *Astrophys.J.Suppl.* **208** (2013) 19, [arXiv:1212.5226].

- [26] M. Gell-Mann, *A schematic model of baryons and mesons*, *Physics Letters* **8** (1964), no. 3 214–215.
- [27] G. Zweig, *An $SU(3)$ model for strong interaction symmetry and its breaking. Version 1*, .
- [28] G. Zweig, *An $SU(3)$ model for strong interaction symmetry and its breaking. Version 2*, .
- [29] R. P. Feynman, *Very high-energy collisions of hadrons*, *Phys.Rev.Lett.* **23** (1969) 1415–1417.
- [30] J. Bjorken, *Asymptotic Sum Rules at Infinite Momentum*, *Phys.Rev.* **179** (1969) 1547–1553.
- [31] C.-N. Yang and R. L. Mills, *Conservation of Isotopic Spin and Isotopic Gauge Invariance*, *Phys.Rev.* **96** (1954) 191–195.
- [32] R. U. Sexl and H. K. Urbantke, *Relativity, groups, particles*. Springer, 2001.
- [33] D. Gross and F. Wilczek, *Ultraviolet Behavior of Nonabelian Gauge Theories*, *Phys.Rev.Lett.* **30** (1973) 1343–1346.
- [34] H. D. Politzer, *Reliable Perturbative Results for Strong Interactions?*, *Phys.Rev.Lett.* **30** (1973) 1346–1349.
- [35] A. G. Grozin, *Lectures on QED and QCD: Practical Calculations and Renormalization of One-and Multi-loop Feynman Diagrams*. World Scientific, 2007.
- [36] P. A. Dirac, *Quantum theory of emission and absorption of radiation*, *Proc.Roy.Soc.Lond.* **A114** (1927) 243.
- [37] S. Tomonaga, *On a relativistically invariant formulation of the quantum theory of wave fields*, *Prog.Theor.Phys.* **1** (1946) 27–42.
- [38] S.-I. Tomonaga and J. Oppenheimer, *On Infinite Field Reactions in Quantum Field Theory*, *Phys.Rev.* **74** (1948) 224–225.
- [39] J. S. Schwinger, *On Quantum electrodynamics and the magnetic moment of the electron*, *Phys.Rev.* **73** (1948) 416–417.
- [40] R. Feynman, *The Theory of positrons*, *Phys.Rev.* **76** (1949) 749–759.
- [41] R. Feynman, *Space - time approach to quantum electrodynamics*, *Phys.Rev.* **76** (1949) 769–789.
- [42] R. Feynman, *Mathematical formulation of the quantum theory of electromagnetic interaction*, *Phys.Rev.* **80** (1950) 440–457.

- [43] E. Fermi, *Versuch einer Theorie der β -Strahlen. I*, *Z.Phys.* **88** (1934) 161–177.
- [44] E. Fermi, *Tentativo di una teoria dei raggi beta*, *Nuovo Cim.* **11** (1934) 1–19.
- [45] S. Glashow, *Partial Symmetries of Weak Interactions*, *Nucl.Phys.* **22** (1961) 579–588.
- [46] A. Salam, *Weak and Electromagnetic Interactions*, *Conf.Proc.* **C680519** (1968) 367–377.
- [47] S. Weinberg, *A Model of Leptons*, *Phys.Rev.Lett.* **19** (1967) 1264–1266.
- [48] N. Cabibbo, *Unitary Symmetry and Leptonic Decays*, *Phys.Rev.Lett.* **10** (1963) 531–533.
- [49] M. Kobayashi and T. Maskawa, *CP Violation in the Renormalizable Theory of Weak Interaction*, *Prog.Theor.Phys.* **49** (1973) 652–657.
- [50] Y. Nambu and G. Jona-Lasinio, *Dynamical Model of Elementary Particles Based on an Analogy with Superconductivity. 1.*, *Phys.Rev.* **122** (1961) 345–358.
- [51] J. Goldstone, *Field Theories with Superconductor Solutions*, *Nuovo Cim.* **19** (1961) 154–164.
- [52] G. 't Hooft and M. Veltman, *Regularization and Renormalization of Gauge Fields*, *Nucl.Phys.* **B44** (1972) 189–213.
- [53] J. C. Collins, *Renormalization*. Cambridge University Press, 1986.
- [54] S. Larin and J. Vermaseren, *The Three loop QCD Beta function and anomalous dimensions*, *Phys.Lett.* **B303** (1993) 334–336, [[hep-ph/9302208](#)].
- [55] E. Byckling and K. Kajantie, *Particle Kinematics*. Wiley, 1973.
- [56] A. Gehrmann-De Ridder, T. Gehrmann, and G. Heinrich, *Four particle phase space integrals in massless QCD*, *Nucl.Phys.* **B682** (2004) 265–288, [[hep-ph/0311276](#)].
- [57] R. Feynman, *Space-time approach to nonrelativistic quantum mechanics*, *Rev.Mod.Phys.* **20** (1948) 367–387.
- [58] G. 't Hooft and M. Veltman, *DIAGRAMMAR*, *NATO Adv.Study Inst.Ser.B Phys.* **4** (1974) 177–322.
- [59] P. Nogueira, *Automatic Feynman graph generation*, *J.Comput.Phys.* **105** (1993) 279–289.
- [60] J. Vermaseren, *New features of FORM*, [math-ph/0010025](#).

- [61] J. Kuipers, T. Ueda, J. Vermaseren, and J. Vollinga, *FORM version 4.0*, *Comput.Phys.Commun.* **184** (2013) 1453–1467, [[arXiv:1203.6543](#)].
- [62] W. Pauli and F. Villars, *On the Invariant regularization in relativistic quantum theory*, *Rev.Mod.Phys.* **21** (1949) 434–444.
- [63] G. 't Hooft, *Dimensional regularization and the renormalization group*, *Nucl.Phys.* **B61** (1973) 455–468.
- [64] A. Slavnov, *Ward Identities in Gauge Theories*, *Theor.Math.Phys.* **10** (1972) 99–107.
- [65] J. Taylor, *Ward Identities and Charge Renormalization of the Yang-Mills Field*, *Nucl.Phys.* **B33** (1971) 436–444.
- [66] W. A. Bardeen, A. Buras, D. Duke, and T. Muta, *Deep Inelastic Scattering Beyond the Leading Order in Asymptotically Free Gauge Theories*, *Phys.Rev.* **D18** (1978) 3998.
- [67] G. 't Hooft, *Renormalizable Lagrangians for Massive Yang-Mills Fields*, *Nucl.Phys.* **B35** (1971) 167–188.
- [68] G. 't Hooft, *Renormalization of Massless Yang-Mills Fields*, *Nucl.Phys.* **B33** (1971) 173–199.
- [69] S. Catani and M. Seymour, *A General algorithm for calculating jet cross-sections in NLO QCD*, *Nucl.Phys.* **B485** (1997) 291–419, [[hep-ph/9605323](#)].
- [70] D. A. Kosower, *Antenna factorization of gauge theory amplitudes*, *Phys.Rev.* **D57** (1998) 5410–5416, [[hep-ph/9710213](#)].
- [71] J. M. Campbell, M. Cullen, and E. N. Glover, *Four jet event shapes in electron - positron annihilation*, *Eur.Phys.J.* **C9** (1999) 245–265, [[hep-ph/9809429](#)].
- [72] S. Frixione, Z. Kunszt, and A. Signer, *Three jet cross-sections to next-to-leading order*, *Nucl.Phys.* **B467** (1996) 399–442, [[hep-ph/9512328](#)].
- [73] A. Gehrmann-De Ridder, T. Gehrmann, and E. N. Glover, *Antenna subtraction at NNLO*, *JHEP* **0509** (2005) 056, [[hep-ph/0505111](#)].
- [74] A. Daleo, T. Gehrmann, and D. Maitre, *Antenna subtraction with hadronic initial states*, *JHEP* **0704** (2007) 016, [[hep-ph/0612257](#)].
- [75] G. Altarelli, R. K. Ellis, and G. Martinelli, *Leptonproduction and Drell-Yan Processes Beyond the Leading Approximation in Chromodynamics*, *Nucl.Phys.* **B143** (1978) 521.

- [76] T. Binoth and G. Heinrich, *An Automated algorithm to compute infrared divergent multiloop integrals*, *Nucl.Phys.* **B585** (2000) 741–759, [[hep-ph/0004013](#)].
- [77] T. Binoth and G. Heinrich, *Numerical evaluation of phase space integrals by sector decomposition*, *Nucl.Phys.* **B693** (2004) 134–148, [[hep-ph/0402265](#)].
- [78] C. Anastasiou and A. Lazopoulos, *Automatic integral reduction for higher order perturbative calculations*, *JHEP* **0407** (2004) 046, [[hep-ph/0404258](#)].
- [79] C. Anastasiou, F. Herzog, and A. Lazopoulos, *On the factorization of overlapping singularities at NNLO*, *JHEP* **1103** (2011) 038, [[arXiv:1011.4867](#)].
- [80] F. Herzog, *QCD corrections and non-linear mappings*. PhD thesis, ETH Zürich, 2012.
- [81] S. Buehler and A. Lazopoulos, *Scale dependence and collinear subtraction terms for Higgs production in gluon fusion at N3LO*, *JHEP* **1310** (2013) 096, [[arXiv:1306.2223](#)].
- [82] S. Buehler, F. Herzog, A. Lazopoulos, and R. Mueller, *The Fully differential hadronic production of a Higgs boson via bottom quark fusion at NNLO*, *JHEP* **1207** (2012) 115, [[arXiv:1204.4415](#)].
- [83] J. C. Collins, D. E. Soper, and G. F. Sterman, *Factorization of Hard Processes in QCD*, *Adv.Ser.Direct.High Energy Phys.* **5** (1988) 1–91, [[hep-ph/0409313](#)].
- [84] V. Gribov and L. Lipatov, *Deep inelastic $e p$ scattering in perturbation theory*, *Sov.J.Nucl.Phys.* **15** (1972) 438–450.
- [85] Y. L. Dokshitzer, *Calculation of the Structure Functions for Deep Inelastic Scattering and $e^+ e^-$ Annihilation by Perturbation Theory in Quantum Chromodynamics.*, *Sov.Phys.JETP* **46** (1977) 641–653.
- [86] G. Altarelli and G. Parisi, *Asymptotic Freedom in Parton Language*, *Nucl.Phys.* **B126** (1977) 298.
- [87] M. Botje, J. Butterworth, A. Cooper-Sarkar, A. de Roeck, J. Feltesse, *et al.*, *The PDF4LHC Working Group Interim Recommendations*, [arXiv:1101.0538](#).
- [88] M. Whalley, D. Bourilkov, and R. Group, *The Les Houches accord PDFs (LHAPDF) and LHAGLUE*, [hep-ph/0508110](#).
- [89] T. Kinoshita, *Mass singularities of Feynman amplitudes*, *J.Math.Phys.* **3** (1962) 650–677.
- [90] T. Lee and M. Nauenberg, *Degenerate Systems and Mass Singularities*, *Phys.Rev.* **133** (1964) B1549–B1562.

- [91] G. F. Sterman and S. Weinberg, *Jets from Quantum Chromodynamics*, *Phys.Rev.Lett.* **39** (1977) 1436.
- [92] Y. L. Dokshitzer, G. Leder, S. Moretti, and B. Webber, *Better jet clustering algorithms*, *JHEP* **9708** (1997) 001, [[hep-ph/9707323](#)].
- [93] M. Wobisch and T. Wengler, *Hadronization corrections to jet cross-sections in deep inelastic scattering*, [hep-ph/9907280](#).
- [94] G. P. Salam, *Towards Jetography*, *Eur.Phys.J.* **C67** (2010) 637–686, [[arXiv:0906.1833](#)].
- [95] M. Cacciari, G. P. Salam, and G. Soyez, *FastJet user manual*, *Eur.Phys.J.* **C72** (2012) 1896, [[arXiv:1111.6097](#)].
- [96] G. Passarino and M. Veltman, *One Loop Corrections for $e^+ e^-$ Annihilation Into $\mu^+ \mu^-$ in the Weinberg Model*, *Nucl.Phys.* **B160** (1979) 151.
- [97] K. Chetyrkin and F. Tkachov, *Integration by Parts: The Algorithm to Calculate beta Functions in 4 Loops*, *Nucl.Phys.* **B192** (1981) 159–204.
- [98] F. Tkachov, *A Theorem on Analytical Calculability of Four Loop Renormalization Group Functions*, *Phys.Lett.* **B100** (1981) 65–68.
- [99] T. Gehrmann and E. Remiddi, *Differential equations for two loop four point functions*, *Nucl.Phys.* **B580** (2000) 485–518, [[hep-ph/9912329](#)].
- [100] S. Laporta, *High precision calculation of multiloop Feynman integrals by difference equations*, *Int.J.Mod.Phys.* **A15** (2000) 5087–5159, [[hep-ph/0102033](#)].
- [101] Maplesoft a division of Waterloo Maple Inc., *Maple*, Version 18 (2014).
- [102] U. Aglietti, R. Bonciani, G. Degrassi, and A. Vicini, *Two loop light fermion contribution to Higgs production and decays*, *Phys.Lett.* **B595** (2004) 432–441, [[hep-ph/0404071](#)].
- [103] M. Argeri and P. Mastrolia, *Feynman Diagrams and Differential Equations*, *Int.J.Mod.Phys.* **A22** (2007) 4375–4436, [[arXiv:0707.4037](#)].
- [104] E. Remiddi and J. Vermaseren, *Harmonic polylogarithms*, *Int.J.Mod.Phys.* **A15** (2000) 725–754, [[hep-ph/9905237](#)].
- [105] Wolfram Research, Inc., *Mathematica*, Version 9.0, Champaign, IL (2012).
- [106] T. Huber and D. Maitre, *HypExp: A Mathematica package for expanding hypergeometric functions around integer-valued parameters*, *Comput.Phys.Commun.* **175** (2006) 122–144, [[hep-ph/0507094](#)].

- [107] T. Huber and D. Maitre, *HypExp 2, Expanding Hypergeometric Functions about Half-Integer Parameters*, *Comput.Phys.Commun.* **178** (2008) 755–776, [arXiv:0708.2443].
- [108] D. Maitre, *HPL, a mathematica implementation of the harmonic polylogarithms*, *Comput.Phys.Commun.* **174** (2006) 222–240, [hep-ph/0507152].
- [109] D. Maitre, *Extension of HPL to complex arguments*, *Comput.Phys.Commun.* **183** (2012) 846, [hep-ph/0703052].
- [110] S. Buehler and C. Duhr, *CHAPLIN - Complex Harmonic Polylogarithms in Fortran*, arXiv:1106.5739.
- [111] A. B. Goncharov, *Multiple polylogarithms, cyclotomy and modular complexes*, *Math.Res.Lett.* **5** (1998) 497–516, [arXiv:1105.2076].
- [112] A. B. Goncharov, *Multiple polylogarithms and mixed tate motives*, arXiv preprint math/0103059 (2001).
- [113] S. Laporta and E. Remiddi, *Analytic treatment of the two loop equal mass sunrise graph*, *Nucl.Phys.* **B704** (2005) 349–386, [hep-ph/0406160].
- [114] F. Chavez, *Two-loop integrals in diboson production*. PhD thesis, ETH Zürich, 2014.
- [115] F. Chavez and C. Duhr, *Three-mass triangle integrals and single-valued polylogarithms*, *JHEP* **1211** (2012) 114, [arXiv:1209.2722].
- [116] R. Ree, *Lie elements and an algebra associated with shuffles*, *Annals of Mathematics* **62** (1958) 210–220.
- [117] C. Duhr, *Hopf algebras, coproducts and symbols: an application to Higgs boson amplitudes*, *JHEP* **1208** (2012) 043, [arXiv:1203.0454].
- [118] C. Duhr, H. Gangl, and J. R. Rhodes, *From polygons and symbols to polylogarithmic functions*, *JHEP* **1210** (2012) 075, [arXiv:1110.0458].
- [119] **ATLAS Collaboration**, G. Aad *et al.*, *Observation of a new particle in the search for the Standard Model Higgs boson with the ATLAS detector at the LHC*, *Phys.Lett.* **B716** (2012) 1–29, [arXiv:1207.7214].
- [120] **CMS Collaboration**, S. Chatrchyan *et al.*, *Observation of a new boson at a mass of 125 GeV with the CMS experiment at the LHC*, *Phys.Lett.B* (2012) [arXiv:1207.7235].
- [121] **ATLAS Collaboration**, G. Aad *et al.*, *Search for the Standard Model Higgs boson in the diphoton decay channel with 4.9 fb⁻¹ of pp collisions at sqrt(s)=7 TeV with ATLAS*, *Phys.Rev.Lett.* **108** (2012) 111803, [arXiv:1202.1414].

- [122] **CMS Collaboration**, S. Chatrchyan *et al.*, *Search for the standard model Higgs boson decaying into two photons in pp collisions at $\sqrt{s}=7$ TeV*, *Phys.Lett.* **B710** (2012) 403–425, [[arXiv:1202.1487](#)].
- [123] **ATLAS Collaboration**, G. Aad *et al.*, *Search for the Standard Model Higgs boson in the $H \rightarrow WW^{(*)} \rightarrow l \nu l \nu$ decay mode with 4.7 /fb of ATLAS data at $\sqrt{s} = 7$ TeV*, [arXiv:1206.0756](#).
- [124] **CMS Collaboration**, S. Chatrchyan *et al.*, *Search for the standard model Higgs boson decaying to a W pair in the fully leptonic final state in pp collisions at $\sqrt{s} = 7$ TeV*, *Phys.Lett.* **B710** (2012) 91–113, [[arXiv:1202.1489](#)].
- [125] **ATLAS Collaboration**, G. Aad *et al.*, *Search for the Standard Model Higgs boson in the decay channel $H \rightarrow ZZ^{(*)} \rightarrow 4l$ with 4.8 fb⁻¹ of pp collision data at $\sqrt{s} = 7$ TeV with ATLAS*, *Phys.Lett.* **B710** (2012) 383–402, [[arXiv:1202.1415](#)].
- [126] **CMS Collaboration**, S. Chatrchyan *et al.*, *Search for the standard model Higgs boson in the decay channel H to ZZ to 4 leptons in pp collisions at $\sqrt{s} = 7$ TeV*, *Phys.Rev.Lett.* **108** (2012) 111804, [[arXiv:1202.1997](#)].
- [127] **CMS Collaboration**, S. Chatrchyan *et al.*, *Search for the standard model Higgs boson in the H to ZZ to $2l 2\nu$ channel in pp collisions at $\sqrt{s} = 7$ TeV*, *JHEP* **1203** (2012) 040, [[arXiv:1202.3478](#)].
- [128] **CMS Collaboration**, S. Chatrchyan *et al.*, *Search for the standard model Higgs boson decaying to bottom quarks in pp collisions at $\sqrt{s}=7$ TeV*, *Phys.Lett.* **B710** (2012) 284–306, [[arXiv:1202.4195](#)].
- [129] **CMS Collaboration**, S. Chatrchyan *et al.*, *Search for the standard model Higgs boson produced in association with a W or a Z boson and decaying to bottom quarks*, *Phys.Rev.* **D89** (2014) 012003, [[arXiv:1310.3687](#)].
- [130] **ATLAS Collaboration**, G. Aad *et al.*, *Search for the Standard Model Higgs boson produced in association with a vector boson and decaying to a b-quark pair with the ATLAS detector*, [arXiv:1207.0210](#).
- [131] J. M. Butterworth, A. R. Davison, M. Rubin, and G. P. Salam, *Jet substructure as a new Higgs search channel at the LHC*, *Phys.Rev.Lett.* **100** (2008) 242001, [[arXiv:0802.2470](#)].
- [132] A. Abdesselam, E. B. Kuutmann, U. Bitenc, G. Brooijmans, J. Butterworth, *et al.*, *Boosted objects: A Probe of beyond the Standard Model physics*, *Eur.Phys.J.* **C71** (2011) 1661, [[arXiv:1012.5412](#)].
- [133] R. Hamberg, W. van Neerven, and T. Matsuura, *A Complete calculation of the order $\alpha - s^2$ correction to the Drell-Yan K factor*, *Nucl.Phys.* **B359** (1991) 343–405.

- [134] H. Baer, B. Bailey, and J. Owens, *O (α -s) Monte Carlo approach to $W + Higgs$ associated production at hadron supercolliders*, *Phys.Rev.* **D47** (1993) 2730–2734.
- [135] J. Ohnemus and W. J. Stirling, *Order α -s corrections to the differential cross-section for the WH intermediate mass Higgs signal*, *Phys.Rev.* **D47** (1993) 2722–2729.
- [136] J. Campbell and K. Ellis, *MCFM - Monte Carlo for FeMtobarn processes*, <http://mcfm.fnal.gov>.
- [137] M. Ciccolini, S. Dittmaier, and M. Kramer, *Electroweak radiative corrections to associated WH and ZH production at hadron colliders*, *Phys.Rev.* **D68** (2003) 073003, [[hep-ph/0306234](https://arxiv.org/abs/hep-ph/0306234)].
- [138] A. Denner, S. Dittmaier, S. Kallweit, and A. Muck, *Electroweak corrections to Higgs-strahlung off W/Z bosons at the Tevatron and the LHC with HAWK*, *JHEP* **1203** (2012) 075, [[arXiv:1112.5142](https://arxiv.org/abs/1112.5142)].
- [139] O. Brein, A. Djouadi, and R. Harlander, *NNLO QCD corrections to the Higgs-strahlung processes at hadron colliders*, *Phys.Lett.* **B579** (2004) 149–156, [[hep-ph/0307206](https://arxiv.org/abs/hep-ph/0307206)].
- [140] G. Ferrera, M. Grazzini, and F. Tramontano, *Associated WH production at hadron colliders: a fully exclusive QCD calculation at NNLO*, *Phys.Rev.Lett.* **107** (2011) 152003, [[arXiv:1107.1164](https://arxiv.org/abs/1107.1164)].
- [141] G. Ferrera, M. Grazzini, and F. Tramontano, *Higher-order QCD effects for associated WH production and decay at the LHC*, *JHEP* **1404** (2014) 039, [[arXiv:1312.1669](https://arxiv.org/abs/1312.1669)].
- [142] E. Braaten and J. Leveille, *Higgs Boson Decay and the Running Mass*, *Phys.Rev.* **D22** (1980) 715.
- [143] M. Drees and K.-i. Hikasa, *NOTE ON QCD CORRECTIONS TO HADRONIC HIGGS DECAY*, *Phys.Lett.* **B240** (1990) 455.
- [144] C. Anastasiou, F. Herzog, and A. Lazopoulos, *The Fully differential decay rate of a Higgs boson to bottom-quarks at NNLO in QCD*, *JHEP* **1203** (2012) 035, [[arXiv:1110.2368](https://arxiv.org/abs/1110.2368)].
- [145] O. Latunde-Dada, *MC and NLO for the hadronic decay of Higgs bosons in associated production with vector bosons*, *JHEP* **0905** (2009) 112, [[arXiv:0903.4135](https://arxiv.org/abs/0903.4135)].
- [146] S. Gieseke, D. Grellscheid, K. Hamilton, A. Papaefstathiou, S. Platzer, *et al.*, *Herwig++ 2.5 Release Note*, [arXiv:1102.1672](https://arxiv.org/abs/1102.1672).

- [147] K. Hamilton, P. Richardson, and J. Tully, *A Positive-Weight Next-to-Leading Order Monte Carlo Simulation for Higgs Boson Production*, *JHEP* **0904** (2009) 116, [arXiv:0903.4345].
- [148] J. Cancino, *Higgs decay to bottom quarks*, Master's thesis, ETH Zürich, 2011.
- [149] Ho-Kim, Quang and Pham, Xuan-Yem, *Elementary particles and their interactions*. Springer, 1998.
- [150] A. Martin, W. Stirling, R. Thorne, and G. Watt, *Parton distributions for the LHC*, *Eur.Phys.J.* **C63** (2009) 189–285, [arXiv:0901.0002].
- [151] A. Djouadi, M. Spira, and P. Zerwas, *QCD corrections to hadronic Higgs decays*, *Z.Phys.* **C70** (1996) 427–434, [hep-ph/9511344].
- [152] **LHC Higgs Cross Section Working Group**, S. Dittmaier *et al.*, *Handbook of LHC Higgs Cross Sections: 1. Inclusive Observables*, arXiv:1101.0593.
- [153] M. Rubin, *Non-Global Logarithms in Filtered Jet Algorithms*, *JHEP* **1005** (2010) 005, [arXiv:1002.4557].
- [154] M. Klasen and G. Kramer, *Large transverse momentum jet production and DIS distributions of the proton*, *Phys.Lett.* **B386** (1996) 384–388, [hep-ph/9605210].
- [155] S. Frixione and G. Ridolfi, *Jet photoproduction at HERA*, *Nucl.Phys.* **B507** (1997) 315–333, [hep-ph/9707345].
- [156] A. Banfi and M. Dasgupta, *Dijet rates with symmetric $E(t)$ cuts*, *JHEP* **0401** (2004) 027, [hep-ph/0312108].
- [157] M. Cacciari, G. P. Salam, and G. Soyez, *The Anti- $k(t)$ jet clustering algorithm*, *JHEP* **0804** (2008) 063, [arXiv:0802.1189].
- [158] M. Dasgupta, L. Magnea, and G. P. Salam, *Non-perturbative QCD effects in jets at hadron colliders*, *JHEP* **0802** (2008) 055, [arXiv:0712.3014].
- [159] J. Ohnemus and J. Owens, *An Order α^-s calculation of hadronic ZZ production*, *Phys.Rev.* **D43** (1991) 3626–3639.
- [160] J. Ohnemus, *Hadronic $Z\gamma$ production with QCD corrections and leptonic decays*, *Phys.Rev.* **D51** (1995) 1068–1076, [hep-ph/9407370].
- [161] J. Ohnemus, *Hadronic ZZ, W^-W^+ , and $W^\pm Z$ production with QCD corrections and leptonic decays*, *Phys.Rev.* **D50** (1994) 1931–1945, [hep-ph/9403331].
- [162] U. Baur, T. Han, and J. Ohnemus, *QCD corrections to hadronic $W\gamma$ production with nonstandard $WW\gamma$ couplings*, *Phys.Rev.* **D48** (1993) 5140–5161, [hep-ph/9305314].

- [163] U. Baur, T. Han, and J. Ohnemus, *QCD corrections and anomalous couplings in $Z\gamma$ production at hadron colliders*, *Phys.Rev.* **D57** (1998) 2823–2836, [[hep-ph/9710416](#)].
- [164] U. Baur, T. Han, and J. Ohnemus, *QCD corrections and nonstandard three vector boson couplings in W^+W^- production at hadron colliders*, *Phys.Rev.* **D53** (1996) 1098–1123, [[hep-ph/9507336](#)].
- [165] U. Baur, T. Han, and J. Ohnemus, *WZ production at hadron colliders: Effects of nonstandard WWZ couplings and QCD corrections*, *Phys.Rev.* **D51** (1995) 3381–3407, [[hep-ph/9410266](#)].
- [166] S. Catani, L. Cieri, D. de Florian, G. Ferrera, and M. Grazzini, *Diphoton production at hadron colliders: a fully-differential QCD calculation at NNLO*, *Phys.Rev.Lett.* **108** (2012) 072001, [[arXiv:1110.2375](#)].
- [167] T. Gehrmann, L. Tancredi, and E. Weihs, *Two-loop master integrals for $q\bar{q} \rightarrow VV$: the planar topologies*, *JHEP* **1308** (2013) 070, [[arXiv:1306.6344](#)].
- [168] T. Gehrmann, A. von Manteuffel, L. Tancredi, and E. Weihs, *The Two-Loop Master Integrals for $q\bar{q} \rightarrow VV$* , [arXiv:1404.4853](#).
- [169] F. Cascioli, T. Gehrmann, M. Grazzini, S. Kallweit, P. Maierhöfer, *et al.*, *ZZ production at hadron colliders in NNLO QCD*, [arXiv:1405.2219](#).
- [170] F. Caola, J. M. Henn, K. Melnikov, and V. A. Smirnov, *Non-planar master integrals for the production of two off-shell vector bosons in collisions of massless partons*, [arXiv:1404.5590](#).
- [171] J. M. Henn, K. Melnikov, and V. A. Smirnov, *Two-loop planar master integrals for the production of off-shell vector bosons in hadron collisions*, [arXiv:1402.7078](#).
- [172] T. Gehrmann and L. Tancredi, *Two-loop QCD helicity amplitudes for $q\bar{q} \rightarrow W^\pm\gamma$ and $q\bar{q} \rightarrow Z^0\gamma$* , *JHEP* **1202** (2012) 004, [[arXiv:1112.1531](#)].
- [173] T. Gehrmann, L. Tancredi, and E. Weihs, *Two-loop QCD helicity amplitudes for $g g \rightarrow Z g$ and $g g \rightarrow Z \gamma$* , *JHEP* **1304** (2013) 101, [[arXiv:1302.2630](#)].
- [174] F. Brown, *On the decomposition of motivic multiple zeta values*, [arXiv:1102.1310](#).
- [175] C. Anastasiou, C. Duhr, F. Dulat, and B. Mistlberger, *Soft triple-real radiation for Higgs production at N3LO*, [arXiv:1302.4379](#).
- [176] Z. Bern, L. J. Dixon, and D. A. Kosower, *Dimensionally regulated pentagon integrals*, *Nucl.Phys.* **B412** (1994) 751–816, [[hep-ph/9306240](#)].
- [177] S. Catani, *The Singular behavior of QCD amplitudes at two loop order*, *Phys.Lett.* **B427** (1998) 161–171, [[hep-ph/9802439](#)].

-
- [178] S. Catani and M. Grazzini, *Infrared factorization of tree level QCD amplitudes at the next-to-next-to-leading order and beyond*, *Nucl.Phys.* **B570** (2000) 287–325, [[hep-ph/9908523](#)].